UNIVERSITY OF OKLAHOMA

GRADUATE COLLEGE

CHARACTERIZATION OF POLY(PROPYLENIMINE) AND POLY(N-METHYLPROPYLENIMINE) AS POLYMER ELECTROLYTES WITH N,N'-DIMETHYLETHYLENEDIAMINE AND N,N'-DIMETHYLPROPYLENEDIAMINE AS MODEL COMPOUNDS

A DISSERTATION

SUBMITTED TO THE GRADUATE FACULTY

in partial fulfillment of the requirements for the

Degree of

DOCTOR OF PHILOSOPHY

by

RACHEL NASH MASON
Norman, Oklahoma
2009

CHARACTERIZATION OF POLY(PROPYLENIMINE) AND POLY(METHYLPROPYLENIMINE) AS POLYMER ELECTROLYTES WITH N,N'-DIMETHYLETHYLENEDIAMINE AND N,N'-DIMETHYLPROPYLENEDIAMINE AS MODEL COMPOUNDS

A DISSERTATION APPROVED FOR THE
DEPARTMENT OF CHEMISTRY AND BIOCHEMISTRY

BY

Roger E. Frech

Ralph A. Wheeler

Wai Tak Yip

Charles. V. Rice

Daniel T. Glatzhofer

John E. Moore Furneaux

DEDICATION

What you leave behind is not what is engraved in stone monuments, but what is woven into the lives of others.

-- Pericles[1]

To Linda, from whom I learned you have to be comfortable in your own skin first;

To Charles, who taught me to view learning as a life long quest and to value precise expression;

To Babe, whose practice of unconditional acceptance and patience provided me a safe place to fail and the challenge to see other through new eyes;

To Roy, who showed me the importance of refusing to take yourself too seriously because even the best men are sometimes wrong;

To Larry, who gave me the gift of honest bliss from others' joy and instilled the power to strive for the improbable while being content with the present.

Thank you for journeying with me as far as you did. I miss you all terribly.

ACKNOWLEDGEMENTS

One can never pay in gratitude; one can only pay "in kind" somewhere else in life.

--Anne Morrow Lindbergh[2]

(You might as well get ready – I was here forever, so the list is long)

I gratefully acknowledge the funding agencies that supported this work and/or kept my belly full during this quest: The University of Oklahoma Alumni Foundation, The United States Department of Education Graduate Assistantship in Areas of National Need (GAANN) Program and The University of Oklahoma Department of Chemistry and Biochemistry.

Funding is pointless without mentors from whom to learn. I am thankful for the collection of wonderful guides I have had. **Dr. Roger Frech**, I am profoundly grateful for your example of balance and your insistence on viewing students as multi-faceted individuals, as well as your vast knowledge of all things PChem. **Dr. John Moore Furneaux**, I am indebted to you for your willingness to teach me to tinker methodically yet fearlessly and for your encouragement to keep jumping when it felt like too many hoops. **Dr. Daniel Glatzhofer**, I appreciate that you challenged me to consider all the options instead of (or at least before) settling for the most comfortable answer. **Dr. Ralph Wheeler**, you ARE initially intimidating. Thank you for the best college course I have had and for reminding me to always strive to be a better teacher, as well as a better scientist. **Dr. Wai Tak Yip**, I am thankful for your humble attitude that never made my most basic questions feel trivial. It has been a pleasure to be supervised by you in the PChem Lab. **Dr. Charles Rice**, your

love of Heisenberg is admirable and your enthusiasm for your work is contagious. Thanks to you all for agreeing to shepherd me through this process.

I would be remiss if I failed to mention the fabulous folks who tried to keep me out of practical problems. To the entire **Chemistry Office Staff,** thank you for all your help with accounting, various paperwork and room scheduling. **Carol Jones**, your readiness to go above & beyond for students is not valued enough. **Jean Keil**, I appreciate that you take care of the Frech Group even though it isn't your job anymore. To the **Research Support Staff**, you all work so hard for us and we don't say thank you enough. **Susan Lauterbach**, I learned much from your conversation. **Jim Cornell** , thank you for always having the time to do "this one little thing." **Carl Van Buskirk**, you are an electronic/mechanical god who is welcome at my table anytime. **Dr. Doug Powell**, thank you so much for all your efforts to coax something useful out of my sad little crystals. Finally, I owe a huge debt (probably literally in a few cases) to all the babysitters: **Whitney Smith, Tami Martyn, Gary & Heather Nunnery Smith, Bobby Fleshman, Adam Warhausen, Leslie Quinalty, Favorite Aunt Stephanie Lawler, Allison Frech and Julia Kinchen** as well as all the members of the Frech group.

I might have given up this endeavor as too difficult if it weren't for my colleagues in lab and life. To the Frechians past, (**Shawna York, Varuni Seneviratne, Fred McKenna, Rebecca Sanders, Chris Burba, Nathalie Rocher, Matt Petrowsky, and Dilhani Jayathalaka)** thank you for your advice and models of diverse ways to succeed. To the Frechians present, (**Gwen Giffin, Allison McCoy Fleshman, and Dharshani Nimali Bopege)** I count our time together as one of the

best parts of the last few years and value your friendships greatly. To the Glatzhoferites (**Lieyu "Richard" Hu, Frank Yepez-Castillo, Matthew Meredith & Rahul Kadam)** thank you for your patience with my crazy schedule and your frequent participation in "Name That Molecule." Richard, you were a great and incredibly flexible collaborator. I miss having your sense of humor and cultural exchanges around. Frank, thanks for being a sounding board for sanity. To **Scott Boesch**, my computing superman, I am happy and you should be too!

I also want to extend grateful lauding to those who diligently read this work in its various incarnations. **Nathalie Rocher**, your insight was invaluable. **Rhonda Kyncl**, your patience (and knowledge of the semicolon) is unending.

Finally, my family has been amazingly supportive of my wild hair to quit a perfectly good engineering job in order to pursue yet more education. Thanks to you all: **Uncle Larry Duree** (Boomer Sooner); my in-laws **Linda Mason** and **Eddie Mason**; my grandmother **Ruth Hoffman**; and my sister **Melodie Nash** for understanding. To my dad, **Larry Nash**, it pains me beyond belief not to share this moment with you. To my mom, **Amelia Nash,** I am so grateful for your encouragement, especially when you felt helpless to help. To my ebullient daughter, **Miriana**, I hope this experience has made your early years fun and exciting – or least hasn't warped you too badly. To my husband, **Rob**, thank you showing me "I am deeply loved and highly valued" always and everywhere. I love you both around the world, to the moon and back.

TABLE OF CONTENTS

Nature uses only the longest threads to weave her patterns, so that each small piece of her fabric reveals the organization of the entire tapestry.

--Richard Feyman[3]

LIST OF TABLES

Order is the shape upon which beauty depends.

-- Pearl Buck[4]

LIST OF FIGURES & SCHEMES

Order is a lovely thing;
on disarray it lays it wing,
teaching simplicity to sing.

-- Anna Hempstead Branch[5]

ABSTRACT

Let me explain. No, there is too much.
Let me sum up.

--Mandy Patinkin as Inigo Montoya[4]

Many factors including light weight, flexible form factor, processing ease and environmental friendliness make solid polymer electrolytes (SPEs) desirable materials for use in lithium ion battery systems. However, consistently low room temperature conductivities have precluded the realization of a true solid polymer battery. Despite nearly forty years of extensive study, fundamental interactions occurring within SPEs are not thoroughly understood. Knowledge gained from poly(ethyleneoxide), the most well-characterized SPE, has spurred the quest for understanding of other systems.

This dissertation examines complexes of poly(propylenimine), PPI and poly (methylpropylenimine), PMPI with lithium triflate with the goal of identifying the primary interactions taking place in the systems and determining how these interactions impact ionic conductivity. The polymers are compared against their better-characterized homologs poly(ethylenimine), PEI and poly(methyl-ethylenimine), PMEI. Vibrational spectroscopy was used to probe interactions between cations, anions and the polymers, while differential scanning calorimmetry and ac impedance measurements were used to characterize the thermal and ionic conductivity behaviors of the systems. Conductivities of both PPI and PMPI were determined to be insufficient for use in battery systems, but interesting results in

terms of ionic associations were obtained. Additionally, significant amounts of hydrogen bonding were shown to be present in PPI and the PPI:salt complex.

Two small molecule model compounds, N,N'-dimethylethylenimine and N,N'-dimethylpropylenimine, were utilized to meet the second goal of this research. This objective set included: establishing what types of the hydrogen bonding interactions occur within the model compounds and their salt complexes, identifying the spectral signatures of those interactions and determining how the cation, anion and polymer interactions change in the presence of salt. Dilution of the compounds and their salt complexes in carbon tetrachloride aided significantly in discerning the various hydrogen bonding interactions by eliminating, to a great extent, the intermolecular interactions. This allowed for the identification of six unique NH species based on spectral evidence. Unexpectedly, dilution of the salt complexes also resulted in the collapse of an apparent network involving cation, anion and polymer interactions.

REFERENCES (FOR ALL FRONT MATTER):

(1) Pericles, as quoted in *The Resilient Child: Seven Essential Lessons for Your Child's Happiness and Success* George Everly, J.; Brown, S., Eds. DiaMedica Publishing: New York, 2009.

(2) Lindbergh, A. M., *North to the Orient*. First Harvest ed.; Harcourt Brace & Company: Orlando, FL, 1967.

(3) Feynman, R. P., The Character of Physical Law (1965). In *Great Physicists: The Life and Times of Leading Physicists from Galileo to Hawking,* Cropper, W. H., Ed. Oxford University Press: New York, 2004; p 397.

(4) Buck, P. S., In *Simple Abundance*, Breathnach, S. B. Warner Books, Inc. : New York, 1995.

(5) Branch, A. H., The Monk in the Kitchen. In *Modern American Poetry: Revised and Enlarged Edition*, Untermeyer, L., Ed. Harcourt, Brace & Company, Inc.: New York, 1921; p 128. Accessed via GoogleBooks 11 October 2009.

(6) Reiner, R., The Princess Bride. Screenplay by William Goldman; MGM Home Entertainment: United States, 1987.

CHAPTER 1: CONTEXT FOR THE RESEARCH

Science is a pyramidal endeavor, each layer of discovery arising out of previous ideas and research.

--George Jeffery[1]

1.1 RESEARCH OBJECTIVES

Solid polymer electrolytes (SPEs) have been the subject of extensive study for a number of years, yet the fundamentals of interactions within the systems remain largely enigmatic. This lack of understanding is a significant factor inhibiting the design of a SPE viable in a commercial battery. As the subject of nearly 40 years of research, poly(ethyleneoxide), PEO, is the most well-characterized SPE. Similar polymers have been studied in an effort to gain understanding of the cation-anion-polymer interactions within the systems. Two polymers are addressed in the present work: poly(propylenimine), PPI and poly (methylpropylenimine), PMPI. One goal of the project was to identify the types of interactions occurring the systems and to ascertain how they impact ionic conductivity. Model compounds, N,N'-dimethylethylenediamine and N,N'-dimethylpropylenediamine were employed to aid in interpretation of the spectral data of the polymers. These compounds were also utilized to meet a second objective of indentifying various types of the hydrogen bonding interactions occurring within the model compounds and how these interactions change in the presence of salt. A more detailed summary of this work is given in Section 1.5 below.

1.2 BATTERY BASICS

A battery, or more precisely a cell, is an electrochemical device which converts chemical energy into electric current though the use of a reduction/oxidation couple. Technically, a battery is a collection of cells connected in parallel and/or series to give the desired capacity and/or voltage. However, in practice the terms 'battery' and "cell" are often used interchangebly. Batteries (and cells) may be divided into two broad categories: primary and secondary. Primary batteries are designed for a single use. Once the cell is completely discharged, it can not be recharged and is discarded. Examples of primary batteries are the carbon-zinc and alkaline cells used in numerous devices, such as radios and flashlights. Secondary batteries are rechargeable. In stationary and assist applications, these batteries draw charge from a primary power supply and deliver that energy only when the primary source is not available or is unable to deliver the full energy demand of the load. The battery is then immediately replenished to its maximum state of charge. The nickel cadmium (NiCad) emergency lighting batteries and lead-acid batteries used in automobiles and uninterrupted power supplies are examples of this sort of secondary battery. The other variety of secondary batteries, often referred to as portable batteries, serves as the primary power supply for a given device. Once the battery has been drained, it can be placed in a charger, which inputs energy into the system forcing the reverse reaction to occur. This restores the battery to a useable state of charge and it can be employed again to power a device. Common types of portable secondary batteries are nickel metal hydride power tool

batteries and lithium ion batteries used for everything from laptop computers to MP3 players. In either type of secondary battery, the recharging process is rarely 100% efficient (for safety reasons it is actually designed not to be)[3] so each time a secondary battery is recharged some capacity is lost. Eventually, the secondary battery will fail to hold charge sufficient to drive the device and require replacement by a new battery. Lead-acid is the dominant chemistry for stationary and assist applications, while in the portable secondary battery market, lithium ion chemistry is by far the most prevalent.[4,5]

1.2.1 The Context for Lithium Ion Batteries

The global market for all batteries was estimated to be about $71 billion in 2008.[6] Secondary batteries constitute roughly two thirds of that[6] and lithium ion batteries now account for about 75% of the portable rechargeable market.[5] Worldwide sales of lithium ion secondary batteries in 2008 were estimated at $911 million.[7] As the disposable income levels of the developing world rise, this market is expected to increase significantly, since nearly every form of portable consumer electronic product, from cell phones and laptop computers to portable digital media players are powered by lithium ion batteries.[6,8] This is expected to push worldwide sales to $9.1 billion by 2015 according WinterGreen Research Inc.'s most recent market survey.[7] The growth in the domestic U.S. market is anticipated to be around 6% annually from 2009, reaching $1.9 billion by 2012.[4] This demand is driving research interest in building a better lithium ion battery. In fact, the chemistry was

the recipient of more research dollars in 2008 than all other battery systems collectively.[5]

1.2.2 The Lithium Ion Technology

Like all electrochemical cells, the lithium ion cell consists of an anode, cathode and electrolyte material. The terms 'anode' and 'cathode' designate the electrode at which oxidation and reduction occur respectively. In a secondary battery, the roles of the electrodes would be reversed upon recharge. That is to say the electrode that was reduced during discharge will be oxidized during charge. Thus, in a strict sense the labels 'anode' and 'cathode' also should be exchanged. However in practice, the jargon retains the labeling designated by the discharge cycle.

The earliest lithium ion cell utilized lithium metal as the anode material. While it provided an extremely high energy density, this proved impractical due to safety issues arising from dendrite growth upon cycling. Lithium alloys (*e.g.* LiAl) solved the dendrite problem and found some commercial use.[9,10] However, the large volume changes experienced by these materials with intercalation/deintercalation limited the cycle life of the cell and they have been abandoned in favor of carbonaceous materials which do not suffer large volume changes upon intercalation.[9-12] Lithiated 3-d metal nitrides, amorphous tin composite metal oxide and intermetallic alloy material have been explored, but not commercialized to date due to performance issues.[10,11] Recently, carbon nanotubes have been investigated as

potential anode materials. However, the high cost and large irreversible capacity losses must be overcome before these are serious contenders.[11] Presently, the anode is most often a powdered lithiated carbon coated onto a copper foil current collector.[12,13] The carbon material is usually a mixture of graphite (or graphitized carbon) and a hard carbon coke.[12-14]

The lithium ion cell's cathode material is composed of a powered metal oxide, capable of lithium intercalation, coated onto an aluminum foil current collector.[13,14] The lithiated metal oxide may be a layered material such as $LiCoO_2$, a spinel like $LiMn_2O_4$, or an olivine such as $LiFePO_4$.[10,11,13] The layered materials host the lithium ions in the spaces between the layers, while in spinel materials the lithium ions occupy tunnels in the materials.[14] $LiCoO_2$ was the most common cathodic material in the commercial cells. However, environmental concerns have pushed toward the use of mixed metal oxides which substitute some or all of the cobalt with Mn, Ni, and/or Ti. The important factor is the capability of the cathode to reversibly accept lithium ions into its structure without damaging the integrity of the structure.

During use, lithium ions are shuttled through the electrolyte between the anode and cathode according to the equations shown in Figure 1-1. Due to this action, these batteries are also called rocking chair batteries. During discharge, lithium ions are extracted from the cathodic material as it is oxidized and inserted between the graphitic layers of the carbonaceous anode as it is reduced. When the cell is charged, the process is reversed with the lithium ions moving from the

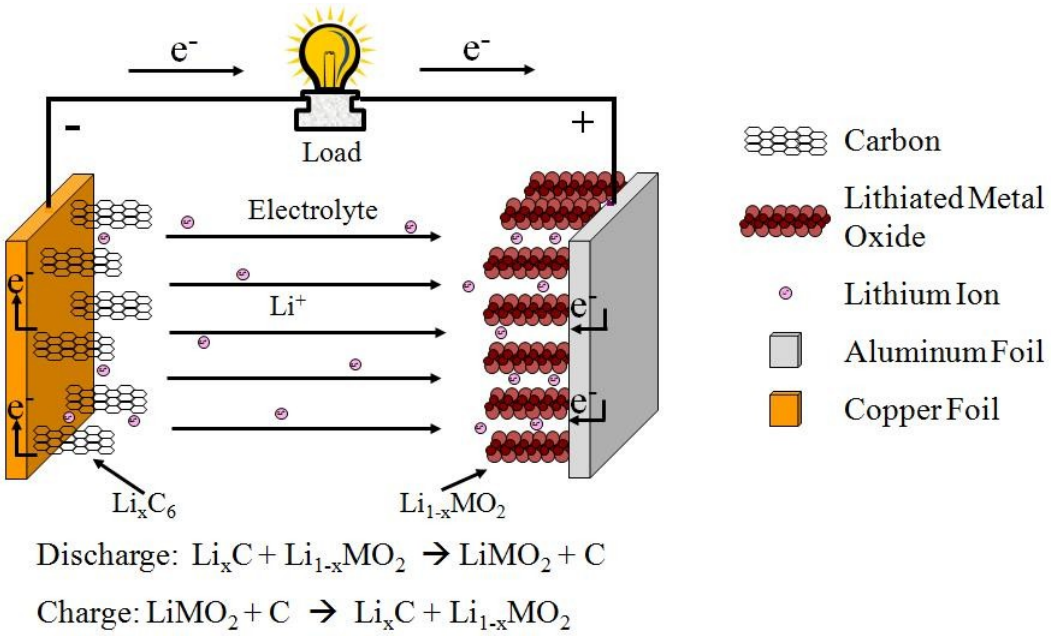

Figure 1-1: Schematic of a lithium ion battery. Drawn to illustrate the cell components and flow of electrons and Li^+ during discharge. The "electrolyte" area is occupied by a solid polymer electrolyte or in the case of commercial cells a polymer membrane swollen with an organic carrier mixture and dissolved lithium salt.

carbonaceous material to the cathode material. Electrolytic media between the anode and cathode serves to conduct both the lithium ions and counter anions.

In general, secondary lithium ion cells can be grouped in to two categories: non-aqueous electrolytes and polymer electrolytes. Both types of lithium ion cells utilize the same basic chemistry. In the case of non-aqueous electrolytes, a solid separator material is required to prevent direct contact between the anode and cathode. This material is usually a microporous polyolefin, such as poly(propylene) or poly(ethylene).[13] Poly(vinylendinefluroride) and poly(vinylendinefluroride) coated polyolefins are also widely used.[15] The separator functions not only as a physical barrier preventing contact between the anode and cathode, but often also is

a safety mechanism designed to lose porosity if the temperature of the system increases above a threshold value. This prevents ion movement between the electrodes and effective "turns off" the battery.[13,15] The separator also serves as a host for the organic electrolyte mixture. The electrolyte consists of a low lattice energy salt dissolved in an organic carrier. The salts most commonly used are $LiPF_6$, $LiBF_4$, $LiAsF_6$, $LiClO_4$ and $LiAlCl_4$.[9,14,16] These salts are dissolved in small linear and/or cyclic ethers, esters and carbonates, with ethylene carbonate, propylene carbonate and dimethyl carbonate being the most frequently used in commercial cells.[11,13,14] Often a combination of carriers is used to achieve the best results. The best performing electrolyte mixtures should have high dielectric constants, low viscosity, low freezing points and be compatible with the electrode materials.[14] The dry components of the cell system (anode, cathode and separator) are stacked or wound to form the desired cell geometry (*e.g.* cylindrical, prismatic, *etc*) then placed in a rigid metal can. The can is flooded with the electrolyte solution, which is absorbed by the microporous separator to form a swollen polymer host material.[16] Any excess electrolyte is decanted before the can is sealed. The organic liquids are often referred to as plasticizers. These materials enhance the conductivity of the system by providing a liquid-like environment for ion conduction. However, because they are contained within the polymeric matrix of the separator, the overall system appears to be solid. Though these cells are sometimes marketed as "solid" systems, this is inaccurate since they require the liquid to function. They are more accurately called "hybrid" or "swollen polymer" systems. A closely related cell

technology, often called “plastic lithium ion” incorporates the electrolyte swelling into separator processing and laminates the anode, separator/electrolyte and cathode together before punching plates and packing the cell in pouches. Plastic and hybrid cell technologies account for the vast majority of currently available lithium ion cells.

The second type of lithium ion cell utilizes a true solid polymer electrolyte. The chemistry is identical to that used in non-aqueous cells described above in terms of anode and cathode materials and the salts. The difference is that the solid polymer itself serves as the electrolyte carrier *and* the separator, so no organic solvent is required. The same types of low lattice energy salts can be dissolved directly into the polymer. Usually, the polymer is dissolved in a solvent to form a liquid solution; the salt is added to the solution. The mixture is cast and the solvent evaporated. The result is a free standing polymer electrolyte film, which is layered between the anode and cathode to form a secondary cell. Alternately, the various materials may be cast directly onto the previous layer. In the end, the completed stack is usually hot pressed or laminated to ensure good contact between the layers. Long strips of the stack are wound into cylinders or are cut into smaller plates which are layered and placed into foil-backed plastic pouches. These cells do not require the use of organic carriers. Due to low conductivity at ambient temperatures (0-30°C), true solid polymer electrolyte based lithium ion cells are not yet commercially viable.

1.2.3 The Crucial Need for Improvement over Non-Aqueous Cells

Though the conductivity of the current state-of-the-art solid polymer electrolytes is not high enough for widespread commercial use, the materials are of interest. Non-aqueous electrolyte lithium ion batteries are far from ideal. The carrier must be carefully chosen to avoid detrimental interactions, which cause the breakdown of electrode materials and shorten cell life.[14] The use of an organic carrier comes with the inherent risk of leakage and a flammability concern. The 2007 recall of nearly 7 million Sony® cells in the wake of several battery sourced laptop fires illustrates this point.[6] Additionally, the organic carrier adds weight to the battery. While for compact applications, like portable personal electronics, the added weight is not an issue, in more specialized applications such as electric vehicles and space craft, it is a strong consideration. The need to contain the volatile organic carriers requires hermetically sealed metal containers which also add weight to finished product. Containment of the organic also limits the flexibility in terms of design. The battery and device must be designed to accommodate the container so only a limited number of form factors are practical.

Solid polymer electrolyte based lithium ion cells offer freedom from the organic carrier, thereby eliminating the leakage and flammability concerns. Polymer electrolytes do not diffuse into the bulk of the electrodes, so cannot cause the same types of damage as the organic carriers. The lower density of polymer electrolytes also offers a weight savings versus the non-aqueous electrolytes. Further weight savings is realized through packaging the SPE cells in foil-backed plastic pouches

rather than sealed metal canisters. The flexible form factor of polymer electrolytes offers design advantage over non-aqueous electrolytes, since, in principal, the SPE cells can be manufactured in virtually any shape or dimension. For these reasons, solid polymer electrolytes continue to garner interest from the battery community.

1.2.3 The Critical Flaw of Solid Polymer Electrolytes

The main drawback to SPEs to date, is their low conductivity. Ions are not able to diffuse as rapidly through the solid polymer as through liquid carriers, so conductivity values are lower. Some of this may be overcome through the use of thin film solid polymer electrolytes. However, conductivity of even the best SPEs remains under the 1mS cm^{-1} threshold at ambient temperatures. Numerous studies aimed at understanding these systems better have been undertaken, but questions remain regarding fundamental interactions in the system. These interactions largely determine the conductivity of the systems, so thorough comprehension of them is imperative to system improvement. The work presented here strives to offer some insight into cation-polymer, cation-anion, anion-polymer and polymer-polymer interactions occurring in two polymer electrolyte systems: poly(propylenimine) and poly(methylpropylenimine). These interactions are also probed in small organic molecules modeling parts of the secondary polymeric system.

1.3 POLYMER ELECTROLYTES

Polymer electrolytes are a class of ionic conducting materials. In their simplest form, polymer electrolytes consist of an ionic salt dissolved in a polymer host matrix. Other materials, such as organic plasticizers and inorganic fillers are sometimes added to optimize certain properties of the systems. Polymer electrolytes have potential applications in the field of electrochromic devices, sensors, photoelectrochemical cells, fuel cells and batteries.[17,18] The most well- characterized system is poly(ethyleneoxide), PEO, which initially sparked interest in the possibility of a thin flexible solid-state battery.[19]

1.3.1 Brief Review of Polymer Electrolytes for Battery Applications

Poyl(ethyleneoxide) was the first polymeric material in which ionic conduction was observed.[20,21] The relatively recent (to that time) discovery of intercalation electrode materials eventually prompted the suggestion that polymer electrolytes could be paired with these materials for use in batteries.[19,22,23] A number of investigations ensued, aimed both at characterizing various systems and at identifying the basic issues associated with the materials. Understanding the guest-host interactions governing the salt complexes, the mechanism of charge transport, the factors governing conductivity of the systems, were (and to a large extent remain) the focus research in the field.[24-42]

When pure PEO polymer electrolytes failed to realize the conductivity levels needed to be viable as a battery electrolyte, a wide variety of measures were

employed in hopes of increasing conductivity. Side chains were added in an effort to decrease crystallinity thereby improving conductivity.[25,33,43-45] New backbones were tried in hopes of increasing polymer motion and controlling ion solvation, both of which facilitate ion conduction.[43,46-48] Crosslinking of polymers into networks was used to give conducting polymers better mechanical properties.[49-51] Gels, consisting of liquid electrolytes stiffened by polymers, were created (often through crosslinking).[52-54] Organic plasticizers were added to create a liquid-like conduction environment within a polymer matrix.[55-57] Inorganic additives were employed to disrupt crystallinity and aid ion transport.[58-61] Copolymers and blends, which combined the mechanical and conduction benefits of multiple polymers, were synthesized.[62-65] Whole new classes of polymers were explored.[43,46,66-68] In some cases, multiple approaches were undertaken simultaneously.[69-73] Many of these efforts, such as the gels and the plasticized materials, resulted in the required conductivity levels, but did so at the expense of the desired mechanical properties. Other approaches maintained the desired mechanical characteristics, but failed to meet the conductivity goal. The most successful of these efforts has been the addition of organic small molecule plasticizers to polymeric hosts. The materials are not truly solid polymer electrolytes, but technically gel electrolytes. Nonetheless, this approach has resulted in the non-ideal lithium ion hybrid cell technology described in Sections 1.2.2 and 1.2.3, which has colloquially become called a polymer or plastic battery and has been widely commercialized.[74]

1.3.2 Polyimines

Polymines are among the new classes of polymers investigated. These systems are similar to the ether oxygen compounds, but utilize nitrogen, rather than oxygen heteroatoms. The lone pair on the nitrogen atom allows the system to retain the capability to coordinate cations, while the secondary nature of the nitrogen offers a degree of synthetic flexibility not available with oxygen as functional groups may be added to the nitrogen atom.

1.3.2.1 Poly(ethylenimine)

The most well studied of the polyamines is linear poly(ethylenimine), PEI. The polymer is structurally analogous to PEO, with both materials containing two methylene groups between heteroatoms. Chatani, *et al* provided a crystal structure for anhydrous PEI, which shows double stranded helices having five repeat units per complete turn.[75] The helices are connected via interchain hydrogen bonding between NH groups.[75] PEI is an able host for electrolytic salts and has been shown to dissolve many of the same salts as PEO, including $Na(SO_3CF_3)$,[76,77] NaI,[78] NaCl,[79] LiI,[80] LiBr,[80] LiCl,[80] $LiClO_4$,[80,81] LiSCN,[80] $LiBF_4$,[80] $LiSbF_6$,[82,83] $Li(SO_3CF_3)$.[77,81-83] Likewise, it exhibits many of the same trends as PEO in terms of conductivity, such as reaching a maximum at salt composition around a 10:1 to 15:1 heteroatom:Li^+ molar ratio. Also like PEO, conductivity of pure PEI:salt systems at ambient temperature (10^{-8} to 10^{-6} Scm^{-1}) is considerably below that necessary for battery use, requiring temperatures of around 150°C to reach the 10^{-3} Scm^{-1} mark.[76,78,80,81,84]

Branching, crosslinking, plasticizing and blending with other polymers have been tried in efforts to improve conductivity of PEI systems.[62,85-89]

1.3.2.2 Poly(methylethylenimine)

One culprit contributing to the lower-than-desired conductivity of PEI:salt systems is the extensive hydrogen bonding present. The opportunity for hydrogen bonding to occur can be eliminated through substitution of the secondary nitrogen. The simplest option is methylation, which forms poly(N-methylethylenimine) or PMEI. The material has been the focus of subject of some research, but is not as well characterized as PEI. PMEI is a viscous liquid whose viscosity increases with salt content. PMEI is known to solvate $LiClO_4$,[81] $Li(CF_3SO_3)$[81,90,91] and $Na(CF_3SO_3)$.[90] PMEI displayed low conductivity when complexed with these salts. The highest values were obtained by 15:1 $N:Li^+$ molar ratio, but at 10^{-6} S cm^{-1} around 60ºC, this is not sufficient for battery use.

1.3.2.3 Poly(propylenimine)

Poly(propylenimine), PPI, is a homolog to PEI, having three rather than two methylene groups separating heteroatoms. Branched and dendritic PPI has mainly been studied for biological applications, such as drug delivery.[16,92,93] PPI has not been examined as a potential polymer electrolyte for battery applications. The lack of interest in PPI based electrolytes probably stems from the failure of the analogous ether oxygen system to conduct better than PEO. Based on the performance of the ether oxygen systems, two backbone carbons has been identified as the optimum inter-heteroatom spacing.[19] This hypothesis has not been tested in imine systems.

PPI is not expected to be an exceptional ion conductor owing to the potential for extensive hydrogen bonding within the system. However, information garnered from the system can lead to a deeper understanding of the interactions within the system and how these impact conductivity, which in turn can be applied to related systems.

1.3.2.4 Poly(N-methylpropylenimine)

Poly(methylpropylenimine), PMPI, is obtained via methylation of PPI. It is not a well characterized system. This work explores the vibrational spectroscopy of neat PMPI and complexes of PMPI and lithium trifluoromethanesulfonate, Li(CF_3SO_3) or LiTf, of various compositions. Differential scanning calorimetry data and temperature dependent conductivity data are also reported.

1.3.3 Factors Influencing Conductivity

The first step to improving conductivity of solid polymer electrolytes is understanding the factors that determine it. Ionic conductivity in polymer electrolytes is a complex process that depends on the specific polymer-salt complex. Polymer-ion interactions, ion-ion interactions, and polymer structure and motion all influence ion concentration and mobility, which are the primary factors in ionic conductivity.

1.3.3.1 Formation of Polymer Electrolyte

In order to form an ionically conducting electrolyte, a salt must dissolve into a host polymer. This is governed by the change in Gibbs free energy of dissolution

which can be described by $\Delta G=\Delta H-T\Delta S$ where ΔG is the change in Gibbs free energy upon dissolution, ΔH is the accompanying change in enthalpy, T is temperature and ΔS is the associated change in entropy. In order for salts to dissolve in the polymer, ΔG must be negative. ΔS for these systems may be either positive or negative depending on the balance between the entropy gained in the breaking up of the salt lattice and the entropic loss resulting from order induced in the polymer chains due to ion-polymer interactions.[94] ΔH also requires balancing competing contributions to the term. The lattice energy of the salt and the creation of coordination sites in the polymer contribute toward a positive ΔH, while the coordination between the cation and the polymer and the interaction between ions make negative ΔH contributions.[94] In the end, it is the lattice energy of the salt and the coordinative interaction between the polymer and the cation that primarily governs the dissolution. The latter interaction weighs heavily in the determining the degree of restriction experienced by the polymer chains (ΔS) and in solvation enthalpy (ΔH). For these reasons, the salts used tend to be of low lattice energy and composed of alkali-metal cations (most often Li^+ for battery applications) and monovalent polyatomic anions with charge distributed over all the atoms.[94] Some monatomic anions of large radii have also been successfully solvated.

1.3.3.1 Structure of the Polymer Electrolyte

When a salt dissolves in a polymer, the resulting polymer electrolyte is not a homogenous mixture of the salt and polymer. Instead a number of local domains exist within the bulk system. As shown Figure 1.2, there are at least three types of microscopic environments possible. A region of pure polymer may exist where no salt is present (a). This region may have either an amorphous or crystalline character depending on the polymer. A crystalline region of salt-containing polymer may also be present (b). The final region is composed of amorphous salt-containing polymer (c).

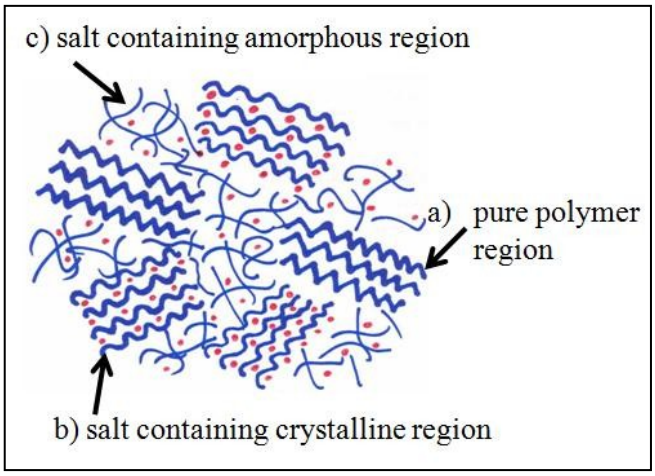

Figure 1-2: Possible local environments within the bulk polymer electrolyte. Figure used with permission.[2]

Motion of the polymer chains in the crystalline regions is suppressed, while in the amorphous regions the chains move more freely. Since ion transport is largely dependent on polymer motion, it occurs mainly within the amorphous salt-containing region. Thus, maximizing these regions is desirable. For this reason, polymer hosts are usually selected to have low T_g and flexible backbones, since these factors increase polymer motion and ion transport and are most likely to maximize the percentage of amorphous material. Likewise, measures to reduce crystallinity, such

as addition of side chains of high motion or steric hindrance can often improve conductivity.

1.3.3.2 Ion Transport

In general, polymer electrolytes are anion conductors since the cation motion is restricted by coordination to the polymer chain. Unlike liquid electrolytes, where the cation moves freely surrounded by a solvation sphere, in solid polymer electrolytes, the cation moves via polymer segmental motion. The length of the polymer chain prevents long range translation, so the cation must be transported through a series of short range local motions requiring partial desolvation. This requires finding the optimum strength of cation coordinative interaction with the polymer chain. The interaction must be strong enough to promote solvation, but not so strong as to render the cation completely immobile. In general, anions are not known to coordinate directly to the polymer chain, but rather any chain association comes through interaction with the coordinated cation. The present work presents the possibility of direct anion interaction with polymer chain through hydrogen bonding.

1.3.3.3 Ionic Association

As salts are dissolved in aqueous solutions, ions gain a solvation shell of water. This effectively isolates the ions from one another and, due to the polarity of the water molecules, reduces the effective charge fields of the ions. In turn, this reduces ion-ion interactions. However, this is not the case in the polymer electrolyte. While the cation is solvated by the polymer chain, it is not completely encompassed

in a solvation shell. Thus, the effective charge of the cation is not as efficiently reduced as in a liquid system and the possibility of ion-ion interaction exists. These interactions result in the clustering of ions.

The most commonly seen aggregates in the systems presented here are contact ion pair (LiTf), and the triple ion $(Li_2Tf)^+$, though some evidence of higher order association is occasionally observed.[95] Aggregation is detrimental to ionic conductivity since it reduces the number of charge carriers available in the system and most likely hinders mobility. The maximum number of charge carriers and therefore maximum conductivity occurs when the free ion, consisting of Li^+ and Tf^- well-separated from one another, is the dominate species. In the polyimine systems investigated in this study, "free" ion occurs at low salt concentrations and degree of association increases with increasing salt concentration. It should be noted that associations in this study are determined based on vibrational spectroscopy, which can not distinguish between truly free ions and those which are solvent separated pairs. For this reason the designation "free" will be used to represent the indeterminate species, which may be truly free or may be a solvent separated pair.

1.4 SMALL MOLECULES AS MODEL COMPOUNDS

Solid polymer electrolyte systems are complex with many interactions occurring simultaneously and many factors concurrently influencing the behaviors of the systems. Dissecting the contributions from various factors can be difficult or impossible from analysis of the polymer electrolyte alone. Complete interpretation

using analytical techniques, in particular vibrational spectroscopy, is hindered by the complexity of the systems. One useful approach is to use small molecules to model parts of the system.

Model compounds are chosen to closely imitate the structure or chemical environment of the polymer or polymer segment of interest. In some cases the use of multiple model compounds may be warranted in to order to model different aspects of the system. In addition to supplying a simplified spectral signature, it is often possible to obtain crystals structures from the small molecules that would be impossible, or at the very best extremely difficult, to acquire from the polymers. Additionally, model compounds can be used in computational studies that would be too time and resource extensive to be feasible on the full polymeric system. The information gained through all these techniques can render important insights into the polymer electrolyte system.

The use of model compounds has been successful for multiple polymer electrolyte systems. The study of short chain ethoxides (glymes) and low molecular weight poly(ethyleneglycols) has proven invaluable in the investigation of PEO and closely related systems.[29,31,37,39,41,96-99] PEI based systems have also benefited from knowledge gained through the use of model compounds.[100-102] Most notably, the competing effects of cation induction and hydrogen bonding in branched poly(ethylenimine), BPEI, were clarified through studies on several amines models. In that case, three compounds (dipropylamine, hexylamine and N,N-

dimethylethylendiamine) were needed to model the primary and secondary nitrogen components within BPEI.[103,104]

The purpose of using model compounds is two-fold. The primary goal is to use the more simplified model system to identify characteristic bands in the IR and Raman spectra. The vibrational spectra of the model compounds are generally more straightforward than those of the polymer system. Thus, it is easier to identify and assign particular spectral bands to their vibrational modes or to recognize spectral trends due to known changes in the system. This knowledge can then be extended to the polymeric system. A second objective is to characterize the behavior of the model compound under given conditions. In many instances this information can be extended to make predictions about the behavior of the polymeric systems. However, this is not always the case. Some significant intermolecular interactions, such as formation of dimers, can occur in the model compound, but not in the polymer. The same type of interactions may manifest differently in the polymer due structural differences such as chain length. Nonetheless, model compounds can be a powerful tool for investigation of polymer electrolyte systems and are well-utilized in this study.

1.5 SUMMARY OF THIS WORK

The work constituting this dissertation is comprised of several interrelated, but independent projects. These endeavors all relate to polymer electrolytes for application in lithium ion batteries. Much of the research was performed in

collaboration with Lieyu Hu and is noted as such when appropriate. In constructing the dissertation document itself, attempts were made to create largely self-contained and free standing chapters, thus each chapter contains introductory material and several concepts are addressed different chapters. It should be noted, however, that the work is interlinked.

Chapter 1: Context for the Research contains an overall introduction to the basic concepts of lithium ion batteries, polymer electrolytes and the primary factors which influence ionic conductivity. It is not intended as a primer on any of those subjects, but instead, its purpose it to give the reader a framework from which to approach the research presented in following chapters.

Chapter 2: Experimental Methods contains descriptions of sample preparation and analytical techniques used to conduct this research. These procedures are not repeated within each chapter.

Chapter 3: Poly(propylenimine) addresses the investigation of PPI as a potential polymer electrolyte material when complexed with lithium trifluoromethanesulfonate, LiTf. As previously mentioned linear PPI is a homolog material to linear PEI, whose conductivity behavior has not been well characterized. The PPI investigated here was synthesized by Leiyu Hu. The material and its complexes with lithium trifluoromethanesulfonate were characterized using differential scanning calorimmetry, IR spectroscopy and AC impedance measurements. The results were compared against the more thoroughly characterized PEI.

PPI is a highly crystalline pale yellow solid, which is not hygroscopic. When the LiTf concentration is low, domains of pure highly ordered crystalline PPI dominate the system. At a composition between 10:1 and 5:1 $N:Li^+$, the system is transformed into a single amorphous phase of salt containing polymer. IR spectra of anionic vibrational modes indicate addition of LiTf beyond this level continues to add to the contact ion pair population, with slight indications of a higher order aggregates. Further, these data show the degree of association is not significantly impacted by either temperature or excessive LiTf concentration. Conductivity measurements performed over a range of compositions from 20:1 to 3:1 $N:Li^+$ molar ratio show increasing conductivity until reaching a plateau, the value of which is dependent on temperature. Conductivity is less than 10^{-7} S cm^{-1} at room temperature, but increases to 10^{-4} S cm^{-1} at 80 ºC The steady increase in conductivity indicates that the improvement is likely a function of thermally driven mobility enhancement rather than a change in ionic association or local environment.

The performance is disappointing, but not unexpected given the hydrogen bonding within the system. The hydrogen bonding in PPI appears to be weaker than that observed in the analogous PEI samples, yet less aptly disrupted by salt or heat addition.

Chapter 4: Poly(methylpropylenimine) discusses PMPI. This material was also synthesized by Lieyu Hu. Hydrogen bonding was eliminated through Eschweiler-Clark methylation of PPI. It was hoped this would result in increased conductivity. Again, differential scanning calorimmetry, FT-IR spectroscopy and

AC impedance measurements were used to characterize neat PMPI and complexes with lithium triflate. Results were compared against those of the homologous system, PMEI.

In stark contrast to PPI, PMPI is a highly viscous, dark amber fluid. In this regard it is very similar to PMEI. Spectral differences exist between PMEI and PMPI however, particularly in the backbone region. These distinctions are heightened with addition of even moderate amounts of LiTf. These spectral data, when combined with differential scanning calorimmetry data, indicate that the differences are likely caused by local environmental differences arising from variations in the nature of polymer-salt interactions in two systems. IR data suggest that ionic association in PMPI:LiTf electrolytes is highly aggregated even at low salt concentration, while PMEI:LiTf complexes exhibit significant higher order association only at higher salt concentration. The additional flexibility provided by the third backbone carbon may be the source the differences in cation-polymer interaction. While the spectra of neat PMPI shows evidence of kinetic effects of heating, PMPI:LiTf complexes show virtually no temperature dependence, most especially no change in ionic association. This suggests that the PMPI:LiTf salt complex is in a thermodynamically stable amorphous configuration between 25 ºC and 80 ºC. Ionic conductivity is poor at room temperature (10^{-9} and 10^{-8} Scm^{-1}) and increases steadily up to 80ºC (10^{-5} Scm^{-1}) further indicating a lack any significant long range structural changes in the systems. This conductivity is low for a polymer electrolyte and renders the PMPI:LiTf system unsuitable for battery applications.

Chapter 5: Model Compounds for PEI and PPI discusses the use of N,N'-dimethylethylenediamine (N,N'-DMEDA) and N,N'-dimethylpropylenediamine (N,N'-DMPDA) to model the hydrogen bonding interactions in the polymers poly(ethylenimine) and poly(propylenimine). Initially conceived of as a way to recognize and assign the IR and Raman bands resulting from various NH stretching species, the work expanded to include other spectral regions, as well as some preliminary density functional theory computations. The model compounds and their LiTf complexes were diluted in carbon tetrachloride to eliminate significant hydrogen bonding interactions. This resulted in the identification of six different NH species: non-hydrogen bonded NH, intermolecularly hydrogen bonded NH, singly intramolecularly hydrogen bonded NH, n-mer type hydrogen bonded NH, doubly intramolecularly hydrogen bonded NH, and Li^+ coordinated NH.

Intermolecular and intramolecular hydrogen bonding are present in both N,N'-DMEDA and N,N'-DMPDA. Intermolecular interactions are predominant in N,N'-DMEDA, while intramolecular interactions are more prevalent in N,N'-DMPDA. This may be due to the additional backbone carbon allowing a wider range of molecular conformations (including a pseudo-six-membered ring) as compared to N,N'-DMEDA. In both systems, the vast majority of the of the intermolecular hydrogen bonding is disrupted with the addition of CCl_4, but the intramolecular hydrogen bonding is, for the most part, unchanged by the CCl_4. Addition of lithium triflate to the compounds results in cation coordination to the nitrogen atoms and partial disruption of all types of hydrogen bonding interactions,

depending on salt concentration. Spectral data indicate that multiple types of hydrogen bonding are present in the compound:salt complexes of N,N'-DMEDA, but the salt associated NH species is virtually the only species present in N,N'-DMPDA:LiTf complexes. In general, the N,N'-DMPDA system is more highly aggregated than the N,N'-DMEDA system. Dilution of both complexes in CCl_4 results in higher degrees of anion association and dramatic reduction of cation interaction with the nitrogen atoms. This appears to be due to a collapse of a network involving cation, anion and polymer interactions which happens at a higher level of dilution in N,N'-DMPDA than in N,N'-DMEDA.

Chapter 6: The G Series contains a summary of some very preliminary work with model compounds for polymers based on N-2-methoxyethylamine. The results presented here are far from a complete characterization of the system. They are addressed out of an attachment to the systems. This, my first project at OU, was plagued with issues including the seeming creation of water from nothing. A "short" break to run some PPI spectra for Leiyu Hu turned into Chapters 3-5 and a four year hiatus from the G-Series materials and their infuriating affinity for water. Matt Meredith's work measuring the conductivity of the model compounds brought the materials back into my sphere. Alas, my remaining time was not sufficient for a complete characterization.

This is a family of exciting and promising compounds containing both oxygen and nitrogen heteroatoms. The compounds are capable of dissolving ludicrous amounts of LiTf (upwards of 1:1 heteroatom:Li^+ mole ratio). Ionic

association is heavily dependent on salt concentration and ranges from “free” ions at low salt concentrations to triple ions at high salt concentrations.

It is hoped the reader will find something of value in this summary of the last seven years of my academic life. This is indeed my year of Julibee!

1.6 REFERENCES

(1) Jeffery, G. A. *An Introduction to Hydrogen Bonding*; 1st ed.; Oxford Unviersity Press: New York 1997.

(2) Seneviratne, V. Doctoral Dissertation, University of Oklahoma, 2004.

(3) Jacobi, W. In *Battery Technology Handbook*; 2nd Ed. ed.; Kiehne, H. A., Ed.; Marcel-Dekker, Inc. : New York, 2003.

(4) *US Industry Forecasts for 2012 & 2017: Batteries*, The Freedonia Group, 2009.

(5) *Advanced Storage Battery Market: from Hybrid/Electric Vehicles to Cell Phones*, SBI 2009.

(6) Bulkeley, B. In *Wall Street Journal*; 28 Oct 2008 ed.; Dow Jones & Company of News Corporation: New York 2008.

(7) Curtiss, E.; Eustis, S. *Worldwide Nanotechnology Thin Film Lithium-Ion Battery Market Shares, Strategies and Forecasts 2009-2015*, WinterGreen Research Inc. , 2009.

(8) *World Batteries: Industry Study with Forecasts for 2012 & 2017*, The Freedonia Group, 2008.

(9) Daniel, C. *JOM* **2008**, *60*, 43-48.

(10) Tarascon, J. M.; Armand, M. *Nature (London, United Kingdom)* **2001**, *414*, 359-367.

(11) Shulka, A. K.; Kumar, T. P. *Current Science* **2008**, *94*, 314-331.

(12) Vincent, C. A. *Solid State Ionics* **2000**, *134*, 159-167.

(13) Erlich, G. M. In *Handbook of Batteries, 3rd Edition*; Linden, D., Reddy, T. B., Eds.; McGraw-Hill: New York, 2002.

(14) Jacobi, W. In *Battery Technology Handbook*; 2nd ed.; Kiehne, H. A., Ed.; Marcel Dekker: New York, 2003, p 401-466.

(15) Arora, P.; Zhang, Z. *Chem. Rev.* **2004**, *104*, 4419-4462.

(16) Zhang, W.; Jiang, J.; Qin, C.; Perez, L. M.; Parrish, A. R.; Safe, S. H.; Simanek, E. E. *Supramol. Chem.* **2003**, *15*, 607-616.

(17) Gray, F. M. *Solid Polymer Electrolytes: Fundamentals and Technological Applications*; 1st ed.; VCH Publishers Inc.: New York, 1991.

(18) MacFarlane, D. R.; Forsyth, M. *Chem. Aust.* **1996**, 72-74

(19) Armand, M. B.; Chabagno, J. M.; Duclot, M. J. In *Fast Ion transport in Solids - Electrodes and Electrolytes*; Vashishta, P., Mundy, J. N., Shenoy, G. K., Eds.; North-Holland: New York, 1979, p 131-136.

(20) Fenton, D. E.; Parker, J. M.; Wright, P. V. *Polymer* **1973**, *14*, 589-589.

(21) Wright, P. V. *British Polymer Journal* **1975**, *7*, 319-327.

(22) Armand, M. B. *Solid State Ionics* **1994**, *69*, 309-319.

(23) Meyer, W. H. *Adv. Mater.* **1998**, *10*, 439-448.

(24) Schantz, S.; Sandahl, J.; Borjesson, L.; Torell, L. M.; Stevens, J. R. *Solid State Ionics* **1988**, *28-30*, 1047-53.

(25) Rhodes, C. P.; Khan, M.; Frech, R. *J. Phys. Chem. B* **2002**, *106*, 10330-10337.

(26) Rhodes, C. P.; Frech, R. *Macromolecules* **2001**, *34*, 2660-2666.

(27) Isaac, A.; Peter, B. *Philos. Mag. A* **1991**, *64*, 1113-1118.

(28) Anantha, P. S.; Hariharan, K. *Solid State Ionics* **2004**, *176*, 155-162.

(29) Ansari, S. M.; Brodwin, M.; Stainer, M.; Druger, S. D.; Ratner, M. A.; Shriver, D. F. *Solid State Ionics* **1985**, *17*, 101-106.

(30) Berthier, C.; Gorecki, W.; Minier, M.; Armand, M. B.; Chabagno, J. M.; Rigaud, P. *Solid State Ionics* **1983**, *11*, 91-5.

(31) Bhattacharja, S.; Smoot, S. W.; Whitmore, D. H. *Solid State Ionics* **1986**, *18-19*, 306-314.

(32) Caruso, T.; Capoleoni, S.; Cazzanelli, E.; Agostino, R. G.; Villano, P.; Passerini, S. *Ionics* **2002**, *8*, 36.

(33) Chintapalli, S.; Frech, R. *Electrochim. Acta* **1995**, *40*, 2093-2099.

(34) *Polymer Electrolyte Reviews 1*; 1st ed.; MacCallum, J. R.; Vincent, C., Eds.; Elsevier Applied Science: New York, 1987; Vol. 1.

(35) Ferry, A. *J. Phys. Chem. B* **1997**, *101*, 150-157.

(36) Frech, R.; Chintapalli, S.; Bruce, P. G.; Vincent, C. A. *Macromolecules* **1999**, *32*, 808-813.

(37) Frech, R.; Huang, W. *Solid State Ionics* **1994**, *72*, 103-7.

(38) Huang, W.; Frech, R. *Polymer* **1994**, *35*, 235-42.

(39) Johansson, P.; Tegenfeldt, J.; Lindgren, J. *J. Phys. Chem. B* **1998**, *102*, 4660-4665.

(40) Papke, B. L.; Ratner, M. A.; Shriver, D. F. *J. Electrochem. Soc.* **1982**, *129*, 1434-8.

(41) Petersen, G.; Jacobsson, P.; Torell, L. M. *Electrochim. Acta* **1992**, *37*, 1495-1497.

(42) Weston, J. E.; Steele, B. C. H. *Solid State Ionics* **1981**, *2*, 347-354.

(43) Shriver, D. F.; Papke, B. L.; Ratner, M. A.; Dupon, R.; Wong, T.; Brodwin, M. *Solid State Ionics* **1981**, *5*, 83-88.

(44) Hubbard, H. V. S. A.; Southall, J. P.; Cruickshank, J. M.; Davies, G. R.; Ward, I. M. *Electrochim. Acta* **1998**, *43*, 1485-1492.

(45) Ikeda, Y.; Wada, Y.; Matoba, Y.; Murakami, S.; Kohjiya, S. *Electrochim. Acta* **2000**, *45*, 1167-1174.

(46) Allcock, H. R.; Napierala, M. E.; Olmeijer, D. L.; Cameron, C. G.; Kuharcik, S. E.; Reed, C. S.; O'Connor, S. J. M. *Electrochim. Acta* **1998**, *43*, 1145-1150.

(47) Dupon, R.; Papke, B. L.; Ratner, M. A.; Shriver, D. F. *J. Electrochem. Soc.* **1984**, *131*, 586-9.

(48) Lee, Y.-C.; Ratner, M. A.; Shriver, D. F. *Solid State Ionics* **2001**, *138*, 273-276.

(49) Watanabe, M.; Nagano, S.; Sanui, K.; Ogata, N. *Solid State Ionics* **1986**, *18-19*, 338-342.

(50) Killis, A.; Le Nest, J. F.; Gandini, A.; Cheradame, H. *Macromolecules* **2002**, *17*, 63-66.

(51) Callens, S.; Le Nest, J. F.; Gandini, A.; Armand, M. *Polym. Bull.* **1991**, *25*, 443-450.

(52) Reiche, A.; Steurich, T.; Sandner, B.; Lobitz, P.; Fleischer, G. *Electrochim. Acta* **1995**, *40*, 2153-2157.

(53) Prasad, P. S. S.; Munshi, M. Z. A.; Owens, B. B.; Smyrl, W. H. *Solid State Ionics* **1990**, *40-41*, 959-963.

(54) Kono, M.; Nishiura, M.; Ishiko, E.; Sada, T. *Electrochim. Acta* **2000**, *45*, 1307-1312.

(55) Yang, L.; Lin, J.; Wang, Z.; Wang, C.; Zhou, R.; Liu, Q. *Solid State Ionics* **1990**, *40-41*, 616-619.

(56) MacFarlane, D. R.; Sun, J.; Meakin, P.; Fasoulopoulos, P.; Hey, J.; Forsyth, M. *Electrochim. Acta* **1995**, *40*, 2131-2136.

(57) Banara, L. R. A. K.; Dissanayake, M. A. K. L.; Mellander, B. E. *Electrochim. Acta* **1998**, *43*, 1447-1451.

(58) Wieczorek, W.; Florjanczyk, Z.; Stevens, J. R. *Electrochim. Acta* **1995**, *40*, 2251-2258.

(59) Capuano, F.; Croce, F.; Scrosati, B. *J. Electrochem. Soc.* **1991**, *138*, 1918-1922.

(60) Weston, J. E.; Steele, B. C. H. *Solid State Ionics* **1982**, *7*, 75-79.

(61) Kumar, B.; Scanlon, L.; Marsh, R.; Mason, R.; Higgins, R.; Baldwin, R. *Electrochim. Acta* **2001**, *46*, 1515-1521.

(62) Tanaka, R.; Sakurai, M.; Sekiguchi, H.; Mori, H.; Murayama, T.; Ooyama, T. *Electrochim. Acta* **2001**, *46*, 1709-1715.

(63) Andrieu, X.; Fauvarque, J. F.; Goux, A.; Hamaide, T.; M'Hamdi, R.; Vicedo, T. *Electrochim. Acta* **1995**, *40*, 2295-2299.

(64) Saunier, J.; Alloin, F.; Sanchez, J. Y. *Electrochim. Acta* **2000**, *45*, 1255-1263.

(65) Tsuchida, E.; Ohno, H.; Tsunemi, K.; Kobayashi, N. *Solid State Ionics* **1983**, *11*, 227-233.

(66) Forsyth, M.; MacFarlane, D. R.; Hill, A. J. *Electrochim. Acta* **2000**, *45*, 1243-1247.

(67) Karatas, Y.; Pyckhout-Hintzen, W.; Zorn, R.; Richter, D.; Wiemhoefer, H. D. *Macromolecules (Washington, DC, United States)* **2008**, *41*, 2212-2218.

(68) Blonsky, P. M.; Shriver, D. F.; Austin, P.; Allcock, H. R. *Solid State Ionics* **1986**, *18-19*, 258-264.

(69) Albinsson, I.; Mellander, B. E.; Stevens, J. R. *Polymer* **1991**, *32*, 2712-2715.

(70) Cowie, J. M. G.; Sadaghianizadeh, K. *Solid State Ionics* **1990**, *42*, 243-249.

(71) Sun, J.; Macfarlane, D. R.; Forsyth, M. *Electrochim. Acta* **1995**, *40*, 2301-2304.

(72) Huq, R.; Koksbang, R.; Tonder, P. E.; Farrington, G. C. *Electrochim. Acta* **1992**, *37*, 1681-1684.

(73) Lee, K.-H.; Park, J.-K.; Kim, W.-J. *Electrochemica Acta* **2000**, *45*, 1301-1306.

(74) Gozdz, A. S.; Schmutz, C. N.; Tarascon, J.-M.; Bell Communications Research, Inc.: United States, 1994.

(75) Chatani, Y.; Kobatake, T.; Tadokoro, H.; Tanaka, R. *Macromolecules* **1982**, *15*, 6.

(76) Harris, C. S.; Shriver, D. F.; Ratner, M. A. *Macromolecules* **1986**, *19*, 987-9.

(77) York, S.; Frech, R.; Snow, A.; Glatzhofer, D. *Electrochim. Acta* **2001**, *46*, 1533-1537.

(78) Chiang, C. K.; Davis, G. T.; Harding, C. A.; Takahashi, T. *Macromolecules* **1985**, *18*, 825-7.

(79) Kobayashi, S.; Shirasaka, H.; Kyung-Do, S.; Uyama, H. *Polym. J.* **1990**, *22*, 442-446.

(80) Chiang, C. K.; Davis, G. T.; Harding, C. A.; Takahashi, T. *Solid State Ionics* **1986**, *18-19*, 300-5.

(81) Tanaka, R.; Fujita, T.; Nishibayashi, H.; Saito, S. *Solid State Ionics* **1993**, *60*, 119-23.

(82) York, S. S.; Buckner, M.; Frech, R. *Macromolecules* **2004**, *37*, 994-999.

(83) Buckner, M.; York, S. S.; Frech, R.; Glatzhofer, D. T. *Polym. Prepr.* **2003**, *44*, 1085.

(84) Harris, C. S.; Ratner, M. A.; Shriver, D. F. *Macromolecules* **1987**, *20*, 1778-1781.

(85) Erickson, M. J.; Frech, R.; Glatzhofer, D. T. *Polymer* **2004**, *45*, 3389-3397.

(86) Ren, Z.; Sun, K.; Liu, Y.; Zhou, X.; Zhang, N.; Zhu, X. *Solid State Ionics* **2009**, *180*, 693-697.

(87) Takahashi, T.; Davis, G. T.; Chiang, C. K.; Harding, C. A. *Solid State Ionics* **1986**, *18-19*, 321-325.

(88) Ionescu-Vasii, L. L.; Garcia, B.; Armand, M. *Solid State Ionics* **2006**, *177*, 885-892.

(89) Harris, C. S.; Ratner, M. A.; Shriver, D. F. *Macromolecules* **2002**, *20*, 1778-1781.

(90) Sanders, R. A.; Snow, A. G.; Frech, R.; Glatzhofer, D. T. *Electrochim. Acta* **2003**, *48*, 2247-2253.

(91) Frech, R.; Giffin, G. A.; Castillo, F. Y.; Glatzhofer, D. T.; Eisenblaetter, J. *Electrochim. Acta* **2005**, *50*, 3963-3968.

(92) Lee, J.; Lee, K.; Kim, H. *Bull. Korean Chem. Soc.* **1996**, *17*, 115-16.

(93) Borkovec, M.; Koper, G. J. M. *Prog. Colloid Polym. Sci.* **1998**, *109*.

(94) Bruce, P. G. *Solid State Electrochemistry*; 1st ed.; Cambridge University Press: New York, 1995.

(95) Huang, W.; Frech, R.; Wheeler, R. A. *J. Phys. Chem.* **1994**, *98*, 100-10.

(96) Ferry, A.; Oradd, G.; Jacobsson, P. *J. Chem. Phys.* **1998**, *108*, 7426.

(97) Frech, R. *Macromolecules* **2000**, *33*, 9342-9436.

(98) Frech, R.; Chintapalli, S.; Bruce, P. G.; Vincent, C. A. *Chem. Commun. (Cambridge)* **1997**, 157-158.

(99) Huang, W.; Frech, R.; Johansson, P.; Lindgren, J. *Electrochim. Acta* **1995**, *40*, 2147-2151.

(100) Sanders, R. A.; Boesch, S. E.; Snow, A. G.; Hu, L.; Frech, R.; Wheeler, R. A.; Glatzhofer, D. T. *Polym. Prepr. (Am. Chem. Soc., Div. Polym. Chem.)* **2003**, *44*, 966-967.

(101) York, S. S.; Boesch, S. E.; Wheeler, R. A.; Frech, R. *Macromolecules* **2003**, *36*, 7348-51.

(102) Boesch, S. E.; York, S. S.; Frech, R.; Wheeler, R. A. *PhysChemComm* **2000**, *1*, 1.

(103) Rocher, N. M.; Frech, R. *Macromolecules* **2005**, *38*, 10561-10565.

(104) Rocher, N. M.; Frech, R.; Khan, M. *J. Phys. Chem. B* **2005**, *109*, 20697-20706.

CHAPTER 2: EXPERIMENTAL METHODS

In science it is not enough to think of an important problem on which to work. It is also necessary to know the means which could be used to investigate the problem.

-- *Leo Szilard*[1]

2.1 NEAT MATERIALS

All materials were used and stored in an inert atmosphere glovebox maintained at less than 1 ppm water and 10 ppm oxygen, unless otherwise noted. The glovebox was under an argon atmosphere for the duration of the polymer experiments and under a nitrogen atmosphere during the work with the amine model compounds. Investigation of the mixed heteroatom systems occurred in both argon and nitrogen atmospheres.

2.1.1 Polymers

2.1.1.1 Polypropylenimine (PPI)

All the linear poly(propylenimine) used in the work was synthesized by Lieyu Hu. Initially, a one pot reaction of 3-amino-1-propanol and propionitrile was used to create the 2-ethyl-5,6-dihydro-4-H-1,3-oxazine monomer, which underwent a cationic opening polymerization to produce linear poly(2-ethyl-5,6-dihydro-4-H-1,3-oxazine). This material was hydrolyzed to obtain the linear PPI. Details of the synthesis may be found in other publications[2,3].

The PPI is a light yellow solid, which is fairly brittle and highly crystalline. The molecular weight of the synthesized PPI was calculated to be ~3000 g/mol, which gives an average degree of polymerization of about 53 repeat units per chain. DSC data indicate a melting point of 60.5^{o}C. The material was dried under vacuum for 24 hours at 50^{o}C followed by 48 hours at 65^{o}C to ensure the absence of water. However, unlike poly(ethylenimine), PEI, which is extremely hygroscopic, PPI appears to exclude water, with the as-synthesized sample being just as dry as the sample which underwent the drying process.

2.1.1.2 Poly(N-methylpropylenimine) (PMPI)

Like the PPI, all the linear poly(N-methylpropylenimine) employed in this investigation was synthesized by Lieyu Hu. PMPI was obtained through the Eschweiler-Clarke methylation of the PPI, which requires the formation of the ammonium chloride salt followed by neutralization via ion exchange. A more detailed description of the synthesis is given in previous publications.[3,4] The process yielded a pale yellow material that was highly viscous and appeared visually similar to honey. The molecular weight was estimated to be approximately 3700 g/mol and displayed a DSC determined glass transition temperature of -88^{o}C.

2.1.2 Amine Model Compounds

N,N'-dimethylethylenediamine (99%) (N,N'-DMEDA) was purchased from Sigma-Aldrich. N,N'-dimethylpropylenediamine (N,N'DMPDA) was purchased from TCI (99%) and Aldrich (97%). The materials were analyzed for water via IR

by looking at the OH stretch in the 3300 cm^{-1} region and distilled if needed; otherwise they were used as received.

2.1.3 Mixed Heteroatom Model Compounds

N,N-dimethyl-(2-methoxyethyl)amine (G1MC) was synthesized by Matthew Meredith using the Eishwieler-Clarke methylation of 2-methoxyethylamine by formaldehyde in formic acid[5]. The product was purified by distillation over sodium carbonate, followed by distillation over sodium metal, and was stored over molecular sieves in the glovebox. G1MC is an amber liquid with a viscosity comparable to water. The material is capable of dissolving a large molecular equivalent of lithium trifluoromethanesulfonate, LiTf, (upwards of 1 mole of LiTf for each mole of G1MC).

Likewise, N,N'-dimethyl-(2-(2-methoxyethoxy)ethyl)amine (G2MC) was synthesized by Lieyu Hu using the Eschwieler-Clarke methylation of methoxy-ethoxyethylamine with formaldehyde in formic acid[5]. This material was purified by distillation over sodium carbonate and stored over molecular sieves. G2MC is a thick dark amber liquid of medium viscosity (thick molasses) able to solvate LiTf in concentrations greater than 2 moles of LiTf to each 1 mole of G2MC.

2.1.4 Salts

Lithium trifluoromethanesulfonate (LiTf) (99.995%), sodium trifluoromethanesulfonate (NaTf) (98%), lithium tetrafluoroborate ($LiBF_4$)

(99.999%) and tetrabutylammonium trifluoromethanesulfonate (TBATf) (≥99.9%) were purchased from Aldrich. LiTf and NaTf were dried for 96 hours at 120°C under vacuum of 20-25 mm Hg. $LiBF_4$ and TBATf were used as received. All salts were tested for water with via IR as potassium bromide (puriss or FT-IR grade Aldrich) pellets.

2.1.5 Solvents

Methanol (Fisher 99.99%) was distilled over sodium metal prior to use. Carbon tetrachloride, CCl_4, (ACS 99.9%) was purchased from Aldrich and distilled as needed to obtain dryness before being placed over molecular sieves. All solvents were maintained in an inert atmosphere glovebox.

2.2 SOLUTION PREPARATION

2.2.1 Polymer Electrolytes

Salt concentrations are given as mole ratios of nitrogen to cation (i.e. $N:Li^+$ or $N:Na^+$). PEI and PPI electrolytes were prepared by dissolving the required mass of polymer in anhydrous methanol prior to salt addition. PMEI and PMPI were viscous liquids, consequently salts could be added directly to the materials without the use of a co-solvent. In either case, after the desired mass of salt was added, the sample was stirred with a magnetic stirring bar for a minimum of 24 hours before being cast for the specific uses described below in 2.3. Several samples of PMPI electrolytes were prepared using methanol as a co-solvent. There were no visually or spectrally

observable differences between the PMPI films cast with methanol as a co-solvent and those cast without the methanol. Electrolyte solutions of PEI and PPI were colorless to pale yellow with viscosity dependent on the volume of MeOH present and the salt concentration, with the higher salt concentrations being more viscous. PMEI electrolytes ranged from dark amber goos to dark amber gels, while PMPI electrolytes varied from dark amber fluids to dark amber tacky gels. All polymer electrolyte preparation occurred in the room temperature argon atmosphere glovebox.

2.2.2 Model Compounds

Salt solutions of model compounds were prepared by adding the desired mass of salt to the desired mass of model compound. Solutions were magnetically stirred for a minimum of 24 hours before use. G1MC and G2MC electrolyte solutions were amber fluids ranging in viscosity from water to thick molasses. Even at high salt concentrations, G1MC materials flowed. Concentrations are expressed as ratios of moles of heteroatom to moles of cation counting both oxygen and nitrogen as heteroatoms. N,N'-DMEDA and N,N'-DMPDA electrolyte solutions were colorless clear liquids with less variation in viscosity over the range of 20:1 to 3:1 than seen in the G1MC and G2MC. Concentrations for N,N'-DMEDA and N,N'-DMPDA are given as the mole ratio of nitrogen to cation ($N:Li^+$).

2.2.3 CCl_4 Dilutions

Solutions of N,N'-DMEDA and N,N'-DMPDA with carbon tetrachloride were prepared by adding the required mass of CCl_4 to the desired mass of previously prepared model compound-salt solution. The mixture was then sealed in a glass vial and manually agitated for two minutes before use. Solutions were colorless, clear liquids with the viscosity dependent on the CCl_4 concentration. After standing for several days, some amber color became apparent. This was of minimal concern as sample analysis was completed within a few hours of preparation. No samples had any visible changes within the analysis timeframe. Concentration of these samples are given as carbon to nitrogen mole ratios (C:N) and nitrogen to cation mole ratios ($N:Li^+$).

2.3 SAMPLE PREPARATION

2.3.1 Fourier Transform Infrared Spectroscopy (FTIR)

Solid polymer and polymer electrolyte samples for IR analysis were cast from solution directly onto 25 mm zinc selenide windows in an argon atmosphere glovebox, where they dried for a minimum of 24 hours at room temperature. If a co-solvent was used in the electrolyte solution preparation, the samples underwent an additional 12-24 hours drying under reduced pressure (20-25 mbar) to ensure solvent removal. The supporting window was placed into a Harrick temperature controlled liquid cell holder with the sample up. A second zinc selenide window was placed on

top of this, sandwiching the sample between the two windows, before the holder top piece was screwed into place.

Liquid polymers, G1MC and G2MC and the salt solutions of these materials were placed dropwise onto zinc selenide windows in a Wilmad demountable FT-IR liquid cell. A second zinc selenide window was placed on top of this, and the holder top screwed into place. Occasionally, fringing in the resulting spectrum necessitated the placement of a small sliver of Teflon between the windows to avoid the windows being exactly parallel. Cell loading was performed in an inert (nitrogen or argon) atmosphere glovebox.

Amine model compounds (N,N'-DMEDA and N,N'-DMPDA) were transferred via injection from a Luer-lock syringe into the Wilmad cell. The cell consisted of two 25 mm zinc selenide windows with a Teflon spacer of 0.05, 0.10 or 0.15 mm thickness. This cell was useful for samples with viscosities on the order of water or higher and low vapor pressures. However, it was not possible to form sufficiently tight seals to use this cell with materials of high vapor pressures, such as CCl_4.

N,N'-DMEDA and N,N'-DMPDA salts solution in CCl_4 dilutions were placed in one of two potassium bromide cell configurations. Initially a 16 x 8 mm sealed cell of undetermined pathlength (vendor unknown) was used. Later samples were run in a New Era demountable amalgamated dispersive liquid cell consisting of two potassium bromide windows separated by 0.05 mm or 0.10 mm lead spacers. The switch to the New Era cell was necessitated by the fouling of two of the sealed

cells. Both cells were filled via Luer-lock syringe in a nitrogen atmosphere glovebox.

Solid samples were ground in an inert atmosphere (either argon or nitrogen) glovebox with potassium bromide (approximately 100:1 KBr:Sample) and pressed at 12 tons for five to ten minutes in a stainless steel dye with a diameter of one centimeter. Prior to use, the dye was dried for a minimum of 24 hours at 125^{o}C. Pressing was performed in ambient environment. Samples did not appear to gain an appreciable amount of water during pressing.

2.3.2 Fourier Transform Raman Spectroscopy

Polymer and polymer electrolyte samples for Raman spectroscopic analysis were cast from solution directly onto small store-bought craft quality mirrors approximately 2 cm by 2 cm. Samples were dried at room temperature in an argon atmosphere glovebox for a minimum of 24 hours before being further dried in a room temperature vacuum oven at 20-25 inch Hg, to ensure solvent removal.

Liquid samples were sealed in a clean, dry Raman tube in the inert atmosphere glovebox. Tubes were covered with plastic NMR tube caps and wrapped with dried Parafilm®. Raman tubes were prepared from thin wall 5 mm by 20 mm quartz glass NMR tubes cut into thirds, with one end closed by fire polishing. Tubes were stored in an oven at 125^{o}C for a minimum of 48 hours before being moved to the glovebox.

2.3.3 Differential Scanning Calorimetry

Polymer electrolyte samples were cast from solution directly into 40 μl aluminum pans inside the room temperature glovebox. Samples were allowed to evaporate 12-24 hours, before more solution was added to the pan. This process was continued, until the pan was half to three quarters filled with solid polymer electrolyte. Following the final the evaporation, pans were transferred to a room temperature vacuum oven for an additional 24 hours at 20-25 inches Hg. Sealing of the pans was performed in the glovebox.

Liquid samples were placed in the 40 μl aluminum pans and sealed in the inert atmosphere glovebox.

2.3.4 AC Complex Impedance

Polymer electrolyte samples were cast from solution onto a 12.5 mm diameter stainless steel disk mounted in a ceramic insulating block. They were allowed to evaporate at room temperature in an argon atmosphere glovebox for a minimum of 24 hours before being transferred to a room temperature vacuum oven at 20-25 in Hg for another 12-24 hours. A second stainless steel disk in a ceramic insulator was placed on top of the sample and compressed slightly with a micrometer to ensure uniform contact. The entire airtight assembly was removed to an oven fitted with a nitrogen purge.

Liquid samples were placed via fine gauge syringe into a length of Teflon® tubing (ID=0.5 cm) fitted with 0.6 cm diameter stainless steel electrodes separated

by 1 cm. As the liquid samples were injected, displaced air in the tube was removed by a second syringe, until the liquid sample entered the second syringe's body. This allowed the tube space to be completely filled. If the process was performed sufficiently slowly, no air bubbles were visible in the tube or on the electrodes. The cell constant was calculated from conductivity data of 0.1 demal potassium chloride solutions.

2.4 INSTRUMENTATION AND METHODS

2.4.1 Fourier Transform Infrared Spectroscopy

Infrared spectra were recorded with a Bruker IFS66V Fourier Transform-Infrared (FT-IR) spectrometer with a potassium bromide beamsplitter at a resolution of 1 cm^{-1} over the range 500-4000 cm^{-1}. Generally, 64 scans were averaged. Solid samples were evaluated between zinc selenide windows as described in Section 2.3.1 under a reduced pressure of 12-15 mbar. Liquid samples were tested with either zinc selenide or potassium bromide windows as described in Section 2.3.1 under a dry air purge. A purge time of 300 seconds elapsed before data collection. Temperature dependent data was collected in 10^{o}C increments over the range of 20-80^{o}C. The Harrick temperature controlled cell was heated via resistance heaters with the input voltage to the heaters varied by an Omega CN9000A PID controller. Samples were held at constant temperature for one hour after the target temperature was reached, before data were collected.

Analysis of spectral data was performed with commercially available software Thermo Galactic Grams 3.2 version 7.0. Spectra were fitted using the least squares method, utilizing a straight baseline and a mixed Gaussian-Lorenzian product function for each band.

2.4.2 Fourier Transform Raman Spectroscopy

Raman spectra were recorded with a Bruker system comprised of an Equinox 55 and FRA 106/S Raman Module with a liquid nitrogen cooled germanium detector. Spectra were collected using a quartz beamsplitter. Excitation was provided by the 1064 cm^{-1} line of a Nd:YAG laser. Depending on the system to be studied, 1000 or 5000 scans were apodized. Samples with lower salt concentrations or those with high CCl_4 dilution were re-run at 5000 scans, if the spectrum resulting from 1000 scans was too noisy to allow adequate fitting of the band of interest.

Polymer samples were run in 180^o backscattering arrangement on commercially available non-optical grade mirrors as described in Section 2.3.1. Liquid samples, prepared as described in Section 2.3.2, were run in quartz glass Raman sample tubes prepared as previous described. An optical mirror was placed behind the sample to create an 180^o backscattering configuration.

As with the FT-IR spectra, analysis of Raman spectra was accomplished with Thermo Galactic's Grams 3.2 version 7.0 using a least squares method to fit a mixed Gaussian-Lorenzian product function from a straight baseline for each band.

2.4.3 Differential Scanning Calorimetry

Differential Scanning Calorimetry (DSC) thermograms were obtained using a Mettler Toledo DSC 820. Samples were sealed in 40 μl aluminum pans and placed under nitrogen flow of 87 ml/min. An identical empty pan was used a reference.

PEI and PPI samples, both neat and those with dissolved salt, were cycled three times from 0^oC to 100^oC at a heating/cooling rate of either 2 or 5^oC per minute. One cycle is defined as 0^oC to 100^oC to 0^oC. Prior to the initial heating/cooling cycle, the control profile brought the sample from room temperature to 100^oC at the same rate that the cycling was to be executed. At the conclusion of the third cycle, the sample was brought to 25^oC before removal from the sample chamber.

Analysis of the data was performed using software from Mettler Toledo ($STAR^e$ version 6.10 or version 9.10). Glass transition temperatures (T_g) for each cycle were calculated by the software, from the inflection tangent and the half step height, between the onset and endpoint as defined by intersections of the inflection tangent, and the baseline before and after transition, respectively. T_g data from the first cycle was ignored due to the inability to consistently load the materials with homogenous pan contact. After the first cycle, the materials were uniformly distributed within the pan. Glass transition temperatures for the second and third cycle were averaged to obtain the T_g for the sample. Reported data are the averages of at least different two samples.

2.4.3 AC Complex Impedance

Conductivity data were calculated from complex AC impedance measurements performed with a Hewlett-Packard 4192A LF impedance analyzer. The instrument was controlled through an in-house coded Labview 5.1 (National Instruments) interface. Measurements were made over the range of 5 Hz to 10 MHz kHz. Data plotted in the complex impedance form (also called a Nyquist or Cole-Cole plot) were fit using an elliptical function in Origin 7.0 from OriginLab Corporation.

Samples were prepared as described in Section 2.3.4. The thickness of solid samples was determined using the micrometer built into the sample holder. The area of these samples was 122.7 mm^2, as the 12.5 mm diameter of the electrode was completely covered by the sample. The conductivity, formerly specific conductivity, was determined by the formula:

$$\sigma = t/(R \bullet A) \qquad (2.1)$$

where σ is the conductivity in S/cm, t is the sample thickness in cm, R is resistance in ohms and A is the sample area in cm^2.

Variable temperature data for PPI, PMPI, PEI and PMEI electrolytes were obtained over the range of room temperature to 80^oC using the following protocol. After an initial room temperature measurement, the sample was heated from room temperature to 80^oC over about two hours. The sample was held at temperature for one hour, before an 80^oC measurement was conducted. The sample was cooled over approximately four hours and held at room temperature for 1 hour. A room

temperature measurement was taken, and the cycle repeated two times. After reaching room temperature on the last RT-80^{o}C cycle, the temperature was increased back to 80^{o}C in 10^{o}C increments. The sample was maintained at temperature for one hour prior to data collection. The sample was then cooled to room temperature and the 10^{o}C incremental increase repeated to 80^{o}C. This process allowed the reproducibility of the data to be confirmed relatively quickly by comparing the first three room temperature and 80^{o}C readings. If this data were inconsistent, the experiment was stopped and then restarted with a new sample. If the data were consistent, the experiment was continued with the 10^{o}C increment heating for two cycles.

2.5 REFERENCES

(1) Lanouette, W. *Genius in the Shadows: A Biography of Leo Szilard*; 1st ed.; Charles Scribner's Sons: New York, 1992.

(2) Hu, L.; Frech, R.; Glatzhofer, D. T.; Mason, R.; York, S. S. *Solid State Ionics* **2008**, *179*, 401-408.

(3) Hu, L., University of Oklahoma, 2005.

(4) Mason, R. N.; Frech, R.; Hu, L.; Glatzhofer, D. T. *Solid State Ionics*, *(Accepted)*.

(5) Clarke, H. T.; Gillespie, H. B.; Weisshaus, S. Z. *J. Am. Chem. Soc.* **1933**, *55*, 4571-87.

CHAPTER 3: POLY(PROPYLENIMINE)

Glory lies in the attempt to reach one's goal and not in reaching it.

--Mohandas Ghandi[1]

3.1 INTRODUCTION

Linear poly(propyleneimine) (PPI) is a homolog of poly(ethylenimine) (PEI) which varies only by the presence an additional backbone methylene group (see Figure 3-1). Most interest in PPI has stemmed from the potential for PPI-based dendrimers to act as drug delivery systems; therefore, research has focused on conformational changes occurring in various biologically relevant environments.[2&3] In this project, PPI was investigated for its potential application as a polymer electrolyte host for lithium ion batteries. Its chemical and structural similarity to PEI suggests it may be a viable candidate due to its ability to solvate lithium salts and transport cations. This work utilizes lithium trifluoromethanesulfonate (lithium triflate, LiTf), as LiTf is a commonly used salt in experimental polymer electrolyte systems. To that end, Fourier Transform infrared

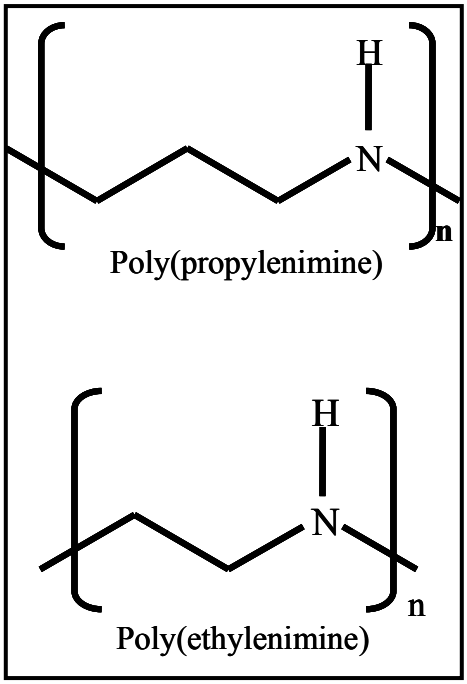

Figure 3-1: Structures of poly(propylenimine) and poly(ethylenimine)

spectroscopy (FT-IR), differential scanning calorimmetry (DSC) and alternating current (AC) complex impedance measurements were made as described in sections 2.3 and 2.4.

The investigation of poly(propylenimine) was part of a joint project between the organic chemistry laboratory of Professor Daniel Glatzhofer and the physical chemistry laboratory of Professor Roger Frech. Synthesis of the polymer was performed by Dr. Lieyu Hu, all analytical samples were prepared by me, but data collection responsibilities were shared equally. The Glatzhofer group performed the initial analysis of DSC data, with later data interpreted by the Frech group, who also held primary responsibility for conductivity and spectroscopic analysis. Due to the collaborative nature of the project, much of this work is also presented in Dr. Hu's dissertation.[4]

3.2 SYNTHESIS AND APPEARANCE

The synthesis of poly(propylenimine) was conducted by Dr. Lieyu Hu. As such, the synthesis is not the focus of this discussion and is therefore described here in brief. A detailed synthetic route is given in Dr. Hu's dissertation[4] and in a journal article.[5]

The precursor monomer, 2-ethyl-5,6-dihydro4-H-1,3-oxazine, was prepared from 3-amino-1-propanol and propionitrile following the protocol of Lee, *et al.*[6] A cationic ring opening polymerization produced the intermediate polymer, poly(ethyloxazine). This polymer was precipitated into diethyl ether and then dried

under reduced pressure before being hydrolyzed with HCl. The resultant polymer, PPI, was dissolved in water and neutralized with NaOH. The solution was filtered to obtain the PPI, which was then dried. This process resulted in PPI of approximately 53 repeat units and having a molecular mass of ~3025 g/mol. The synthetic route is summarized in Scheme 3-2. The PPI formed irregular chunks, approximately pea sized, which were light yellow in color. The material is a highly crystalline solid that is fairly brittle and breaks into large lumps easily. PPI is readily soluble in methanol and appears to exclude water.

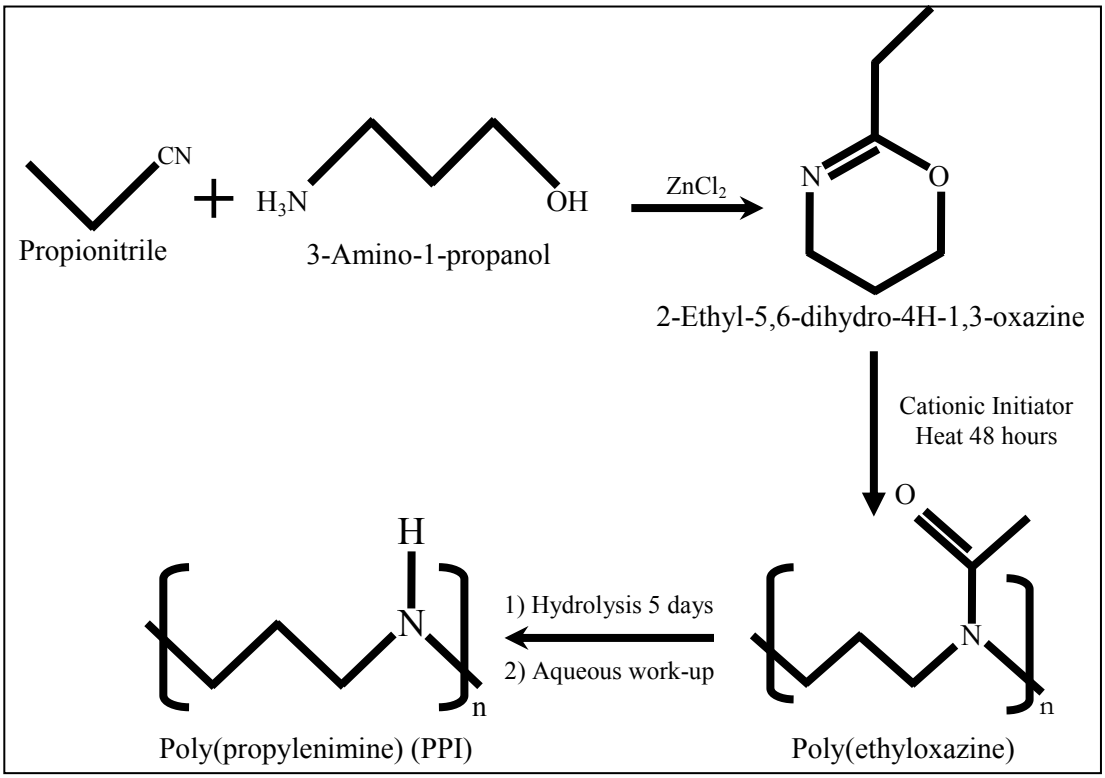

Scheme 3-2: Synthetic route for poly(propylenimine)

3.3 THERMAL ANALYSIS

Melting point (T_m) and glass transition (T_g) temperatures for PPI:LiTf complexes at several compositions ranging from neat PPI to 3:1 N:Li^+ are given in Table 3-1. These transition temperatures were obtained from DSC measurements conducted on samples cast from solutions directly into 40μL aluminum pans and cycled in the DSC from 0°C to 100°C at 2° C/min or 5°C/min. Details of the experiments are described in sections 2.3.3 and 2.4.3.

Table 3-1: Melting Points and Glass Transition of PPI:LiTf Salt Complexes

	T_g Onset (°C)	T_g Midpoint (°C)	T_m Onset (°C)	T_m Peak (°C)	Crystalline: Amorphous Phase Ratio
Neat PPI	---	---	56±4	70±3	1.00
20:1 N:Li^+	-33±3	-26±2	46±1	60±1	0.75
15:1 N:Li^+	-27±3	-22±2	33±6	51±1	0.45
10:1 N:Li^+	-24±7	-18±5	undetermined	undetermined	0.41
5:1 N:Li^+	-27±4	-18±3	---	---	0
3:1 N:Li^+	-31±2	-24±3	---	---	0

Neat PPI has a melting onset of approximately 56°C but exhibits no glass transition, suggesting that it is virtually 100% crystalline. This is similar to PEI, which is also highly crystalline and exhibits a T_m of approximately 65°C for the pure

material. The approximately 10°C difference in T_m may stem from differences in hydrogen bonding interactions. Spectroscopic evidence presented in section 3.4.2 suggests PPI experiences a relatively weaker hydrogen bonding network than PEI. Spectroscopic data also indicate the presence of some amount of non-crystalline domains, even in the neat materials which appear to be 100% crystalline according to the DSC data. This is not surprising as the analysis from DSC experiments provides a macroscopic view of the sample structure while the spectroscopic analysis such as IR provides information on the local environment of the sample. Thus, the crystalline to amorphous ratios given in Table 3.1 should be considered as qualitative comparisons between the various compositions, rather than strict quantitative measurements.

A glass transition temperature appears with the addition of lithium triflate to the polymers. At the lowest salt concentration (20:1 N:Li^+), this new transition, T_g, is seen at -33°C, while the melt transition, originally present at 56° in the pure PPI is reduced by about 10°C. The onset of T_m continues to fall with salt addition until at 5:1 and 3:1 N:Li^+, the level of crystallinity is sufficiently low, so that no T_m is observed. Increasing salt concentration does not significantly raise T_g; even at relatively high LiTf concentrations (3:1 N:Li^+) the complex exhibits a T_g of approximately -31°C, which is similar to the T_g in the 20:1 N:Li^+ sample. A slight increase in T_g at intermediate concentrations is not significant considering the error associated with the measurements. Thus, while addition of salt does not appreciably increase $T_{g,,}$ it does effectively reduce crystallinity of the overall sample. This is in

marked contrast to the behavior of PEI, where salt addition also results in a disordering of the system from a primarily crystalline to amorphous character, but the change is accompanied with a monotonic increase in T_g.[7] This difference in T_g behavior suggests that PEI and PPI experience different interactions with LiTf. This assertion is reflected in the spectral behavior of the two systems as well.

The T_g and T_m reported here vary some from that presented previously by myself and coworkers.[4,5] This variance is due to the availability of additional data, which slightly altered the average values. However, the trends seen remain constant.

3.4 VIBRATIONAL SPECTROSCOPY

3.4.1 OH Stretching

Figure 3.3 shows the FT-IR spectra from 3600 cm^{-1} to 3000 cm^{-1} of neat PPI immediately following synthesis (lower trace) and after drying under vacuum for 24 hours at 50°C then 48 hours at 65°C (upper trace). The lack of any band in the OH stretching region of the spectra indicates that neither vacuum-dried nor as-synthesized PPI contains water. This is of particular interest in terms of potential use as a polymer electrolyte host material, as many SPE systems utilize lithium salts as charge carriers and/or lithium metal based electrodes. In both cases, the presence of water is deleterious to the performance of the battery. PEI is known to be highly hygroscopic and must be extensively dried before use and meticulously stored away from moisture. However, PPI appears to behave in the opposite manner, with its crystalline structure excluding water. Naturally, the addition of lithium salts

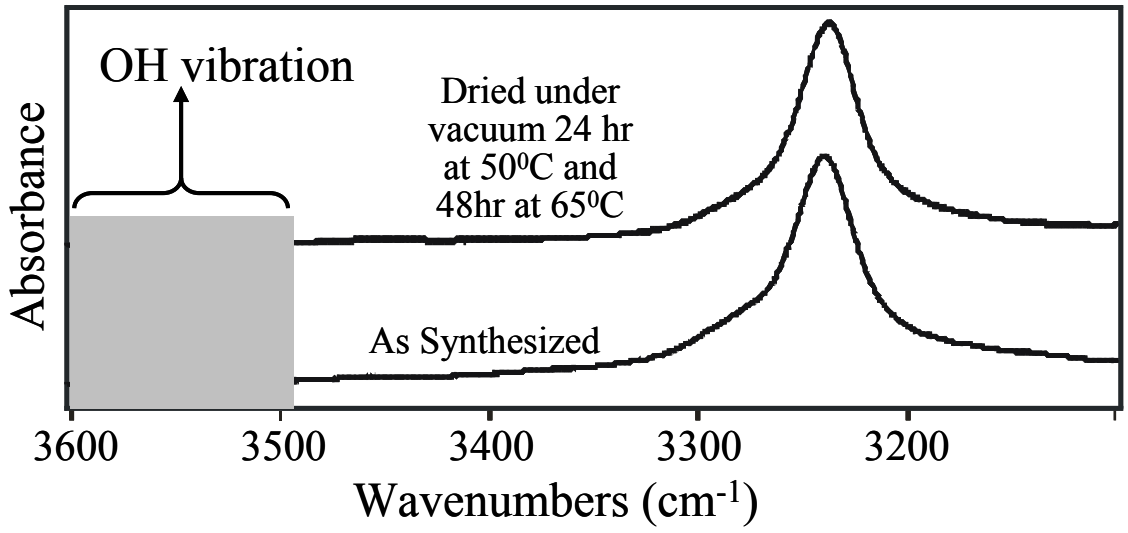

Figure 3-3: OH stretching region of the IR spectra of the as-synthesized and thoroughly dried neat PPI

increases the susceptibility of the polymer:salt complex to water absorption, but this appears to be a factor of the salt's hygroscopic nature rather than a property of the PPI polymer.

3.4.2 NH Stretching

3.4.2.1 Neat Material

The spectra of pure PEI and pure PPI in the NH stretching region (~3000-3500 cm^{-1}) are similar, with both materials having a relatively sharp band with a less intense broad shoulder centered at a higher frequency. As shown in Figure 3-4, in room temperature PEI, these two bands occur at 3218 cm^{-1} and 3270 cm^{-1}, respectively, while they are seen at 3240 cm^{-1} and 3288 cm^{-1} in PPI. Previous work by the Frech group with PEI determined that the sharp band is due to highly ordered crystalline domains undergoing hydrogen bonding.[7-9] This work also determined the

broader shoulder band to be the result of domains which, while less ordered, still experience a significant degree of hydrogen bonding[7,8]. These assignments utilized the crystal structure of Chatani *et al*[10], which showed linear PEI to exist in an extensively hydrogen-bonded double helix to explain the shift of the PEI NH stretching bands to frequencies lower than anticipated for primary amine NH stretches.[8]

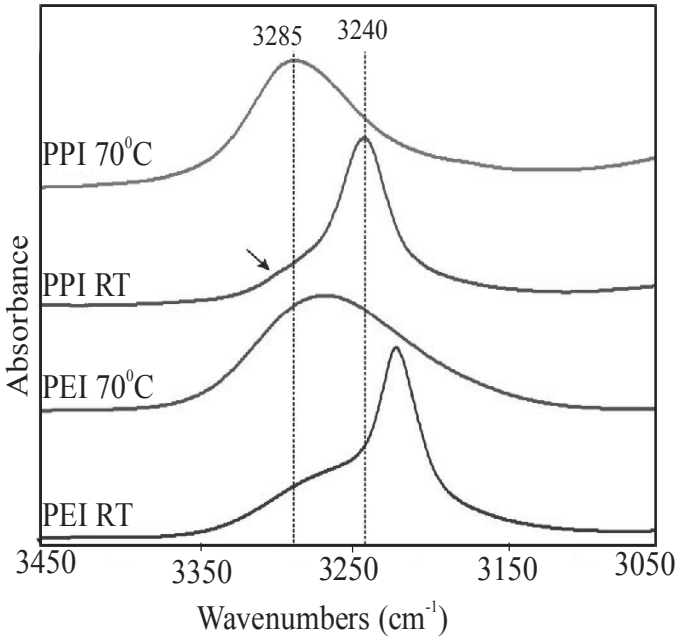

Figure 3-4: NH Stretching Region of the IR spectra of PPI and PEI at 70°C and room temperature

Though no crystal structure of linear PPI has been published, the same thinking can be extended to the NH stretching bands in PPI. The presence of analogous band structures in PPI suggests that, like PEI, neat linear PPI exists in two distinct domains, highly ordered and more disordered, both of which are heavily hydrogen-bonded. The lower NH stretching frequencies in PPI compared to PEI suggest that the hydrogen bonding in PPI is somewhat weaker than in PEI. This is in agreement with the thermal analysis measurements where the T_m in PEI was found to be approximately 10°C higher than in PPI.

In both cases, the intensity of the sharp band corresponding to more highly ordered domain is larger at room temperature than the broader band related to the more disordered, or amorphous, region. This indicates that the vast majority of the material in both systems is crystalline at room temperature. However, the PPI sample has a significantly smaller proportion of disordered domains at room temperature than the PEI polymer, as evidenced by the nearly absent higher frequency band associated with the disordered domains. With heating to 70°C, which is well above the T_m of both materials, the sharp crystalline band disappears entirely, yielding to the much broader amorphous domain band for both PEI and PPI. The 3285 cm^{-1} band in PPI is narrower than the corresponding PEI amorphous band centered at 3265 cm^{-1}, suggesting the possibility of a smaller distribution of amorphous states in PPI. This may be related to the comparative degree of hydrogen bonding present in the systems. PPI experiences weaker hydrogen bonding interactions at room temperature and is therefore more readily converted to disordered states with an increase in temperature than PEI. In the PEI system, the initial extensive hydrogen bonding network can maintain a certain degree of order as the temperature is increased, but it also allows for the formation of a more "disturbed" network therefore having the potential for a wider distribution of hydrogen bonding interactions.

At this point, there is no convincing explanation for this difference in the degree of hydrogen bonding experienced by PPI and PEI. It is expected that PPI will exist in a helical structure, though its helicity is expected to be different from PEI

due to the additional backbone carbon. Perhaps the difference in spacing the nitrogen atoms results in longer N-H···N distances or N-H···N angles less conducive to hydrogen bonding interactions. However, the possible formation of a six membered created by an intramolecular hydrogen bonding between an amine hydrogen and the adjacent nitrogen (N-C-C-C-N-H···) is supported by computational work presented in a later chapter.

3.4.1.2 Addition of Lithium Triflate

The addition of lithium triflate to PPI renders several changes to the NH stretching region of the IR spectrum. Many of these are similar to those which occur in PEI with the addition of LiTf; a few are unique to PPI. The room temperature IR spectra of neat PPI, neat PEI and the 5:1 $N:Li^+$ salt complexes of each system are shown in Figure 3-5. As previously reported, adding LiTf to PEI results in the suppression of the 3218 cm^{-1} crystalline band and the growth of two broad, but intense, bands at 3326 cm^{-1} and 3301 cm^{-1}.[7,8] This suggests a change from a highly ordered crystalline domain in the neat material to two distinct amorphous domains in

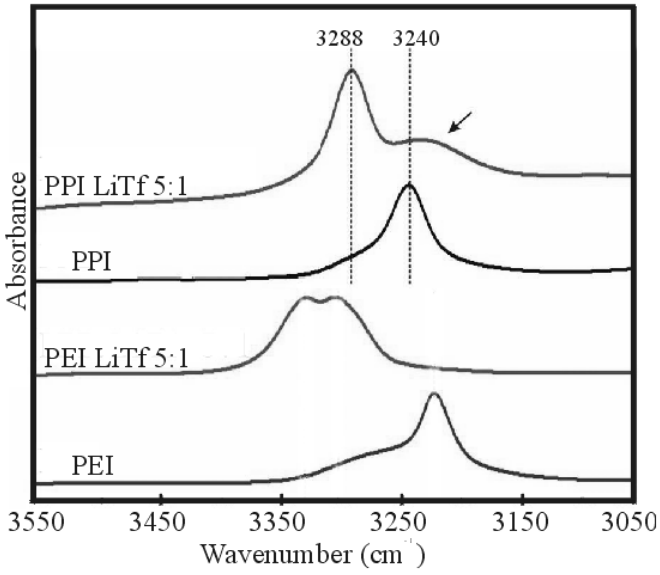

Figure 3-5: NH stretching region of the IR spectra for neat PPI, neat PEI, and 5:1 N:Li+ complex of PPI and PEI with LiTf

the salt complex. PPI also experiences partial suppression of the crystalline band at 3240 cm^{-1} and the growth of one higher frequency band at 3288 cm^{-1} indicating the presence of a new NH environment, which probably corresponds to the amorphous region of the sample. However, this feature is a single band rather than two bands as seen in PEI, suggesting the presence of a single NH environment, rather than two distinct environments.

In general, upon addition of LiTf to the polymer, there are two simultaneous effects on the NH stretching vibrational mode. Hydrogen bonding interactions are disturbed, which may result in shift of the NH stretching band to higher frequencies if these bonding interactions are significantly weakened or disrupted entirely.[11-13] Secondly, the lithium cation coordinates to the polymer nitrogen atom. The inductive effect of the coordination shifts the NH vibration to a lower frequency.[11-13] The frequency of the 3288 cm^{-1} band in PPI is significantly lower than the analogous feature in PEI. The lower frequency may result from the disruption of a smaller percentage of hydrogen bonding in the PPI system than in the PEI system, or it may also be caused by a stronger $Li^{+\cdots}N$ interaction in PPI:LiTf than that seen in the PEI:LiTf complex. Either or both of these factors would result in a lower frequency of the NH stretching vibration in the PPI sample.

Finally, the broad feature present on the low frequency side of the of the 3288 cm^{-1} band in the PPI:LiTf spectrum, indicated by the arrow in Figure 3-5, has no analogous feature in the PEI:LiTf spectra. The physical significance of this feature is not known at this time. However, according to DSC data, shown in Table 3-1, by

a composition of 5:1 N:Li^+ the PPI:LiTf complex is completely amorphous at room temperature. This feature must, therefore, correspond to a second distinct amorphous domain. These two domains represent two different NH environments, which probably result from differing degrees of hydrogen bonding, different coordination of the lithium cation with the backbone nitrogen atoms or some combination of these two factors.

Heating the PEI:LiTf complex has previously been shown to elicit behavior in the NH stretching region quite similar to that observed with salt addition by inducing a shift toward higher frequencies.[8,9] As expected, this is also true of the PPI:LiTf system. As noted earlier, heating the neat material well above its T_m to 70°C results in a change from a virtually completely crystalline material with a sharp band centered at 3235 cm^{-1} to a completely amorphous material with a broad asymmetric band at 3288 cm^{-1} (Figure 3-4). Likewise, addition of LiTf also develops the 3288 cm^{-1} band (Figure 3-5). As discussed earlier, the band at 3288 cm^{-1} suggests the presence of a new NH environment. It is expected that heating the PPI:LiTf complexes forces any remaining ordered domains into disorder, resulting in weaker hydrogen bonding interactions, just as seen in the PEI:LiTf system.[8,9]

IR spectra of neat PPI, 10:1 PPI:LiTf and 5:1 PPI:LiTf at room temperature and at 70°C are shown in Figure 3-6. The behavior of the 10:1 PPI:LiTf complex upon heating is particularly intriguing. At room temperature, the sharp band at 3240 cm^{-1} is much more intense than the broader band at 3288 cm^{-1}. However, at 70°C the intensities of the two bands are reversed with the bandwidth of the lower frequency

band markedly increasing and becoming a shoulder on the low frequency side of the 3288 cm^{-1} band. This is in contrast to the PEI:LiTf system[9] and the 5:1 PPI:LiTf complex where this intensity reversal is not seen, but only a broadening of the two modes with no frequency shift or intensity difference.

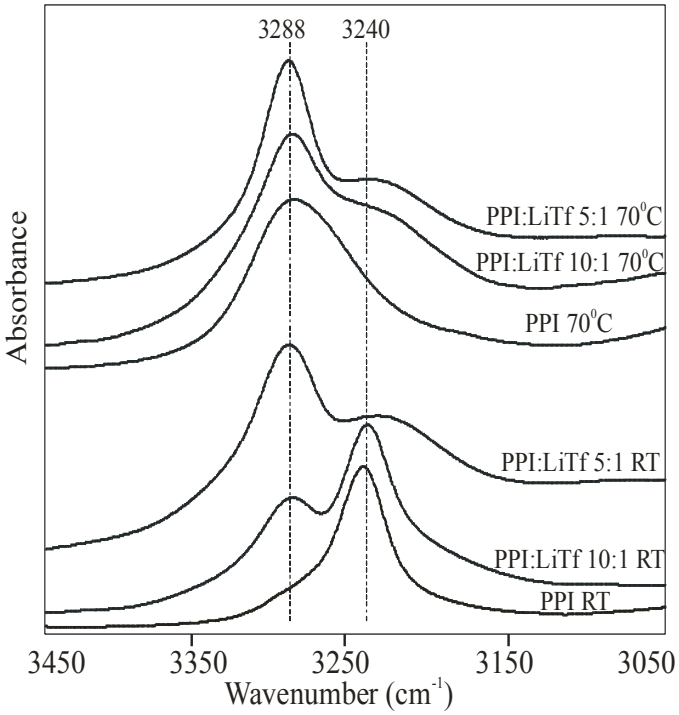

Figure 3-6: NH stretching region of the IR spectra of PPI and PPI:LiTf with $N:Li^+$ of 10:1 and 5:1 at room temperature and 70°C

It was suggested earlier that the frequency difference between the two bands observed at 3240 cm^{-1} and 3288 cm^{-1} could be due to differences in cation coordination to the backbone nitrogen atoms, strengths of hydrogen bonding or a combination of the two factors. Differences in cation coordination to the backbone nitrogen can be discounted largely on the grounds of glass transition temperatures. The T_g of the 10:1 PPI:LiTf and the 5:1 PPI:LiTf complexes, as determined by DSC (Table 3-1), are identical within the bounds of error, indicating that the two complexes experience the same sort of cation-nitrogen coordination. If the nature of the cation-nitrogen interaction was dissimilar, the segmental motion of the polymer would be affected, which would

in turn result in a disparity in T_g. The lack of variance in T_g implies equivalent cation-nitrogen coordination and leaves the alternate explanation - differing strengths of hydrogen bonding - as the more likely cause. Thus, the spectral changes observed with heating and increased LiTf concentration in PPI result from changes in the degree of hydrogen bonding interactions present in the system.

3.4.3 Backbone and Conformational Regions

This region covers the spectral range from about 1400 cm^{-1} to approximately 1100 cm^{-1}, where the observed modes are CN stretching and mixtures of CH twisting and wagging motions. A small amount of NH in-plane bending is also seen here. A number of published articles have thoroughly examined the vibrational spectroscopy of this region, both experimentally and computationally, in PEI and in short chain PEI-like oligmers[7,14-17]. Assignments made in these papers have been utilized for the current work.

Figure 3-7 shows this spectral region for neat PPI and neat PEI at room temperature and at 70°C, which is above the T_m for both polymers. IR spectra of the room temperature neat materials contain several similar general spectral features but are distinctly different in the region. Sharp bands are present in the room temperature PEI spectra at 1246, 1281 and 1330 cm^{-1} and a broader band appears at 1364 cm^{-1}. The former two bands may be attributed to CH_2 twists and latter two bands to CH_2 wags.[16] These four features may be roughly correlated to four features seen in neat room temperature PPI at 1273, 1302, 1338 and 1367 cm^{-1} (dashed lines) which also can be ascribed to CH_2 twists and CH_2 wags.

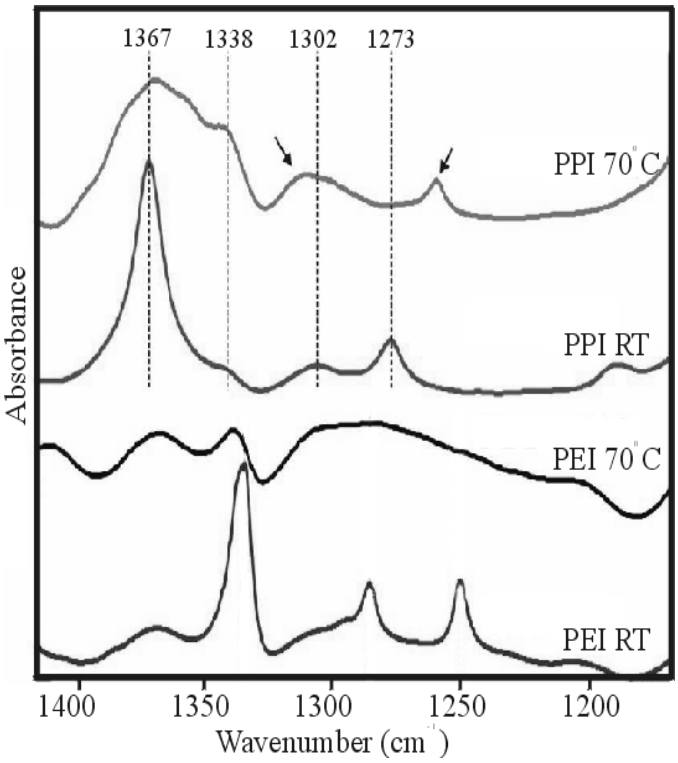

Figure 3-7: 1400-1200 cm^{-1} region of the IR spectra of PPI and PEI at 70°C and room temperature

Upon heating to 70°C, the spectra become further divergent. In PEI, the lower frequency bands are completely lost in the very broad feature ranging from around 1200 cm^{-1} to just above 1300 cm^{-1}. The 1330 cm^{-1} band decreases significantly in intensity compared to the other modes present and shifts upfield slightly, while the higher frequency band at 1364 cm^{-1} remains largely unchanged. In contrast, when PPI is heated above T_m, all four spectral features remain distinct, though in the case of the 1367 and 1338 cm^{-1} significant broadening and some intensity changes occur. Additionally, shoulders develop on both sides of the 1367 cm^{-1} mode. The band at 1302 cm^{-1} shifts to a higher frequency while the band at 1273 cm^{-1} shifts to a lower frequency (see arrows).

The differences with change in temperature between the PEI and PPI systems are very likely due to the additional methylene group present in the PPI backbone.

The added methylene group creates inequivalency among the three methylene units. Two of the methylene groups reside alpha to a nitrogen heteroatom, but the third is beta to the heteroatom. This may result in an increased degree of complexity in these backbone modes. The extra backbone CH_2 also results in a larger separation of the PPI heteroatoms than in PEI; this greater separation may be less conducive to intramolecular hydrogen bonding than the separation found PEI. However, the possibility of a pseudo-six membered ring formed via hydrogen bonding interactions between an amino hydrogen and its adjacent nitrogen would be expected to lead to increased intermolecular hydrogen bonding. Use of a model compound such as N,N' dimethylethylendiamine would be useful in probing these effects. This compound, its complexes with lithium triflate and their respective spectra are discussed in a later chapter.

In the backbone region of the spectrum, as well as in the NH stretching region (previously discussed in section 3.4.1.2), the addition of lithium triflate appears to mimic the effects of heating: band broadening and loss of intensity.[8] Figure 3-8 contains the spectra of neat and 5:1 ($N:Li^+$) LiTf complexes of PEI and PPI in the 1400 to 1100 cm^{-1} region. In addition to the CH_2 wag and twist bands previously mentioned at 1330, 1281 and 1246 cm^{-1}, PEI exhibits two sharp bands at 1132 and 1107 cm^{-1}, which both arise from CN stretching motions.

In PPI, the band at 1368 cm^{-1} can be correlated to the PEI band at 1330 cm^{-1}. However, rather than the two bands at 1132 and 1107 cm^{-1} seen in PEI, an asymmetric band with fairly broad high frequency side shoulder at 1116 cm^{-1}

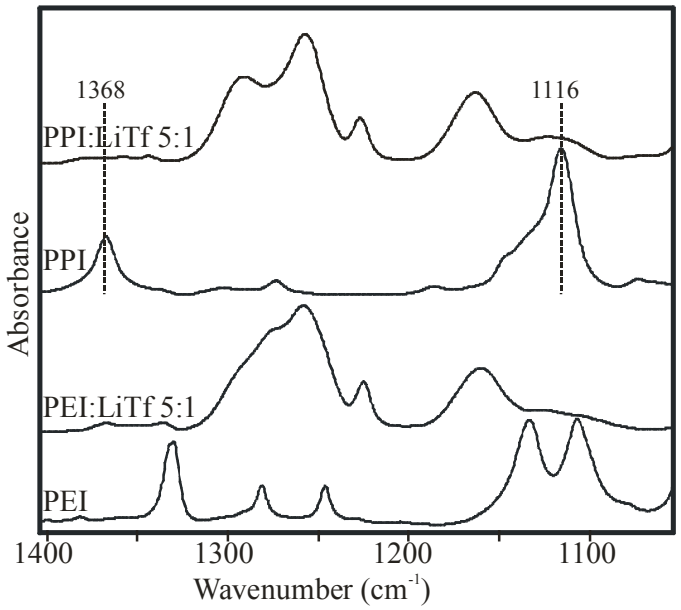

Figure: 3-8: 1400-1200 cm-1 region of the IR spectra of neat PPI and PEI and their 5:1 N:Li+ complexes with LiTf

appears (dashed line) in the PPI spectrum. These bands can be assigned to CN stretching motions. The asymmetry and increased breadth of these bands upon LiTf addition, as compared to those found in PEI, is attributed to the broader distribution of conformations possible as a result of the additional methylene group. With the addition of salt, all of these CH_2 mode bands, in both PEI and PPI, suffer a loss of intensity similar to that seen with upon heating.[8] However, the broad feature spanning 1250 to 1300 cm^{-1} in both the PEI:LiTf and PPI:LiTf spectra results from the triflate anion antisymmetric SO_3 stretch, $\nu_{as}(SO_3)$; the breadth and intensity of this feature greatly impairs any substantial analysis of the neighboring modes. Likewise, the anion's symmetric and antisymmetric CF_3 stretching modes, $\nu_s(CF_3)$ and $\nu_{as}(CF_3)$, are responsible for significantly intense bands seen in the spectra of both the PEI:LiTf and PPI:LiTf complexes at 1220 and 1170 cm^{-1}, respectively. These bands will be further addressed in Section 3.4.3.

Bands resulting from CC stretching and CH_2 rocking are observed in the region from 1100 to 700 cm^{-1}. Assignments given to PEI in previous work[14]

reasonably may be extended to the PPI polymer. These modes have been shown to be sensitive to conformational changes of the polymer backbone.[14-16] Spectra from this region for neat PPI and PPI:LiTf complexes with 10:1 and 5:1 $N:Li^+$ at room temperature and at 70°C are shown in Figure 3-9. The sharp bands present in room temperature neat PPI at 913, 859, 793 and 767 cm^{-1} disappear to be replaced by a single, extremely broad asymmetric feature at 731 cm^{-1} and a small peak at 782 cm^{-1} in the 70°C spectrum; however, this does not occur in spectra of the salt complexes. Bands at 946, 859 and 810 cm^{-1} in the room temperature 10:1 and 5:1 PPI:LiTf complexes remain unchanged even at 70°C, suggesting that the local structures involving the anion and the cation formed in the complexes are more stable against temperature changes than the salt-free local structures present in the neat material.

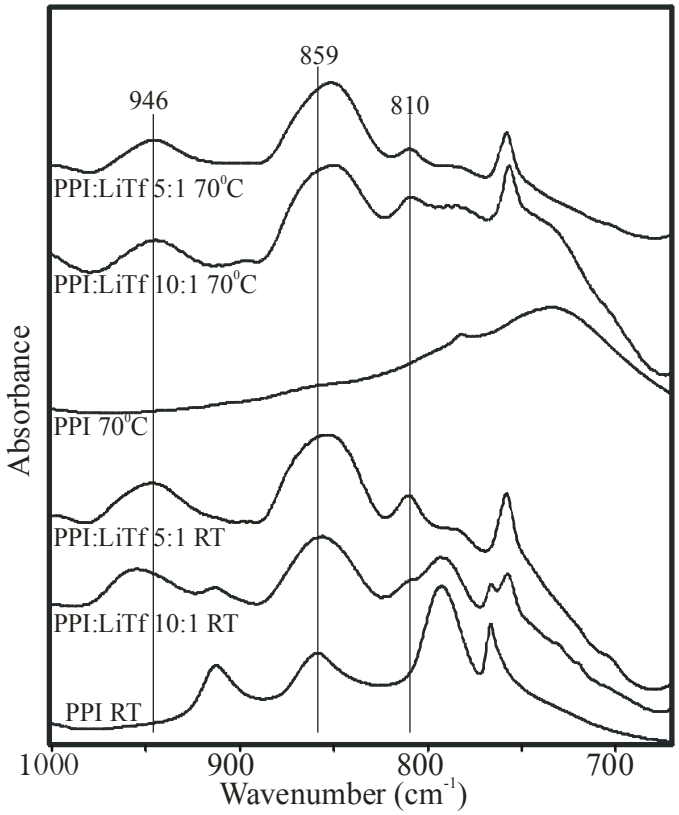

Figure 3-9: 1000-700 cm^{-1} region of the IR spectra of PPI and PPI:LiTf with $N:Li^+$ of 10:1 and 5:1 at room temperature and 70°C

3.4.4 Ionic Association

A substantial body of work studying the association of the triflate ion with PEO and PEO oligomers using experimental[18-24] and computational techniques[15,25] exists. These studies have identified three basic types of ion associations: "free" ions, contact ion pairs and more highly aggregated species. Characteristic frequencies for each of these associations have been assigned in several vibrational modes sensitive to association in the PEO systems. For the symmetric deformation of the triflate CF_3, $\delta_s(CF_3)$, bands for "free" ions, defined as Tf^-, are seen at 752-753 cm^{-1} in PEO systems, bands due to contact ions pairs, [LiTf], appear at 756-758 cm^{-1} and the triple cations ,$[Li_2Tf]^+$, exists around 761-762 cm^{-1}. These assignments do not transfer identically to PEI, but the trend of increasing aggregation leading to higher frequency has been found to be valid for several different organic systems[26] and specifically in PEI and PEI oligomeric systems.[7,15] In PEI, the "free" band has been identified as having a frequency of 754 cm^{-1}.[7,15] As can be seen in Figure 3-10, adding lithium triflate to PEI

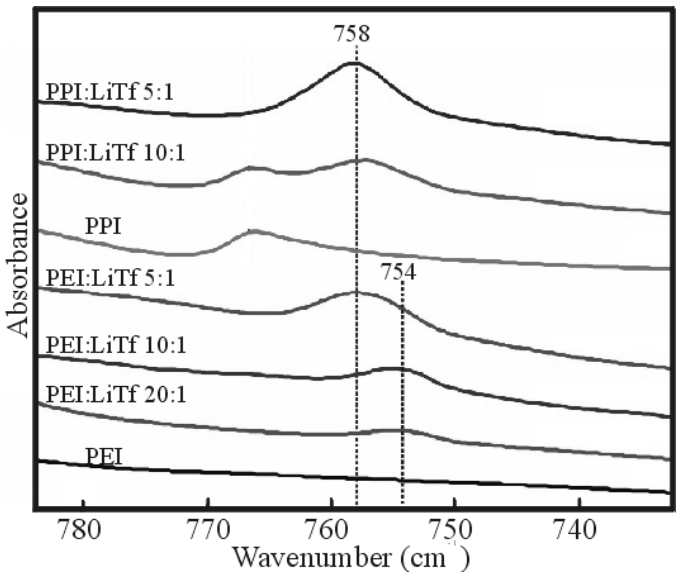

Figure 3-10: Symmetric CF_3 deformation region of the IR spectra of neat and LiTf complexed (N:Li+ = 20:1, 10:1, 5:1) for PEI and PPI

results in the development of this symmetric CF_3 deformation band at 754 cm^{-1} indicating the presence of mainly "free" ion at 20:1 PEI:LiTf ($N:Li^+$). As salt concentration is increased, association changes to mainly contact ion pairs, as evidenced by the shift of the $\delta_s(CF_3)$ band to 758 cm^{-1} at a ratio of 5:1 PEI:LiTf. In marked contrast to this behavior, a $\delta_s(CF_3)$ band appears in dilute PPI:LiTf at 758 cm^{-1}; however, increasing the salt concentration, even up to 5:1 PPI:LiTf does not shift this band any higher. Figure 3-9 illustrates the frequency of this band does not shift with heating either. This behavior indicates PPI:LiTf contains triflate ions that are not "free" ions, but rather are contact ion pairs or possibly more highly aggregated species.[25] This assertion is strengthened by spectra of tetrabutylammonium triflate (TBATf) in PPI, in which a single $\delta_s(CF_3)$ band is observed at 753 cm^{-1}. Since the bulky nature of this cation prevents any significant interactions with the anion, this effectively benchmarks 753 cm^{-1} as the frequency associated with the "free" triflate anion in PPI. Thus, $\delta_s(CF_3)$ bands higher than 753 cm^{-1} must correlate to contact ion pair and/or species of higher aggregation.

Another indicator of ionic association which has been well studied in PEO-type systems[25,27-30] and may be extended to PEI[15] and PPI is the SO_3 symmetric stretching mode, $\nu_s(SO_3)$. As shown in Figure 3-11, this band appears in PEI-LiTf complexes at 1032 cm^{-1} at low salt concentrations and develops a higher frequency asymmetric tail as salt concentration is increased to a 5:1 PEI:LiTf ratio. This suggests that the ions are present in the PEI-LiTf complex predominately as "free" ions at low salt concentration with some contact ion pairs present at higher triflate

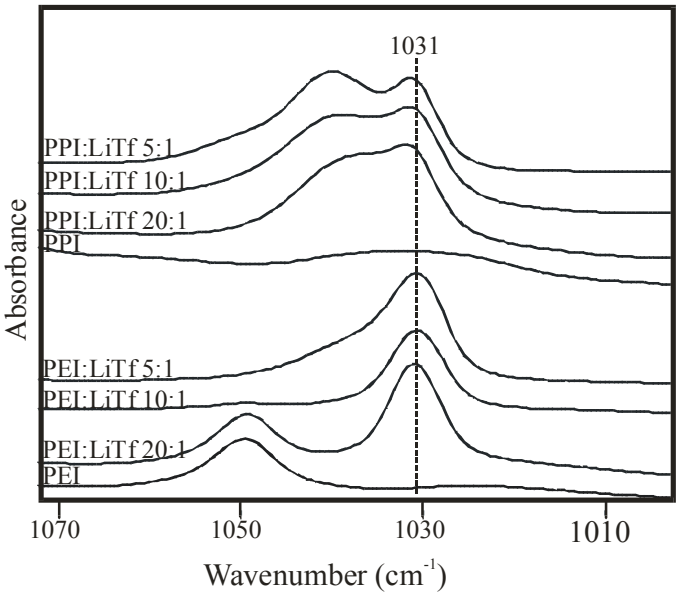

Figure 3-11: Symmetric CF_3 deformation region of the IR spectra of neat and LiTf complexed (N:Li+ = 20:1, 10:1, 5:1) for PEI and PPI

concentrations, while the $\delta_s(CF_3)$ region implied a more marked shift toward contact ion pair with nominal remaining "free" ion at high salt concentration. Rather than the single band observed in the PEI-LiTf system, the spectra of PPI-LiTf complexes have two intense bands. These bands are centered at 1040 and 1031 cm^{-1} and do not shift position with added salt, though the intensity of the 1040 cm^{-1} band relative to the 1031 cm^{-1} band does increase with increasing salt concentration. These frequencies are indicative of the presence of contact ion pairs and "free" ions. This is inconsistent with the $\delta_s(CF_3)$ region that suggests that the anions are present as contact ion pairs and more highly aggregated species (Fig 3-10).

While disconcerting, this contradiction is not without precedent. In a published study of tetrabutylammonium triflate and lithium triflate in water and numerous organic solvents, researchers noted that, in the case of 2-propanol, while the observed $\delta_s(CF_3)$ frequency suggested aggregate species, the $\nu_s(SO_3)$ frequency indicated "free" anions. In that case, researchers explained the phenomenon in terms

of the alteration of bond force constants resulting from hydrogen bonding electrophilic interactions between the protic solvent and the oxygen anion atom of the triflate, with the SO bonds being affected to a larger degree than the CF bonds on the opposite end of the molecule.[26] In fact, in solvents with electron pair acceptance polarities, $E_T(30)$, less than about 42 kcal/mol, there was extremely limited impact on the $\delta_s(CF_3)$ modes.[26] The same argument can be applied to the case of poly(imino)-triflate systems. When the SO_3 end of the anion interacts with the amino hydrogen, possibly forming the six-membered ring shown in Figure 3-12, the accompanying redistribution of electron density shifts most anion modes to higher frequencies. This has greatest on impact on the SO_3 modes. The CF_3 modes, separated from direct association by the CS single bond, are less affected. Additionally, PPI-type systems would be expected to have $E_T(30)$ values less than 42 kcal/mol[31], so based on the previous work[26], changes in the $\delta_s(CF_3)$ mode frequencies would not be anticipated. Thus, in these types of systems, the $\delta_s(CF_3)$ is the more accurate reflection of the ionic association. The six-membered ring suggested in Figure 3-12 may also contribute to the apparent stability of the ionic association, since the association seems to be affected little by either salt concentration or temperature.

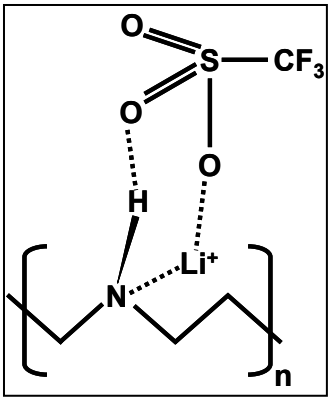

Figure 3-12: Possible interaction between the Li+ ion contact pair and the secondary amine backbone

3.5 IONIC CONDUCTIVITY

Temperature dependent ionic conductivity data, collected at 20:1, 10:1 and 5:1 N:Li^+ for PEI:LiTf and PPI:LiTf over the temperature range from 22°C to 70°C are presented in Figure 3-13. The conductivity of PEI:LiTf increases as a function of increasing salt concentration at low temperatures (<40°C), but decreases with added salt at higher temperatures (>60°C). The seemingly contradictory behavior is explained by the competing factors of charge carrier concentration and ionic mobility. Initially, the increase in charge carriers due to increased salt concentration enhances the conductivity. Eventually, at high salt concentrations, ionic associations begin to occur, which reduces the number of charge carriers available. Mobility may be negatively impacted by increased salt concentration, but aided by increased temperature. Thus at higher temperatures, complexes with higher salt concentrations actually have fewer charge carriers with the optimum mobility than complexes with lower salt concentrations.

In contrast to PEI:LiTf, the conductivity of PPI:LiTf maintains the initially present pattern of reaching a maximum somewhere between N:Li^+ of 10:1 and 5:1 across the entire temperature range studied. The conductivity of PPI:LiTf also exhibits a fairly constant increase with heating, as opposed to the PEI:LiTf, in which the slopes vary widely across the temperature and concentration ranges. This is most likely due to the relatively minimal change in the ionic species that are present in the system with the addition of salt or heat, which occurs in PPI:LiTf. Therefore, the

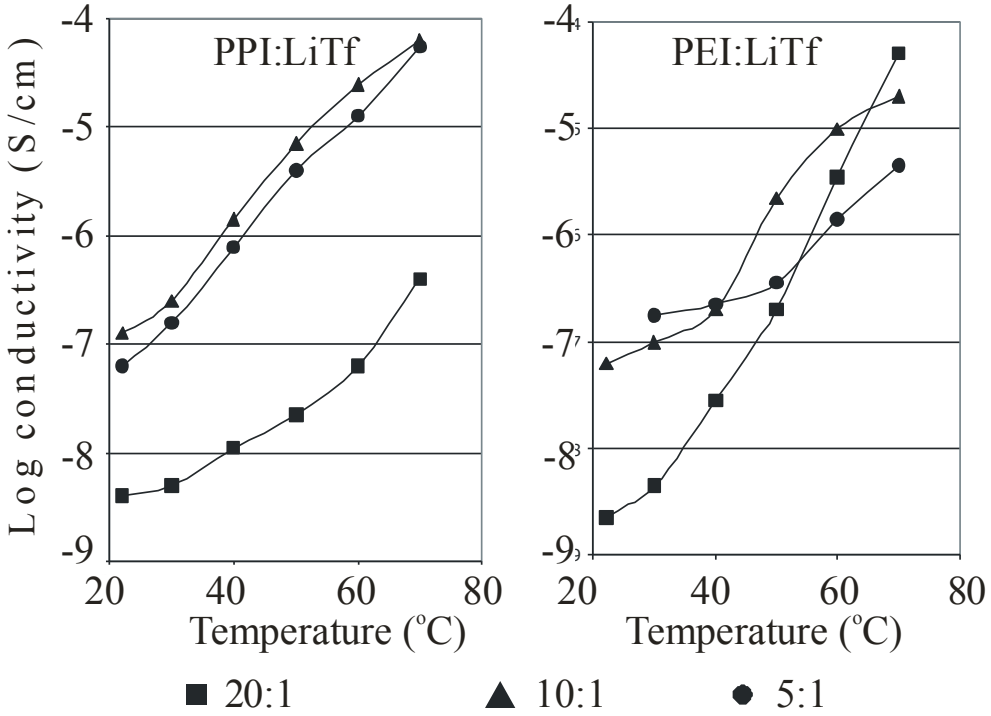

Figure 3-13: Ionic Conductivity of PEI:LiTf and PPI:LiTf complexes of N:Li+ = 20:1, 10:1 and 5:1 over the temperature range from 22°C to 70°C

conductivity enhancement seen with increasing temperature is more likely due to the greater percentage of amorphous rather than crystalline domains present in the sample at higher temperatures. It is widely accepted that the salt dissolved in the amorphous domains are primarily responsible for ionic conductivity, consequently increasing the proportion of these domains would yield higher ionic conductivity.[32-35] Balancing this contribution against the ionic mobility in the system would result in an expected conductivity maxima just at the point where 100% of the salt-containing domains are amorphous. According to the DSC data, PPI:LiTf reaches a completely amorphous condition at a composition between 10:1 and 5:1 N:Li^+, which correlates

quite well with the conductivity data. Unfortunately, even at this maximum, the conductivity falls short of the 10^{-5} to 10^{-3} S cm^{-1} needed over the targeted temperature range to be truly viable as a solid polymer electrolyte for batteries without the addition of a co-solvent or plasticizer.[36-39]

3.6 CONCLUSIONS

PPI is a pale yellow crystalline material, which melts at 54±3°C. Salt addition suppresses and eventually eliminates T_m, while creating a T_g, which varies only slightly with increased salt concentration. Local specific structure and composition of domains present in PPI-LiTf complexes vary with salt concentration and temperature. According to DSC data, while the neat material is completely crystalline, at room temperature an entirely amorphous material is obtained at a salt concentration between 10:1 and 5:1 $N:Li^+$.

FT-IR data from the OH stretching region indicates neat PPI is not hygroscopic. Data from the NH stretching region show hydrogen bonding interactions occur in both the neat and salt-complexed material. The hydrogen bonding interactions appear to be weaker than those in the PEI system and are less disrupted by salt addition or heating. Likewise, PPI polymer backbone and conformation modes appear to be less dependent on salt concentration and temperature than analogous modes in the PEI system, indicating weaker hydrogen bonding in the PPI system or at the least more stable local structures. While the ionic association in PEI-LiTf complexes change from “free” ions to contact ion pairs

with increasing LiTf concentration and temperature, in the PPI-LiTf electrolyte ionic association appears as contact ion pairs or aggregates at low salt concentrations and does not change with temperature increase. This stability in ionic association may be due to: (1) to the less extensive intermolecular hydrogen bonding network in PPI as compared to PEI, (2) the presence of a third backbone methylene group (as compared to only two such groups in PEI), (3) the formation of a six membered ring by anion association with the amino hydrogen or (4) some combination of these three factors. All of these could make PPI-LiTf complexes less sensitive to changes in salt concentration and temperature then PEI-LiTf electrolytes. An apparent discrepancy in the nature of the ionically associated species determined by the analysis $\delta_s(CF_3)$ and $\nu_s(SO_3)$ is resolved by previous work[26] with the triflate ion in various protic organic solutions. That work suggests that interaction of the triflate oxygen with protic solvents results in a redistribution of electronic density, which, in turn, shifts the anion modes to higher frequencies. The $\nu_s(SO_3)$ modes more perturbed than the $\delta_s(CF_3)$, leaving the later mode as the more accurate indicator of ionic association species in poly(imino)-LiTf electrolytes.

The ionic conductivity of the PPI-LiTf system is fairly low (10^{-7} S cm^{-1}) at room temperature. With the addition of heat, it continues to rise with an even, steep slope within the temperature range presented here, reaching a maximum of about $10^{-4.5}$ S cm^{-1} at 80°C. This is in contrast to PEI-LiTf, where ionic conductivity trends are heavily dependent on the combination of salt concentration and temperature. Increasing salt concentration of the PPI system initially raises conductivity; however,

a maximum in ionic conductivity is reached somewhere between 10:1 and 5:1 N:Li^+. This directly corresponds with the change to an entirely amorphous material as indicated by the DSC data.

Unfortunately, it appears that the PPI is not a suitable candidate for solid polymer battery applications. Even at 80°C, the most highly conductivity PPI:LiTf complex fails to achieve the 10^{-3} S cm^{-1} goal.[36-39] Since the system is entirely amorphous under those conditions, the conductivity may be limited by hydrogen bonding interactions occurring within the system and/or by the formation of highly associated ionic species with lower mobilities. In order to achieve better conductivity, modifications must be made to the system.

3.7 REFERENCES

(1) Gandhi, M. K. *The Collected Works of Mohatma Gandhi*; 1st ed.; Publications Division, Ministry of Information and Broadcasting, Government of India, 1960-1994; Vol. 26. GandhiServe Foundation. http://www.gandhiserve.org/cwmg/cwmg.html (accessed: 9 May 2009).

(2) Lee, J.; Lee, K.; Kim, H. *Bull. Korean Chem. Soc.* **1996**, *17*, 115-16.

(3) Zhang, W.; Jiang, J.; Qin, C.; Perez, L. M.; Parrish, A. R.; Safe, S. H.; Simanek, E. E. *Supramol. Chem.* **2003**, *15*, 607-616.

(4) Hu, L., University of Oklahoma, 2005.

(5) Hu, L.; Frech, R.; Glatzhofer, D. T.; Mason, R.; York, S. S. *Solid State Ionics* **2008**, *179*, 401-408.

(6) J. Lee, K. L., H. Kim *Bulletin of the Korean Chemical Society* **1996**, 115-116.

(7) York, S.; Frech, R.; Snow, A.; Glatzhofer, D. *Electrochim. Acta* **2001**, *46*, 1533-1537.

(8) York, S. S.; Buckner, M.; Frech, R. *Macromolecules* **2004**, *37*, 994-999.

(9) Buckner, M.; York, S. S.; Frech, R.; Glatzhofer, D. T. *Polymer Preprints* **2003**, *44*, 1085.

(10) Chatani, Y.; Kobatake, T.; Tadokoro, H.; Tanaka, R. *Macromolecules* **1982**, *15*, 6.

(11) Rocher, N. M.; Frech, R. *Macromolecules* **2005**, *38*, 10561-10565.

(12) Rocher, N. M.; Frech, R.; Khan, M. *The Journal of Physical Chemistry B* **2005**, *109*, 20697-20706.

(13) Rocher, N. M.; Frech, R.; Powell, D. R. *The Journal of Physical Chemistry B* **2006**, *110*, 15117-15126.

(14) York, S. S.; Boesch, S. E.; Wheeler, R. A.; Frech, R. *Macromolecules* **2003**, *36*, 7348-51.

(15) York, S. S.; Boesch, S. E.; Wheeler, R. A.; Frech, R. *PhysChemComm* **2002**, *5*, 99-111.

(16) Boesch, S. E.; York, S. S.; Frech, R.; Wheeler, R. A. *PhysChemComm* **2000**, *1*, 1.

(17) Sanders, R. A.; Frech, R.; Khan, M. A. *J. Phys. Chem. B* **2004**, *108*, 12729-12735.

(18) Frech, R.; Chintapalli, S.; Bruce, P. G.; Vincent, C. A. *Macromolecules* **1999**, *32*, 808-813.

(19) Frech, R. *Macromolecules* **2000**, *33*, 9342-9436.

(20) Huang, W.; Frech, R. *Polymer* **1994**, *35*, 235-42.

(21) Frech, R.; Huang, W. *Solid State Ionics* **1994**, *72*, 103-7.

(22) Chintapalli, S.; Frech, R. *Electrochim. Acta* **1995**, *40*, 2093-2099.

(23) Muhuri, P. K.; Das, B.; Hazra, D. K. *The Journal of Physical Chemistry B* **1997**, *101*, 3329-3332.

(24) Huang, W.; Frech, R.; Johansson, P.; Lindgren, J. *Electrochim. Acta* **1995**, *40*, 2147-2151.

(25) Huang, W.; Frech, R.; Wheeler, R. A. *J. Phys. Chem.* **1994**, *98*, 100-10.

(26) Frech, R.; Huang, W. *J. Solution Chem.* **1994**, *23*, 469-81.

(27) Schantz, S.; Torell, L. M.; Stevens, J. R. *J. Appl. Phys.* **1988**, *64*, 2038-43.

(28) Schantz, S.; Sandahl, J.; Borjesson, L.; Torell, L. M.; Stevens, J. R. *Solid State Ionics* **1988**, *28-30*, 1047-53.

(29) Ferry, A. *J. Phys. Chem. B* **1997**, *101*, 150-157.

(30) Petersen, G.; Jacobsson, P.; Torell, L. M. *Electrochim. Acta* **1992**, *37*, 1495-1497.

(31) Reichardt, C. *Chem. Rev.* **1994**, *94*, 2319-2358.

(32) Berthier, C.; Gorecki, W.; Minier, M.; Armand, M. B.; Chabagno, J. M.; Rigaud, P. *Solid State Ionics* **1983**, *11*, 91-5.

(33) Papke, B. L.; Ratner, M. A.; Shriver, D. F. *J. Electrochem. Soc.* **1982**, *129*, 1694-701.

(34) Ratner, M. A.; Nitzan, A. *Faraday Discuss.* **1989**, *88*, 19-42.

(35) Gray, F. M. *Solid Polymer Electrolytes: Fundamentals and Technological Applications*; 1st ed.; VCH Publishers Inc.: New York, 1991.

(36) Meyer, W. H. *Adv. Mater.* **1998**, *10*, 439-448.

(37) Armand, M. B. *Solid State Ionics* **1994**, *69*, 309-319.

(38) Reddy, T. B.; Hossain, S. In *Handbook of Batteries, 3rd ed*; 3rd ed.; Linden, D. S., Ed.; McGraw-Hill: New Tork, New York, 2002.

(39) Erhlich, G. M. In *Handbook of Batteries, 3rd ed*; 3rd ed.; Linden, D. S., Ed.; McGraw-Hill: New York, New York, 2002.

CHAPTER 4: POLY(N-METHYLPROPYLENIMINE)

Guess what I've done!
Invented a light bulb that plugs into the sun.
The sun is bright enough,
The bulb is strong enough,
But, oh, there's only one thing wrong ...
The cord ain't long enough.

Shel Silverstein[1]

4.1 INTRODUCTION

Poly(N-methylpropylenimine) is similar in structure to poly(propylenimine), PPI, differing only in the substitute of an amino methyl group in PMPI for the amino hydrogen present in PPI. PMPI may also properly be explained as an homolog of poly(N-methylethyl enimine), PMEI, which is itself a methyl substituted version of the widely studied polymer poly (ethyleneimine), PEI. Structures of all four materials are given in figure 4-1.

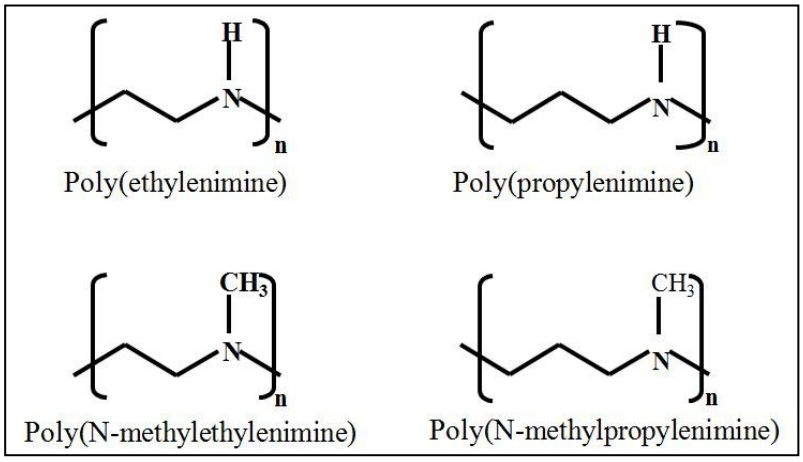

Figure 4-1: Structures of PEI, PPI, PMEI and PMPI

As discussed in Chapter 3, PEI has been offered as an alternative to PEO for use as polymer electrolyte. The potential detrimental effects of both inter- and

intramolecular hydrogen within PEI have been addressed by substituting the amino hydrogen with a functional group. This offers a range of interesting synthetic options for polymer electrolytes and other applications.[2-8] The simplest of the substitutions, methylation, creates poly(N-methylethylenimine), or PMEI, and has been thoroughly studied by several groups including Tanaka, *et al*[9,10] and Frech, *et al.*[11-14] These investigations have offered insight into the ionic associations and conductivity behavior of PMEI but have shown mixed results for conductivities of PMEI:LiTf salt complexes versus those for PEI:LiTf complexes. This work builds on this approach by methyl substituting the PEI homolog PPI to create the PMEI homolog PMPI, which should maintain many of the characteristics of PPI while eliminating hydrogen bonding. This project explores PMPI as a potential polymer electrolyte host for dissolved lithium trifluoromethanesulfonate (LiTf). Details of the investigative techniques used, Fourier Transform infrared spectroscopy (FT-IR), differential scanning calorimmetry (DSC) and alternating current (AC) complex impedance, are described in sections 2.3 and 2.4.

This study of the poly(N-methylpropylenimine), PMPI, system was performed as a collaboration between Dr. Roger Frech's physical chemistry laboratory and Dr. Daniel Glatzhofer's organic chemistry laboratory. Like the PPI project, Dr. Leiyu Hu was responsible for the synthesis of the PMPI, I prepared all of the analytical samples, and we shared in data collection. A preliminary analysis of these data may be found in Dr. Hu's dissertation.[15] However, in the time since the

completion of Dr. Hu's degree, additional work has yielded new interpretation of some data.

4.2 SYNTHESIS AND APPEARANCE

The poly(N-methylpropylenimine) used for this work was synthesized by Dr. Leiyu Hu and is described in detail in his dissertation.[15] The present work is concerned with the analysis of the polymer, consequently the synthetic route will be only briefly summarized. Interested readers should refer to Dr. Hu's dissertation[15] for details.

Poly(N-methylpropylenimine) was produced via Eschweiler-Clarke methylation of poly(propylenimine), PPI, which was synthesized as explained in Section 3.2 and detailed elsewhere.[15-18] The methylation process is illustrated in Scheme 4.2. PPI was dissolved in excess formic acid and formalin, and the solution heated to reflux for 12 hours before concentrated HCl was added. This mixture was heated to reflux for an additional period of time. This resulted in PMPI•HCl,

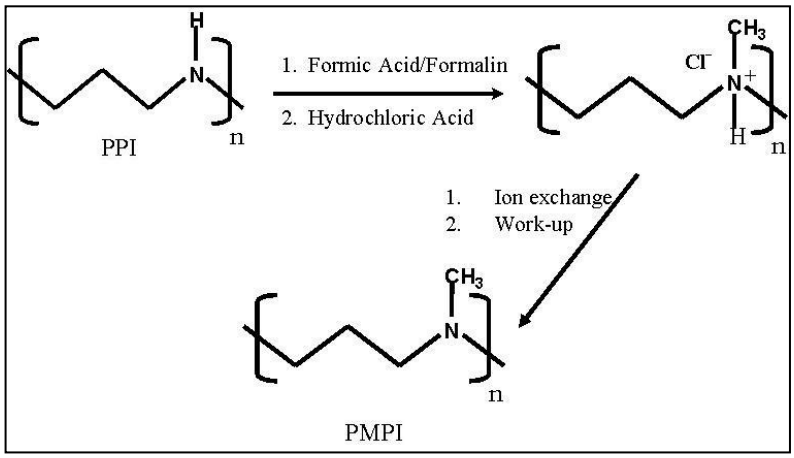

Scheme 4-2: Synthesis of poly(N-methyl propylenimine) via Eschweiler-Clarke methylation of poly(propylenimine)

which was isolated by the removal of solvent under reduced pressure to give the polymer ammonium chloride salt. This salt was neutralized by ion exchange in water with Amberlite ® IRA 400 (OH•) resin to yield the PMPI after water removal. The molecular weight of the obtained polymer is estimated to be approximately 3700 g/mol. PMPI is a dark amber liquid very similar in appearance and viscosity to honey. It has a glass transition temperature of -88°C, as determined by DSC, and is soluble in methanol.

4.3 THERMAL ANALYSIS

Glass transition (T_g) temperatures for PMPI:LiTf complexes were determined by DSC and are given in Table 4-1. Neat PMPI as glass transition temperature (T_g) of -88°C, while neat PMEI displays a T_g of -93°C. A melting point (T_m) was not observed in either sample below 150°C, suggesting both systems are entirely amorphous. Though addition of lithium triflate increases T_g in both PMEI and PMPI, the effect is much greater in the PMEI:LiTf system where the Tg is raised nearly 80°C to -14°C by increasing salt to 5:1 N:Li^+. At a like composition, T_g of PMPI:LiTf increases by only 60°C to -28°C. Interestingly, at lower concentrations of LiTf, the T_g climbs in comparable increments in the two

Table 4-1: Glass Transitions of PMPI:LiTf and PMEI:LiTf Complexes

	PMPI Tg (ºC)	PMEI Tg (ºC)
Neat Polymer	-88	-93
20:1 N:Li^+	-73	-79
10:1 N:Li^+	-47	-60
5:1 N:Li^+	-28	-14

systems. The largest variation is seen only at the highest salt concentration. The overall shifts in T_g are comparable to those experienced in related polymer-salt systems.[12,13,19-22] The change in both T_g without evidence of additional thermal transitions suggests that while salt addition "stiffens" the system, no major long range changes in structure occur in either the PMEI:LiTf or PMPI:LiTf system. As discussed in a following section (4.4.3), this lack of major structural alteration is consistent with the temperature dependent IR data, which show no significant changes in any region up to 80°C.

4.4 VIBRATIONAL SPECTROSCOPY

PMEI and PMPI share the same basic structure in terms of connectivity however, the additional backbone in carbon in PMPI separates the nitrogen atoms further. This may well result in different interactions with the lithium triflate salt. As in the case of PPI and PEI, the additional backbone creates an inequivalency between the CH_2 groups alpha to the heteroatom and those beta to it. It also allows for the formation of different conformations than those available in the ethyl system, by adding a dihedral angle and additional rotational bond axis not present in PMEI. These differences may be responsible for the significant differences seen in the IR spectra of the materials.

4.4.1 Backbone & Conformational Regions

Features in this region (~1400 cm^{-1} to ~900 cm^{-1}) result mainly from CN stretching modes (ν_{CN}), CC stretching modes (ν_{CC}) and complex mixtures of CH

motion, including wagging (ω_{CH}) rocking (ρ_{CH}) and twisting (τ_{CH}). Assignments made in the present work are based on experimental and computational studies published by other workers examining vibrational modes in IR for PEI and PEI-like small molecules,[23-25] as well as PMEI and PMEI-like small molecules.[13,26] Computational studies on model compounds for PPI and PMPI are not currently available in the literature. Some unpublished computations on a PPI model compound, dimethylethylendiamine, are presented in Chapter 5 of this work. Those results are consistent with those previously published for PEI-like and PMEI-like small molecules.

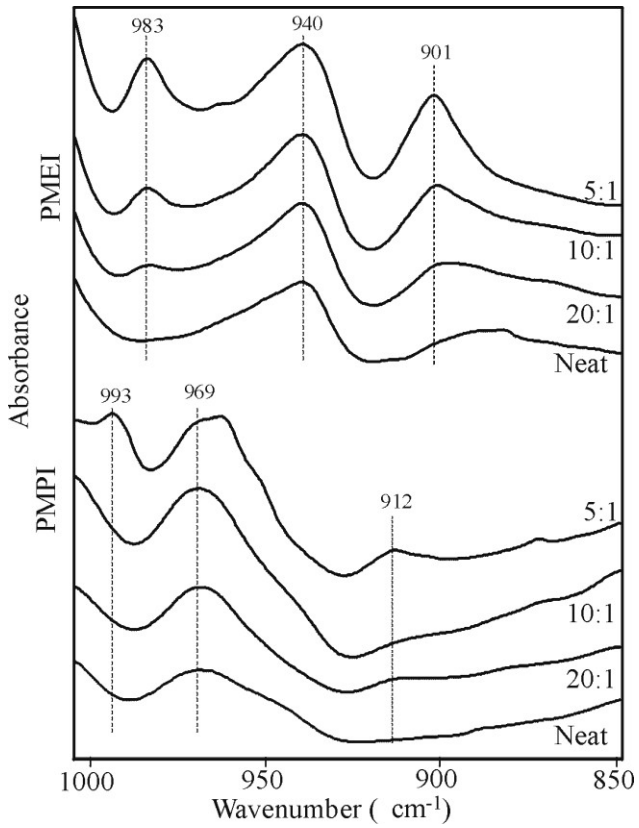

Figure 4-3: IR spectra from 1000 to 850 cm^{-1} for PMPI, PMPI:LiTf ($N:Li^+$ = 20:1, 10:1, 5:1) , PMEI and PMEI:LiTf ($N:Li^+$ = 20:1, 10:1, 5:1)

Several features in this region of the IR spectra of PMEI and PMPI can be well correlated to provide information about the backbone modes in the two materials and in their polymer:salt complexes with lithium triflate. For example, Figure 4-3 shows the IR spectra from 850 to 1000 cm^{-1} for neat PMEI and PMEI and salt complexes with lithium triflate of 20:1, 10:1 and 5:1 $N:Li^+$. The

spectra of both the PMEI and PMPI complexes change from consisting of a single broad feature to containing three distinct features. These features, while occurring at different frequencies, show the same development pattern in both materials. The intensity increase of the bands at 993 cm^{-1} and 912 cm^{-1} in PMPI mirrors a similar intensity increase seen in the bands at 983 cm^{-1} and 901 cm^{-1} in PMEI. In both instances, these bands bookend a third band (969 cm^{-1} in PMPI and 940 cm^{-1} in PMEI), which seems to slightly increase in intensity with increasing LiTf concentration.

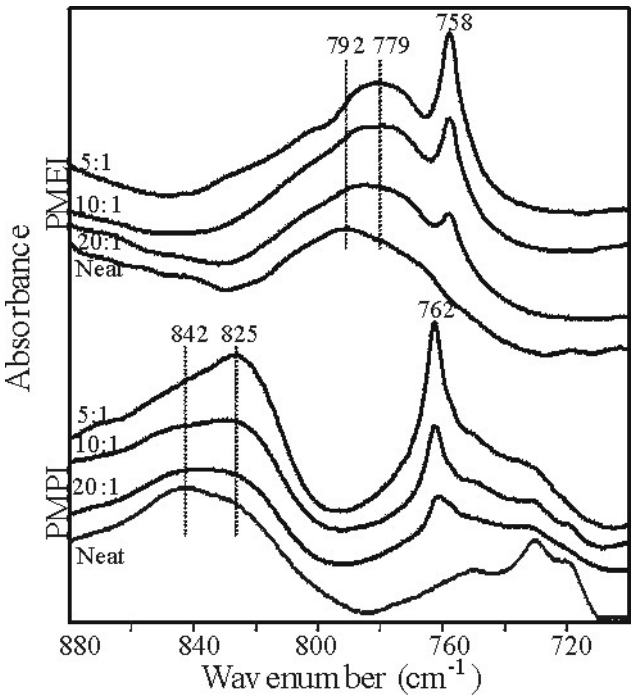

Figure 4-4: IR spectra from 880 to 720 cm^{-1} for PMPI, PMPI:LiTf (($N:Li^+$ = 20:1, 10:1, 5:1), PMEI and PMEI:LiTf ($N:Li^+$ = 20:1, 10:1, 5:1)

The correlation between the two systems can be extended to the regions shown in Figure 4-4. Again, the spectra of the two materials consist of the same general features: a higher frequency broad band and a lower frequency sharp band. In the PMPI spectra, the features are separated by a larger frequency than the analogous bands in the PMEI spectra. In PMPI, the broad band is seen at 842 cm^{-1} with a shoulder at 825 cm^{-1}. With increasing LiTf concentration, this

shoulder exhibits such a significant increase in intensity that the 842 cm^{-1} band eventually becomes indistinguishable from the high frequency tail of the strong asymmetric 825 cm^{-1} band. The same behavior is observed in the PMEI spectra, where the 792 cm^{-1} band has a lower frequency broad shoulder, whose intensity grows with increasing LiTf to become the broad band at 779 $cm^{-1,}$ from which the 792 cm^{-1} can not be distinguished. Based on these similarities, it seems practical to assign the bands in PMPI to the same or similar vibrations as those occurring in the PMEI system.

The behavior seen in Figure 4-3 and 4-4 common to PMEI and PMPI has also been observed in PEO:LiTf systems.[27] Therefore, it seems reasonable to look to the well-studied and structurally similar PEO:LiTf system for guidance in assigning these bands. The broad band present in the PEO spectrum has been assigned to a predominate mixture of CH_2 rocking, $\rho(CH_2)$, and CO stretching motions, $\nu(CO)$, with some small contribution from CC stretching, $\nu(CC)$, motions.[28-30] Neat, crystalline PEO exists as a 7/2 helix, having O-C-C-O dihedral angles of approximately 64° and C-C-O-C dihedral angles of about 188°.[30] The complex formed upon LiTf addition has a 3:1 stoichiometry. According to the crystal structure of this $P(EO)_3LiTf$ complex solved by Lightfoot, Mehta and Bruce, the PEO:Li^+ complex is a 2/1 helix with five-fold coordinate Li^+ interacting with three ether oxygens and two triflic oxygens.[31] Based on the spatial atomic coordinates of this crystal structure, two distinct O-C-C-O dihedral angles, having values of 44° and 64°, were determined by Frech and Huang.[27] These angles are different from that of

64° found in the neat PEO, suggesting that Li^+ addition changes the conformation of the polymer backbone. These changes are reflected in a number of polymer vibrational modes whose frequencies shift upon LiTf addition.[32] Unfortunately, no crystal structures of PMEI or PMPI complexed with LiTf have been published; therefore, this behavior can not be quantitatively confirmed in either PMEI or PMPI. However, the spectral behavior of the two systems is conspicuously similar to that of the PEO:LiTf system in the 750-1000 cm^{-1} region. Given this, it is reasonable to conclude that similar backbone conformational changes occur in the PMPI and PMEI systems upon LiTf addition. Further, these conformational changes are probably due to coordination of the Li^+ to the backbone nitrogen heteroatoms in a style comparable to that occurring in the PEO:LiTf system.

The frequencies of the PMPI bands shown in Figure 4-4, are lower than the corresponding PMEI bands. However, the frequencies of the PMPI bands in Figure 4-4 are higher than the corresponding PMEI bands. These differences are likely due to the presence of the additional backbone CH_2 group in PMPI. This additional unit may also be responsible for the variation in the frequency difference between the broad bands and shoulders shown in Figure 4-4. In PMPI, the frequency difference between the 842 cm^{-1} and 825 cm^{-1} bands is 17 cm^{-1}, while in PMEI, the difference between the 792 cm^{-1} and 779 cm^{-1} bands is 13 cm^{-1}. This may reflect a difference in the coordinative interaction between the lithium cation and the nitrogen heteroatoms in the two systems, with PMPI having a slightly stronger interaction than PMEI. However this data alone is insufficient to make a certain claim.

Despite the similarities in the two systems, strong spectral differences do occur. For example, in Figure 4-4, the three overlapping bands from about 715 cm^{-1} to 760 cm^{-1} in the neat PMPI have no analog in the PMEI spectrum. This suggests a definite difference in the two backbone structures. Modes in this region have been assigned to CH_2 rocking, $\rho(CH_2)$, wagging , $\omega(CH_2)$, and twisting, $\tau(CH_2)$, bands.[25] The absence of a similar feature in the PMEI spectrum may be taken as a strong suggestion that these bands are associated with the CH_2 group beta to the nitrogen in PMPI since this unit is non-existent in PMEI. That the three individual bands merge into a single broad band at modest (20:1 $N:Li^+$) salt concentrations indicates some change in the local backbone structure occurs with salt addition.

4.4.2 Ionic Associations

Four main vibrations offer the most insight into the ionic associations occurring in PMPI with addition of lithium triflate. These are the symmetric CF_3 bend, $\delta_s(CF_3)$, from around 750-760 cm^{-1}; the symmetric SO_3 stretch, $\nu_s(SO_3)$ from about 1030-1060 cm^{-1}; the asymmetric CF_3 stretch, $\nu_{as}(CF_3)$, centered around 1170 cm^{-1}; and the symmetric SO_3 bend, $\delta_s(SO_3)$ from about 630-650 cm^{-1}. Careful analysis of these bands provides knowledge about the types the ionic associations forming in the polymer: salt complex and about how these associations change as a function of salt concentration and temperature. Understanding the types of ionic association present in a system is crucial to understanding charge transport and therefore, conductivity in the system.

To this end, the ionic associations present in the PEO:LiTf have been thoroughly examined in both the polymer and small model glyme molecules.[33-35] Through these studies, the $\delta_s(CF_3)$ band at 751-752 cm^{-1} has been assigned to the "free" triflate ion, Tf^-, in which the cation and anion are solvent separated. Likewise, the band at 756-758 cm^{-1} has been assigned to the contact ion pair, LiTf, and the band at 761-762 cm^{-1} has been associated with higher aggregate species, such as $[Li_2Tf]^+$. While these modes are not expected to have precisely identical vibrational frequencies in the polyether and polyimine systems, the general trend of increasing degree of association yielding increased vibrational frequencies reasonably can be expected to be maintained in both systems. Thus, in the polyamines, the expectation is that the frequency of "free" triflate would be less than that of contact ion pair, which would be less that of triple cation, which would be less than that of higher order aggregate species. These assignments have been extended previously into very similar imine systems, including PEI, PMEI and model compounds for the both polymers.[12,24,36]

Therefore, higher frequency of the $\delta(CF_3)$ band (762 cm^{-1}) seen in PMPI:LiTf spectra in Figure 4-4, as compared to the same band (758 cm^{-1}) in the PMEI:LiTf spectra suggests the ions in PMPI experience an overall higher degree of aggregation than their counterparts in PMEI. Deconvolution of both features reveals multiple overlapping bands, summarized in Table 4-2. As a general trend, ionic association increases with increasing salt concentration in both systems. The band present in the 20:1 $N:Li^+$ PMEI:LiTf spectra resolves in to three bands: 755 cm^{-1} (37%

integrate intensity), 757 cm^{-1} (58%) and 761 cm^{-1} (5%). The latter two bands may be assigned to the contact ion pair and the triple ion respectively. It is possible that the 755 cm^{-1} population may be the "free" ion. However, 755 cm^{-1} is on upper edge of what may be designated as the "free" ion with confidence, so this population may represent a second variety of contact ion pairing. With additional salt, the degree of association increases. By a composition of 5:1 $N:Li^+$, the triple ion accounts for just over a quarter (26%) of the ion population in PMEI:LiTf. The frequencies and integrated of the PMEI:LiTf given above are in close proximity to publish results.[11] It should be noted that in that study, the lowest frequency assigned to the "free" ion was 752 cm^{-1}.

Table 4-2: Summary of band center frequencies in cm^{-1} (integrated intensities) of $\delta_s(CF_3)$ bands of PMEI:LiTf and PMPI:LiTf at 20:1, 10:1 and 5:1 $N:Li^+$ ratios

	20:1 $N:Li^+$	10:1 $N:Li^+$	5:1 $N:Li^+$
PMEI:	761 cm^{-1} (5%)	760 cm^{-1} (22%)	760 cm^{-1} (26%)
	757 cm^{-1} (58%)	757 cm^{-1} (52%)	758 cm^{-1} (36%)
	757 cm^{-1} (37%)	755 cm^{-1} (26%)	754 cm^{-1} (38%)
PMPI:LiTF	(0%)	764 cm^{-1} (26%)	766 cm^{-1} (80%)
	762 cm^{-1} (64%)	762 cm^{-1} (27%)	762 cm^{-1} (7%)
	758 cm^{-1} (36%)	758 cm^{-1} (48%)	757 cm^{-1} (13%)

In comparison, only contact ion pairs (758 cm^{-1}) and triple ions (762 cm^{-1}) are present in the 20:1 $N:Li^+$ PMPI:LiTf system, with the triple ions accounting for nearly two thirds of the ion population (64%). Increasing salt content increases ion

association further. By a composition of 5:1 $N:Li^+$ a third population at an even higher frequency (766 cm^{-1}) accounts for 80% of the total population. That the integrated intensity of the triple ion population is less than that of the contact ion population is unexplained at this time.

This difference in degree of association in the two systems is also reflected in the $\nu_s(SO_3)$ band. Figure 4-5 illustrates the spectra of PMPI, PMEI and their LiTf complexes from 20:1 to 5:1 $N:Li^+$ over the range from 900-1200 cm^{-1}. In both systems an underlying host band complicate spectral interpretation. Nonetheless, the development of the $\nu_s(SO_3)$ band is clear in both systems. In the PMEI:LiTf system, the band frequency in the 20:1 $N:Li^+$ is difficulty to determine, but the band is clearly centered at 1041 cm^{-1} in the 10:1 and 5:1 $N:Li^+$ complexes. This frequency has previously been attributed to

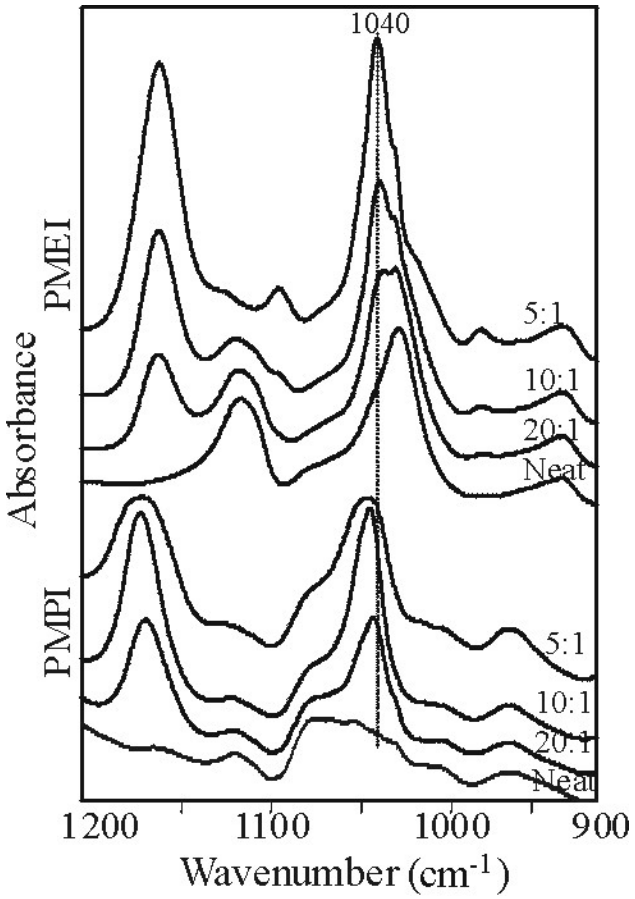

Figure 4-5: IR Spectra from 1200 to 900 cm^{-1} for PMPI, PMPI:LiTf ($N:Li^+$= 20:1, 10:1, 5:1), PMEI and PMEI:LiTf ($N:Li^+$= 20:1, 10:1, 5:1)

contact ion pairs.[33,35,37,38] The higher frequency of the same band in the PMPI:LiTf spectra indicates higher order aggregates are present. The band steadily grows n both width and intensity and shifts center from 1044 cm^{-1} to 1046 cm^{-1}. These changes are interpreted as a widening of potential energy environments present in the system as the population experiences a increased variety of ionic associations. The bandwidth and possible changes in the underlying PMPI band present from about 1060 cm^{-1} to 1090 cm^{-1} may obscure the detail of the overlying $\nu_s(SO_3)$ band and make deconvolution impossible.

The IR spectra of $\nu_s(SO_3)$ and $\delta_s(CF_3)$ regions of PMPI and its precursor analog PPI are shown in Figure 4-6. PMPI and PPI share the same backbone structure, but PPI is a secondary amine, while PMPI is a methyl-substituted tertiary amine. As previously discussed, the $\nu_s(SO_3)$ band appears in PMPI around 1044-1046 cm^{-1}

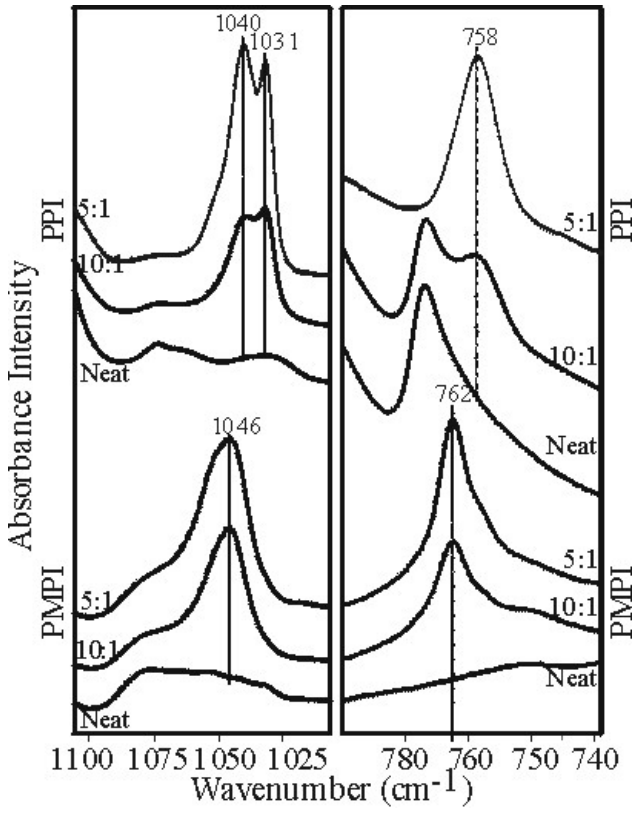

Figure 4-6: IR Spectra for the triflate ion SO_3 symmetric stretch, $\nu_s(SO_3)$, region (left) and the CF_3 symmetric stretch, $\nu_s(CF_3)$, region fir PPI, PPI:LiTf ($N:Li^+$ = 10:1, 5:1), PMPI and PMPI:LiTf ($N:Li^+$ = 10:1, 5:1)

and grows in intensity and width, with increasing salt concentration. This suggests the presence of aggregated species even at salt concentrations as low as 20:1 N:Li^+. Deconvolution of band reveals an even higher order aggregate population represented by a band at 1053 cm^{-1}. In PPI, this mode, $\nu_s(SO_3)$, appears at a lower frequency and is split into two distinct bands at 1031 cm^{-1} and 1040 cm^{-1}. The 1031 cm^{-1} band, due to "free" ions, is favored at lower salt concentrations, while the 1040 cm^{-1} band, due to contact ion pairs, is favored at higher salt concentrations. This tendency toward a higher degree of association is also present in the $\delta_s(CF_3)$ mode, shown on the right side of Figure 4-6. In the PMPI spectra, the band centered at 760 cm^{-1} indicates the prevalence of the triple ion. In the PPI spectra, a band centered at 758 cm^{-1} is present suggesting the species present are predominantly contact ion pair. The band centered at 779 cm^{-1} in the neat PPI and in the 10:1 N:Li^+ spectra is not related to the anion, but is a polymer band which is engulfed by in the $\delta_s(CF_3)$ band at higher salt compositions.

These two modes, $\delta_s(CF_3)$ and $\nu_s(SO_3)$, indicate that PMPI experiences a higher degree of ionic association than does PPI. This behavior is consistent with that of the homolog systems of PMEI and PEI. PMEI appears to contain contact ion pairs and higher aggregate species even at modest salt concentrations, while PEI appears to develop triple ions only at high salt concentration, but exhibits "free" ions and contact ion pairs at lower LiTf concentrations.[11,12] A possible explanation for this trend is the interaction of the amine hydrogen in PEI and PPI with the anion. This would, in turn, free the cation to interact with the backbone heteroatoms. A

second explanation may lie in the presence of the amino methyl group in PMEI and PMPI. This group may spatially hinder the approach of the cation to the backbone heteroatoms making cationic association with the anion favored, and thereby resulting in more highly aggregated ionic species.

A high degree of ionic association in the PMPI:LiTf system is also illustrated Figure 4-7, which contains the IR spectra of PMPI and PMEI in the $\delta_s(SO_3)$ region. The band and shoulder structure in the 640-630 cm^{-1} region increases in intensity and breadth, but does not shift position or shape with increasing LiTf concentration. In contrast, in the PMPI:LiTf system the $\delta_s(SO_3)$ band initially appears centered at 640 cm^{-1}. With increased salt content, the band increases in intensity and width experiences a cumulative shift of approximately 5 cm^{-1} as LiTf concentration is increased from 20:1 to 5:1 $N:Li^+$. In addition, it develops a high frequency shoulder. Some researchers have attempted assignments of frequencies to

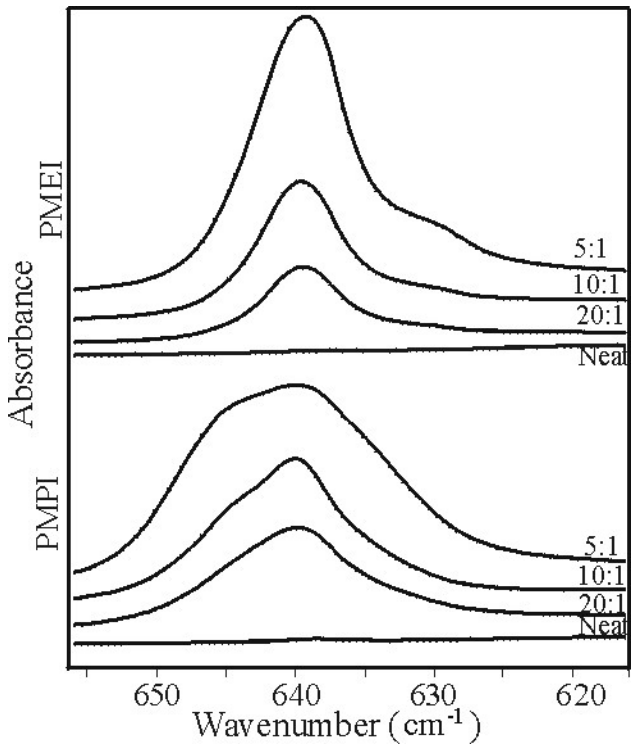

Figure 4-7: IR Spectra for the triflate ion SO_3 symmetric deformation, $\delta_s(SO_3)$, region for PMPI, PMPI:LiTf ($N:Li^+$= 20:1, 10:1, 5:1), PMEI and PMEI:LiTf ($N:Li^+$= 20:1, 10:1, 5:1)

specific ionic association; those assignments are tentative and are not used here.[39] However, the general trend of increased frequency relating to increased aggregation holds. This indicates the overall degree of ionic association experienced by PMPI:LiTf is higher than that in the PMEI:LiTf system.

4.4.3 Temperature Dependence

The behavior of the IR spectrum as a function of temperature of the PMPI system was also investigated. IR spectra were collected over the range of 30° to 80°C in 10°C increments. Additionally, spectra were taken at room temperature before the sample was heated, and again after it had cooled from 80°C. Spectra from 1200 cm^{-1} to 1500 cm^{-1} are presented in Figure 4-8. Bands in this region have been assigned to a complex mixture of CH_2 and CH_3 twists, wags and deformations in PMEI and the closely related poyl(ethylethyleneimine), PEEI, which has pendent ethyl, rather than methyl, groups attached to the nitrogen atom.[13] The spectra in this figure are stacked in order of increasing temperature, beginning with the initial room temperature scan and progressing upward to 80°C. The uppermost spectra is the final room temperature scan, collected after the sample had cooled from 80°C to room temperature and allowed to equilibrate for one hour. Essentially no changes occur in this region of the neat PMPI spectra below 40°C or above 60°C, while significant changes occur between 40°C and 60°C. Some spectral changes incurred at elevated temperatures are retained even after cooling. The most dramatic example of this is the band pair at 1450 cm^{-1} and 1375 cm^{-1}. Other modes in the region

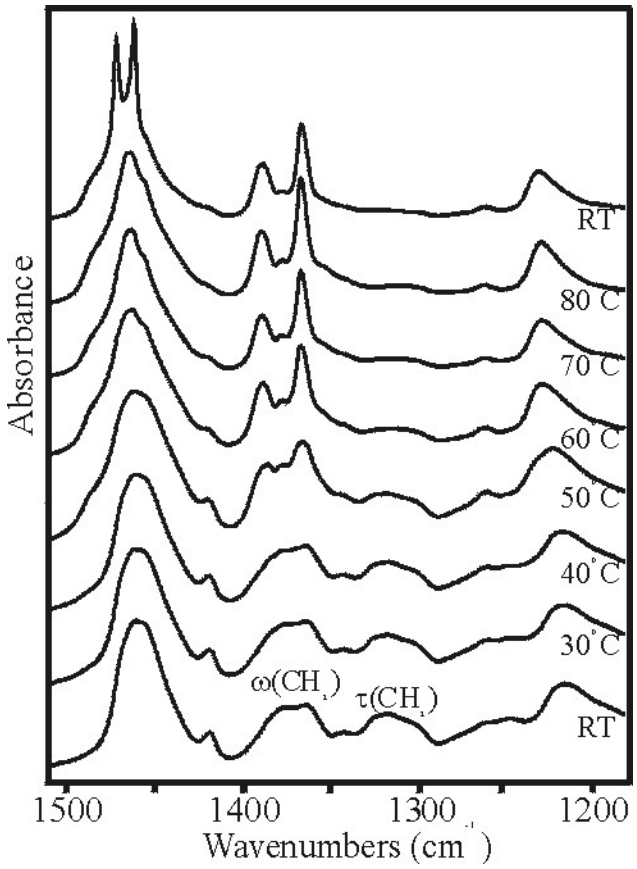

Figure 4-8: IR spectra from 1500 to 1200 cm^{-1} for PMPI from room temperature (RT) to 80°C in 10°C increments. Uppermost spectrum is at RT after polymer cooled from 80°C

simply decrease in intensity, eventually disappearing, and do not return with cooling. An example of this behavior is the CH_2 twist, $\tau(CH_2)$, at 1317 cm^{-1}, which slowly loses intensity as temperature increases, until it disappears into the baseline at 80°C. This feature does not reappear in the uppermost spectra taken after the sample was returned to room temperature. In contrast, the CH_2 wag, $\omega(CH_2)$, at 1365-1390 cm^{-1} changes from a broad band feature to three distinct peaks by 50°C; these peaks are largely retained upon the sample return to room temperature. This change implies that the structure of the polymer change from a broad distribution of numerous different local structures at temperature below 40°C to three distinct local structure populations at temperatures above 50°C. In PEO systems, frequency shifts in this region have been attributed to changes in local conformations.[27] Unfortunately, knowledge of the PMPI system is not sufficient to

allow confident assignment of the observed changes to particular conformational alterations. One possible reason for the retention of the spectral changes upon cooling to room temperature is that an energy barrier to a more thermodynamically favorable state is surmounted between 40°C and 50°C. Once the polymer achieves this lower energy state at elevated temperature, it remains in this lower energy state upon cooling. An alternate explanation is that structural relaxation kinetics slower than the cooling rate may be present. This would result in the apparent retention of local structures achieved at elevated temperatures upon cooling, but if the sample were re-examined after many hours or days, the spectrum would return to the initial room temperature state. Unfortunately, these data were not collected; therefore, no definitive statement can be made regarding the cause.

However, the kinetics argument is strengthened by the behavior of the asymmetric CH_3 deformation, $\delta_s(CH_3)$, band at 1460-1475 cm^{-1} and the CH_2 rock, $\rho(CH_2)$, at 710-730 cm^{-1}. In both instances, a new population develops upon heating, as evidenced by the emergence of a second band. Upon cooling back to room temperature, the new band is retained, but the original band is also present. For example, the δ_sCH_3 band initially appears at 1461 cm^{-1} in the room temperature spectrum (Figure 4-8). With heating, a band at 1473 cm^{-1} develops. When the sample is cooled, both bands are present. This is seen even more spectacularly in Figure 4-9, which contains the $\rho(CH_2)$ region (710-310 cm^{-1}) of neat PMPI at room temperature before heating, at 80°C and at room temperature after heating. The initial room temperature spectrum contains a dominant band at 730 cm^{-1} and a

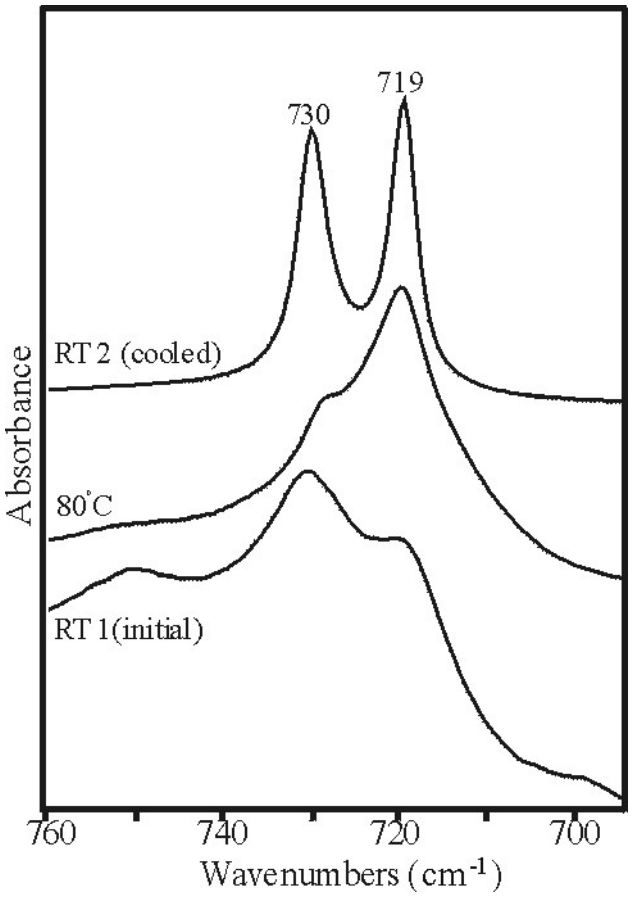

Figure 4-9: IR spectra from 690 to 760 cm^{-1} for neat PMPI at room temperature (lower), 80°C (middle) and room temperature after cooling from 80°C (upper)

smaller side band to 719 cm^{-1}. At elevated temperatures the relative intensity of the two bands shifts so that the 719 cm^{-1} band is much more intense than the barely visible 730 cm^{-1} band. Upon return to room temperature, both bands are present as narrow symmetric features of approximately the same intensity. Additionally, n the cooled sample, the bands are narrower than in either the initial room temperature spectrum or the 80ºC spectrum, indicating a narrower distribution of states clustered around two distinct populations in the cooled sample. This may mean that two time scales are active: one of which is a relaxation step slower than the cooling rate, which prevents a total return to the original population within the time frame of the cooling rate. These changes are most likely on a local scale, since while they are clearly seen in the IR spectra, no evidence of macro-scale or long range phase changes is present in the DSC data over the same temperature range. Therefore,

these changes are probably conformational and local in nature and do not impact the long-range order or macro-level behavior of the system.

It is worth noting that adding salt to the system effectively eliminates the IR dependence on temperature, at least up to 80°C. Sample compositions of 20:1, 10:1 and 5:1 N:Li^+ show virtually no temperature induced changes in the IR spectra, with the room temperature, the elevated temperature and the return to room temperature spectra exhibiting essentially no variation. This implies that a thermodynamically favorable structure is already in place in the salt containing systems, and that this structure is effectively "locked" into place via strong cation-heteroatom interactions. Though this behavior is not common, it has precedence. IR spectra of PMEI also show negligible temperature dependence upon the introduction of lithium triflate into the polymer, likewise suggesting a "locked-in" local structure.[13]

4.5 CONDUCTIVITY BEHAVIOR

The absence of changes in local structure as a function of temperature is also apparent in the conductivity behavior of the PMPI:LiTf system shown in Figure 4-10. No dramatic increase conductivity occurs between room temperature and 80°C in either PMEI:LiTf or PMPI:LiTf. This implies that no major changes in ionic mobility occur over this temperature range. The steady climb in conductivity with increasing temperature instead suggests that this increase is due to slight enhancements in ionic mobility associated with greater kinetic energy due to increased temperature rather than a significant change in local structure or ionic

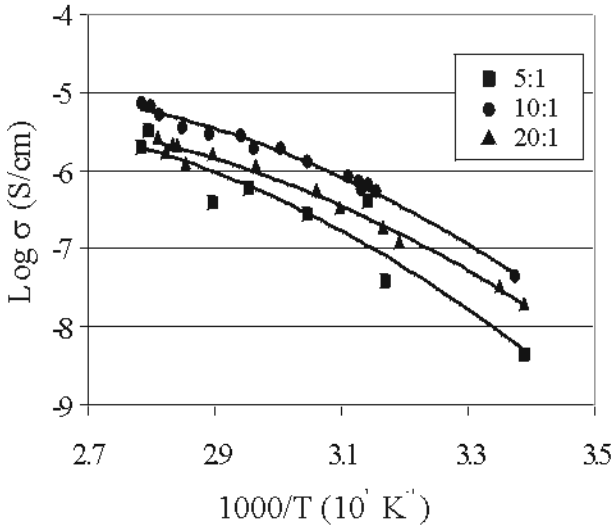

Figure4-10: Log of conductivity of PMPI:LiTf (N:Li^+= 20:1, 10:1, 5:1) as a function of 1000/T over the range 20°C to 80°C

association. Such a change would be expected to engender a large, abrupt jump in conductivity. Likewise, the half order of magnitude increase in conductivity seen between the 20:1 and 10:1 N:Li^+ compositions most likely stems from the increased number of charge carriers present at the higher salt concentration rather than a significant change in ionic association or local structure. At both 20:1 and 10:1 N:Li^+, PMPI:LiTf exhibits lower conductivity than that reported by either Tanaka, *et al*[10] or Sanders, *et al*[11] for PMEI:LiTf. This is not surprising given that the spectral data show PMPI:LiTf experiences a higher degree of association than PMEI:LiTf, which would result in fewer available charge carriers in PMPI:LiTf than are present in PMEI:LiTf at the same salt concentration.

Of the compositions shown in Figure 4-11, 10:1 N:Li^+ demonstrates the highest conductivity at all temperatures in the 25°C to 80°C range. This behavior is common in many polymer electrolytes. Increasing conductivity with increasing salt concentration up to a maximum, followed by a decrease in conductivity has been reported in a number of related polymer electrolyte systems, with PEO[40,41],

poly(propyleneoxide),[42-44] PMEI[10] and branched PEI[45] also exhibiting conductivity maxima at around10:1 N:Li^+.

4.6 CONCLUSIONS

PMPI is a thick amber liquid, strongly resembling dark honey in both viscosity and color. The neat material exhibits a glass transition around -88°C, which increases steadily with addition of LiTf, reaching -28°C at N:Li^+ ratio of 5:1. No indications of major phase transitions are present in DSC data between 25°C and 80°C, suggesting a stable macroscopic structure in the material at all temperatures and salt concentrations addressed in this study.

Infrared spectra suggest that ionic association in PMPI:LiTf electrolytes is highly aggregated even at low salt concentration. This is notably different than PMEI:LiTf electrolytes in which ionic association is a strong function of salt concentration with "free" and contact ion pair prevalent at low salt concentrations. The differences in association type and dependence on salt concentration are most likely due to the increased conformational degrees of freedom present in PMPI as a result of the third backbone carbon, which offers an additional dihedral angle and rotational bond axis not present in PMEI with only two backbone carbons. These added degrees of freedom may allow stronger cation-heteroatom associations, which would, in turn, force anions to associate more readily with cations not already associated to the backbone heteroatoms.

Spectral evidence also suggests the presence of kinetic effects upon heating the neat PMPI polymer. PMPI fails to completely return to its initial room temperature state after heating, but instead retains some spectral features of the elevated temperature state, as well as the initial room temperature state. This behavior indicates the presence of relaxation kinetics occurring on a time scale slower than the cooling rate. Unfortunately, this cannot be conclusively proven with the data presented here. In contrast, the IR spectra of the PMPI:LiTf complexes do not exhibit this behavior but show virtually no temperature dependence in any region, including those affiliated with ionic association. This suggests that the system exists in a thermodynamically stable amorphous configuration over the temperature range studied here. DSC data show no thermal transitions in the 25-80°C range, supporting the assertion that any structural changes are local, rather than long range macroscopic effects. Likewise, the absence of an abrupt rise in conductivity with addition of either heat or salt also supports the hypothesis of a "locked-in" structure.

The ionic conductivity of the PMPI:LiTf system is between 10^{-9} and 10^{-8} S cm^{-1} at room temperature, depending on salt concentration. Throughout the 25°C to 80°C temperature range, the 10:1 N:Li^+ composition exhibits a higher conductivity than either the 20:1 or 5:1 N:Li^+ composition. Though the conductivity of all compositions increases with the addition of heat, it reaches only about 10^{-5} S cm^{-1} at the highest performing salt composition (10:1 N:Li^+) at 80°C. This is

disappointingly low for a polymer electrolyte and renders the PMPI:LiTf system unsuitable for most applications.

4.5 REFERENCES

(1) Silverstein, S. *Where the Sidewalk Ends* 30th Anniversary Special Edition ed.; HarperCollins Publishers, 2004.

(2) Villoslada, R.; Alonso, B.; Casado, C. M.; GarciÌ□a-Armada, P.; Losada, J. *Organometallics* **2009**, *28*, 727-733.

(3) Lakard, B.; Herlem, G.; de Labachelerie, M.; Daniau, W.; Martin, G.; Jeannot, J.-C.; Robert, L.; Fahys, B. *Biosens. Bioelectron.* **2004**, *19*, 595-606.

(4) Martinovic, J.; Chiorcea-Paquim, A.-M.; Diculescu, V. C.; Van Wyk, J.; Iwuoha, E.; Baker, P.; Mapolie, S.; Oliveira-Brett, A.-M. *Electrochim. Acta* **2008**, *53*, 4907-4919.

(5) Maurice W. P. L. Baars; Söntjens, S. H. M.; Fischer, H. M.; Peerlings, H. W. I.; Meijer, E. W. *Chemistry - A European Journal* **1998**, *4*, 2456-2466.

(6) Murugan, E.; Sherman, R. L.; Spivey, H. O.; Ford, W. T. *Langmuir* **2004**, *20*, 8307-8312.

(7) Paul, J. L.; Jegat, C.; Lassègues, J. C. *Electrochim. Acta* **1992**, *37*, 1623-1625.

(8) Bringley, J. F.; Harder, J. W.; Qiao, T. A.; Penner, T. L.; Wang, R., inventors. U.S. Patent Application No. 20080241266. United States Patent and Trademark Office, Washington D.C., 2008.

(9) Tanaka, R.; Ueoka, I.; Takaki, Y.; Kataoka, K.; Saito, S. *Macromolecules* **1983**, *16*, 849-853.

(10) Tanaka, R.; Fujita, T.; Nishibayashi, H.; Saito, S. *Solid State Ionics* **1993**, *60*, 119-23.

(11) Sanders, R. A.; Snow, A. G.; Frech, R.; Glatzhofer, D. T. *Electrochim. Acta* **2003**, *48*, 2247-2253.

(12) York, S.; Frech, R.; Snow, A.; Glatzhofer, D. *Electrochim. Acta* **2001**, *46*, 1533-1537.

(13) Frech, R.; Giffin, G. A.; Castillo, F. Y.; Glatzhofer, D. T.; Eisenblaetter, J. *Electrochim. Acta* **2005**, *50*, 3963-3968.

(14) York, S. S.; Buckner, M.; Frech, R. *Macromolecules* **2004**, *37*, 994-999.

(15) Hu, L., University of Oklahoma, 2005.

(16) Lee, J.; Lee, K.; Kim, H. *Bull. Korean Chem. Soc.* **1996**, *17*, 115-16.

(17) Hu, L.; Frech, R.; Glatzhofer, D. T.; Mason, R.; York, S. S. *Solid State Ionics* **2008**, *179*, 401-408.

(18) Mason, R. N.; Frech, R.; Hu, L.; Glatzhofer, D. T. *Solid State Ionics*, *(Submitted)*.

(19) Hubbard, H. V. S. A.; Southall, J. P.; Cruickshank, J. M.; Davies, G. R.; Ward, I. M. *Electrochim. Acta* **1998**, *43*, 1485-1492.

(20) Angell, C. A.; Fan, J.; Liu, C.; Lu, Q.; Sanchez, E.; Xu, K. *Solid State Ionics* **1994**, *69*, 343-53.

(21) Anantha, P. S.; Hariharan, K. *Solid State Ionics* **2004**, *176*, 155-162.

(22) Rocher, N. M.; Frech, R. *Macromolecules* **2005**, *38*, 10561-10565.

(23) York, S. S.; Boesch, S. E.; Wheeler, R. A.; Frech, R. *Macromolecules* **2003**, *36*, 7348-51.

(24) York, S. S.; Boesch, S. E.; Wheeler, R. A.; Frech, R. *PhysChemComm* **2002**, *5*, 99-111.

(25) Boesch, S. E.; York, S. S.; Frech, R.; Wheeler, R. A. *PhysChemComm* **2000**, *1*, 1.

(26) Sanders, R. A.; Boesch, S. E.; Snow, A. G.; Hu, L.; Frech, R.; Wheeler, R. A.; Glatzhofer, D. T. *Polym. Prepr. (Am. Chem. Soc., Div. Polym. Chem.)* **2003**, *44*, 966-967.

(27) Frech, R.; Huang, W. *Macromolecules* **1995**, *28*, 1246-51.

(28) Dissanayake, M. A. K. L.; Frech, R. *Macromolecules* **1995**, *28*, 5312-19.

(29) Matsuura, H.; Fukuhara, K. *J. Polym. Sci., Part B: Polym. Phys.* **1986**, *24*, 1383-400.

(30) Tadokoro, H.; Chatani, Y.; Yoshihara, T.; Tahara, S.; Murahashi, S. *Makromol. Chem.* **1964**, *73*, 109-27.

(31) Lightfoot, P.; Mehta, M. A.; Bruce, P. G. *Science* **1993**, *262*, 883-5.

(32) Papke, B. L.; Ratner, M. A.; Shriver, D. F. *J. Electrochem. Soc.* **1982**, *129*, 1434-8.

(33) Schantz, S.; Sandahl, J.; Borjesson, L.; Torell, L. M.; Stevens, J. R. *Solid State Ionics* **1988**, *28-30*, 1047-53.

(34) Frech, R.; Huang, W. *Solid State Ionics* **1994**, *72*, 103-7.

(35) Huang, W.; Frech, R.; Wheeler, R. A. *J. Phys. Chem.* **1994**, *98*, 100-10.

(36) Sanders, R. A.; Frech, R.; Khan, M. A. *J. Phys. Chem. B* **2004**, *108*, 12729-12735.

(37) Frech, R.; Huang, W. *J. Solution Chem.* **1994**, *23*, 469-81.

(38) Petersen, G.; Jacobsson, P.; Torell, L. M. *Electrochim. Acta* **1992**, *37*, 1495-1497.

(39) Seneviratne, V.; Furneaux, J. E.; Frech, R. *Macromolecules* **2002**, *35*, 6392-6396.

(40) Caruso, T.; Capoleoni, S.; Cazzanelli, E.; Agostino, R. G.; Villano, P.; Passerini, S. *Ionics* **2002**, *8*, 36.

(41) Tominaga, Y.; Takizawa, N.; Ohno, H. *Electrochim. Acta* **2000**, *45*, 1285-1289.

(42) Armand, M. B. *Solid State Ionics* **1994**, *69*, 309-319.

(43) Ferry, A.; Jacobsson, P.; Stevens, J. R. *J. Phys. Chem.* **1996**, *100*, 12574-12582.

(44) Watanabe, M.; Ogata, N. In *Polymer Electrolyte Reviews I*; MacCallum, J. R., Vincent, C. A., Eds.; Elsevier Science: New York, 1987; Vol. I.

(45) Ferry, A. *J. Phys. Chem. B* **1997**, *101*, 150-157.

CHAPTER 5: MODEL COMPOUNDS FOR PEI AND PPI

The cords of passion and desire weave a binding net around you. Worldly confrontation makes you stiff and inflexible. The trap of duality is tenacious. Bound, rigid, and trapped, you cannot experience liberation.

Lao Tzu[1]

5.1 INTRODUCTION

As seen in the previous chapters, the vibrational signatures of polymer electrolytes can be complex and difficult to confidently interpret, particularly in the absence of a definitive crystal structure. One method available to make sense of such complicated systems is the use of model compounds. Often, by employing small organic molecules that mimic the structure and behavior of given aspects of the polymer electrolyte, insight into the complex nature of the polymer electrolyte can be acquired.[3-12] Model compounds are usually small monomeric or oligomeric versions of the polymer, though for polymers with multiple functional groups, the model may imitate only a portion of the polymer. As such, these model compounds normally exhibit less complicated spectra than the polymer and often are able to form crystals when complexed with salts, which are impossible or at least difficult, to obtain from the polymer. Additionally, computations involving the small molecules are feasible, where it is impractical, if not impossible, to perform like computations on the polymer itself. These features allow vibrational assignments to be made more concretely and the simplified spectra offer the possibility of straightforward

interpretation. Knowledge gained from the model compounds can then be applied to the more intricate polymer electrolyte.

5.1.1 Selection of Model Compounds

Two model compounds are employed in this study: N,N'-dimethylethylenediamine (N,N'-DMEDA) and N,N'-dimethylpropylenediamine (N,N'-DMPDA). These materials are used to model poly(ethylenimine), PEI, and poly(propylenimine), PPI, respectively. The molecular structures of all four materials are given in Figure 5-1.

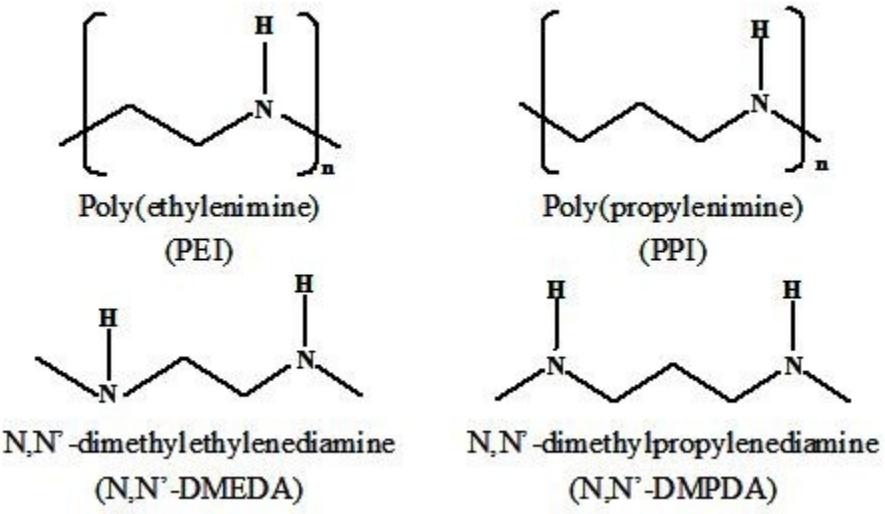

Figure 5-1: Structures of PEI and PPI and their model compounds N,N'-DMEDA and N,N'-DMPDA

While the overarching goal is to use the model compounds to gain general insight into the polymer electrolytes, some specific points of interest are the hydrogen bonding interactions and the ionic associations when the compound forms a complex with lithium triflate. Behaviors of the backbone vibrational modes are

also relevant. As seen in Figure 5-1, the model compounds mimic the polymers in both backbone structure and presence of NH functional groups. Diamines were selected for two basic reasons: ease of handling and potential interactions between intramolecular NH groups and between heteroatoms in a common molecule and the salt cations. Diamines are the smallest compounds that allow for both chemical functions and are of sufficiently low volatility to be easily handled. Having multiple heteroatoms in the backbone is important for exploring both inter- and intramolecular hydrogen bonding and the possibility of ionic associations involving multiple heteroatoms on the same molecule.

5.1.2 Investigation of Model Compounds

This investigation was divided into three segments: addition of lithium triflate, dilution in carbon tetrachloride, CCl_4, and simultaneous salt addition and CCl_4 dilution. These routes were chosen based on results of previously published studies on similar materials.[9,13,14] The addition of a salt to the model compound is logical method of investigation since the polymer electrolyte is formed by the dissolution of a salt into a polymer. This technique simply imitates that used to study the polymer. This should give information about the types of ionic associations taking place in the systems and hint at changes occurring in the backbone conformation of the polymer upon ionic associations, both of which can be related to the polymer electrolytes. Dilution with CCl_4 was chosen in an effort to elucidate the hydrogen bonding interactions in the systems. The combination of the two methods may yield

additional insight into the hydrogen bonding behavior and ionic associations of the system

Extensive hydrogen bonding is believed to exist within the PPI system, but no studies have directly addressed this. It is hoped that the use of the N,N'-DMPDA model compound will be able to provide meaningful information regarding the types and behaviors of the hydrogen bonding interactions present in PPI. Published

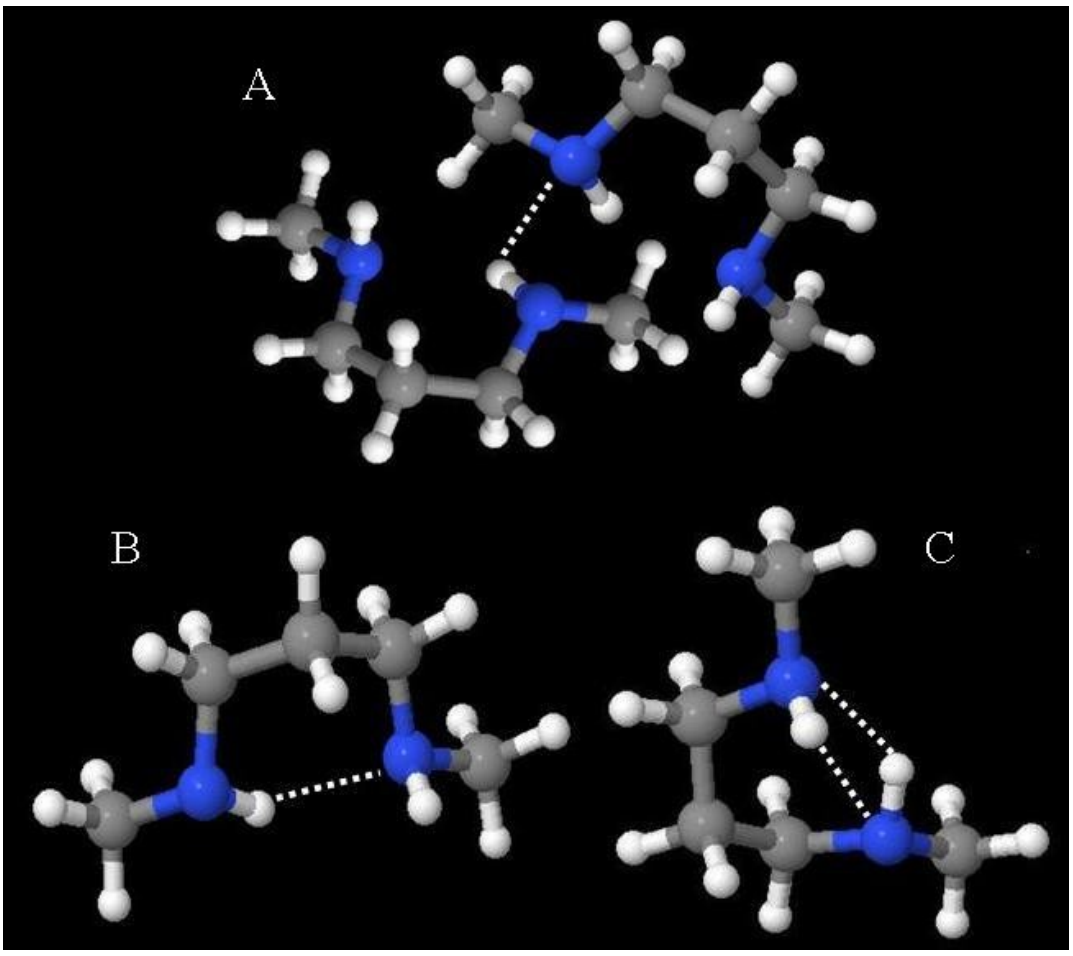

Figure 5-2: Proposed types of hydrogen bonding interactions in N,N'-DMEDA and N,N'-DMPDA.
A) Intermolecular hydrogen bonding.
B) Intramolecular hydrogen bonding involving one N-H interaction
C) Intramolecular hydrogen bonding involving both N-H interactions

computational studies have suggested that N,N'-DMEDA is capable of three distinct types of hydrogen bonding interactions.[3] The first type is hydrogen bonding between amine groups on two different N,N'-DMEDA molecules, known as intermolecular hydrogen bonding (Fig 5-2.A). The other two types are forms of intramolecular hydrogen bonding. One type involves the interaction between a single nitrogen on one end of the diamine and the amino hydrogen on the other end (Fig 5-2.B). The last type entails simultaneous interaction of both possible pairs of complementary amino hydrogen and heteroatom (Fig 5-2.C). For simplicity sake, representations of all three proposed hydrogen bonding interactions are provided in Figure 5-2. These drawings are shown utilizing the N,N'-DMPDA molecule. Previously published work[3] addressed only N,N'-DMEDA, but it is reasonable to suppose that the same types of interactions may be present in N,N'-DMPDA and by extension in PPI. Some preliminary computations with N,N'-DMPDA supporting this hypothesis are presented later in this chapter (5.4).

The types of hydrogen bonding interactions that may be present in the system under any given condition are unknown. It is hoped that by progressively diluting the model compounds with CCl_4, knowledge about the hydrogen bonding interactions may be attained. Since the CCl_4 serves as a physical obstruction separating the model compound molecules, at a sufficiently high concentration, it should disperse the model compound molecules enough to prevent interactions between different molecules. This would break almost all intermolecular hydrogen bonding interactions, while leaving intramolecular hydrogen bonding interactions

largely intact. It is not expected that, even at extremely large concentrations, CCl_4 will cause significant disruption of intramolecular hydrogen bonding interactions. However, cation association is expected to impact these interactions in a nontrivial way. Thus, examining the behavior of the systems as a function of lithium triflate concentration is also an important factor in determining the nature of hydrogen bonding interactions in the systems.

5.2 PROCUREMENT AND APPEARANCE

Both model compounds were purchased from commercial suppliers. N,N'-dimethylethylenediamine (99%) was purchased from Sigma-Aldrich. N,N'-dimethylpropylenediamine was purchased from TCI (99%) and Aldrich (97%). N,N'-DMEDA and N,N'-DMPDA are liquids at room temperature. Both compounds are colorless clear liquids with a viscosity comparable to cough syrup. Viscosity of the materials increases with salt addition. Lithium trifluoromethanesulfonate (LiTf) was dissolved in both model compounds up to a composition of 3:1 N:Li^+ molar ratio without precipitating out of solution. These solutions appeared highly viscous colorless liquids. Efforts to increase the amount of LiTf present beyond a 3:1 N:Li^+ composition were not consistently successful.

Samples with LiTf were covered and stored for several months. During this time, crystals were formed, but these were not suitable for X-ray diffraction analysis (XRD), so no crystal structures were obtained. Since a crystal structure for N,N'-DMEDA with sodium triflate (NaTf) has previously been published,[15] N,N'-

DMPDA:NaTf crystals were also attempted. As in the efforts with LiTf, crystals were formed but were not useable for XRD analysis.

Addition of CCl_4 resulted in miscible colorless clear solutions whose viscosity decreased with increasing CCl_4 concentration. Solutions ranging from 40:1 to 1:5 C:N were made. These solutions turned cloudy amber to dark brown after standing for several days, but all IR and Raman analyses were performed well before and any color change was observed.

5.3 VIBRATIONAL SPECTROSCOPY

5.3.1 NH Stretching Region

5.3.1.1 Introduction to Hydrogen Bonding and the Inductive Effect

In the basic sense, a hydrogen bond occurs when a hydrogen atom already covalently bonded to one atom forms a simultaneous link to another atom. In 1939, Pauling attributed this to the electronegativity difference between the hydrogen and its covalently bonded partner allowing a shift in electron density away from the hydrogen atom, which "descreens" the hydrogen atom[16]. This proton is then able to interact with an acceptor atom having unpaired electrons or polarizable π electrons. In the intervening years, hydrogen bonding interactions have been defined by less stringent criteria. More current works seem to favor the expanded definition given in 1960 by Pimentel and McClellan. This definition requires two criteria be met in order to declare an interaction between A-H and B a hydrogen bond[17]:

"1) there is evidence of hydrogen bond formation (association or chelation)

2) there is evidence of that this new bond linking A-H and B specifically involves a hydrogen atom already bonded to A"

This definition allows for a wide variety of interactions which do not meet Pauling's standard, particularly those in biological systems, to be included as hydrogen bonds. However, it does little to clarify the nature hydrogen bonding. Electrostatics does not completely explain the complex phenomenon of hydrogen bonding. Nonetheless, it does offer an excellent basis for understanding the spectral changes associated with hydrogen bonding interactions.

The NH stretching vibration is sensitive to hydrogen bonding.[16,18] Knowing the expected spectral impacts of H-bond formation, strengthening, breakage, *etc.* allows for more complete correlation of the data to the system behavior. The influence of hydrogen bonding interactions on IR and Raman spectral data are well studied and clear. Hydrogen bonding interactions shift the NH stretching, ν(NH), to a lower frequency, broaden the bandwidth and increase the intensity of the band.[16,17,19] The electronic redistribution that occurs upon hydrogen bond formation withdraws electron density from the N-H bond. This lengthens and weakens the bond, which in turns shifts the vibrational frequency of the bond lower as compared to the stronger, shorter unassociated N-H bond[16]. The cause of the band broadening is less clear. Normally, it is assumed that an increase in bandwidth is due to

heterogeneous broadening of the potential energy distribution within the population[9]. In this case, formation of hydrogen bonds is known to broaden the potential energy curve of the N-H group.[16] It is likely that the increase in the number of potential energy environments of the N-H with the imposition of the hydrogen bonding is the source of the band broadening in the spectra, since not every N-H group will simultaneously experience an identical hydrogen bonding interaction.[20] The intensity change is due to changes in the dipole moment due to hydrogen bonding which increases the first derivative of the dipole moment, thereby increasing the IR intensity.[19]

Taking the Pauling definition of hydrogen bonding, in which electron density shifts away from the hydrogen onto its bonded partner atom, in this case nitrogen, it is a simple matter to see how a dipole ($\mapsto$) is created in the N-H bond. Now, consider the selection rules for Raman and IR. IR activity is a function of the first derivative of the dipole moment and as such favors molecules/groups/bonds which experience larger dipole moments[21]. Thus, the stronger the dipole induced on the N-H bond by the hydrogen bonding interaction, the stronger the IR activity of the mode. Conversely, Raman activity is governed by the derivative of polarizability and favors molecules/groups/bonds which can be polarized – that is which are not already strong dipoles.[21] Thus, in Raman scattering, the weaker the dipole experienced by the N-H bond, the stronger the Raman activity. In this way, Raman and IR are complementary techniques. This can exploited as a powerful tool with which to explore changes in hydrogen bonding, since Raman and IR will

preferentially sample different populations of the hydrogen bonding interactions. Stronger hydrogen bonded populations are favored in IR, while weaker hydrogen bonded populations are favored in Raman. Figure 5-3 illustrates the spectral effects of hydrogen bonding. The upper chart represents the intensities of the band relative to the strength of hydrogen bonding present. The lower drawing generalizes the ν(NH) frequencies of Raman and IR bands relative to the hydrogen bonding strengths of the populations sampled by the techniques. Again, IR tends to preferentially sample N-H groups undergoing stronger hydrogen bonding interactions, while Raman preferentially samples weaker hydrogen bonding interactions.

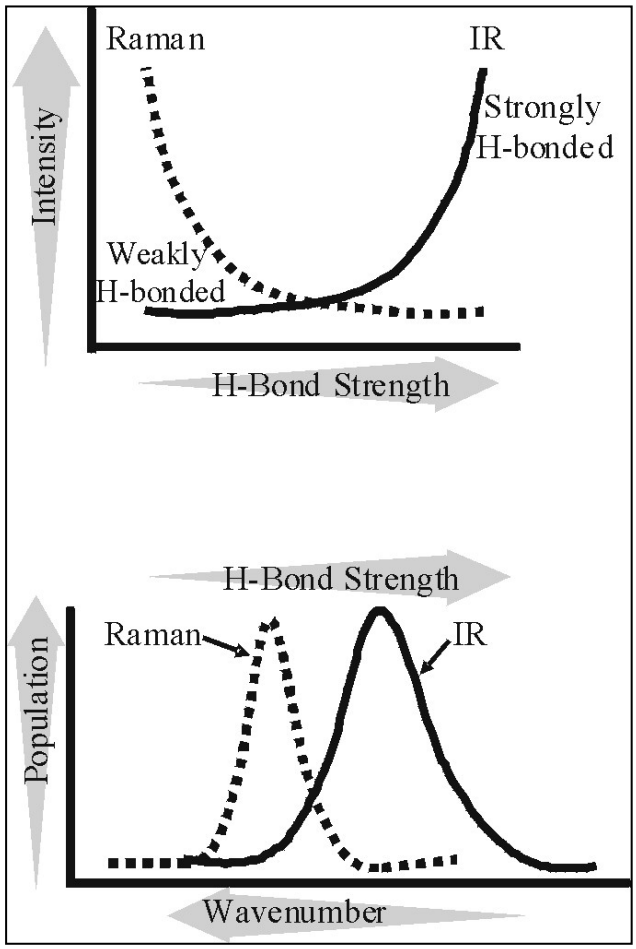

Figure 5-3: Differences in Raman and IR sampling of hydrogen bonded species based on ν(NH).
Upper: Stronger bonding increases intensity of IR band, but decreases intensity of Raman bands leading IR to favor stronger H-bonds and Raman to favor weaker H-bonds.
Lower: Stronger hydrogen bonding shifts ν(NH) frequencies lower and broadens bandwidth. Breaking the hydrogen bonding shifts frequencies higher and narrows bandwidth.

From the perspective of Pauling's definition, hydrogen

bonding is basically an inductive effect. It is therefore, not surprising that other inductive effects would have similar impacts on IR and Raman spectra. Spectral changes seen upon lithium association with N,N'-DMEDA and N,N'-DMPDA, particularly in the ν(NH) region can be explained with an electrostatic argument largely the same as that used to justify the spectral changes due to hydrogen bonding interactions. Cation association with the nitrogen atom withdraws electron density from the N-H bond, lengthening and weakening it. This results in a lower force constant for the bond which translates to lower ν(NH) frequency[22]. A very slight broadening of the ν(NH) band has also been observed upon coordination with positively charged metal atoms.[23] These authors offer no explanation for the band broadening, though it is likely heterogenous broadening due to a widened distribution of potential energy environments. An increase in intensity of the IR band is also to be expected and, like the intensity increase seen with hydrogen bonding, has been attributed to the greater dipole experienced by the N-H bond.[22] Due to its inductive nature, cation association follows the same trend as hydrogen bonding interaction with lower frequency signaling stronger association.[13,24]

5.3.1.2 Neat Materials

Before beginning any of the salt addition or CCl_4 dilutions, it is imperative to understand the base spectra of the two model compounds. Figure 5.4 contains the IR and Raman spectra of N,N'-DMEDA and N,N'-DMPDA in the NH stretching region, ν(NH). In this figure, the top set of spectra is N,N'-DMPDA and the bottom set is N,N'-DMEDA. In both cases the lower of the two spectra is IR absorbance

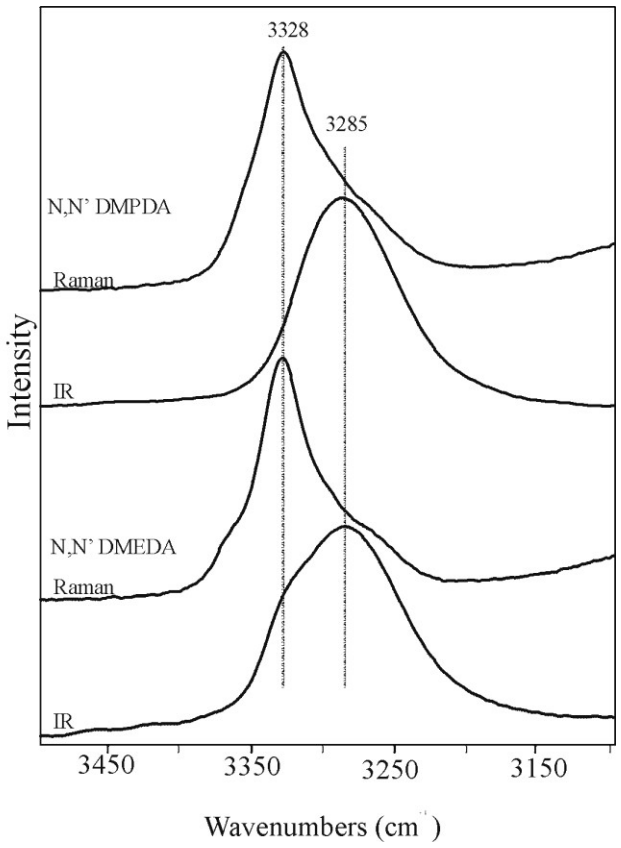

Figure 5-4: Raman and IR spectra of the NH stretching region of neat N,N'-DMEDA (lower) and neat N,N'-DMPDA (upper)

and the upper is Raman scattering. The first feature of note is the remarkable similarity between the spectra of the two materials. Both N,N'-DMEDA and N,N'-DMPDA have an IR band centered at approximately 3285 cm^{-1} and a Raman band centered at 3328 cm^{-1}, suggesting the presence of two distinct populations of H-bonding interactions of varying strengths. Additionally, the Raman spectra of both compounds exhibit a low frequency tail or shoulder coincident with the 3285 cm^{-1} IR band.

Since shifts to lower wavenumbers are expected with stronger H-bonding interactions[16-19], it is postulated that the ~3285 cm^{-1} band is due an intermolecular hydrogen bonded species, while the 3328 cm^{-1} band results from a weaker interaction, perhaps an intramolecular hydrogen bonded species. That these bands correspond exactly in the two materials is not surprising since the materials are homologs of one another and could reasonably be expected to have largely the same

chemical nature and interactions. However, they are not identical compounds, so should not be expected to behave identically. Thus, the slight differences seen in the spectra of the two compounds are not surprising either. The Raman spectrum of N,N'-DMEDA contains a very high frequency shoulder, but no such shoulder is evident in the N,N'-DMPDA spectrum. The high frequency of the shoulder (>3350 cm^{-1}) indicates a species that experiences either very weak or no hydrogen bonding at all. This is consistent with computational work on gas phase N,N'-DMEDA which gives a non-hydrogen bonded NH stretching frequency of 3363 cm^{-1} for N,N'DMEDA.[3] Previous experimental results assign a free ν(NH) for N,N'-DMEDA in tetrachloroethylene to 3371 cm^{-1}.[14] Both of these are higher frequencies than those identified as free ν(NH) in dipropylamine in CCl_4 (3346 cm^{-1})[9] and dimethylamine in CCl_4 (3356 cm^{-1}).[25] Unfortunately, the shoulder in this N,N'-DMEDA spectrum is too weak to be properly deconvoluted so a specific frequency cannot be assigned.

Another difference between the spectra of the two model compounds is that while the ν(NH) band of N,N'-DMPDA appears symmetrical in IR, the analogous band in the N,N'-DMEDA IR spectra has a high frequency shoulder at 3328 cm^{-1}. This shoulder occurs at the identical frequency as the ν(NH) band in the Raman spectra of both compounds. Small differences in the normal coordinates of the N,N'-DMEDA and N,N'-DMPDA probably result in a slightly different dipole moment derivative in N,N'-DMEDA than in N,N'-DMPDA which allows the 3328 cm^{-1} mode to be both Raman and IR active in N,N'-DMEDA, but mutually exclusive in

N,N'-DMPDA. This behavior will be repeated in the spectra upon salt addition and upon dilution with carbon tetrachloride. It is not particularly surprising since strict mutual exclusion applies only to molecules with an inversion center.[24] No such center is present in either compound, so strict adherence to mutual exclusion is not expected. It generally recognized that modes strongly active in IR are weakly active in Raman and vice versa. In some cases the mode may be so weakly active as to be below the signal to noise threshold. In other instances, such as those of the 3328 cm^{-1} band in N,N'-DMEDA IR and the 3285 cm^{-1} in both compounds' Raman spectra, the weakly active modes may appear as a low intensity band or shoulder.

5.3.1.3 CCl_4 Dilution

The hypothesis of the ~3285 cm^{-1} and 3328 cm^{-1} bands representing the inter- and intramolecular hydrogen bonded populations can be tested by diluting the neat materials in carbon tetrachloride. CCl_4 should not interact with the diamine model compounds, so it serves as an inert solvent, which interposes between diamine molecules pushing them further and further away from each other; thereby disrupting any intermolecular hydrogen bonding interactions at high dilution levels.[25,26] However, the lack of interaction between CCl_4 and the diamine means the intramolecular hydrogen bonding should remain unperturbed.[27] This will allow differentiation between spectral bands since the band associated with intermolecular hydrogen bonding interactions should decrease in relative intensity with increasing CCl_4 concentration while the band linked to intramolecular hydrogen bonding will remain largely unchanged.

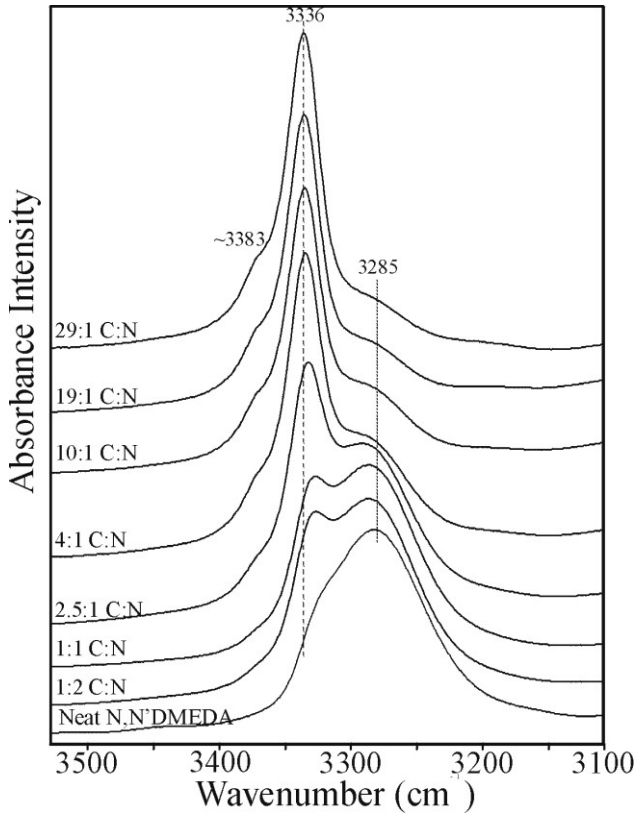

Figure 5-5: IR spectra of NH stretching region for neat N,N'-DMEDA and for dilutions of C:N = 1:5, 1:2, 1:1, 3:1, 5:1, 10:1 and 30:1

The IR spectra for N,N'-DMEDA diluted in carbon tetrachloride shown in Figure 5-5 illustrate this point perfectly. The lowermost spectrum is neat N,N'-DMEDA with CCl_4 concentration increasing up the spectral stack from 1:1 C:N molar ratio to 29:1 C:N molar ratio. The neat band is centered at 3285 cm^{-1} with a shoulder at 3328 cm^{-1}. As the CCl_4 concentration increases, the 3285 cm^{-1} band decreases in intensity as the 3328 cm^{-1} grows and shifts slightly to 3336 cm^{-1}. At the highest dilution (29:1 C:N), the 3285 cm^{-1} band is little more than a bump in the baseline next to the narrow symmetric 3336 cm^{-1} band which has a very slight high frequency shoulder (>3350 cm^{-1}). This suggests a change from two distinct NH environments in neat N,N'-DMEDA, one weakly and the other more strongly hydrogen bonded, to a single weakly hydrogen bonded environment in the most dilute system, with the possibility of a small amount of non-hydrogen bonded NH represented by the high frequency shoulder.

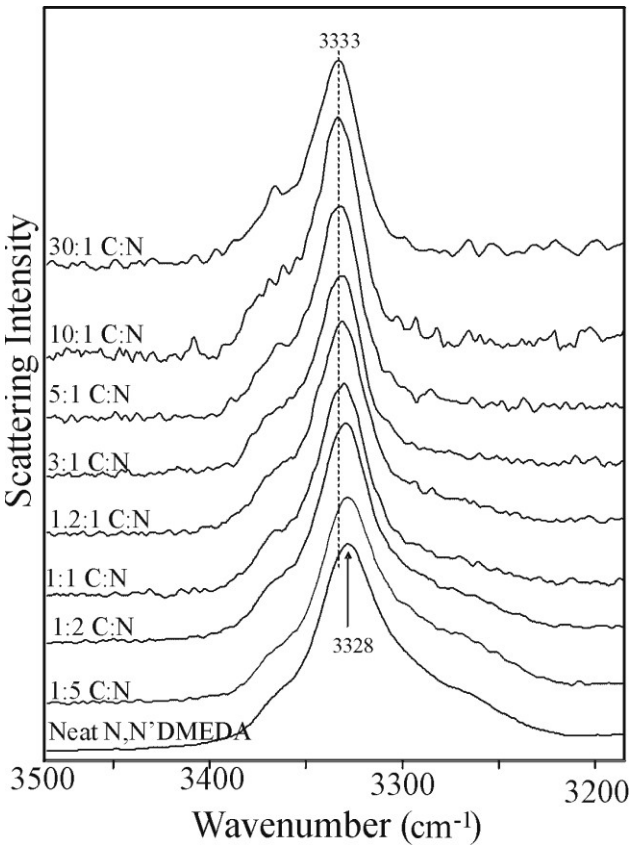

Figure 5-6: Raman spectra of NH stretching region for neat N,N'-DMEDA and for dilutions of C:N = 1:5, 1:2, 1:1, 3:1, 5:1, 10:1 and 30:1

This trend is repeated in the Raman spectra, shown in Figure 5-6, where the band centered at 3328 cm^{-1} in the neat N,N'-DMEDA grows in intensity and shifts upfield with increasing CCl_4 concentration while the shoulder band at 3285 cm^{-1} decreases with CCl_4 addition. All Raman spectra show a very weak high frequency shoulder (>3350 cm^{-1}). The intensity of the shoulder as compared to the noise is insufficient for its deconvolution or assignment of a specific frequency. However, the shoulder consistently appears at the same location in all trials, which compares favorably with the obvious shoulder in the IR spectra and is probably representative of free NH groups. Again, these data indicate a change from a weaker and a stronger hydrogen bonded NH environments to a single weakly interacting NH environment with the potential for a minimal amount of non-hydrogen bonded NH. This would correspond to both inter- and intramolecular hydrogen bonding interactions existing

in the neat material with only the weaker intramolecular hydrogen bonding interactions retained in the diluted system.

These assignments can be extended to the N,N'-DMPDA Raman spectra shown in Figure 5-7. Here again, the low frequency tail present in the neat N,N'-DMPDA is lost with the addition of a modest amount of carbon tetrachloride, and the 3328 cm^{-1} band increases in intensity and shifts slightly upfield to 3333 cm^{-1} with increased CCl_4 concentration. However, the high frequency shoulder seen in N,N'-DMEDA is completely absent in the N,N'-DMPDA spectra. Even at CCl_4 concentrations as low as 4:1 C:N, the system appears to have reached its final state. Like N,N'-DMEDA, the Raman spectra of N,N'-DMPDA seem to suggest the presence of both strong and weak hydrogen bonding interactions in the neat material, but only a single, weakly hydrogen bonded NH environment in the diluted system.

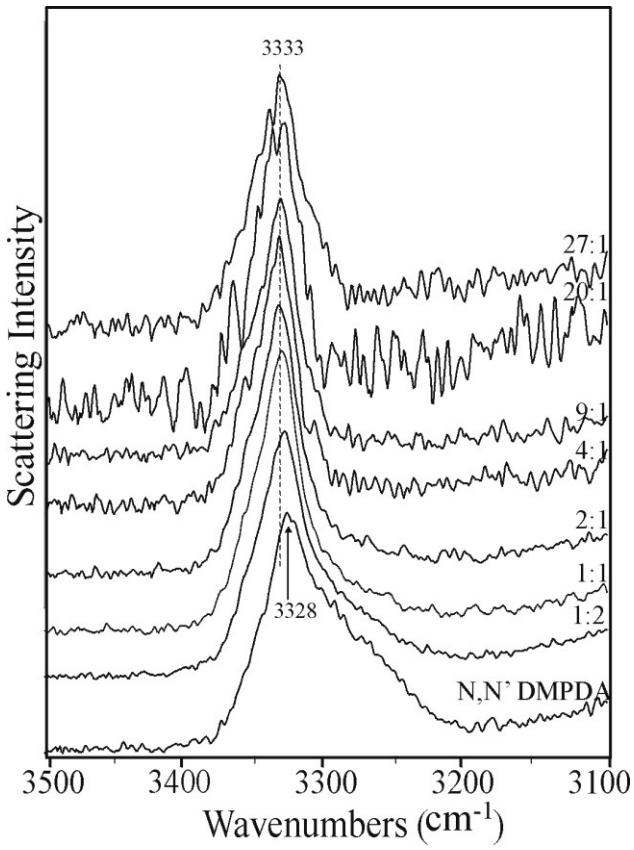

Figure 5-7: Raman spectra of NH stretching region for neat N,N'-DMPDA and for dilutions of C:N = 1:2, 1:1, 3:1, 4:1, 9:1, 20:1 and 27:1

The IR spectra of N,N'-DMPDA, however, do not follow same behavior as that seen in N,N'-DMEDA. Figure 5-8 contains IR spectra for N,N'-DMPDA ranging from the neat solution to the CCl_4 dilution of C:N 27:1. As previously noted, the band centered at 3285 cm^{-1} is the only band present in the neat N,N'-DMPDA IR spectra. This fairly symmetric band shifts and narrows with increased CCl_4 concentration until a C:N ratio of around 9:1 is reached. At this concentration, the band is narrow, symmetric and centered at 3314 cm^{-1}. Additional CCl_4 dilution (up to C:N=27:1) does not change the shape or location of the band. This is in contrast to the N,N'-DMEDA IR spectra which continue to show slight spectral changes to 29:1 C:N. It is only at the highest dilution levels that a high frequency shoulder appears. This suggests very limited amounts of free NH. A second, and more important, distinction between N,N'-DMEDA IR spectra and N,N'-DMPDA IR spectra is the final frequency of the band. Both neat

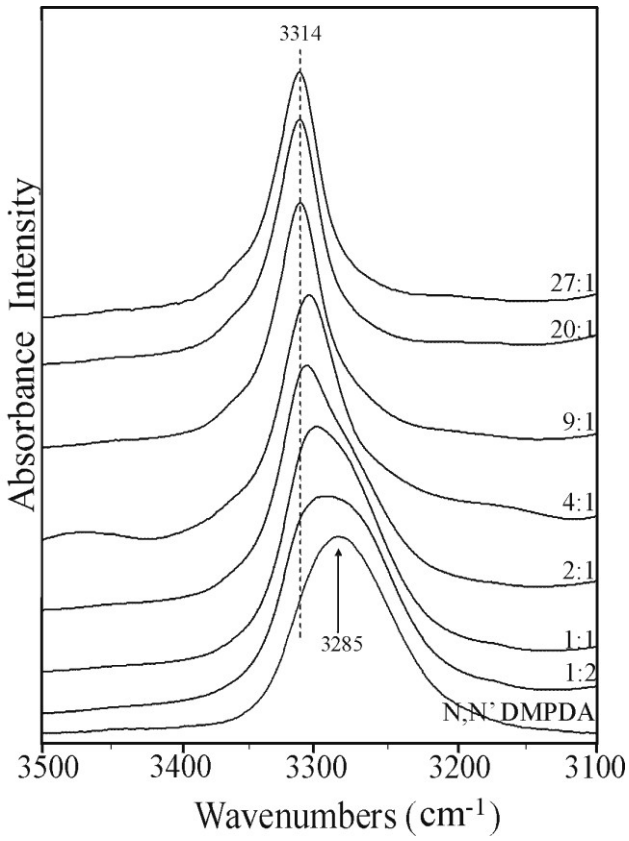

Figure 5-8: IR spectra of NH stretching region for neat N,N'-DMPDA and for dilutions of C:N = 1:2, 1:1, 3:1, 4:1, 9:1, 20:1 and 27:1

systems show a band at 3285 cm^{-1}. In N,N'-DMEDA, this band shifts to 3336 cm^{-1} which is quite similar to the final frequency (3333 cm^{-1}) seen in the N,N'-DMEDA Raman spectra. However, in N,N'-DMPDA, the 3285 cm^{-1} IR band shifts to 3314 cm^{-1}, which is rather different from the final frequency of 3333 cm^{-1} seen the N,N'-DMPDA Raman. It seems to imply the presence of another NH environment which experiences hydrogen bonding interactions of a moderate strength – less than the hypothesized intermolecular, but greater than the hypothesized intramolecular. Combined, the Raman and IR spectra suggest that neat N,N'-DMPDA contains two distinct populations of NH groups: strongly hydrogen bonded (3285 cm^{-1}) and weakly hydrogen bonded (3328 cm^{-1}). With CCl_4 dilution, rather than converging to a single weakly intramolecular hydrogen bonded environment (3333 cm^{-1}) as seen in N,N'-DMEDA, this system has both that weak intramolecular hydrogen bonded environment and a second, different, environment which undergoes slightly stronger hydrogen interactions.

Figure 5-9 is a composite of the previous four figures, showing Raman (upper) and IR (lower) spectra for selected compositions of CCl_4 dilutions of N,N'-DMEDA (left) and N,N'-DMPDA (right). Here, the similarities between the systems are apparent. Both systems begin with two distinct NH environments: intermolecular hydrogen bonded signified by the 3285 cm^{-1} band and intramolecular hydrogen bonded associated with the 3328 cm^{-1} band. In both systems, the Raman data indicate these two environments converge to a single intramolecular hydrogen

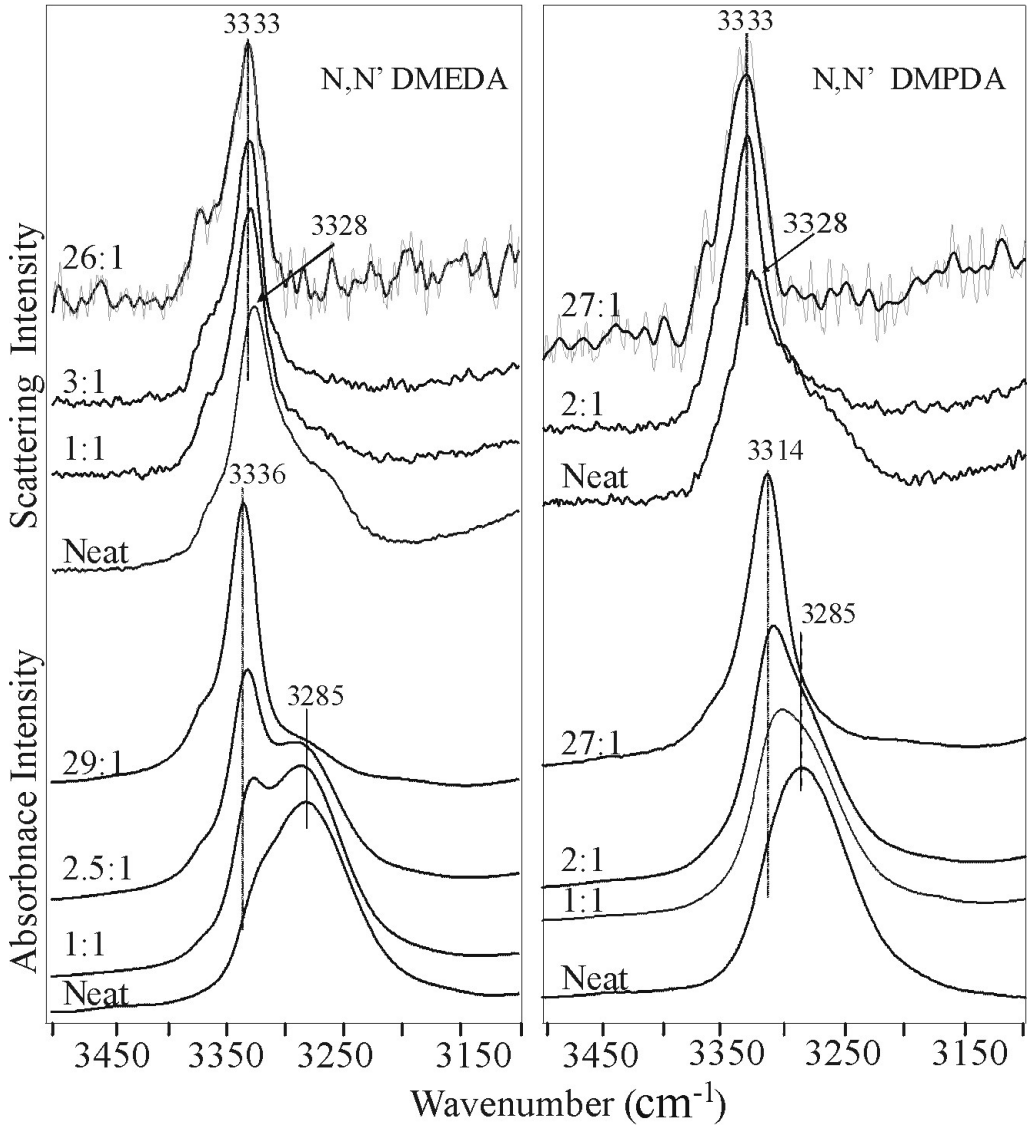

Figure 5-9: IR (lower) and Raman (upper) spectra of the NH stretching region of neat N,N'-DMEDA (left) and neat N,N'-DMPDA (right) and their dilutions in CCl_4 ranging from C:N=1:1 to 30:1

bonded environment denoted by the 3333 cm^{-1} band. In the case of N,N'-DMEDA, the IR also supports this assertion.

Rocher and Frech note very similar frequencies in dipropylamine (DPA) diluted in CCl_4.[13] They report neat DPA spectra to contain a single broad band

centered at 3289 cm^{-1} in the IR spectrum and two broad overlapping weak bands at 3327 cm^{-1} and 3315 cm^{-1} in the Raman spectrum. When diluted in CCl_4, the 3289 cm^{-1} band is lost and replaced by a broad band at 3346 cm^{-1} with a shoulder at 3328 cm^{-1} in the IR spectrum. In the Raman spectrum, the band at 3315 cm^{-1} disappears with dilution while the 3328 cm^{-1} band decreases in intensity. The 3346 cm^{-1} band was assigned to non-hydrogen bonded NH and the 3328 cm^{-1} band was attributed to a "hydrogen-bonded population of molecules that are dilute in CCl_4."[13] Assignments beyond this were not made, though the possibility of dimerization was suggested based on Wolff and Gamer's work with methylamine in CCl_4.[25] The coincident frequencies between DPA and N,N'-DMEDA and N,N'-DMPDA could be troubling because DPA, having only one nitrogen atom, is unable to form intramolecular hydrogen bonds. This makes the assignment of the 3328 cm^{-1} and 3314 cm^{-1} bands in N,N'-DMEDA and N,N'-DMPDA somewhat dubious. However, factors beyond mere frequency coincidence must be considered. The markedly dissimilar behaviors of these bands in DPA and in N,N'- DMEDA with respect to bands of similar frequencies in N,N'-DMPDA is of tremendous importance.

In N,N'-DMEDA, a band in the 3310-3320 cm^{-1} region is not observed in either the IR or Raman spectra. In DPA, the 3315 cm^{-1} band slowly disappears with CCl_4 dilution. In N,N'-DMPDA, the 3314 cm^{-1} band is not initially present in the neat spectra, but develops into a strong, narrow, symmetric band out of and at the expense of the 3285 cm^{-1} band with CCl_4 dilution. This very different behavior of the bands suggests that they do not arise from the identical sources, but instead the

frequencies in the neat liquids are truly coincidental. Rocher's explanation of the DPA band as arising from dimers is reasonable. It is likely such linkages could have two N-H groups participating in N···H bonding with each other. As shown in Figure 5-10, this would be very similar to the two-fold intramolecularly hydrogen bonded species shown in Figure 5-2.C and could reasonably be expected to have similar force constants and therefore similar frequencies. In DPA, this dimer would be separated by the interposition of CCl_4, which would account for its loss with CCl_4 addition. However, in N,N'-DMPDA this interaction involves atoms on the *same* molecule. Consequently, increasing CCl_4 concentration actually affords *more* opportunity to form the species as intermolecular hydrogen bonding is disrupted, leaving only intramolecular options. Thus, the presence of the 3315 cm^{-1} band in DPA does not preclude the assignment of the 3314 cm^{-1} band in N,N'-DMPDA to an intramolecular species.

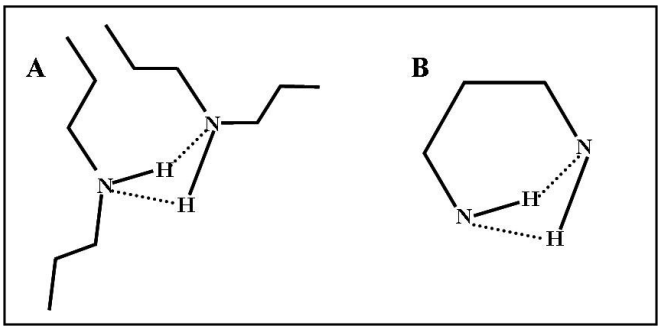

Figure 5-10: Possible hydrogen bonding interactions in dipropylamine (DPA) and N,N'-DMPDA in which two N-H groups form N···H bonds with each other
A: Possible dimer of DPA
B: Doubly intramolecular hydrogen bonded N,N'-DMPDA

The models in Figure 5-2 are drawn from the computational work of Boesch, *et al*,[3] which found that N,N'-DMEDA hydrogen bonding interactions involving two heteroatoms in a single molecule are theoretically possible, but are not the lowest

energy state for N,N'-DMEDA. This is probably due to the strain induced by the N-C-C-N dihedral angle required to form both hydrogen bonds. However, the third carbon atom in N,N'-DMPDA allows for an additional degree of conformational freedom by providing another rotational bond axes. The presence of this additional dihedral angle allows the two-fold bonded structure to be essentially a six-membered ring, lending stability to the structure.

The coincident frequency of the 3328 cm^{-1} band in the model compounds with a similar band in DPA can be likewise explained. In Rocher's DPA Raman spectrum, this band does not shift with CCl_4 addition, but its intensity does reduce at high CCl_4 levels. Some intensity reduction is expected due to Beer's law adherence, but this band reduces faster than its companion 3315 cm^{-1} band, suggesting a more rapid decline of the population. However, in N,N'-DMEDA and N,N'-DMPDA the 3328 cm^{-1} band shifts up in frequency and narrows. It also decreases in intensity (as shown by the increase in signal to noise ratio), but does so commensurate with other bands in the spectra, suggesting the decrease is due to the lower overall concentration rather than the decrease of the specific species. This band is fleeting and stationary in DPA, but persistent and shifting in N,N'-DMEDA and N,N'-DMPDA suggesting a difference in origin. The band's behavior is also dissimilar in the IR spectra. In DPA, the band increases in intensity along with the free band at 3346 cm^{-1} up to a concentration of ~9:1 C:N. At higher CCl_4 concentrations, the band decreases to become a shoulder on the free NH band. In N,N'-DMEDA, a

similar band grows out of a broad shoulder on the 3285 cm^{-1} band, increases in intensity and shifts upward to 3336 cm^{-1} at a composition of ~30:1 C:N.

One possible interpretation is that the 3328 cm^{-1} band in DPA is due to trimers and higher order multi-mers which are broken in DPA with CCl_4 addition resulting in increased numbers of non-hydrogen bonded NH groups. In N,N'-DMEDA, these species are also present and dissociated upon dilution. However, instead of non-hydrogen bonded NH groups, the singly intramolecularly hydrogen bonded species is formed. This would result in the decrease of the 3328 cm^{-1} band at roughly the same rate as the increase of the 3336 cm^{-1}, which would appear as a shifting band center.

These general assignments are consistent with the results found by Krueger upon diluting several amines in tetrachloroethene.[14] In that work, the free NH frequencies are given as 3371 and 3361 cm^{-1} in N,N'-DMEDA and N,N'-DMPDA, respectively. The intramolecular hydrogen bonded frequency is given as 3317 cm^{-1} in N,N'-DMPDA and 3341 cm^{-1} in N,N'DMEDA. It should be noted that those experiments were conducted at concentrations a decade more dilute than the ones presented in this work, which may account for the difference in the N,N'-DMEDA intramolecular frequency and the presence of stronger free NH bands. Unfortunately, Krueger presents only a single concentration (~0.02M) and does not give any Raman spectra, hampering further comparison to this study.

These assignments also make sense in light of the simple models of hydrogen bonding interactions shown previously in Figure 5-2. As CCl_4 is added, the CCl_4

molecules interpose between two intermolecular hydrogen bonded model compound molecules. This breaks the intermolecular hydrogen bonding between those two groups and leaves all four amine groups unassociated. Isolated from other model compound molecules by CCl_4, the unassociated model compound molecule is unable to form new intermolecular hydrogen bonds. This results in the intensity reduction of the 3285 cm^{-1} band and eventually the 3328 cm^{-1}. Instead, the unassociated molecule forms an intramolecular hydrogen bond and causes the increase of the 3333-3336 cm^{-1} band intensity in both materials and the 3314 cm^{-1} band in N,N'-DMPDA.

That the N,N'-DMPDA IR band alone fails to converge to 3333 cm^{-1}, but instead remains as a strong band at 3314 cm^{-1} suggests that two different NH environments are involved in the N,N'-DMPDA system. The narrow shape of the 3314 cm^{-1} IR band and the 3333 cm^{-1} Raman band and the lack of any shoulders on either of these bands imply that all NH in the CCl_4:N,N'-DMPDA system falls into one of these two environments. One, represented by the 3333-3336 cm^{-1} band, is simple intermolecular hydrogen bonding and is present in both N,N'-DMEDA and N,N'-DMPDA. The other is something different. The continued growth of the band at high concentration of CCl_4 (27:1 C:N) leaves it unlikely that the 3314 cm^{-1} band is due to an extremely weakened intermolecular hydrogen bonded interaction and introduces the possibility of a intramolecular hydrogen bonded species different from that represented by the 3333-3336 cm^{-1} band. Its similarity the hypothesized dimer frequency of DPA makes the doubly intramolecular hydrogen bonded species an

attractive, though not concrete, assignment. What is certain is that despite their structure similarities, N,N'-DMEDA and N,N'-DMPDA experience markedly different hydrogen bonding interactions under highly isolated conditions.

5.3.1.4 Lithium Triflate Addition

Addition of lithium trifluoromethanesulfonate, LiTf, to the model compounds also gives insight into the types of hydrogen bonding interactions present in these model compounds systems. Disruptions of both the intermolecular and intramolecular hydrogen bonding interactions are expected due to the formation of associations between the cation and/or anion of the salt and the nitrogen and/or hydrogen atoms of the model compounds.

The Raman and IR spectra collected from N,N'-DMEDA complexed with lithium triflate are shown in

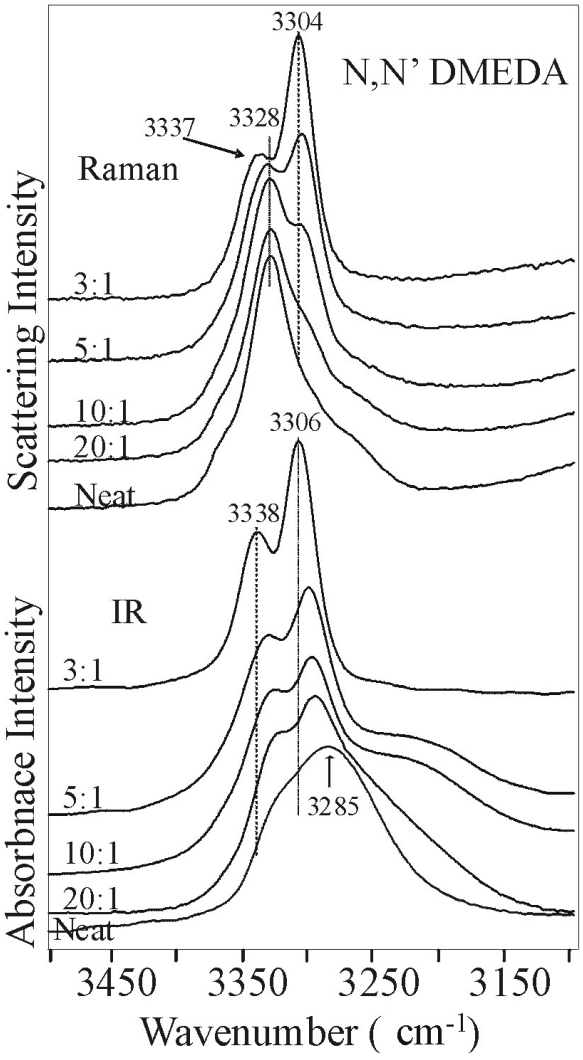

Figure 5-11: IR (lower) and Raman (upper) spectra in the NH stretching region for neat N,N'-DMEDA and N,N'-DMEDA:LiTf complexes of $N:Li^+$ = 20:1, 10:1, 5;1 and 3:1

Figure 5-11. The lower spectra set is IR data, while the upper set is Raman data. The bottommost spectrum is the neat N,N'-DMEDA IR absorbance, which has a band centered at 3285 cm^{-1} and large shoulder at about 3328 cm^{-1}. As lithium triflate is added, these overlapping bands separate into two narrow symmetric bands and shift upward in frequency. The 3328 cm^{-1} shoulder becomes the 3338 cm^{-1} band at a $N:Li^{+}$ composition of 3:1. At the same composition, the 3285 cm^{-1} band shifts to 3306 cm^{-1}. These changes imply that LiTf affects both the inter- and intramolecular hydrogen bonding. This is supported by the Raman data in which the band centered at 3328 cm^{-1} in neat N,N'DMEDA is initially unaffected by the LiTf addition while a second band around 3304 cm^{-1} begins to grow in intensity. At a composition between 10:1 and 5:1 $N:Li^{+}$, the 3328 cm^{-1} band begins shifting to a higher frequency, reaching 3337 cm^{-1} at the 3:1 $N:Li^{+}$ molar ratio. When considered in combination with the IR data, this is a strong argument for the assigning the 3304/3306 cm^{-1} band to an NH environment that involves cation association to the nitrogen atom. The apparent shift of the 3285 cm^{-1} band in IR combined with the gradual growth of the 3304 cm^{-1} band in Raman strongly suggests a breaking of intermolecular hydrogen bonds present in the neat N,N'-DMEDA upon salt addition. The 3337 cm^{-1} band seen in both the IR and Raman of N,N'-DMEDA:LiTf complexes is reminiscent of the 3333/3336 cm^{-1} band seen in the spectra of N,N'-DMEDA diluted in CCl_4 and can most likely be assigned to a form of intramolecular hydrogen bonding. These freed NH groups then associate with the cation or form intramolecular hydrogen bonds. It is not until relatively high salt concentrations are

reached that the intramolecular hydrogen bonds are influenced by the salt presence. At sufficiently high salt concentrations, the intramolecular hydrogen bonds are perturbed, but not completely disrupted.

The shift to lower wavenumber is confusing as first glance, as the breaking of hydrogen bonds would be expected to increase the frequency of the ν(NH) band.[16,18] However this shift can be explained by the cation inductive effect, which would push the frequency lower.[13,23] Upon association with nitrogen, the cation withdraws some electron density from the N-H bond. This results in a lengthened and weakened N-H bond, which vibrates at a lower frequency than the unperturbed N-H bond[24]. As shown in Figure 5-12, the two effects (cation induction and hydrogen bond breakage) occur simultaneously, but result in opposite spectral shifts. Which shift is actually observed depends on both the

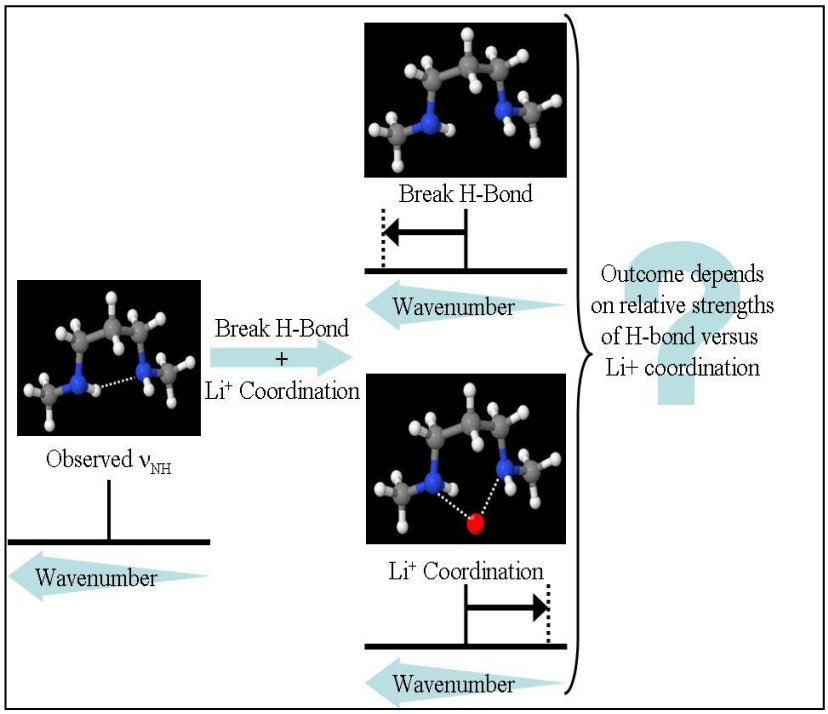

Figure 5-12: Competing nature of hydrogen bond breakage and cation inductive effect on the shift in NH stretching frequency upon cation association

strength of the H-bond broken and the strength of the cationic induction[28]. Replacing a weak H-bond with a strong cation inductive effect will shift the ν(NH) frequency lower, but substituting a strong H-bond with a weak cation induction will increase the ν(NH) frequency. In the case of lithium triflate breaking intermolecular hydrogen bonding upon association with N,N'-DMEDA, the frequency of the NH stretch increases (3285 cm^{-1} → 3306 cm^{-1}). However, when LiTf disrupts the weaker intramolecular hydrogen bonded N,N'-DMEDA, the ν(NH) frequency decreases (3328 cm^{-1} → 3304 cm^{-1}). Since the two wavenumber difference between 3304 cm^{-1} and 3306 cm^{-1} is within the range of error of the experiment, it is reasonable to suggest that the two bands represent the same associated species. Thus, addition of lithium triflate to N,N'-DMEDA moves the system from having two distinct NH environments of inter- and intramolecular hydrogen bonding in the neat material to having other distinct environments as a result of cation coordination. The nature of these environments cannot be definitely determined without the aid of a crystal structure. Unfortunately, even though crystals of N,N'-DMEDA:LiTf were obtained, they were not suitable for XRD analysis so no such data is available for the N,N'-DMEDA:LiTf complex.

Sanders, *et. al.* have reported a crystal structure and IR data for N,N'-DMEDA with sodium triflate.[29] In this crystal structure (space group $P\bar{1}$) a polymer chain-like structure is formed in which sodium atom is 6 fold coordinated to either four N,N'-DMEDA nitrogen atoms and two triflate oxygen atoms or to two N,N'-DMEDA nitrogen atoms and four triflate oxygen atoms. All nitrogen atoms are

coordinated to sodium. At a composition of 7.5:1 N:Li^+ molar ratio, infrared bands occur at 3310 and 3335 cm^{-1}. By a molar composition of 1.5:1 N:Li^+, these have shifted to 3315 and 3344 cm^{-1} and upon crystallization, the bands have reached 3324 cm^{-1} and 3352 cm^{-1}. Based on the computations of York, *et al*[2] this shift is attributed to the breaking of intramolecular bonds and the formation of intermolecular bonds.

In crystals formed by the complex of dipropylamine and lithium triflate, Rocher and Frech observed bands at 3302 and 3289 cm^{-1} in the infrared and Raman spectra.[13] The $P2_1/c$ crystal structure of this complex shows a polymeric chain-like network with each nitrogen atom coordinated to a lithium cation and each NH group in one of two distinct N-H environments. In one of these, the hydrogen atom experiences weak hydrogen bonding interactions with a triflate oxygen atom. In the other, the NH undergoes no hydrogen bonding. Rocher has assigned these populations to the 3302 and 3289 cm^{-1} bands, respectively.

It is important to note that in both crystal structures all nitrogen atoms were coordinated to a lithium cation, yet both systems still showed two distinct N-H environments. It is likely that the N,N'-DMEDA:LiTf system is similarly complexed. Thus, the two distinct bands (3337 cm^{-1} and 3304-3306 cm^{-1}) cannot be attributed strictly to a difference in cation association (inductive effect). Hydrogen bonding interactions must also be considered. It seems likely that the 3304-3306 cm^{-1} band in N,N'-DMEDA:LiTf is representative of a population experiencing both hydrogen bonding interaction and cation association, as seen in Rocher's study.[13]

The source of the higher frequency band is less clear. When making the assignments of 3302 cm^{-1} to the simultaneously hydrogen bonded and lithium coordinated species and 3289 cm^{-1} to the solely lithium coordinated species, Rocher's work with DPA specifically states that the frequencies do not shift and that spectra of liquid solutions of high lithium triflate content strongly resemble those of the crystalline DPA-LiTf system. In contrast, Sanders notes that the frequencies of N,N'-DMEDA:NaTf continue to shift upward with increasing amounts of sodium triflate. A difference of approximately eight wavenumbers is seen between bands in the 1.5:1 $N:Li^+$ solution spectrum and the $(N,N'\text{-DMEDA})_2(NaTf)_5$ crystal spectrum.[15] This indicates continued changes in the structure up to the point of crystallization. Rocher and Frech note that the N-H···O bond appears to be weaker than the N-H···N bond.[13] With this in mind, the continued upward shift in Sanders' N,N'-DMEDA:NaTf could be explained by progressive replacement of intermolecular hydrogen bonding interactions (N-H···H) with weaker interactions with the triflate oxygen atoms (N-H···O) as cation association disrupts intermolecular associations. This explanation could also be applied to the N,N'-DMEDA:LiTf system, whose behavior appears similar (though compositions more lithium rich than 3:1 $N:Li^+$ were not obtained in the present work.) However, between 5:1 and 3:1 $N:Li^+$, the bands continue a slight upward migration, suggesting a final structure has not been obtained by this point.

A slightly different behavior is seen in the N,N'-DMPDA:LiTf system. IR absorbance (lower) and Raman scattering (upper) data for N,N'-DMPDA in its neat

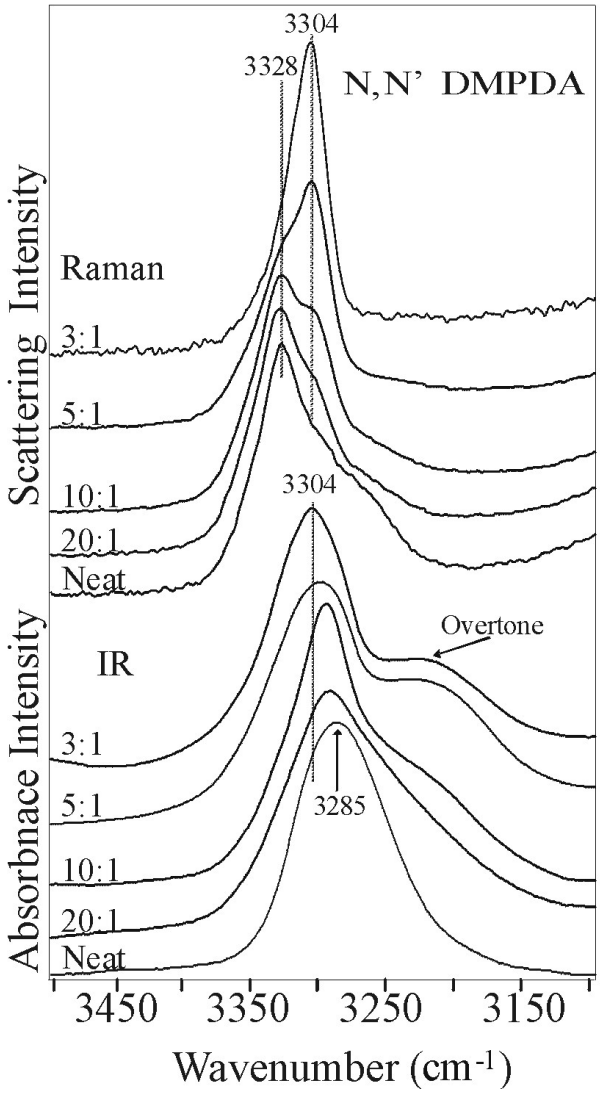

Figure 5-13: IR (lower) and Raman (upper) spectra in the NH stretching region for neat N,N'-DMPDA and N,N'-DMPDA:LiTf complexes of $N:Li^+$ = 20:1, 10:1, 5;1 and 3:1

form and complexed with lithium triflate are given in Figure 5-13. The IR bands which appear to develop around 3214 cm^{-1} are overtone/ combination bands whose intensity is disproportionately impacted by cationic association[13,21]. The 3285 cm^{-1} band present in the IR spectra of neat N,N'-DMPDA shifts to a higher frequency with salt addition, reaching 3304 cm^{-1} at a molar composition of 3:1 $N:Li^+$. Likewise, the 3385 cm^{-1} shoulder in the Raman is reduced with salt addition and is completely eliminated by a composition of 5:1 $N:Li^+$. The 3328 cm^{-1} band initially present in the Raman scattering spectra decreases in intensity as the 3304 cm^{-1} band develops, suggesting coupled populations. At the highest salt concentration (3:1 $N:Li^+$), the 3328 cm^{-1} band is, at best, a high frequency tail on the 3304 cm^{-1} band. This, combined with

the narrow symmetric nature of the same band in the IR absorbance spectra, suggests that all NH in the system experiences the same general environment. This is in marked contrast to the behavior of the N,N'-DMEDA:LiTf complex in which two distinct environments are present even at a composition of 3:1 N:Li^+. Unfortunately, identifying the specific structure of this association is beyond the scope of vibrational spectroscopy without the aid of a crystal structure. While crystals of both N,N'-DMPDA: NaTf and N,N'-DMPDA:LiTf were obtained, they were not of sufficient size or quality to allow successful XRD refinement. Published crystal structures for a number of related compounds indicate that the association is likely through the Li^+ in a manner that allows the cation to be multicoordinate.[10,13,15,27,29-32] The vast majority of these structures present a lithium ion that uses both the compound heteroatoms and the salt anion to obtain four, five, or higher-fold coordination, such as that seen earlier in N,N'-DMEDA with NaTf.[15] For a single NH environment to exist in LiTf complexed N,N'-DMPDA, all NH would need to be somehow drawn into in the association in an identical manner. Rocher's work with DPA, as well as that presented here with N,N'-DMEDA, would suggest such a structure involve all NH in simultaneous lithium coordination and hydrogen bonding.

5.3.1.5 CCl_4 Dilution of LiTf Complexes

In the absence of a crystal structure, dilution of the model compound-salt complexes may offer the best option to gain additional insight into the nature of hydrogen bonding interactions in these systems. As in the previous case, the hope is that progressive addition of CCl_4 to the system will break the intermolecular

hydrogen bonding interactions and leave only non-hydrogen bonded NH groups, those involved in intramolecular interactions and those NH groups associated to lithium.

Figure 5-14 illustrates the impact of CCl_4 addition to 20:1 and 5:1 $N:Li^+$ complexes of N,N'-DMEDA:LiTf. The spectrum of salt-free N,N'-DMEDA is given as the bottommost of the spectra for reference. The IR spectrum of the pure 20:1 $N:Li^+$ complex (lower) consists of two overlapping bands at 3330 and 3295 cm^{-1}, with the lower frequency band being slightly more intense. With addition of CCl_4, both bands shift up in frequency slightly to 3337 and 3305 cm^{-1} and the intensity of the lower frequency band diminishes while the intensity of the higher frequency band increases. Between a CCl_4 molar ratio of 1:1 and 4:1 C:N, the intensity of the higher

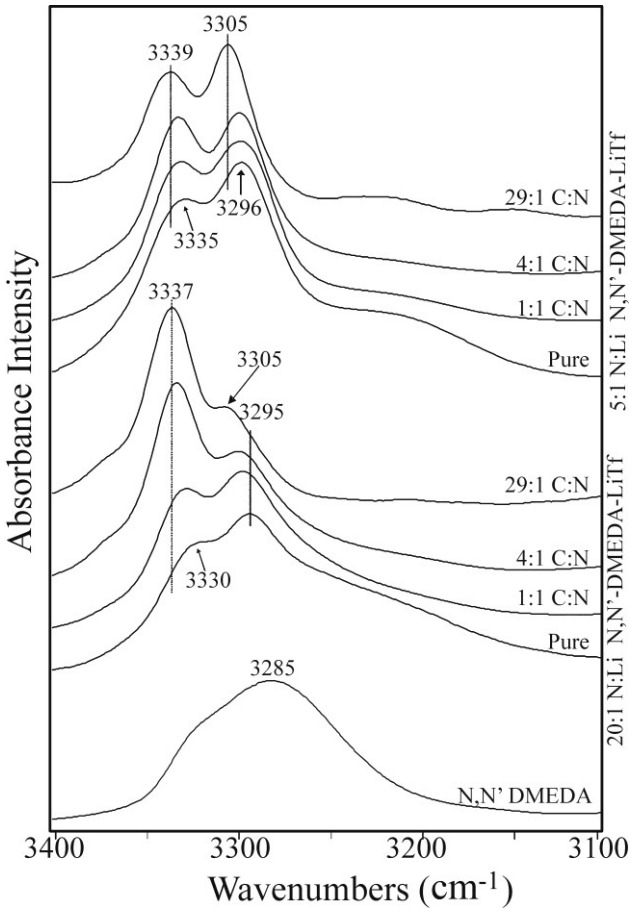

Figure 5-14: IR spectra in the NH stretching region of CCl_4 dilutions of 20:1 $N:Li^+$ (lower) and 5:1 $N:Li^+$ complexes (upper) of N,N'-DMEDA with LiTf. Dilutions are given as C:N molar ratios.

frequency band overtakes that of the lower frequency band. Since the 3305 cm^{-1} band has previously been assigned to NH groups undergoing cation association hydrogen bonding, this seems to indicate a transformation of the local environment in a manner that disrupts the N,N'-DMEDA-salt network. This disruption appears to interfere with the cation associated N-H···O interaction with the triflate oxygen atoms. It is not clear if this due to loss of cation association or loss of anion interaction.

Like its 20:1 $N:Li^+$ counterpart, the spectra of the undiluted (pure) 5:1 $N:Li^+$ (upper) complex of N,N'-DMEDA:LiTf, consists of two broad overlapping bands. In the case of the 5:1 $N:Li^+$ complex, the bands are centered at 3296 and 3335 cm^{-1}. As with the 20:1 $N:Li^+$ upon dilution, the bands narrow slightly and gradually shift upward in frequency to 3339 and 3305 cm^{-1}. However, in this instance, the relative intensity of the bands to one another does not change significantly and the lower frequency band remains the more intense of the two bands. The disruption of the local N,N'-DMEDA-salt network does not seem to be as extensive as that seen in the 20:1 $N:Li^+$ system, indicating the network in the 5:1 $N:Li^+$ complex may be more resistant to dissociation and/or exists in a less interconnected form. In both the 20:1 and 5:1 $N:Li^+$, at the highest dilution two distinct populations of NH groups are present: NH groups experiencing cation coordination through the nitrogen atom and hydrogen bonding to the triflate oxygen atom (3305 cm^{-1}) and NH groups in a different environment (3337-3339 cm^{-1}). The nature of this second environment cannot be definitely identified with these data. Several possibilities compatible with

the observed frequency exist. For instance, the band may be due to non-hydrogen bonded NH which are cation associated. Coordination of the nitrogen atom to the lithium cation lowers the frequency of ν(NH). Since the expected frequency of non-hydrogen bonded NH groups in N,N'-DMEDA is around 3371 cm^{-1},[14] shifting to ~3338 cm^{-1} would be a change of approximately 33 wavenumbers. This is slightly larger than the 25 wavenumber maximum shift due to cation inductive effect seen by Rocher.[28] A second possibility is that the band originates with a species of NH experiencing hydrogen bonding to other NH groups, but not cation association. The band at ~3332 cm^{-1} in the neat N,N'-DMEDA system was previously assigned to intramolecular hydrogen bonded NH groups. The band present at ~3338 cm^{-1} in the dilute salt complexes may indicate a similar species. A third option is that this band originates from a species of NH experiencing hydrogen bonding to the triflate oxygen atoms without being associated to a lithium atom. Rocher observed that hydrogen bonding of the N-H···O type was of higher frequency than that of the N-H···N type in multiple amine-salt systems.[9,13,20,27] Unfortunately, the infrared NH stretching region alone does not provide sufficient spectral clues to exclude any of these possibilities.

Raman scattering data for 5:1 (upper) and 20:1 (lower) $N:Li^+$ complexes of N,N'-DMEDA diluted in CCl_4 are presented in Figure 5-15. Again, the spectrum of salt-free N,N'-DMEDA is provided in the bottommost spectrum for reference. This spectrum is remarkably similar to that of the undiluted (pure) 20:1 $N:Li^+$ complex containing a broad band at about 3337 cm^{-1} with a lower frequency tail and a higher

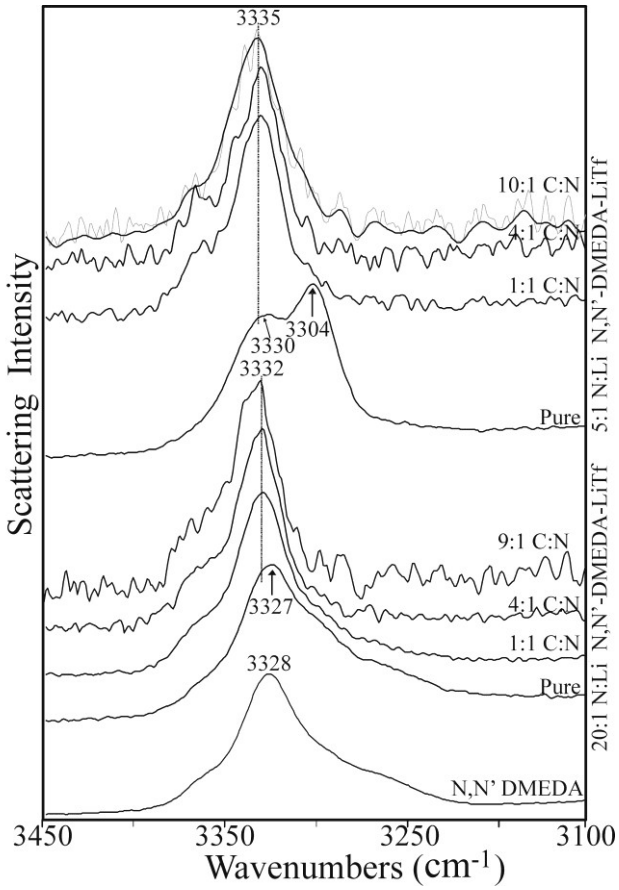

Figure 5-15: Raman spectra in the NH stretching region of CCl_4 dilutions of 20:1 N:Li+ (lower) and 5:1 N:Li+ complexes (upper) of N,N'-DMEDA with LiTf. Dilutions are given as C:N molar ratios

frequency shoulder. In both instances, with CCl_4 dilution the 3327-8 cm^{-1} band shifts up in frequency to 3332 cm^{-1} and gradually looses the tail while maintaining the shoulder. This seems to suggest that at low salt composition the amount of salt present is insufficient to result in large scale disruption of the intramolecular hydrogen bonding of the system, so most of the changes seen are as a result of CCl_4 dilution impacting the N-H···N interactions.

In the 5:1 N:Li^+ complex, the pure Raman scattering spectrum contains two broad overlapping bands centered at 3304 and 3330 cm^{-1}. With addition of even very modest amounts of CCl_4 (1:1 C:N) the band the intensity of the 3304 cm^{-1} band decreases dramatically while the band at 3330 cm^{-1} narrows, shifts to 3335 cm^{-1} and increases in intensity significantly. This suggests a major change to the local environment. This transformation seems to involve the disruption of hydrogen bonding interactions

with triflate oxygens and the formation of some other type of interaction, probably intermolecular N-H···N interactions. That a band at a similar frequency (~3305 cm^{-1}) is maintained in the IR absorbance spectra implies some populations of N-H···O interactions still exist in the system, even at high levels of dilution. It should be noted that the spectral alterations observed in the 5:1 N:Li^+ Raman scattering spectra occur rapidly and at low CCl_4 levels while the changes in the IR absorbance spectra of the same compound occur gradually over a wide range of CCl_4 dilution. This suggests that CCl_4 addition impacts different populations of NH in different ways. The IR absorbance and Raman scattering data combined, show multiple NH environments in the N,N'-DMEDA:LiTf complexes. The 3304-6 cm^{-1} band represents the hydrogen bonded and cation associated NH groups. The 3332 cm^{-1} Raman scattering band has been assigned to intramolecular hydrogen bonded NH groups. The 3337 cm^{-1} band in the IR absorbance spectra may relate to a cation coordinated, though not hydrogen bonded species, a weakened intramolecular hydrogen bonded species or NH groups involved in N-H···O hydrogen bonding. A more certain assignment is not possible with only the data from this region. In subsequent sections, data from the backbone region and ionic association regions will be presented, which will allow a more thorough discussion of the various environments present in the N,N'-DMEDA:LiTf system.

Before addressing those spectral regions, IR absorbance and Raman scattering data from diluting N,N'-DMPDA:LiTf system are presented in Figure 5-16 and Figure 5-17. Infrared absorbance spectra for 20:1 (lower) and 5:1 (upper)

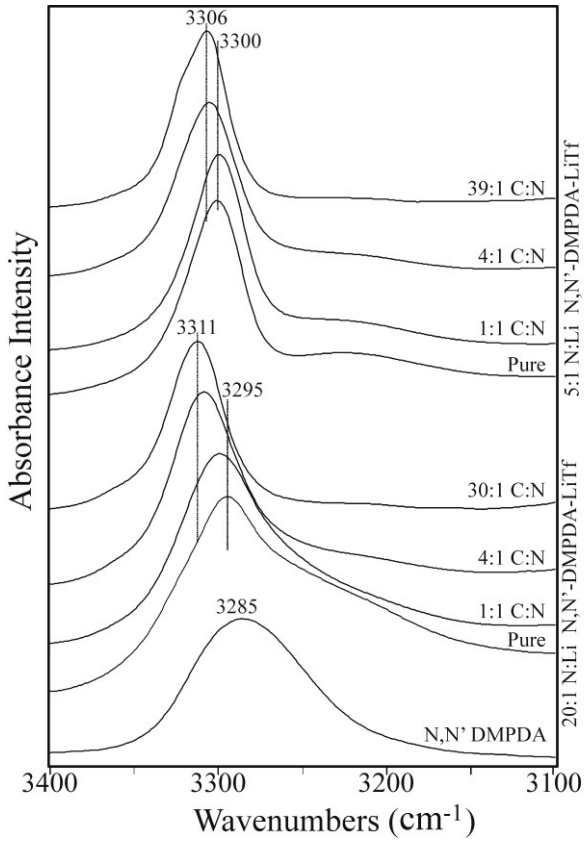

Figure 5-16: IR spectra in the NH stretching region of CCl_4 dilutions of 20:1 $N:Li^+$ (lower) and 5:1 $N:Li^+$ complexes (upper) of N,N'-DMPDA with LiTf. Dilutions are given as C:N molar ratios.

$N:Li^+$ compositions of N,N'-DMPDA:LiTf are given in Figure 5-16. For reference, the spectrum of neat N,N'-DMPDA is provided as the bottommost trace. The spectra of the 20:1 $N:Li^+$ N,N'-DMPDA:LiTf complex consists of a broad band centered at 3295 cm^{-1} with a low frequency tail. With CCl_4 addition, this band narrows and shifts up in frequency. By a dilution level of 4:1 C:N, the low frequency tail is completely lost. In the most dilute solution (30:1 C:N), the band has narrowed and shifted to 3311 cm^{-1} suggesting all the IR active NH groups experience the same environment. This spectral series very closely resembles the series formed in pure N,N'-DMPDA:LiTf with salt addition (Figure 5-13) and the series formed with dilution of pure N,N'-DMPDA (Figure 5-8). In both cases the broad band at 3285 cm^{-1} in the neat material narrows and shifts up in frequency, reaching 3304 cm^{-1} at a composition of 3:1 $N:Li^+$ and 3314 cm^{-1} at a dilution level of 27:1 C:N. While the

3313-14 cm^{-1} band is indicative of a strongly intramolecular hydrogen bonded species in the salt-free system, the 3304 cm^{-1} band represents an NH species undergoing cation association and hydrogen bonding of the NH···O type. This seems to imply that very little of the NH in the 20:1 N:Li^+ N,N'-DMPDA:LiTf is salt associated, since no band is present in the 3304-3306 cm^{-1} range. This is an important difference from the diluted 20:1 N:Li^+ N,N'-DMEDA:LiTf spectra, which retained a weak band at 3305 cm^{-1} even with addition of CCl_4 at a molar ratio of 29:1 C:N.

In the 5:1 N:Li^+ composition, a single band centered at 3330 cm^{-1} shifts upward in frequency to 3306 cm^{-1} and develops a slightly higher frequency shoulder with CCl_4 addition. This seems to suggest that dilution simultaneously drives the N,N'-DMPDA:LiTf system to further salt association and reduces cation-heteroatom interaction, rather than simply breaking a previously existent interconnected network formed through salt association such as that seen by Rocher in N,N-DMEDA-LiTf[27] or in DPA-LiTf[13] or by Sanders in N,N'-DMEDA-NaTf.[15] Instead, the changes to the local environment, seem to diminish salt interaction with the compound resulting in the formation of a new population of NH, not previously seen with N,N'-DMPDA in either the diluted neat material or in the salt-laden systems. The high frequency shoulder is significant in that it develops with a high amount of CCl_4 (>4:1 C:N). The frequency of the shoulder (3323 cm^{-1}) suggests it may represent a population of NH experiencing either n-mer type intermolecular hydrogen bonding or weakened intramolecular hydrogen bonding, but which is not cation associated. This would

seem to support the formation a dimer or higher order type association upon addition of sufficient quantity of CCl_4. Crystals with these sorts of associations have been obtained with other (non-diluted) diamine-triflate complexes, such as tetramethylethylenediamine with sodium triflate and that compound with lithium triflate.[10] Unfortunately, at this time, no crystal structure is available to confirm this claim, though it is bolstered by the Raman scattering data given in Figure 5-17.

This figure contains Raman scattering spectra for 5:1 (upper) and 20:1 (lower) $N:Li^+$ N,N'-DMPDA:LiTf systems diluted with CCl_4. The spectrum of the 20:1 system experiences only a slight shift upward in frequency (to 3331 cm^{-1}) of the broad band centered at 3328 cm^{-1} with virtually no change in the band shape. Again, this is similar to the behavior seen with addition of CCl_4 to the salt-free N,N'-DMPDA system (Figure 5-7), where the band at 3328 cm^{-1} shifts to 3333 cm^{-1} though with some band narrowing. It is important to note

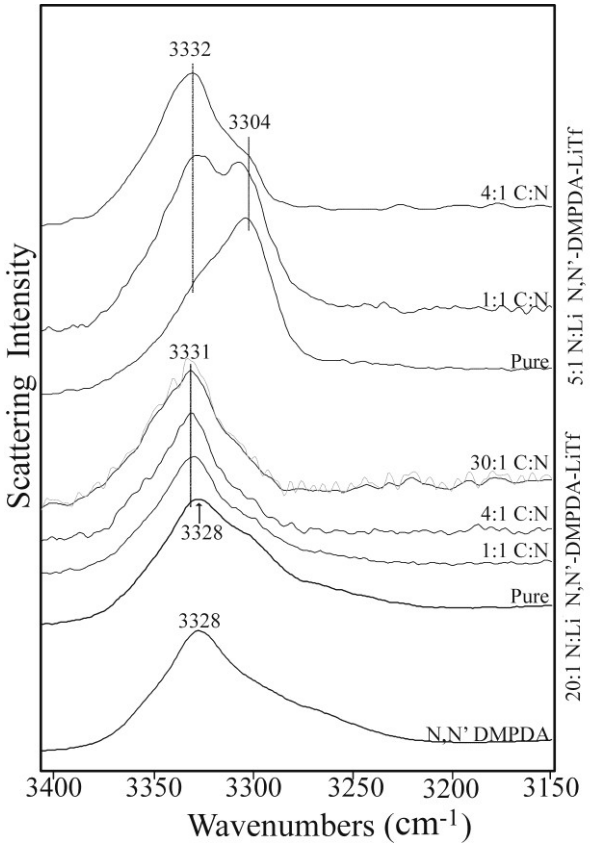

Figure 5-17: Raman spectra in the NH stretching region of CCl_4 dilutions of 20:1 $N:Li^+$ (lower) and 5:1 $N:Li^+$ complexes (upper) of N,N'-DMPDA with LiTf. Dilutions are given as C:N molar ratios.

the presence of a shoulder at 3304 cm^{-1} in the undiluted salt-laden system, which represents a very small population of cation associated N,N'-DMPDA. The intensity of the shoulder appears to decrease in the same proportion as the larger band with increasing CCl_4. However, the low intensity of all the bands at high dilution makes it impossible to make claims about any potential changes to the shoulder band. Like the IR absorbance data, the Raman scattering data seem to indicate that the amount of salt present in the 20:1 $N:Li^+$ N,N'-DMPDA:LiTf system is not sufficient to significantly interfere with the local structure (particularly hydrogen bonding) present in pure N,N'-DMPDA. Together, the IR absorbance and Raman scattering data indicate that at 20:1 $N:Li^+$ three types of NH groups are present in the diluted system: doubly intramolecular hydrogen bonded NH (3313 cm^{-1}), singly intramolecular hydrogen bonded NH (3331 cm^{-1}) and a small amount of cation associated $NH^{\cdots}O$ hydrogen bonded NH (3304 cm^{-1}). This is consistent with the expectation, based on the IR absorbance and Raman scattering data of the diluted neat material and those of the pure material with salt.

In contrast, in the 5:1 $N:Li^+$ N,N'-DMPDA:LiTf system, the hydrogen bonding interactions of the neat N,N'DMPDA have been thoroughly disrupted by the large amount of salt. The Raman scattering spectrum of the 5:1 $N:Li^+$ N,N'-DMPDA:LiTf shows a broad band at 3304 cm^{-1} with a shoulder at 3332 cm^{-1}, representing the NH groups undergoing cation association and $NH^{\cdots}O$ hydrogen bonding and the NH groups experiencing single intramolecular hydrogen bonding, respectively. With CCl_4 addition, the relative intensity of the these two bands

reverses with the 3332 cm^{-1} band becoming more intense than the 3304 cm^{-1} between a C:N ratio of 1:1 and 4:1.

Contrary to the IR absorbance data which seem to indicate that CCl_4 addition encourages cation association, these Raman scattering data seem to suggest that dilution disrupts cation association. This apparent contradiction may be resolved by considering the possibility that the Raman scattering bands at 3332 cm^{-1} and 3304 cm^{-1} are not coupled. Instead the cation associated and NH···O hydrogen bonded 3304 cm^{-1} population may be remaining stable despite CCl_4 addition. However, the NH···N intermolecular hydrogen bonded population seen in the IR absorbance as the low frequency tail of the 3295 cm^{-1} band may be disrupted by dilution. This solvent separated population is then free to form intramolecular hydrogen bonds represented by the 3332 cm^{-1} band in the Raman scattering data. Thus, the change in the relative intensity of the 3332 cm^{-1} and the 3304 cm^{-1} bands in the Raman scattering data results from the growth of the population represented by the 3332 cm^{-1} band at higher dilution levels. This is bolstered by the growth of the higher frequency shoulder (3323 cm^{-1}) in the 5:1 N:Li^+ N,N'-DMPDA:LiTf IR absorbance spectra with large amounts of CCl_4, which may represent n-mer type hydrogen bonding. This explanation would also be consistent with formation of dimer-type N,N'-DMPDA:LiTf complexes. However, claims about the behavior of the N,N'-DMPDA:LiTf cannot be conclusively drawn based on the NH region alone.

5.3.1.6 Summary of the NH Stretching Region

Table 5-1 provides a summary of the behavior of both model compounds and their 20:1 and 5:1 N:Li^+ lithium triflate complexes upon dilution. N,N'-DMEDA has mainly intermolecular (3285 cm^{-1}) and some intramolecular hydrogen bonding or n-mers (3328 cm^{-1}) in the pure form. CCl_4 addition results in the loss of most of the intermolecular hydrogen bonded species while retaining singly intramolecular hydrogen bonded NH groups (3333-3336 cm^{-1}) and gaining some non-hydrogen

Table 5-1: Summary of the frequencies of the major bands in the ν(NH) regions of the IR and Raman spectra of N,N'-DMEDA and N,N'-DMPDA and their 20:1 and 5:1 N:Li^+ complexes both pure and diluted with CCl_4

			Neat Sample (cm^{-1})	20:1 Sample (cm^{-1})	5:1 Sample (cm^{-1})
N,N'-DMEDA	IR	Pure	3285 + 3328 (sh)	3295 > 3330	3296 > 3335
		Dilute	3336 +higher sh	3337 > 3305	3305 > 3339
	Raman	Pure	3328 + 3285 (sh)	3327 + lower tail + higher sh	3330 > 3304
		Dilute	3333 + higher sh	3332 + higher sh	3335
N,N'-DMPDA	IR	Pure	3285	3295 + lower tail	3300
		Dilute	3314	3311	3306 + higher sh
	Raman	Pure	3328 + lower tail	3328 + lower sh	3304 + 3332 (sh)
		Dilute	3333	33331	3332 + 3306 (sh)

bonded NH groups. Pure N,N'DMPDA contains intermolecular hydrogen bonded NH groups (3285 cm^{-1}), some intramolecularly hydrogen bonded NH groups or n-mers (3328 cm^{-1}) as well as third moderately hydrogen bonded species (3314 cm^{-1}). Diluting pure N,N'-DMPDA results in the loss of the intermolecular hydrogen bonding, leaving only singly intramolecularly hydrogen bonded NH groups and the species undergoing moderately strong hydrogen bonding. It is suggested that this moderately strong hydrogen bonding population may be experiencing double intramolecular hydrogen bonding of both NH groups to each other as illustrated in Figure 5-10. The 3333-3336 cm^{-1} band would then correspond to the singly intramolecularly hydrogen bonded species which utilizes only one of the two available hydrogen atoms.

Upon complexation with lithium triflate, spectra of both N,N'-DMEDA and N,N'-DMPDA develop bands near 3304-3306 cm^{-1}. Comparison with spectra of dipropylamine-LiTf [13] and N,N'-DMEDA-NaTf,[15] for which crystal structures are available, allows this band to be assigned to NH groups undergoing both association to the cation and hydrogen bonding to triflate oxygen atoms. In N,N'-DMEDA a band at 3339 cm^{-1} persists even at a composition of 3:1 $N:Li^{+}$. This band has not been positively assigned. It may represent intramolecular hydrogen bonding slightly weakened by interactions with the cation or may result from non-bonded NH groups strongly associated to the cation. In N,N'-DMPDA addition of lithium triflate drives all NH groups into a single environment (3300-3304 cm^{-1}) of simultaneous cationic

association and hydrogen bonding (N-H···O) to the oxygen atoms of the triflate anion.

Diluting the 20:1 N:Li^+ salt complexes of N,N'-DMEDA and N,N'-DMPDA indicates that the small amount of salt present is insufficient to create large scale changes in the local hydrogen bonding environment as compared to the pure materials. Dilution of the 5:1 N:Li^+ complexes of both N,N'-DMEDA and N,N'DMPDA resulted in the disruption of the interconnected network formed through cation and anion association with the compounds. In N,N'-DMEDA:LiTf this resulted in two NH environments: the cationic associated and hydrogen bonded species (3304-3306 cm^{-1}) and the second environment (3336-3339 cm^{-1}). The frequency of the second species suggests either a non-hydrogen bonded species, but cationic associated species or a species experiencing weak hydrogen bonding and association. Unfortunately, assignment of this band to a specific species is not possible at this time. Dilution of 5:1 N:Li^+ N,N'-DMPDA:LiTf leads to three NH environments: the cationic associated and hydrogen bonded species (3304-3306 cm^{-1}), the singly intramolecular hydrogen bonded species (3332 cm^{-1}) and a small amount of a third species (3323 cm^{-1}). This third species was not seen in either dilution of neat N,N'-DMPDA or in the pure salt-laden system.

The assignments made to the IR and Raman spectral bands in the NH stretching regions for N,N'-DMEDA and N,N'-DMPDA are summarized in Table 5-2. The "free" band frequencies were assigned by Krueger,[14] whose work occurred at dilution factors up to ten times higher than those used in the present work. It should

Table 5-2: Assignments of the major bands in the ν(NH) regions of the IR and Raman spectra of N,N'-DMEDA and N,N'-DMPDA and complexes formed with lithium triflate in neat N,N'-DMEDA and N,N'-DMPDA and in CCl_4 dilutions. †Assigned by Krueger.[2]

Band	N,N'-DMEDA	N,N'-DMPDA
"Free" NH	†3361 cm^{-1}	†3371 cm^{-1}
Intermolecular N-H···N	3285 cm^{-1}	3285 cm^{-1}
Singly Intramolecular N-H···N	3333-3336 cm^{-1}	3332 cm^{-1}
n-mer type N-H···N	3328 cm^{-1}	3328 cm^{-1}
Doubly Intramolecular N-H···N	Not observed	3313-3315 cm^{-1}
Li^+ Associated and N-H···O	3304-3306 cm^{-1}	3304-3306 cm^{-1}
Unassigned	3339 cm^{-1}	3323 cm^{-1}

also be noted that Krueger's experiments utilized methylene chloride rather than the carbon tetrachloride employed here. "Free" NH vibrations were not observed in this study, but are supplied as a point of reference for the reader.

5.3.2 Backbone and Conformation Region

5.4.2.1 Introduction the Backbone Region

The IR and Raman regions from about 1000-800 cm^{-1} are a complex mixture of CH bending, NH bending, CC stretching and CN stretching vibrations. These modes would correlate to the backbone motions of the analogous polymers modeled by these compounds. In well studied systems, bands in this region can give insight into the conformational structure of the backbone. At this time, knowledge of the

N,N'-DMEDA and N,N'-DMPDA (and the related polymers) systems is insufficient to allow detailed conclusions with regard to specific conformations to be drawn from the spectral data in this region. However, useful information is available from spectra in the region. Though specific conformations cannot be identified, spectral changes stemming from interactions of backbone nitrogen atoms with the cations can be seen. These changes confirm cation association with or dissociation from the compound and may be correlated to changes seen in the N-H stretching region. .

5.3.2.2 Neat Materials

It is not possible to make detailed claims about the local conformations of the compounds based only on IR absorbance and Raman scattering spectra in this region. A computational study of N,N'-DMEDA by Boesch, *et al*.[3] suggests that the lowest energy conformation for the neat material is the trans-gauche-trans or TGT structure of N,N'-DMEDA, where the TGT designation refers to the C-N-C-C, N-C-C-N and C-C-N-C dihedral angles being of 180±60°, 60±60°and 180±60° respectively. The computed frequencies compare acceptably with the experimental frequencies presented in the same study. Preliminary computations on the N,N'-DMPDA suggest that the TG'GT structure may be the lowest energy structure for neat N,N'-DMPDA. This structure would have C-N-C-C, N-C-C-C, C-C-C-N and C-C-N-C dihedral angles of 180±60°, -60±60°, 60±60°and 180±60° respectively. These preliminary computational studies of N,N'-DMPDA are further discussed in section 5.4. Spectra of the neat materials are presented in the figures in the following

sections as reference for the changes seen with the addition of lithium triflate and/or carbon tetrachloride.

5.3.2.3 Carbon Tetrachloride Dilution

Carbon tetrachloride has several IR active bands in this region which are near to the bands of interest in the model compounds.[33] This precludes practical analysis of the IR absorbance spectra of the model compounds diluted in CCl_4. However, in the Raman scattering spectra there are fewer CCl_4 bands and little overlap between the CCl_4 and model compound bands.[33]

Figure 5-18 contains Raman scattering spectra for N,N'-DMEDA (lower) and N,N'-DMPDA (upper) at various levels of dilution with carbon tetrachloride. In both cases, the bottommost spectra of the series are the pure, undiluted model compound and the level of dilution increases moving up the stack. Dilution as given as C:N ratios. Most striking is that there are relatively few differences between the spectra of the pure materials and those of the diluted compounds. Several of the N,N'-DMEDA bands experience a gradual slight upward shift in frequency with increased CCl_4 and the band at 1266 cm^{-1} splits into two distinct bands. Similarly, in the NH stretching region (Figure 5-5), the N,N'-DMEDA ν(NH) band undergoes a gradual shift with increased CCl_4. This suggests that as the intermolecular hydrogen bonding in the pure N,N'-DMEDA is gradually broken by the CCl_4 and replaced by other types of hydrogen bonding interactions, the backbone conformation of the molecule is altered. Defining specific changes is beyond the scope of these data.

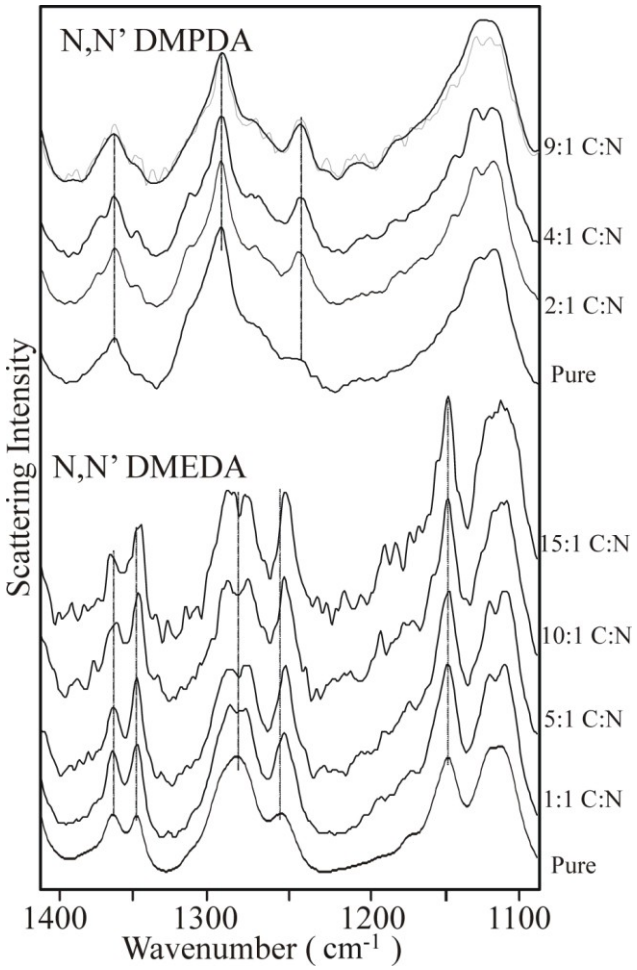

Figure 5-18: Raman scattering spectra of N,N'-DMDPA (upper stack) ranging from pure to 9:1 C:N ratio when diluted with CCl_4 and of N,N'-DMEDA (lower stack) ranging from pure to 15:1 C:N ratio when diluted with CCl_4.

Meanwhile, the N,N'-DMPDA spectra show extremely limited changes with the addition of CCl_4. The lack of change in band frequency or shape with dilution in the N,N'-DMPDA indicates that changes in hydrogen bonding interactions do not involve significant alteration of the backbone conformation. Previously in this chapter, structures for an n-mer type interaction and a doubly intermolecular hydrogen bonded species of N,N'-DMPDA were presented. In both cases, the backbone structure allowing these interactions was largely the same, TG'GT. It is reasonable to suggest that the added rotational axis provided by the third carbon in N,N'-DMPDA offers the more opportunities for different hydrogen bonding interactions from the same conformation than are available in N,N'-DMEDA. The TG'GT conformation strongly resembles that present in traditional six-membered rings. Perhaps TG'GT

N,N'-DMPDA is able to create pseudo-six-membered rings through a number of different interactions, including both inter- and intra-molecular hydrogen bonding. Therefore, the compound moves between these various interactions without changing the backbone conformation greatly. In contrast, N,N'-DMEDA, having only two carbon atoms, must undergo a change to its backbone conformation to shift between, intermolecular and/or n-mer type interactions and intramolecular hydrogen bonding.

5.3.2.4 Lithium Triflate Addition

Figure 5-19 contains IR absorbance (upper) and Raman scattering (lower) spectra for N,N'-DMEDA as a function of lithium triflate concentration in several areas of the backbone region. These regions were selected to avoid bands related to the vibrations of the triflate anion. Those bands will be in a later section (5.3.3). In this figure, neat N,N'-DMEDA is given as the bottommost spectra with LiTf amounts increasing from 20:1 N:Li^+ to 3:1 N:Li^+ moving up the spectral stacks. The far right stack presents the sub-region 925-800 cm^{-1}. This area is composed of bands mainly due to CH_2 motions. Both the IR absorbance and Raman scattering spectra of N,N'-DMEDA consist of a single broad band. In the IR absorbance, this band is of low intensity and centered at 876 cm^{-1}. In the Raman scattering spectra, the band is relatively more intense and centered at 878 cm^{-1}. With the addition of LiTf, this band decreases in frequency and a more intense lower frequency band appears. In the IR absorbance spectra the new band is centered at 841 cm^{-1}, while in the Raman

scattering spectra it is centered at 852 cm^{-1}. Additionally a large band active only in the IR spectra appears at 897 cm^{-1} at extremely high LiTf compositions (>5:1 $N:Li^+$).

The center panel illustrates the changes in the sub-region 1200-1080 cm^{-1}. This area has been attributed to CN stretching, CC stretching and some CH_2 motions.[2,3,15] Again, the Raman scattering and IR absorbance spectra of neat N,N'-DMEDA are very similar. Each of the neat spectra contains two main features: a band at 1148 cm^{-1} with a considerably less intense sideband at ~1170 cm^{-1} and set of overlapping bands present at ~1122 cm^{-1} and 1111 cm^{-1} (Raman) or 1106 cm^{-1} (IR).

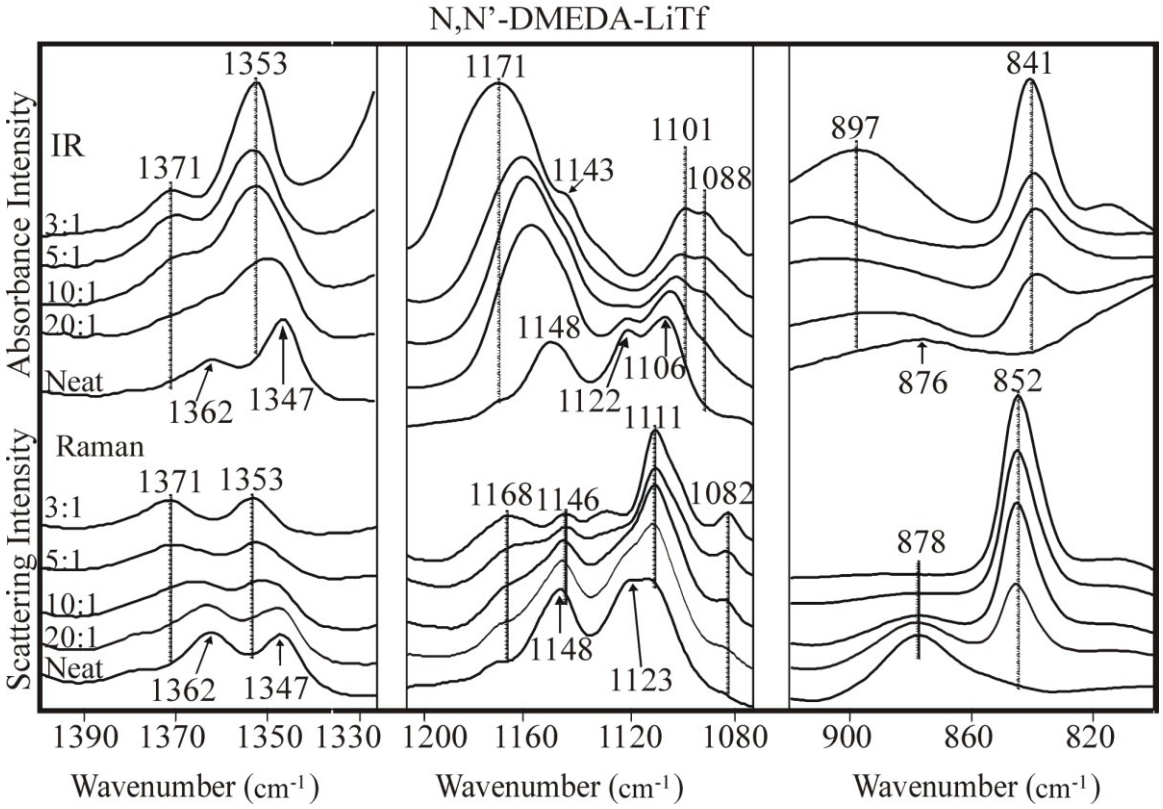

Figure 5-19: IR absorbance and Raman scattering data in the backbone region (1400-800 cm^{-1}) for neat N,N'-DMEDA and LiTf complexes of 20:1, 10:1, 5:1 and 3:1 $N:Li^+$

In the IR absorbance spectra, the overlapping bands are much better differentiated. With the addition of LiTf, the band at 1122 cm^{-1} decreases in intensity, eventually disappearing at LiTf compositions above 20:1 $N:Li^+$. The band at 1106 cm^{-1} shifts to lower in frequency reaching 1101 cm^{-1} at a composition of 5:1 $N:Li^+$, while a band at 1088 cm^{-1} grows in and overlaps with the 1101 cm^{-1} band. A similar trend is seen in the Raman scattering spectra where the band at 1123 cm^{-1} decreases intensity and disappears as compositions higher than 20:1 $N:Li^+$ while the band at 1111 cm^{-1} increase in intensity. Unlike, its IR active counterpart, this band does not appear to shift significantly from its position in the neat Raman spectrum. A band at 1082 cm^{-1} appears at a composition of 20:1 $N:Li^+$ and increases in intensity with greater LiTf addition. The apparent dramatic growth in the intensity and shift in the frequency of the IR absorbance band at 1148 cm^{-1} is a somewhat misleading, since the asymmetric stretch of the triflate anion CF_3 group is expected around 1170 cm^{-1}. It is difficult to discern the behavior of the 1148 cm^{-1} band in the confusion created by the overlying triflate band. However, in the Raman scattering spectra, the $\nu_{as}(CF_3)$ band (1168 cm^{-1}) is considerably less intense and does not overlap the 1148 cm^{-1}, which can be seen to shift to 1146 cm^{-1} while decreasing in intensity. The far left panel contains the sub-region 1400-1320 cm^{-1}, which consists of bands due to symmetric methyl deformations and more CH_2 motions. Both the IR absorbance and Raman scattering bands present in the neat material at 1362 cm^{-1} and 1347 cm^{-1} gradually shift up in frequency with addition of LiTf, reaching frequencies of 1371 cm^{-1} and 1353 cm^{-1}, respectively, by a composition of 3:1 $N:Li^+$. As before, no

specific claims as to the backbone structure can be made based on these data alone. However, it is clear that lithium triflate addition changes the backbone conformation of N,N'-DMEDA in some way. These frequencies are consistent with those calculated and experimentally observed by York *et al* for the N,N'-DMEDA:LiTf system.[2] Unfortunately, no crystal was available in that study, or in this one, to definitively confirm the association. However, Sanders *et al* were able to obtain a crystal structure for the N,N'-DMEDA-NaTf complex which proves cation association.[15] Frequencies in the backbone region in that study were similar to those found by York *et al*[2] and those in the present work. This is strong evidence for cation association with the backbone heteroatoms.

Similar trends are seen with N,N'-DMPDA. Figure 5-20 contains the IR absorbance (upper) and Raman scattering (lower) spectra for the neat N,N'-DMPDA (bottommost) and N,N'-DMPDA complexes with LiTf. The $N:Li^+$ ratio increases from 20:1 to 3:1 $N:Li^+$ moving up the spectral stack. The right hand panel contains the sub-region 925-800 cm^{-1}. The IR absorbance spectrum of the neat material has no strong bands in this region. However, addition of LiTf results in the growth of bands at 849 cm^{-1} and overlapping bands at 903 and 913 cm^{-1}. These bands are not associated with the triflate anion, but are bands developed out of cation interactions with the backbone.[2] In the Raman scattering spectra, the neat material shows a complex broad band feature containing bands centered at 903, 873, 859 and 812 cm^{-1}. With addition of lithium triflate, the band at 873 cm^{-1} decreases in intensity while the 859 cm^{-1} band increases in intensity and shift slightly downward. By a

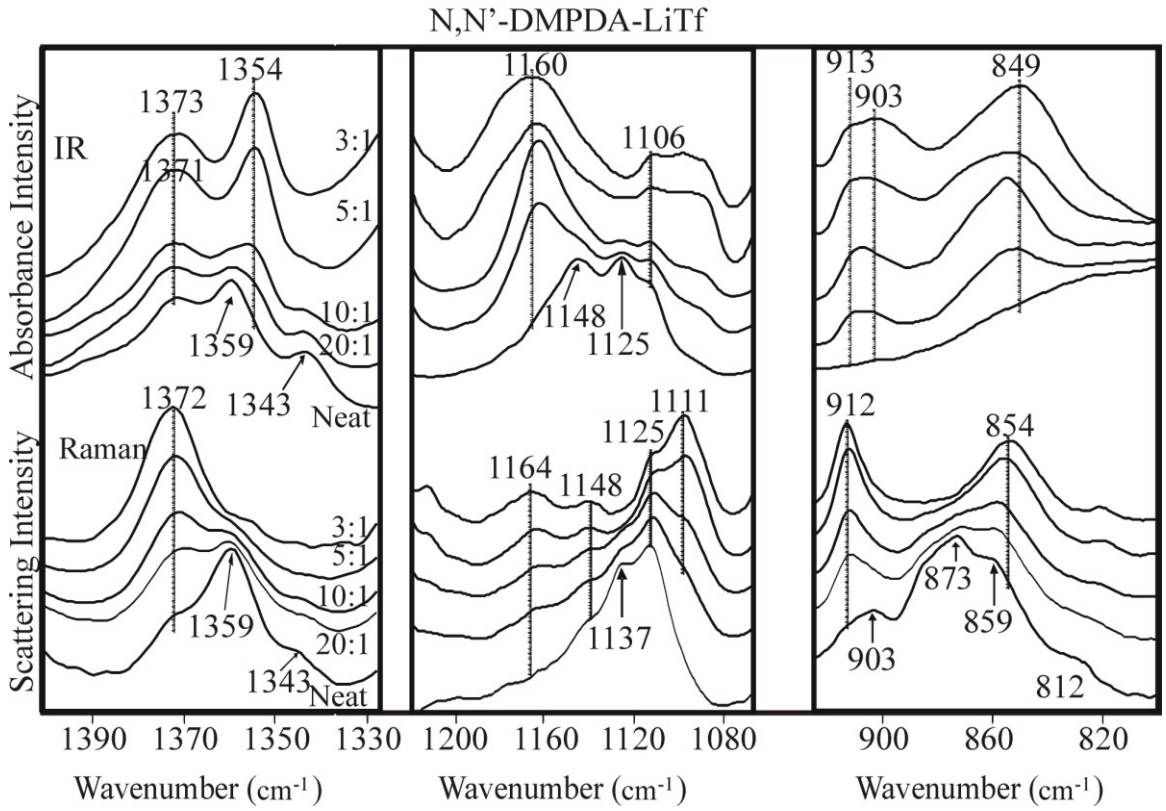

Figure 5-20: IR absorbance and Raman scattering data in the backbone region (1400-800 cm^{-1}) for neat N,N'-DMPDA and LiTf complexes of 20:1, 10:1, 5:1 and 3:1 $N:Li^+$ ratio

molar ratio of 5:1 $N:Li^+$, the 873 cm^{-1} band is completely lost in the broad feature formerly centered 859 cm^{-1}. The latter band reaches a frequency of 854 cm^{-1} at a molar ratio of 3:1 $N:Li^+$. With the addition of even a small amount of LiTf (20:1 $N:Li^+$) a band at 912 cm^{-1} appears. This band grows in intensity with increased lithium triflate. It is unclear whether the band at 903 cm^{-1} decreases in intensity or is simply subsumed by the 912 cm^{-1} band. The central panel contains spectra from the sub-region 1220-1060 cm^{-1}. The IR absorbance spectra of the neat N,N'-DMPDA is composed of three overlapping bands centered at 1148, 1125 and 1106 cm^{-1}. With

LiTf addition, these bands are replaced by two new features: a broad band at 1160 cm^{-1} and a series of overlapping bands beginning at 1106 cm^{-1} and running lower in frequency to about 1090 cm^{-1}. Deconvolution of individual bands in this latter feature proved impossible. The bands at 1160 cm^{-1} (IR) and 1164 cm^{-1} (Raman) must be treated cautiously because the triflate $\nu_{as}(CF_3)$ is expected around 1170 cm^{-1}, but does not appear there. The dramatic growth of the 1160 cm^{-1} band with triflate addition and absence of any other band near 1170 cm^{-1} suggests that the 1160 cm^{-1} (or 1164 cm^{-1}) band is the $\nu_{as}(CF_3)$ band downshifted. At a composition of 10:1 $N:Li^+$ or lower, both the neat N,N'-DMPDA bands and those bands induced by lithium triflate addition are visible. At compositions higher than 10:1 $N:Li^+$, only the bands induced by the lithium triflate addition are seen. In the Raman scattering spectra, the material exhibits a single broad feature composed of many overlapping bands. The three most prominent of these bands are centered at 1148, 1137 and 1125 cm^{-1}. With lithium triflate addition, the band at 1137 cm^{-1} decreases in intensity, while the band at 1148 cm^{-1} increases in intensity slightly. The intensity of band at 1125 cm^{-1} seems to hold relatively steady while a band at 1111 cm^{-1} grows in. Additionally, a broad feature of multiple unresolved bands appears around 1164 cm^{-1} as lithium triflate is increased. The far left panel contains spectra from the sub-region 1400-1325 cm^{-1}. As with the N,N'-DMEDA data in this area, the IR absorbance and Raman scattering spectra of the neat material look very similar. Both spectra contain overlapping bands centered at 1372, 1359 and 1343 cm^{-1}. Like the N,N'-DMEDA, the IR absorbance bands of the N,N'-DMPDA sample are better

differentiated than those in the Raman scattering spectra. With LiTf addition, the IR absorbance bands at 1371 and 1354 cm^{-1} increase in intensity while the intensity of the band at 1343 cm^{-1} decreases. The lower frequency band disappears at compositions greater than 10:1 $N:Li^+$. Similar behavior is seen in the Raman scattering data. The band at 1372 cm^{-1} increases in intensity with LiTf addition and the band at 1343 cm^{-1} decreases, disappearing at lithium triflate compositions larger than 10:1 $N:Li^+$. However, the band at 1359 cm^{-1} also decreases in intensity, becoming a very minor sideband by a composition of 5:1 $N:Li^+$. In all, these spectral changes provide strong evidence of cation association to the N,N'-DMPDA molecule and suggest that some changes to the backbone conformation are likely induced by the association. Specific changes are beyond the scope of this analysis.

5.3.2.5 Carbon Tetrachloride Dilution of LiTf Complexes

As previously mentioned, IR absorbance data are not particularly useful in this region since carbon tetrachloride contains several bands, which lie near or over the compound bands,[33] obscuring any spectral changes that might be occurring. However, this is not the case with the Raman scattering data. Figure 5-21 contains Raman scattering spectra for 5:1 $N:Li^+$ N,N'DMEDA-LiTf (left) and 5:1 $N:Li^+$ N,N'-DMPDA:LiTf (right) complexes diluted with CCl_4. Spectra of the salt-free, undiluted compounds are given as the bottommost spectra for comparison. The spectrum of salt-free, undiluted N,N'-DMEDA, consists of a broad band at 880 cm^{-1}, which has been attributed to a mix of NH bending and CH_2 rocking motions.[3] In the 5:1 $N:Li^+$ N,N'DMEDA-LiTf complex, this band shifts to 845 cm^{-1} due to

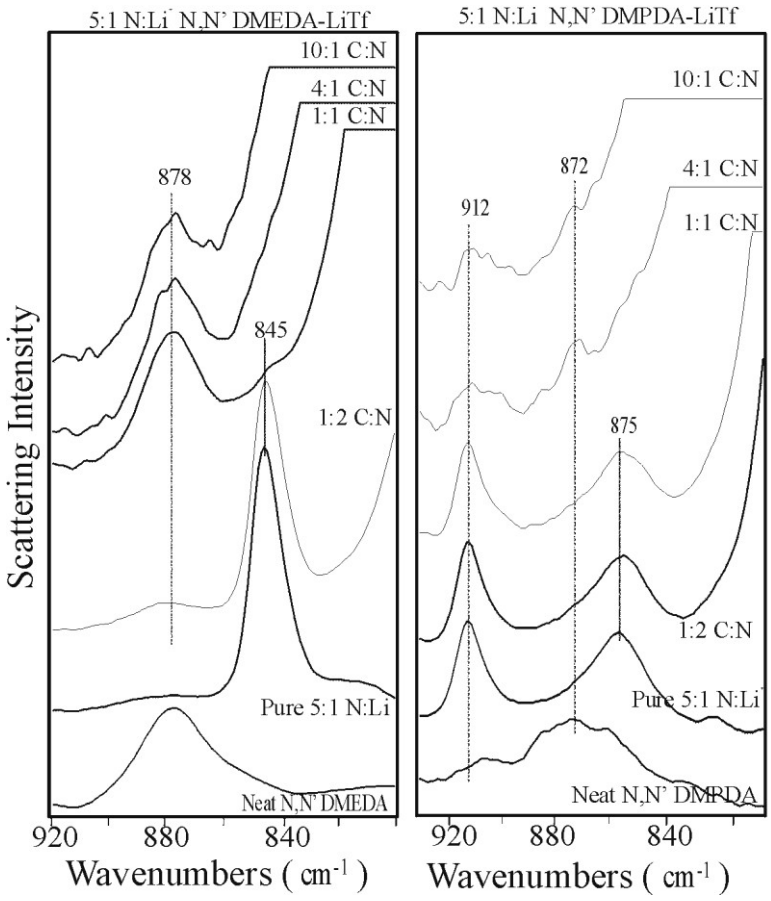

Figure 5-21: Raman scattering spectra of 5:1 N:Li^+ N,N'-DMEDA:LiTf (left) and 5:1 N:Li^+ N,N'-DMPDA-LiTf (right) complexes undiluted and diluted in CCl4 at C:N ratios of 1:2, 1:1, 4:1 and 10:1.

conformational changes occurring upon association.[2] When CCl_4 is added to a ratio of 1:2 C:N, this band is unaffected. However, increased amounts of CCl_4 (even as low as 1:1 C:N) result in a dramatic intensity loss in the band at 845 cm^{-1} and a corresponding increase in intensity in the band at 880 cm^{-1}. The nearby rapidly growing CCl_4 band makes it difficult to determine if the 845 cm^{-1} band is completely eliminated at higher CCl_4 levels, but clearly its intensity is diminished significantly. The growth of the 880 cm^{-1} with CCl_4 addition is unmistakable. This suggests that upon CCl_4 addition at levels above the 1:2 C:N threshold, there is no appreciable cation interaction with the backbone as the spectra strongly resemble that of the salt-free system. This is consistent with Raman

scattering data from the NH stretching region (Figure 5-15) which indicates that a dramatic change in local environment occurs around the same CCl_4 level. These data also show the decrease in salt interaction and the return to spectral features similar to those present in the salt-free system.

A similar scenario occurs with dilution of the N,N'-DMPDA:LiTf system. The broad grouping of overlapping bands centered at 872 cm^{-1} in salt-free undiluted N,N'-DMPDA shifts to a single broad band centered at 875 cm^{-1} and a band at 912 cm^{-1} appears at a composition of 5:1 $N:Li^+$ with LiTf. These bands persist unperturbed with CCl_4 dilution until a dilution ratio somewhere between 1:1 C:N and 4:1 C:N is reached. At this point, the band at 875 cm^{-1} collapses and the 872 cm^{-1} feature returns. Likewise the band at 912 cm^{-1} undergoes a significant intensity loss. The spectra of 4:1 C:N and higher dilutions more closely resemble that of the salt-free undiluted N,N-DMPDA than that of the 5:1 $N:Li^+$ complex. As with the N,N'-DMEDA:LiTf system, this is consistent with the Raman scattering data of the NH stretching region, which also show a decrease in cation-backbone interaction through a resemblance to the salt-free system spectra. This occurs somewhat less dramatically and at a higher dilution level in the N,N'-DMPDA:LiTf system than in the N,N'-DMEDA counterpart, suggesting the N,N'-DMPDA system is more stable against these sorts of changes than the N,N'-DMEDA system. In fact, in both the NH stretching region and the conformation region, the N,N'-DMPDA shows more evidence of residual salt association at high level of dilution than the N,N'-DMEDA system, where virtually all evidence of salt association is lost by dilutions levels

greater than 1:1 C:N. This pattern is repeated for both N,N'-DMEDA and N,N'-DMPDA in several bands across the conformation region. This may be interpreted as evidence of CCl_4 dilution breaking a polymeric network type structure formed through the association of the salt with the compound. As the network is disrupted, discrete dimer-type associations are made with the salt and some compound molecules, but the rest return to their salt-free state.

5.3.3 Ionic Association Region

5.3.1.1 Some Background

As discussed in Chapters 3 (§3.4.4) and 4 (§4.4.2), significant information about ionic associations occurring in the LiTf complexes can be garnered by studying the vibrational bands affiliated with the anion. In general, for lithium triflate, the most informative bands are the symmetric CF_3 bend, $\delta_s(CF_3)$ and the symmetric SO_3 stretch, $\nu_s(SO_3)$. These bands occur around 750-760 cm^{-1} ($\delta_s(CF_3)$), about 1030-1060 cm^{-1} ($\nu_s(SO_3)$). The asymmetric CF_3 stretch, $\nu_{as}(CF_3)$, seen at approximately 1170 cm^{-1} in ether oxygen systems, is also sensitive to changes in ionic associations.

The use of triflate anion bands to identify ionic associations is common practice in ether oxygen based systems and the frequencies have been well characterized.[34-37] These assignments also have been successfully extended to some amine based systems as well.[2,29,38] The amine and polyimine studies found that while the triflate anion modes did not retain precisely identical vibrational

frequencies as those found in the ether oxygen systems, the general trend holds: increased degree of association results in an upward shift of vibrational frequency. Therefore, the frequency of "free" triflate is anticipated to be less than that of contact ion pair, which should be less that of triple cation, which in turn should be less than that of higher order aggregate species.

Understanding the types of ion associations occurring in the system can give insight into ion transport and eventually conductivity mechanisms. Additionally, it has become clear from both the NH stretching and backbone region spectra that dilution of the salt-containing compounds with CCl_4 results in significant changes to the local environment, which probably reduce the degree of interaction between the salt and the the compound. It is hoped examination of spectral regions associated with vibrations of the triflate ion could give insight into this process by indicating the changes in the types of interactions the anion experiences.

5.3.1.2 Lithium Triflate Addition

IR absorbance (lower) and Raman scattering (upper) spectra for neat N,N'-DMEDA and 20:1, 10:1, 5:1 and 3:1 N,N'-DMEDA:LiTf complexes are shown in Figure 5-22. The lowermost spectrum in each panel is of the neat material with the amount of LiTf increasing moving up the spectral stack. The symmetric CF_3 deformation, $\delta_s(CF_3)$, is shown in the right panel of Figure 5-22. York, *et al*[2] and Sanders *et al*[15] have both extended the $\delta_s(CF_3)$ modes assignments given by Huang and Frech[39] for a number of oxygen containing organic compound to N,N'-DMEDA. Based on this, the band produced at 756 and 757 cm^{-1} in the IR absorbance and

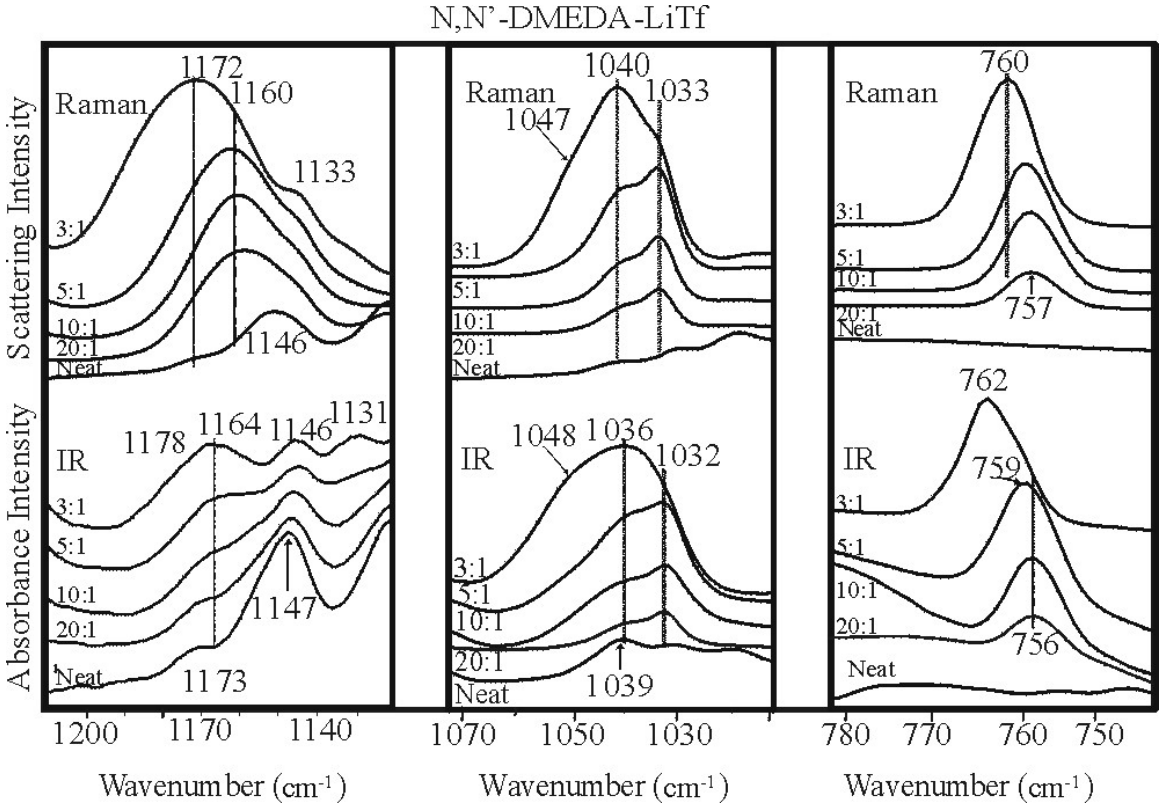

Figure 5-22: IR absorbance and Raman scattering data in the regions affiliated with the $\nu_{as}(CF_3)$, $\nu_s(SO_3)$ and $\delta_s(CF_3)$ vibrations of the triflate anion in N,N'-DMEDA:LiTf complexes of 20:1, 10:1, 5:1 and 3:1 $N:Li^+$ molar ratio

Raman scattering spectra at composition of 20:1 $N:Li^+$ may be attributed to contact ion pairs. By a composition of 3:1 $N:Li^+$, this band shifts to 760 cm^{-1} in the Raman scattering spectrum and 762 cm^{-1} in the IR absorbance spectrum. These frequencies represent contact ion pairs, [LiTf] and the triple ion $[Li_2Tf]^+$ respectively. These data are consistent with those presented by Sanders, *et al*[15] for N,N'-DMEDA-NaTf and York, *et al*[2] for N,N'-DMEDA:LiTf.

The center panel of Figure 5-22 contains the $\nu_s(SO_3)$ region from 1080-1010 cm^{-1}. Neat N,N'-DMEDA has some weak bands underlying this region in both the

IR absorbance and Raman scattering spectra. The addition of lithium triflate to 20:1 $N:Li^+$ broadens and increases the intensity the underlying band at 1039 cm^{-1} and brings about the appearance of a more intense band at 1032 cm^{-1}. By a composition of 3:1 $N:Li^+$, the band broadening becomes such that a single broad band is present. Analysis using mixed Gaussian-Lorentzian distribution reveals the presence of three overlapping bands at 1048, 1036 and 1032 cm^{-1}. The Raman scattering spectrum behaves similarly with only slight differences in band centers (1047, 1040 and 1033 cm^{-1}) of the broad feature at high LiTf compositions. It is clear from the increased frequencies seen with increased LiTf addition that the system moves from "free" anion (1032-3 cm^{-1}) with some contact ion pairs (1036-40 cm^{-1}) at low LiTf compositions to mostly contact ion pairs (1036-40 cm^{-1}) and triple ion or higher aggregates (1047-48cm^{-1}) at higher LiTf compositions. Again, this is consistent with the data presented by York *et al*[2] and Sanders *et al*.[15]

The $\nu_{as}(CF_3)$ region is shown in the far left panel of Figure 5-22. Unfortunately underlying model compound bands make detailed interpretation of this region difficult. The backbone bands at 1147 cm^{-1} (IR) or 1146 cm^{-1} (Raman) and at 1173 cm^{-1} in the IR absorbance somewhat obfuscate the $\nu_{as}(CF_3)$ band, which initially appears at around 1164 cm^{-1} (IR) or 1160 cm^{-1} (Raman) in the 20:1 $N:Li^+$ samples. In both cases, the band increases in intensity and breadth and appears to shift upward in frequency with addition of LiTf. By a composition of 3:1 $N:Li^+$, the broad band appears centered at ~1170-72 cm^{-1}, but can be deconvoluted into distinct bands at 1164 and 1178 cm^{-1} in the Raman scattering spectrum and 1160 and 1178

cm^{-1} in the IR absorbance spectrum. Unfortunately, this region has not been as extensively studied as the $\delta_s(CF_3)$ region, so assignments of the these bands to specific ion species has not been accomplished. However, the upward shift in frequency is consistent with that seen in $\nu_s(SO_3)$ and $\delta_s(CF_3)$. Certainly, the increasing frequency suggests a more highly aggregated species with increased salt concentration.

The trend of increased aggregation with increased salt concentration continues with N,N'-DMPDA. IR absorbance and Raman scattering data for the N,N'-DMPDA:LiTf system are shown in Figure 5-23. This figure is organized just as the N,N'-DMEDA:LiTf figure, with the $\nu_{as}(CF_3)$ region on the far left, the $\nu_s(SO_3)$ in the center panel and the $\delta_s(CF_3)$ region on the far right. In all three panels, the neat N,N'-DMPDA spectrum is the bottommost trace with the amount of LiTf increasing from 20:1 to 3:1 $N:Li^+$ moving upward. Though there are no published data relating directly to ionic association in the N,N'-DMPDA:LiTf complex, it is it is reasonable to expect that the assignments used for N,N'-DMEDA:LiTf could be applied to this system as well. The $\delta_s(CF_3)$ data for N,N'-DMPDA:LiTf, given in the right panel of Figure 5-23, shows a definite move toward higher aggregation with increased lithium triflate addition. In both the IR absorbance and Raman scattering spectra, a triflate band appears at 758 cm^{-1} in the 20:1 $N:Li^+$ composition.

This band remains constant, until abruptly shifting to 760 cm^{-1} at a composition between 5:1 and 3:1 $N:Li^+$. Both these frequencies are in the contact ion pair frequency range suggested by York *et al.*[2] However, the abrupt shift of the

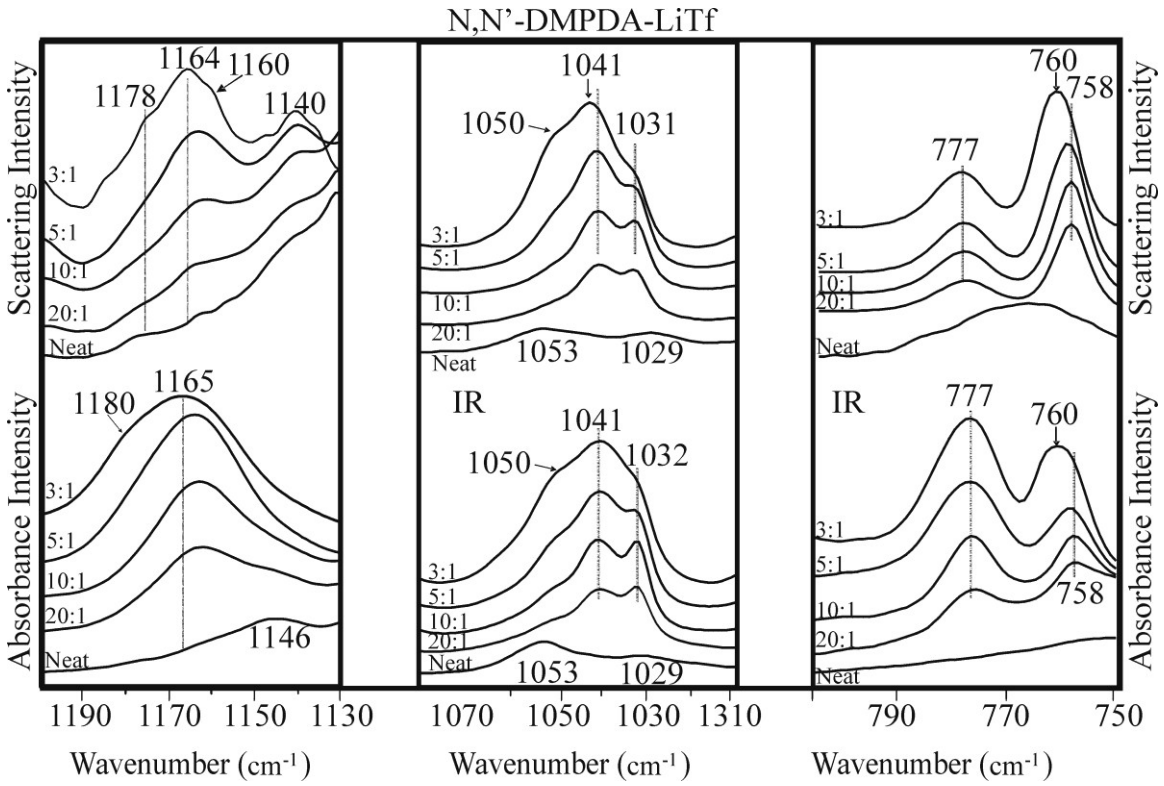

Figure 5-23: IR absorbance and Raman scattering data in the regions affiliated with the $\nu_{as}(CF_3)$, $\nu_s(SO_3)$ and $\delta_s(CF_3)$ vibrations of the triflate anion in N,N'-DMPDA-LiTf complexes of 20:1, 10:1, 5:1 and 3:1 $N:Li^+$ molar ratio

band to 760 cm^{-1} suggests a discrete species. The range given by York, *et al* for the contact ion pairs in N,N'-DMEDA:LiTf[2] is slightly higher than that seen by the same group in the linear PEI-LiTf and linear PEI-NaTf systems.[38] The latter publication put 760 cm^{-1} in the unassigned region between contact ion pair and triple ion. It is reasonable to extend the solvent dependence argument presented by Frech and Huang[39] for oxygen containing organic compounds (given in previous chapters) to amines in order to explain this slight variation. Indeed, York, *et al* warn that anion-solvent interactions in solvents capable of hydrogen bonding may result in alterations of expected anion mode frequencies with CF_3 modes being more susceptible to such

changes than SO_3 modes.[2] Sanders, *et al* also reference this explanation when assigning 761 cm^{-1} firmly to the triple ion $[Na_2Tf]^+$ in N,N'-DMEDA-NaTf.[15] The strong band developed at 777 cm^{-1} is most likely not a triflate band, but a compound band resulting from cation interaction with the nitrogen atoms and can most probably be assigned to an NH bend. The computational evidence for this assignment is found in the N,N'-DMEDA:LiTf and N,N;-DMEDA-LiBr work of York, *et al*.[2] It should however by noted the experimental data in the N,N'-DMEDA-NaTf system shows a band at 770-772 cm^{-1} which is attributed to $[Na_3Tf]^{2+}$.[15] While some solvent dependent shifting is expected, this shifting is anticipated to be in the 1-2 cm^{-1} range rather the 5-7 wavenumber difference seen here.

Like the N,N'-DMEDA system, the situation in the $\nu_s(SO_3)$ region in the N,N'-DMPDA:LiTf system is complicated by broad underlying compound bands centered at 1053 cm^{-1} and 1029 cm^{-1} in both the IR and the Raman spectra. A general trend toward higher aggregation is apparent in both the IR absorbance and Raman scattering data. The triflate band initially appears around 1040 cm^{-1} in the 20:1 $N:Li^+$ complex. The underlying band at 1029 also appears to increase in intensity and shift slightly to 1032 cm^{-1}. This is most likely not a change in the 1029 cm^{-1} band itself, but results of the emergence of the $\nu_s(SO_3)$ band at 1032 cm^{-1}. With increasing LiTf, both the 1032 cm^{-1} and 1040 cm^{-1} bands increase in intensity and breadth, becoming a single intermingled feature by a molar ratio of 3:1 $N:Li^+$. This feature also contains a band centered at 1050 cm^{-1}. According to the assignments given by York *et al*[2] in the N,N'-DMEDA:LiTf system, these frequencies (1032

cm^{-1}, 1040-1041 cm^{-1} and 1050 cm^{-1}) correspond to the "free" ion, contact ion pair and the triple ion, suggesting a shift toward higher aggregation with increased LiTf content.

Again, this trend (more lithium triflate leads to higher order of aggregates) is seen in the $\nu_{as}(CF_3)$ band, shown in the left panel of Figure 5-23. Though to a lesser degree than in N,N-DMEDA, underlying bands in the neat N,N'-DMPDA complicate the spectra of this region. In IR, this band appears at about 1162 cm^{-1} in IR and Raman spectra at a composition of 20:1 $N:Li^+$ and grows in breadth and intensity with the addition of LiTf. The also appears to shift upward in intensity and develop a high frequency shoulder at higher LiTf contents. By a composition of 3:1 $N:Li^+$, three bands are present within the feature. In the IR absorbance spectra, these bands are centered at 1160, 1165 and 1180 cm^{-1}, while in the Raman scattering spectra, they appear at 1160, 1164 and 1178 cm^{-1}. Like the $\delta_s(CF_3)$ and $\nu_s(SO_3)$ bands previously, these frequencies strongly indicate a move toward increased degree of association with increased salt concentration. Given the agreement of these frequencies with those seen in N,N'-DMEDA:LiTf, preliminary assignments are made to the "free" ion at approximately 1160 cm^{-1}, the contact ion pair at around 1164-1165 cm^{-1} and the triple ion at 1178-1180 cm^{-1}. These tentative assignments are based on the species shown to be present by the other anionic vibrations ($\delta_s(CF_3)$ and $\nu_s(SO_3)$). A crystal structure and a systematic analysis of changes in vibration frequencies in this region with a cation known to eschew association (*e.g.*

tetrabutylammoniumtrifluoro-methanesulfonate, TBATf,) would be necessary to confirm these assignments.

5.4.1.3 Carbon Tetrachloride Dilution of LiTf Complexes

Dilution of the samples in CCl_4 causes some experimental problems in these regions, since CCl_4 bands are present very near to the anionic bands of interest. Most noticeably impacted is the $\delta_s(CF_3)$ region where a CCl_4 band at 762 cm^{-1} is present in both the IR absorbance and Raman scattering spectra.[33,40] The superimposed positions of the CCl_4 and $\delta_s(CF_3)$ band render this region unsuitable for use in CCl_4 dilution studies. The $\nu_s(SO_3)$ is free of band interference in both the Raman scattering and IR absorbance spectra and the $\nu_{as}(CF_3)$ IR absorbance spectra are clear of impeding bands as well.

The $\nu_s(SO_3)$ regions of the N,N'-DMEDA:LiTf Raman scattering and IR absorbance spectra are shown in Figure 5-24. In both spectral stacks, the lowermost spectra are pure (undiluted) 5:1 $N:Li^+$ N,N-DMEDA:LiTf, with dilution (CCl_4 content) increasing moving up the stack. In IR absorbance the pure 5:1 $N:Li^+$ sample has more of the "free" species at 1032 cm^{-1} with the band at 1040 cm^{-1}, representing the contact ion pair, being slightly less intense and the higher order aggregate signified by the band at 1051 cm^{-1} minimally present. Increased CCl_4 shifts the system toward higher aggregation and by a ratio of only 1:1 C:N, the contact ion pairs have overtaken the "free" ions as the most populous species. This continues to a ratio of at least 29:1 C:N, by which time the "free" ions are a minor species and the triple ion at 1051 cm^{-1} has significantly increased as evidenced by the growth of the

high frequency side of the band. This is repeated in the Raman scattering spectra where the only species present in the pure 5:1 $N:Li^+$ material are those represented by the 1032 cm^{-1} ("free") and 1040 cm^{-1} (contact ion pair) bands. By a ratio of 1:2 C:N, the contact ion pairs dominate (1032 cm^{-1} < 1040 cm^{-1}) and by 4:1 C:N, the 1049 cm^{-1} (triple ion) is discernable as a substantial side band while the 1032 cm^{-1} band has largely disappeared.

The trend toward higher aggregation with dilution is repeated in the $\nu_{as}(CF_3)$ IR absorbance spectra given in Figure 5-25. Again the lowermost spectrum is the undiluted 5:1 $N:Li^+$ N,N'-DMEDA:LiTf, with the upper spectra being those of increasing

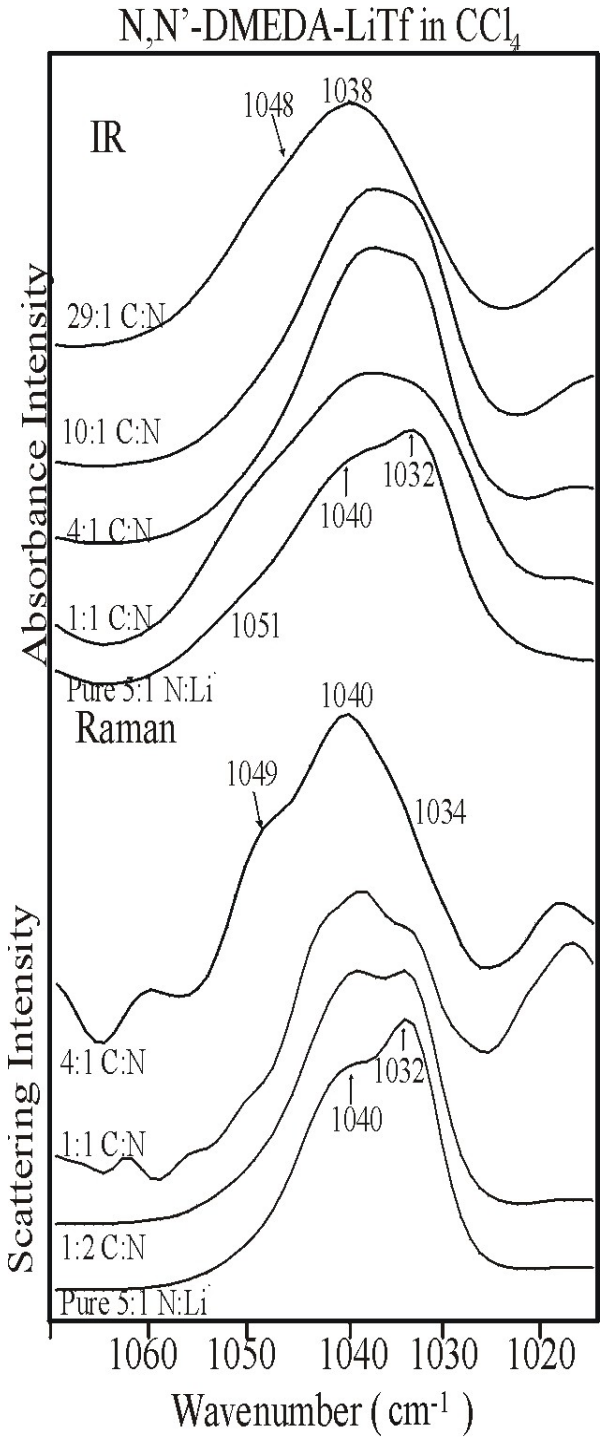

Figure 5-24: Raman scattering (lower) and IR absorbance (upper) spectra in the symmetric SO_3 stretching region, $\nu_s(SO_3)$ for increasing dilutions of 5:1 $N:Li^+$ N,N-DMEDA:LiTf

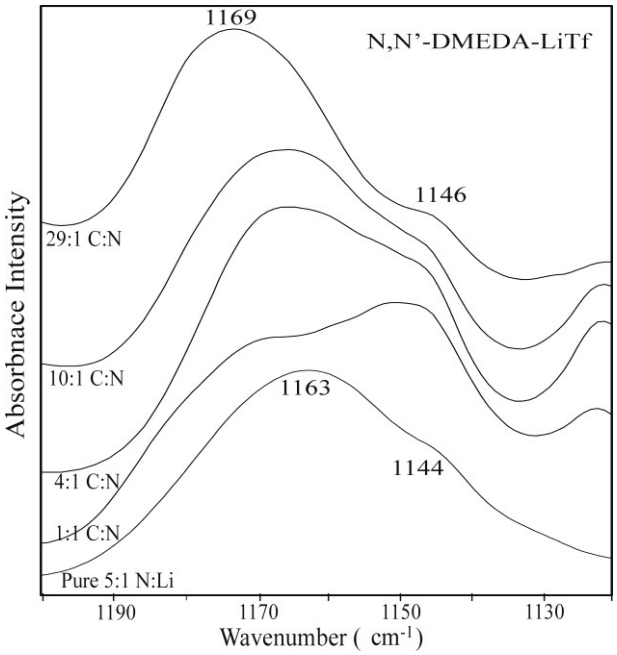

Figure 5-25: IR absorbance spectra in the asymmetric CF_3 stretching region, $\nu_{as}(CF_3)$ for increasing dilutions of 5:1 N:Li^+ N,N-DMEDA:LiTf

dilution given as C:N ratios. The $\nu_{as}(CF_3)$ band is present in the pure 5:1 N:Li^+ material at 1163 cm^{-1}. The large side band centered at 1144 cm^{-1} is a host band inherent to the N,N'-DMEDA. The $\nu_{as}(CF_3)$ band increases in intensity relative to the host band and shifts to a higher frequency with increasing dilution, reaching 1169 cm^{-1} by a C:N ratio of 29:1. This shift to higher aggregation, along with the shift seen in the $\nu_s(SO_3)$ region strongly suggests that with dilution the local structure is radically transformed in a way that very likely involves breaking the interconnected network of hydrogen bonding and ion interaction with the nitrogen heteroatoms by stripping ions from the backbone of the material.

This is seen again in the N,N'-DMPDA:LiTf system. Figure 5-26 contains Raman scattering (lower) and IR absorbance spectra (upper) for various dilutions of 5:1 N:Li^+ N,N'-DMPDA:LiTf starting with the undiluted material at the bottom of the spectral stack and increasing dilution moving up the stack. Deconvolution of the pure 5:1 N:Li^+ N,N'-DMPDA:LiTf Raman scattering spectrum reveals three distinct

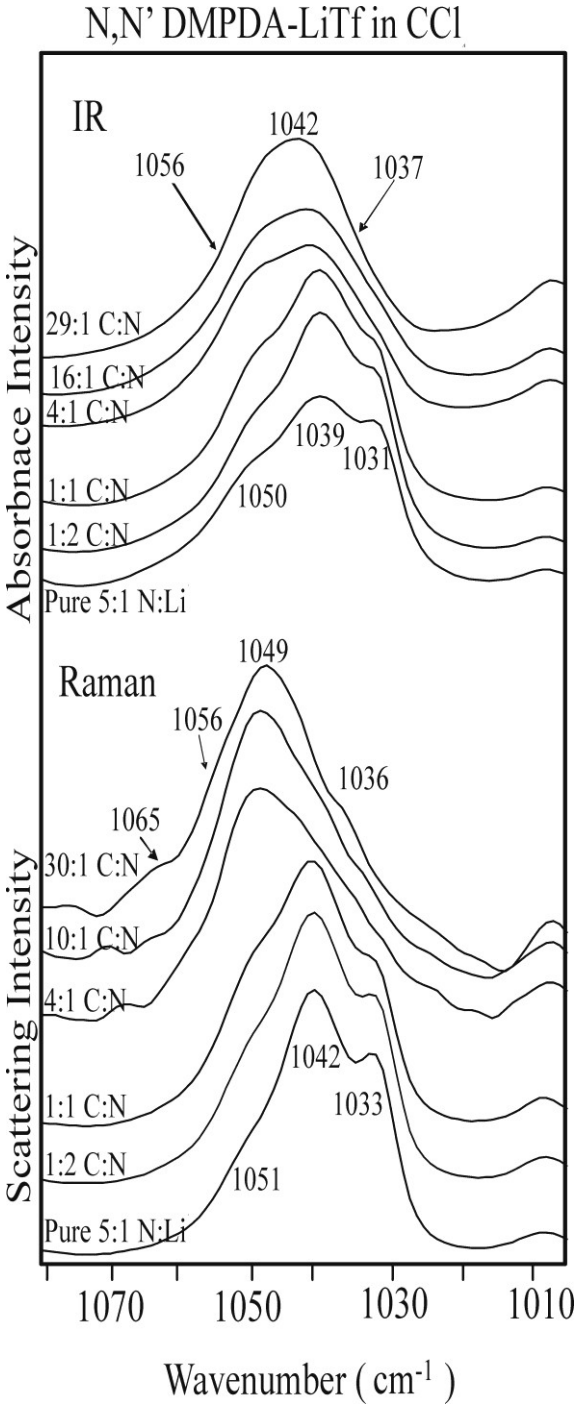

Figure 5-26: Raman scattering (lower) and IR absorbance (upper) spectra in the symmetric SO_3 stretching region, $\nu_s(SO_3)$ for increasing dilutions of 5:1 $N:Li^+$ N,N-DMPDA:LiTf

populations of anions: "free" (1033 cm^{-1}) ions, contact ion pairs (1042 cm^{-1}) and triple ions (1051 cm^{-1}). While these are the same three populations initially present in the N,N'-DMEDA:LiTf system (Figure 5-23), the distribution is significantly different. In N,N'-DMEDA:LiTf, the "free" ion is largest population followed by the contact ion pairing, with any higher order aggregates being negligible in the undiluted system. In contrast, in N,N'-DMPDA:LiTf, the largest population is the contact ion pair followed by "free" ion, but with significant amount of higher aggregate present.

The same trend may be seen in the IR absorbance data where, N,N'-DMPDA:LiTf is dominated by contact ion pair followed by "free" and significantly more higher order

aggregate than seen in the "free" ion dominated N,N'-DMEDA:LiTf system (Figure 5-23). Addition of CCl_4 results in a shift toward higher aggregation. By a ratio of 4:1 C:N, the triple ion has become the dominant species in the Raman scattering spectra with a nearly complete loss of "free" ion and the development of an even higher order aggregate represented by the 1056 cm^{-1} shoulder. Similarly in the IR absorbance spectra, a shift toward higher aggregation is evidenced by the band center shift to 1042 cm^{-1}, which can be deconvoluted into nearly identical populations of contact ion pair and triple ion. Again the presence of an even higher order aggregate is suggested by the shoulder at 1056 cm^{-1}. This general behavior was seen in N,N'-DMEDA:LiTf, but at overall lower frequencies. The highest frequencies seen with N,N'-DMEDA:LiTf were 1048 cm^{-1} (IR) and 1049 cm^{-1} (R). This suggests, as have numerous previous data, the N,N'-DMPDA:LiTf system experience overall higher order

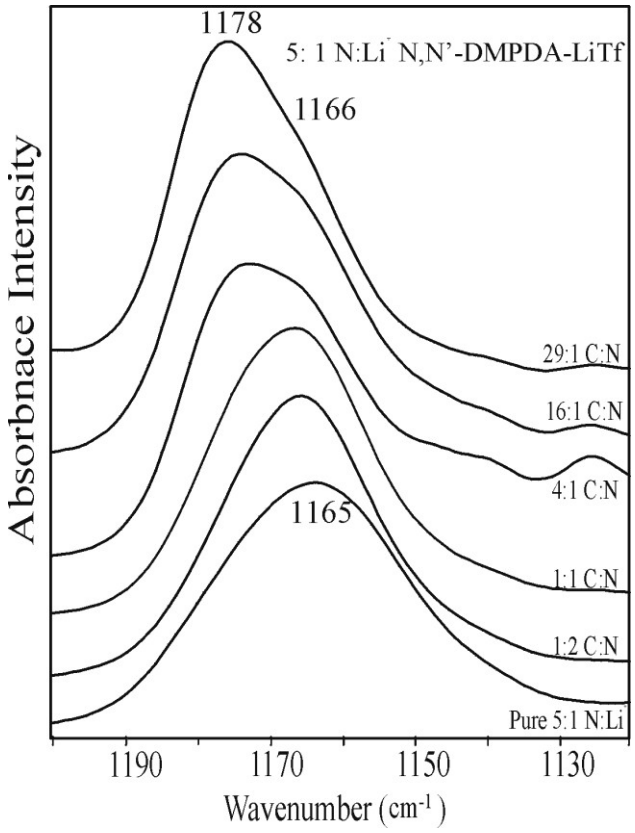

Figure 5-27: IR absorbance spectra in the asymmetric CF_3 stretching region, $\nu_{as}(CF_3)$ for increasing dilutions of 5:1 $N:Li^+$ N,N-DMPDA:LiTf

aggregation than the N,N'-DMEDA:LiTf system. This trend is dramatically shown in the IR absorbance spectra of the $\nu_{as}(CF_3)$ region of N,N'-DMPDA:LiTf illustrated in Figure 5-27.

Here, the undiluted pure 5:1 N:Li^+ N,N'-DMPDA:LiTf appears to have single broad fairly symmetric band centered at 1165 cm^{-1}. Below a ratio of 4:1 C:N minimal changes occur. The band slightly narrows, but remains centered at 1165 cm^{-1}. Increasing CCl_4 addition beyond this ratio causes an abrupt change in the system somewhere between 4:1 C:N and 16:1 C:N. A band at 1178 cm^{-1} rapidly gains in intensity, becoming the primary band while maintaining a shoulder at 1166 cm^{-1}. Similar behavior was seen with N,N'-DMEDA:LiTf (Figure 5-24), but the shift was only 6 wavenumbers from 1163 cm^{-1} to 1169 cm^{-1}. This again indicates a higher overall aggregation in N,N'-DMPDA:LiTf than in N,N'-DMEDA:LiTf. The N,N'-DMPDA:LiTf system, like the N,N'-DMEDA:LiTf system, appears to undergo a change in local structure with the addition of CCl_4 that may involve the breaking of the interconnected network present in the pure and slightly diluted systems and a change in the types of associations formed, as well as a loss of cation association with the backbone.

Initially, it would seem that dilution should result in lower order ionic association as the molecules are spread apart by the diluent. However, this is not the case. Raman scattering data from the NH stretching regions show the loss of the cation associated stretching band, while IR data suggest this association is maintained. Meanwhile, spectral data from the backbone modes indicate high level

of dilutions cause an abrupt change resulting in spectra that more closely resemble the salt-free material. Taken together, these data point to dramatic changes in local structure. The network, especially in N,N'-DMPDA:LiTf is robust against dilution to a certain level, so few spectral changes are initially seen with CCl_4 dilution. At a certain level, the network collapses. The collapse results in much of the model compound returning to its intramolecular hydrogen bonded state or a dimerized state, but some remains cation associated. This cation may be interacting with both hydrogen atoms of a single model compound or may be part of dimer-type group. The former appears more probable in N,N'-DMPDA, while the latter is more likely in N,N'-DMEDA. Meanwhile, the freed ions form clusters of highly aggregated species, as indicated by data from the anion modes. This results in an overall system which is simultaneously highly aggregated and not experiencing significant cation-backbone interaction.

5.4 COMPUTATIONAL RESULTS

A computational study of N,N'-DMEDA has been published by York and Boesch, *et al*.[3] In this work, the vibrational frequencies are calculated and compared to experimental IR absorbance and Raman scattering spectra of neat N,N'-DMEDA. Frequencies are assigned for three forms of the trans-gauche-trans or TGT structure of N,N'-DMEDA, where the TGT designation refers to the C-N-C-C, N-C-C-N and C-C-N-C dihedral angles being of 180±60°, 60±60°and 180±60° respectively.

The authors find reasonable agreement between the scaled calculated vibrational frequencies and those observed experimentally in most regions, but not in the NH stretching region. From frequency matches in other regions, they conclude that pure, neat N,N'-DMEDA is probably a mixture of several conformations of

N,N'-DMEDA, with the non-hydrogen bonded TGT conformation and the singly intramolecularly hydrogen bonded TGT conformation being the most prevalent. Further, they speculate that intermolecular bonding may allow stabilization of higher energy conformations, though the computations presented are single molecule gas phase calculations, which do not account for intermolecular hydrogen bonding. The current work supports these conclusions. The IR absorbance and Raman scattering bands seen in the spectra of pure N,N'-DMEDA indicate predominately intermolecular hydrogen bonding and some singly intramolecular hydrogen bonding are present. However, the current work was unable to confidently associate experimental N,N'-DMPDA frequencies with a particular backbone configuration, due in large part to the small differences in energy and calculated frequencies between conformers.

Dilution of N,N'-DMEDA in CCl_4 mimics the gas phase by separating the N,N'-DMEDA molecules sufficiently far to eliminate significant intermolecular interactions. Thus, comparison of the frequencies found from gas phase computations to those seen experimentally in the highly diluted system is justified. Table 5-3 contains the N-H stretching frequencies calculated by Boesch, *et al*[3] and those obtained experimentally in the pure solution and in the highly diluted (26:1 to

29:1 C:N) solution in the current work. The table uses the notation of Boesch, *et al* to indicate the three different species of TGT N,N'-DMEDA. DMEDA(0) indicates the TGT species experiencing no hydrogen bonding interaction. DMEDA(1) specifies the TGT structure with a single intramolecular hydrogen bond. DMEDA(2) in designates the TGT species in which both NH groups experience simultaneous intramolecular hydrogen bonding interaction with each other, or doubly intramolecular hydrogen bonding.

Table 5-3: N,N'-DMEDA NH stretching frequencies computed by the Hartree-Fock density functional theory method[3] and those experimentally obtained from pure N,N'-DMEDA and from N,N'-DMEDA diluted in CCl_4. (IR data were collected from 29:1 C:N dilution; Raman data were collected from 26:1 C:N dilution.)

Computational[3]			Experimental Pure Material		Experimental Dilute Solution	
DMEDA (0)	DMEDA (1)	DMEDA (2)	IR	Raman	IR	Raman
3373	3338 3363	3347 3353	3284 3328	3284 3328	3336 higher sh	3332 higher sh

As noted by the authors of the computational work[3], the NH stretching frequencies of the pure material are somewhat lower than those predicted by the computation. The model does not allow for intermolecular hydrogen bonding, which would be expected to shift NH stretching frequencies lower. It is a logical step to conclude that some intermolecular interaction may be responsible for the lower frequencies seen experimentally with the pure material. These interactions may be

effectively removed by dilution with CCl_4. In fact, the experimental frequencies of the diluted materials match excellently (difference of 2 and 4 cm^{-1} for IR and Raman respectively) with those computationally predicted for the structure experiencing a single intramolecular hydrogen bond. The higher frequency shoulders on the experimental bands match well with the frequencies predicted for the non-bonded species. This lends further support to the assertion that upon dilution, a network of intermolecular hydrogen bonding interactions is replaced by molecules experiencing single intramolecular hydrogen bonding and some molecules free from any hydrogen bonding.

A second publication by the same group contains calculated and experimental frequencies for N,N'-DMEDA with lithium bromide and lithium triflate salts added.[2] These computations were also performed on single gas phase molecules. For comparison, the calculated NH stretching frequencies from York, *et al*[2] and those experimentally obtained in the current work are given in Table 5-4.

Table 5-4: NH stretching frequencies for N,N'-DMEDA complexed with Li^+ and with LiTf computed by the Hartree-Fock density functional theory method[2] and those experimentally obtained from N,N'-DMEDA: LiTf and from N,N'-DMEDA:LiTf diluted in CCl4. (IR data were collected from 29:1 C:N dilution;

Computational[2] Wavenumber (cm^{-1})			Experimental: N,N'-DMEDA:LiTf Wavenumber (cm^{-1})		Experimental: Dilute 5:1 N:Li^+ N,N'-DMEDA:LiTf Wavenumber (cm^{-1})	
DMEDA (1)	DMEDA w/ Li^+	DMEDA w/ LiTf	IR	Raman	IR	Raman
3338 3363	3312	3332 3334	3296 3335	3304 3330	3305 3339	3305

With the addition of lithium triflate, the calculated and experimental NH stretching frequencies become less similar than with the neat material. The experimental NH stretching frequencies of the pure 5:1 N:Li^+ N,N'-DMEDA are 3335 cm^{-1} in the IR absorbance spectrum and 3334 cm^{-1} in the Raman scattering spectrum. This aggres with the calculated band frequency of 3334 cm^{-1} for N,N'-DMEDA:LiTf. However, the lower frequency bands seen experimentally (3296 cm^{-1} and 3304 cm^{-1}) are not in agreement with the computationally predicted 3332 cm^{-1} band. Interestingly, the NH stretching frequency of 3312 cm^{-1} predicted from N,N'-DMEDA complexed with only the Li^+ cation seems to be much closer in frequency to the experimental band. When the N,N'-DMEDA:LiTf solution is diluted with CCl_4, limited changes are seen in the experimental NH stretching frequencies. The higher frequency IR absorbance band shifts to 3339 cm^{-1}, which is still only 0.15% different from the predicted 3334 cm^{-1}. The lower frequency band changes by only one wavenumber to 3305 cm^{-1} and remains a much closer match to the N,N'-DMEDA:Li^+ at 3312 cm^{-1} than to the N,N'-DMEDA:LiTf at 3332 cm^{-1}. This is troubling as it suggests either issues with the computational model or that the cation in both the undiluted and diluted systems is not closely associated with the triflate anion. The extremely high degree of association suggested by the $\nu_{as}(CF_3)$ region experimental frequencies gives some credence to the latter explanation. It should be noted that the $\nu_{as}(CF_3)$ experimental frequency of 1169 cm^{-1} seen in the diluted (29:1 C:N) 5:1 N:Li^+ suggests a much higher degree of anion association than suggested

by the computational achieved frequency of 1153 cm^{-1}. This results from the fact that the computations consider only a single lithium triflate molecule.

To date, a similarly detailed study on N,N'-DMPDA has not been published. However, some preliminary work is available. Scott Boesch kindly performed a series of calculations on the N,N'-DMPDA molecule, both alone and complexed with Li^+ or with LiTf using GAUSSIAN 03.[41] Geometry optimizations and vibrational frequencies were obtained using the B3LYP hybrid Hartree-Fock/density functional theory method[42,43] with the 6-31G(d) split-valence plus polarization basis set[44]. This Hartree-Fock/density functional theory method combines a weighted sum of Hartee-Fock (E_X^{HF}), local density functional theory and gradient corrected density functional theory expressions to describe the exchange and correlation energies by: $E = aE_X^{Slater} + (1-a)E_X^{HF} + bE_X^{Becke} + CE_C^{LYP} + (1-c)E_X^{VWN}$. In this expression, E_X^{Slater} is Slater's local spin density functional for exchange,[45] E_X^{Becke} is Becke's gradient corrected exchange functional,[46] E_X^{VWN} is the local density functional of Vosko, Wilk and Nusair,[47] and E_C^{LYP} is the gradient corrected functional of Lee, Yang and Parr.[48] A slightly different functional correlation function was used to optimize the weighting coefficients a, b and c through reproduction of thermochemical data for a number of small molecules.[49] Geometry optimizations, from a C_1 symmetry, were accomplished using Berny's optimization algorithm.[50] No correction for anharmoncity was used in determining the vibrational frequencies. However, scaling factors of Scott and Radom were employed.[51] This method multiplied all calculated

frequencies less than 1000 cm^{-1} by 1.0013 and all calculated frequencies less than 1000 cm^{-1} by 0.9614. Specific vibrational mode assignments were made following animation of the mode in XMOL.[52]

Results of fifteen of the geometry optimizations are shown in Table 5-5. Conformations are described according to the dihedral angles of the molecule beginning with the CNCC angle and moving down the molecule as shown Table 5-5. Angles of 60±60º are specified as gauche (G), angles of 180±60º are defined as

Table 5-5: Dihedral angles and energy differences for the fifteen lowest energy conformations of N,N'-DMPDA.

Conformation	CNCC Angle (º)	NCCC Angle (º)	CCCN Angle (º)	CCNC Angle (º)	Energy Difference (kcal/mol)
TḠGT	182	-64	71	182	0.00
TḠḠG	189	-66	69	72	1.72
TḠḠT	176	-67	-67	176	1.95
TTTT	182	183	183	182	2.11
TḠTT	180	-63	183	181	2.28
TGTT	178	66	177	181	2.84
TGGT	181	67	67	181	3.26
TḠTḠ	181	-63	184	-79	3.26
GGGG	72	50	52	60	3.81
TGTG	178	69	173	76	3.81
TGTḠ	177	65	177	-78	3.95
TḠḠG	182	-60	-57	112	4.15
TTḠG	182	186	-64	100	4.81
TḠḠḠ	180	-62	-88	67	5.40
ḠḠḠG	-64	-62	-63	102	6.27

trans (T) and angles of -60±60º are designated as gauche-minus (Ḡ). To facilitate comparison, the energy differences are given with the lowest energy state, TḠGT, being assigned as the zero energy conformation. The actual energy of the TḠGT conformer is calculated to be -308.44515 Hartrees (-193552 kcal/mol).

Labeled three-dimensional renderings of structures of the three lowest energy conformers (TḠGT, TḠḠG and TḠḠT) appear in Figure 5-28, while selected interatomic distances and angles of these structures are provided in Table 5-6. Both the TḠGT and TḠḠG conformers contain N-H distances, N-N distances and N-H···N angles reasonable for intramolecular hydrogen bonding between one nitrogen atom and the opposite amine hydrogen atom. The remaining amine hydrogen atom is

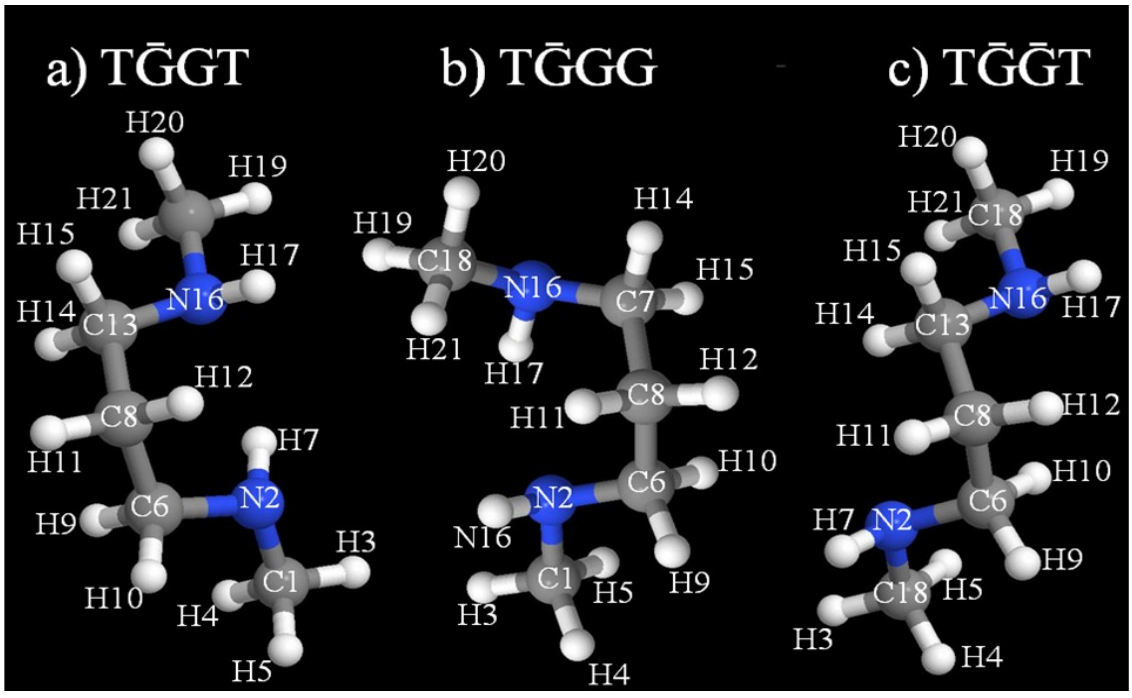

Figure 5-28: Three lowest energy conformations of N,N'-DMPDA: a) TḠGT, b) TḠGG and c) TḠḠ'T where T=trans (180±60º), G=Gauche (60±60º) and Ḡ=Gauche minus (60±60º)

Table 5-6: Selected interatomic distances (Å) and torsional angles (º) of the three lowest energy conformers of N,N'-DMPDA (Dihedral angles are given in Table 5-5.)

	TG̅GT	TG̅G̅G	TG̅G̅T
C1-H3	1.10 Å	1.09Å	1.10 Å
C1-H4	1.11 Å	1.11 Å	1.11 Å
C1-H5	1.10 Å	1.10 Å	1.10 Å
C2-N2	1.46 Å	1.46 Å	1.46 Å
N2-H7	1.02 Å	1.02 Å	1.02 Å
N2-C6	1.46 Å	1.47 Å	1.46 Å
C6-H9	1.11 Å	1.11 Å	1.11 Å
C6-H10	1.10 Å	1.10 Å	1.10 Å
C6-C8	1.53 Å	1.53 Å	1.53 Å
C8-H11	1.10 Å	1.10 Å	1.10 Å
C8-H12	1.10 Å	1.10 Å	1.10 Å
C10-C13	1.53 Å	1.54 Å	1.53 Å
C13-H14	1.10 Å	1.10 Å	1.10 Å
C13-H15	1.11 Å	1.10 Å	1.11 Å
C13-N16	1.47 Å	1.46 Å	1.46 Å
N16-H17	1.02 Å	1.02 Å	1.02 Å
N16-C18	1.46 Å	1.46 Å	1.46 Å
C18-H19	1.09 Å	1.10 Å	1.10 Å
C18-H20	1.11 Å	1.10 Å	1.11 Å
C18-H21	1.10 Å	1.11 Å	1.10 Å
C1-N2-C6	112.9º	112.9 º	113.2 º
N2-C6-C8	112.1 º	112.4 º	111.2 º
C6-C8-C13	115.2 º	114.3 º	113.4 º
C8-C13-N16	112.6 º	117.3 º	111.2 º
C13-N16-C18	113.0 º	114.4 º	113.2 º
N2-H17	3.05 Å	2.29 Å	4.46 Å
N16-H7	2.22 Å	3.25 Å	4.46 Å
N2-N16	2.98 Å	3.06 Å	3.80 Å
N2-H17-N16	130.5 º	131.0 º	45.0 º

pointed away from the opposing nitrogen atom. The distance between the nitrogen atoms (2.98 Å and 3.06 Å) is on the order of those usually found in N-H···B hydrogen bonding (3.10±0.13 Å).[17] The angle of the N-H···N interaction is not linear as is typical due to the intermolecular nature of the interaction. The geometry of the molecule precludes the normal linear bond angle, resulting in a hydrogen bonding interaction somewhat weaker than the typical N-H···N interaction. This is consistent with the experimental vibrational frequency data previously presented. These data show the NH stretch of groups involved in intramolecular hydrogen bonding interactions appearing at a higher frequency than intermolecular hydrogen bonding interactions, indicating the intramolecular hydrogen bonding interaction weakens the N-H bond less than intermolecular hydrogen bonding interaction.

As with N,N'-DMEDA, the computations fail to exactly predict frequencies in the NH stretching region of neat N,N'-DMPDA. Table 5-7 contains the computed NH stretching frequencies and the experimental frequencies of neat N,N'-DMPDA and N,N'-DMPDA heavily diluted with CCl_4.

Table 5-7: N,N'-DMPDA NH stretching frequencies computed by the Hartree-Fock density functional theory method[3] and those experimentally obtained from pure N,N'-DMPDA and from N,N'-DMPDA diluted in CCl_4 at a ratio of 30:1C:N

Computational Wavenumber (cm^{-1})			Experimental Pure Material Wavenumber (cm^{-1})		Experimental Dilute Solution Wavenumber (cm^{-1})	
TGḠT	TGḠG	TḠḠT	IR	Raman	IR	Raman
3332 3341	3338 3339	3336 3336	3285	3328	3314	3333

The computed N···H distances of the TGḠT and TGḠG conformers are favorable for formation of an intramolecular hydrogen bond within the molecule, but these distances are too large to recommend intramolecular hydrogen bonding in the TḠḠT conformation. Non-hydrogen bonded NH could be expected to vibrate at a frequency upwards of 3361 cm^{-1}, which is somewhat higher than that seen in the computational frequencies of the conformers. The non-hydrogen bonded NH in the TGḠT conformer comes closest to this at 3341 cm^{-1}. What is notable about the computations is the similarity of frequencies between the conformations. In spite of having one presumably hydrogen bonded NH group and one "free" NH group, the TGḠG form predicts two very similar frequencies, much like the TḠḠT conformer which undergoes no hydrogen bonding.

None of the conformers calculated frequencies are a direct frequency match for the experimental data of the pure material in this region. However, all three conformers predict a frequency within ten wavenumbers of the Raman band (3328 cm^{-1}) seen in the pure N,N'-DMPDA spectrum. Based on the experimental behavior of the band, it has been assigned to n-mer type intermolecular hydrogen bonding interactions. None of the conformers predicts the experimental IR band at 3285 cm^{-1}. This is to be expected since a single molecule calculation can not predict a band originating in intermolecular interactions.

Experimental data collected from the diluted N,N'-DMPDA contain NH stretching bands at 3314 cm^{-1} (IR) and 3333 cm^{-1}(Raman). The 3314 cm^{-1} band is not predicted by any of the low energy conformers, while all three conformations

show a band coincident with the 3333 cm^{-1} band. The 3333 cm^{-1} band has been assigned to the singly intermolecular hydrogen bond, while the 3314 cm^{-1} band was speculatively assigned to a NH species experiencing intramolecular hydrogen bonding interactions of both NH groups, but conceivably could result from an NH group simultaneously experiencing both inter- and intramolecular hydrogen bonding interaction. The doubly intramolecular hydrogen-bonded form of the molecule was not observed in the preliminary computations, while the inter/intramolecular combination was seen in preliminary computations involving two N,N'-DMPDA molecules. In all, this suggests that this series of single molecule computations may not be an accurate model for the NH stretch in the neat N,N'-DMPDA system. A better model would consider the intermolecular hydrogen bonding interactions which are most assuredly occurring in the system. Some very preliminary computations with two N,N'-DMPDA molecules suggest a low energy configuration may have the two molecules intermolecularly hydrogen bonded on one end and intramolecularly hydrogen bonded on the other end. Frequencies have not yet been calculated for this structure.

In other regions other than the NH stretch, the single molecule computations reproduce the experimentally seen frequencies much better. The backbone region results in numerous matches (± 5 cm^{-1}) between the computed frequencies and those experimentally observed for the pure N,N'-DMPDA and in the diluted system. Unfortunately, the similarities between the computed frequencies for the three different conformers preclude using them as a tool to identify the most prevalent

conformation in the compound. As shown in Table 5-6, the bond lengths and angles in the backbone do not differ significantly between the conformations. This leads to the similarity of vibrational frequencies. The small energy differences between the conformers (less than 2 kcal/mol between the three lowest energy forms) suggest that a single conformation may not be heavily preferred and that the pure material probably exists as a mixture of several conformers with similar energies.

Computations were also performed on N,N'-DMPDA in the presence of a lithium cation and in the presence of lithium triflate salt. In both cases, the calculations utilized a single cation or salt molecule and a single N,N'-DMPDA molecule. This would correspond to the a $N:Li^+$ ratio 2:1. The closest ratio experimentally examined was $N:Li^+$ of 3:1. Solutions more salt-rich than 3:1 $N:Li^+$ could not be reliably produced in the laboratory setting. Unfortunately, the highest salt content included in the dilution study was 5:1 $N:Li^+$. Table 5-8 summarizes the dihedral angles, number of nitrogen atoms coordinated to the lithium cation and the energy differences for the lowest energy conformations of N,N'-DMPDA:Li^+ (upper) and N,N'-DMPDA:LiTf (lower). To obtain these geometries, a cation or salt molecule was placed in proximity to the N,N'-DMPDA molecule in a given starting geometry. The system was then optimized to determine the final structure of the complex. In some cases, multiple starting N,N'-DMPDA geometries lead to the same final geometry of the complex. For example, initial N,N-DMPDA geometries of T$\bar{G}$GT and TGTT both led to the lowest energy doubly coordinated geometry, GG$\bar{G}$T, when complexed with a lithium cation. The effect was also seen with the

Table 5-8: Dihedral angles, number of coordinated nitrogen atoms and energy differences for the lowest energy conformations of N,N'-DMPDA complexed with lithium cation (upper) and with lithium triflate (lower).

Conformation	Coord Nitrogen	CNCC Angle (°)	NCCC Angle (°)	CCCN Angle (°)	CCNC Angle (°)	Energy Difference (kcal/mol)
N,N'-DMPDA with Li^+ (N:Li^+=2:1)						
GGḠT	2	79	73	-77	180	0.00
GGḠḠ	2	79	75	-75	-79	0.87
TḠḠT	2	191	-44	-44	191	1.55
TḠḠḠ	2	192	-43	-44	-65	2.62
TGḠḠ	2	151	49	-90	-90	2.80
GḠḠT	1	99	-57	-62	184	25.11
TḠTT	1	166	-62	172	170	27.91
TḠTḠ	1	164	-62	170	264	28.39
TTTT	1	161	179	169	151	28.83
TGGT	1	172	63	58	150	29.82
TḠḠG	1	174	-54	-95	58	30.99
N,N'-DMPDA with Lithium Triflate (N:Li^+=2:1)						
GGḠT	2	80	69	-75	181	0.00
TḠGG	2	182	-75	68	80	0.60
TḠGT	2	187	-46	-42	193	1.62
TḠḠT	2	188	-45	-43	-69	2.29
GGGG (2)	2	68	43	43	68	3.34
TḠTT	1	176	-62	179	183	13.29
TḠTT	1	176	-63	177	183	13.42
TTTT	1	179	182	181	184	13.93
TḠTḠ	1	177	-62	182	-75	14.45
GGGG (1)	1	73	40	44	64	14.51
TGTT	1	171	65	177	183	15.16
TGGT	1	176	67	65	182	15.64
TGTG	1	171	66	175	73	16.05
TGTḠ	1	168	62	179	-77	16.20
GḠḠT	1	105	-56	-67	184	16.25

N,N'-DMPDA:LiTf complex, where both the initial TTTT and TḠḠḠ N,N'-DMPDA geometries resulted in the lowest energy singly coordinated conformation TḠTT. Similarly, in one case a single initial geometry, GGGG led to two different species in the N,N'-DMPDA:LiTf complex: a lower energy GGGG geometry in which the lithium coordinated to both nitrogen atoms and a higher energy GGGG geometry where the lithium cation coordinated to only a single nitrogen atom. Interestingly, in the singly coordinating species, the non-coordinated nitrogen atom participates in an intramolecular hydrogen bond. The doubly coordinated conformer is 11.17 kcal/mol lower in energy than the singly coordinated conformation. These are designated as GGGG(2) and GGGG(1), respectively in Table 5-8. The actual energy of the N,N'-DMPDA:Li^+ GGḠT conformer is found to be -315.85175 E_h, while the actual energy of the N,N'-DMPDA:LiTf GGḠT conformer is calculated to be -1277.54006 Hartrees (-801669 kcal/mol).

The neat solution is thought to be mixture of several conformations and the salt solution may also contain a variety of conformations, though is likely that salt association to the compound causes preferred conformation(s). However, the energy differences between the lowest energy conformers are small. The frequencies calculated in the backbone region are similar between conformers and are in general agreement with those observed experimentally. Combined, these factors prevent identification of a single most probable conformation. Frequencies of the X-H stretching modes calculated from density functional methods are known to

overestimate experimental values by as much as 100-200 cm^{-1}.[2] This is case for the CH stretching modes in the neat N,N'-DMPDA as well as the cation containing and salt containing system, but not true of the NH stretching frequencies.

The NH stretching vibrations of selected low energy conformations are shown in Table 5-9 along with the experimentally obtained frequencies from the 5:1 $N:Li^+$ N,N'-DMPDA:LiTf complex in both the pure form and diluted in CCl_4. The calculated frequencies for the N,N'-DMPDA with LiTf differ somewhat from those seen experimentally, but not as dramatically as the N,N'-DMEDA:LiTf computations. Experimentally obtained IR and Raman spectra from the 5:1 N,N'-DMPDA:LiTf complex show three distinct bands: 3300/3304 cm^{-1} assigned to the salt associated species, 3332 cm^{-1} designated as intramolecular hydrogen bonding and a higher frequency shoulder, which may be "free" NH. While a frequency similar to the 3300/3304 cm^{-1} band is not predicted in the computations, the latter two bands do match calculated frequencies. The experimental 3332 cm^{-1} band is in the middle of the range (3325-3339 cm^{-1}) determined by the computations for the various conformations. The experimental "free" NH band is expected around 3361 cm^{-1}.[14] Most of the conformers have a slightly lower calculated frequency in the 3340-3350 cm^{-1} range, but the GG$\bar{G}$T conformer has a calculated band at 3365 cm^{-1}.

Much like the N,N'-DMEDA:LiTf system, the NH stretching frequencies predicted by the N,N-DMPDA complexed with only the lithium cation are closer to frequencies seen experimentally. Computations from both the GG$\bar{G}$T and TG$\bar{G}\bar{G}$ conformations predict a band at 3309 cm^{-1}, which is an excellent match for the salt

Table 5-9: NH stretching frequencies for N,N'-DMPDA complexed with Li^+ and with LiTf computed by the Hartree-Fock density functional theory method and those experimentally obtained from N,N'-DMPDA: LiTf and from N,N'-DMPDA:LiTf diluted in CCl4. (IR data were collected from 29:1 C:N dilution; Raman data were collected from 10:1 C:N dilution.)

Sample			Wavenumber (cm^{-1})	
Experimental :	5:1 N,N'-DMPDA: LiTf	Pure 5:1 N:Li^+	3300 (IR) 3304 (R)	3332 + higher shoulder
		Dilute 5:1 N:Li^+	3306	3332 + higher shoulder
Computational:	N,N'-DMPDA w/Li+	GGḠT	3307	3334
		GGḠḠ	3334	3334
		TGḠT	3327	3327
		TḠḠḠ	3322	3329
		TGḠḠ	3309	3310
	N,N'-DMPDA w/ LiTf	GGḠT	3331	3365
		TGḠT	3339	3342
		TḠḠḠ	3338	3344
		TḠGG	3325	3354

associated band seen in the experimental spectra at 3300-3304 cm^{-1}. The GGḠT conformer also calculates a band at 3334 cm^{-1}; again an excellent match for the experimental band at 3332 cm^{-1}. The remarkable agreement between the experimental NH stretching frequencies and those seen from the GGḠT conformer

containing the cation raises some questions about the nature of the interactions between the salt and the N,N'-DMPDA. A crystal structure, which might clarify the manner in which the cation is associated to the compound, has proved elusive, leaving open many questions.

5.5 CONCLUSIONS

In its neat form, N,N'-DMEDA exists predominantly in the TGT conformation, but other low energy conformers may also be present. The molecules experience significant hydrogen bonding – mainly of the intermolecular variety, though intramolecular interaction also play a role in the system. The vast majority of intermolecular interactions are disrupted by dilution in CCl_4. This results in "free" NH groups that are not involved in any hydrogen bonding type interactions. The intramolecular hydrogen bonds remain largely unaffected by the CCl_4 dilution.

Addition of lithium triflate to N,N'-DMEDA results in cation coordination to the nitrogen atoms. The inductive effect from the cation results in a NH stretching band lower in frequency than that either of "free" or intramolecular hydrogen bonded species, but higher than the intermolecular hydrogen bonded species. Significant amounts of intermolecular hydrogen interaction are also present suggesting the formation of a network type structure. The anion vibrational bands suggest that at low salt content, "free" ions and contact ion pairs dominate the system. At higher salt content, contact ion pairs and triple ion are the most common associations. Addition of CCl_4 appears to break the network structure, result in higher anion aggregation

and significant reduction of cation interaction with the nitrogen atoms. This occurs in a dramatic fashion at CCl_4 dilutions between 1:2 and 1:1 C:N molar ratio.

In many ways, the N,N'-DMPDA system behaves similarly, but does have some notable differences. The pure material probably exists as a mixture of several different conformations undergoing a variety of hydrogen bonding interactions. Comparison of experimental data to computationally obtained frequencies was not able to provide a most likely conformer as backbone frequencies of the various conformers were very similar and the energy differences between conformations were small. The hydrogen bonding within the pure material consists of both intramolecular and intermolecular hydrogen bonding, with intramolecular interactions being more common than in the N,N'-DMEDA system. The added degrees of rotational freedom gained by third carbon in the backbone allows the molecule a wider range of conformations as compared to the N,N'DMEDA. Notable is the possibility to form a pseudo-six membered ring through hydrogen bonding interactions (see Figure 5-10). Dilution in CCl_4 interrupts the intermolecular hydrogen bonding and results in a band which may be due to a doubly intramolecularly hydrogen bonded species that involves hydrogen bonding between both NH groups in the same molecule. Some singly intramolecular hydrogen bonded species are also present.

Addition of lithium triflate to N,N'-DMPDA results in a single NH stretching band in the 3:1 $N:Li^+$ complex. This band represents cation association to the nitrogen atoms and is virtually the only species present in the system at high salt

content. A slight shoulder on the band represents a very small population of singly intramolecularly bonded NH groups. Computations involving one N,N'-DMPDA molecule and one lithium triflate molecule are not able to accurately predict the NH stretching vibrations. However, computations on a system containing a single N,N'DMPDA molecule with a lone lithium cation do result in a GG$\bar{G}$T conformation with remarkably similar NH stretching frequencies. Anion vibrations indicate that at low salt contents some "free" ion is present, but that contact ion pair is the dominant species. At higher salt content, the triple ion is present in significant amounts. Overall, the N,N'-DMPDA system experiences a higher degree of association than does the N,N'-DMEDA system. When the N,N'-DMPDA:LiTf complex is diluted with CCl_4, the degree of aggregation increases further and the cation interaction with the nitrogen atoms dramatically reduces. As in the N,N'-DMEDA:LiTf system, this suggests a breaking of a network connecting the compound, the cation and the anion. In N,N'-DMPDA, the network disruptions occurs at a molar ratio of between 1:1 and 4:1 C:N. The N,N'-DMPDA:LiTf system appears to be more robust against this change than the N,N'-DMEDA:LiTf system, as it is able to tolerate a higher level of CCl_4 before the network collapses.

5.6 REFERENCES

(1) Tzu, L. *Hua Hu Ching: The Unknown Teachings of Lao Tzu*; 2nd ed.; HarperCollins Publisher: New York, 1995.

(2) York, S. S.; Boesch, S. E.; Wheeler, R. A.; Frech, R. *PhysChemComm* **2002**, *5*, 99-111.

(3) Boesch, S. E.; York, S. S.; Frech, R.; Wheeler, R. A. *PhysChemComm* **2000**, *1*, 1.

(4) Sutjianto, A.; Curtiss, L. A. *J. Phys. Chem. B* **1998**, *102*, 968-974.

(5) Johansson, P.; Tegenfeldt, J.; Lindgren, J. *J. Phys. Chem. B* **1998**, *102*, 4660-4665.

(6) Torell, L. M.; Jacobsson, P.; Petersen, G. *Polym. Adv. Technol.* **1993**, *4*, 152-163.

(7) Mujica, V.; Malaver, M.; Ruette, F. *J. Phys. Chem. B* **1999**, *103*, 89-94.

(8) Rhodes, C. P.; Khan, M.; Frech, R. *J. Phys. Chem. B* **2002**, *106*, 10330-10337.

(9) Rocher, N.; Frech, D. R. *J. Phys. Chem. A* **2007**, *111*, 2662-2669.

(10) Sanders, R. A.; Frech, R.; Khan, M. A. *J. Phys. Chem. B* **2003**, *107*, 8310-8315.

(11) York, S. S.; Boesch, S. E.; Wheeler, R. A.; Frech, R. *Macromolecules* **2003**, *36*, 7348-51.

(12) Ferry, A.; Oradd, G.; Jacobsson, P. *J. Chem. Phys.* **1998**, *108*, 7426.

(13) Rocher, N. M.; Frech, R.; Khan, M. *J. Phys. Chem. B* **2005**, *109*, 20697-20706.

(14) Krueger, P. J. *Can. J. Chem.* **1967**, *45*, 2143-2149.

(15) Sanders, R. A.; Frech, R.; Khan, M. A. *J. Phys. Chem. B* **2004**, *108*, 2186-2191.

(16) Jeffery, G. A. *An Introduction to Hydrogen Bonding*; 1st ed.; Oxford Unviersity Press: New York 1997.

(17) Pimentel, G. C.; McClellan, A. L. *The Hydrogen Bond*; Freeman: San Francisco, 1960.

(18) Lin-Vien, D.; Colthrup, N. B.; Fately, W. G.; Grasselli, J. G. *The Handbook of Characteristic Infrared and Raman Frequencies of Organic Molecules*; 1st ed.; Academic Press: New York, 1991; Vol. 1.

(19) Vinogradov, S. N.; Linnell, R. H. *Hydrogen Bonding*; 1st ed.; Van Nostrand Reinhold Company: New York, 1971.

(20) Rocher, N. M.; Frech, R. *Macromolecules* **2005**, *38*, 10561-10565.

(21) Colthup, N. B.; Daly, L. H.; Wilberley, S. E. *Introduction to Infrared and Raman Spectroscopy*; 3rd ed.; Academic Press: New York, 1990.

(22) Chatt, J.; Duncanson, L. A.; Venanzi, L. M. *J. Chem. Soc.* **1955**, 4461.

(23) Gerrard, W.; Goldstein, M.; Mooney, E. F. *J. Inorg. Nucl. Chem.* **1969**, *31*, 107-116.

(24) Drago, R. S. *Physical Methods in Inorganic Chemistry*; 1st ed.; Reinhold Publishing Corporation: New York, 1965.

(25) Wolff, H.; Gamer, G. *J. Phys. Chem.* **1972**, *76*, 871-876.

(26) Bellamy, L. J.; Williams, R. L. *Spectrochim. Acta* **1957**, *9*, 341-345.

(27) Rocher, N. M.; Frech, R.; Powell, D. R. *J. Phys. Chem. B* **2006**, *110*, 15117-15126.

(28) Rocher, N. Doctoral Dissertation, University of Oklahoma, 2006.

(29) Sanders, R. A.; Frech, R.; Khan, M. A. *J. Phys. Chem. B* **2004**, *108*, 12729-12735.

(30) Henderson, W. A.; Brooks, N. R.; Young, V. G. *J. Am. Chem. Soc.* **2003**, *125*, 12098-12099.

(31) Lightfoot, P.; Mehta, M. A.; Bruce, P. G. *Science* **1993**, *262*, 883-5.

(32) Rhodes, C. P.; Frech, R. *Macromolecules* **2001**, *34*, 2660-2666.

(33) Chakraborty, T.; Verma, A. L. *Spectrochim. Acta, Part A* **2002**, *58*, 1013-1023.

(34) Schantz, S.; Sandahl, J.; Borjesson, L.; Torell, L. M.; Stevens, J. R. *Solid State Ionics* **1988**, *28-30*, 1047-53.

(35) Frech, R.; Huang, W. *Solid State Ionics* **1994**, *72*, 103-7.

(36) Huang, W.; Frech, R.; Wheeler, R. A. *J. Phys. Chem.* **1994**, *98*, 100-10.

(37) Rhodes, C. P.; Frech, R. *Solid State Ionics* **1999**, *121*, 91-99.

(38) York, S.; Frech, R.; Snow, A.; Glatzhofer, D. *Electrochim. Acta* **2001**, *46*, 1533-1537.

(39) Frech, R.; Huang, W. *J. Solution Chem.* **1994**, *23*, 469-81.

(40) Welsh, H. L.; Crawford, M. F.; Scott, G. D. *J. Chem. Phys.* **1948**, *16*, 97-105.

(41) Frisch, M.; Trucks, G. W.; Schlegel, H. B.; Scuseria, G. E.; Robb, M. A.; Cheeseman, J. R.; Zakrewski, V. G.; Montgomrey, J. A.; Stratman, R. E.; Burant, J. C.; DApprich, S.; Millam, J. M.; Daniels, A. D.; Kudin, K. N.; Strain, M. C.; Farkas, O.; Tomasi, J.; Barone, V.; Cossi, M.; Cammi, R.; Mennucci, B.; Pomelli, C.; Adamo, A.; Clifford, S.; Ochterski, J.; Petersson, G. A.; Aala, P. Y.; Cui, Q.; Morokuma, K.; Lamick, D. K.; Rabuck, A. D.; Rarhavachari, K.; Foresman, J. B.; Cioslowski, J.; Ortiz, J. V.; Stefanov, B. B.; Liu, G.; Liashenko, A.; Piskorz, P.; Komaromi, I.; Gomperts, R.; Martin, R. L.; Fox, D. J.; Keith, T.; Al-Laham, M. A.; Peng, C. Y.; Nanayakara, A.; Gonzalez, C.; Challacombe, M.; Gill, P. M. W.; Johnson, B.; Chen, W.; Wong, M. W.; Andres, J. L.; Gonzalez, C.; Head-Gordon, M.; Replogle, E. S.; Pople, J. A.; revision A.6 ed.; Gaussian, Inc: Pittsburgh, PA, 1998.

(42) Frisch, M. J.; Trucks, G. W.; Schlegel, H. B.; Gill, P. M. W.; Johnson, B. G.; Robb, M. A.; Cheeseman, J. R.; Keith, T.; Petersson, G. A.; Montgomery, J. A.; Ragavachari, K.; Al-Laham, M. A.; Zakrzewski, V. G.; Ortiz, J. V.; Foresman, J. B.; Cioslowski, J.; Stefanov, B. B.; Nanayakkara, N.; Challacombe, M.; Peng, C. Y.; Ayala, P. Y.; CHen, W.; Wong, M. W.; J.L.; Andres; Replogle, E. S.; Gomperts, R.; Martin, R. L.; Fox, D. J.; Binkley, J. S.; Defrees, D. J.; Baker, J.; Stewart, J. P.; Head-Gordon, M.; GOnzalez, C.; Pople, J. A.; revision B.2 ed.; Gaussian, Inc. : Pittsburgh, PA 1995.

(43) Stephens, P. J.; Devlin, F. J.; Chabalowski, C. F.; Frisch, M. J. *J. Phys. Chem.* **2002**, *98*, 11623-11627.

(44) Hehre, W. J.; Radom, L.; Schleyer, P. v. R.; Pople, J. A. *Ab Initio Molecular Oribital Theory* John Wiley & Sons, Inc.: New York, 1986.

(45) Slater, J. C. *Quantum Theory of Molecules and Solids*; McGraw-Hill: New York, 1974; Vol. 4.

(46) Becke, A. D. *Phys. Rev. A: At. Mol. Opt. Phys.* **1988**, 3094.

(47) Vosko, S. H.; Wilk, L.; Nusair, M. *Can. J. Phys.* **1980**, *58*, 1200-1211.

(48) Lee, C.; Yang, W.; Parr, R. G. *Phys. Rev. B: Condens. Matter* **1988**, *58*, 785.

(49) Becke, A. D. *J. Chem. Phys.* **1993**, *98*, 1372-1377.

(50) Schlegel, H. B. *J. Comput. Chem.* **1986**, *3*, 214.

(51) Scott, A. P.; Radom, L. *J. Phys. Chem.* **1996**, *100*, 16502-16513.

(52) Wasikowski, C.; Klemm, S.; Research Equipment, Inc d.b.a. Minnesota Supercomputer Center, Inc.: Minneapolis, MN, 1993.

CHAPTER 6: THE G SERIES – MATERIALS DERIVED FROM N-2-METHOXYETHYLAMINE

It is time for parents to teach young people early on that in diversity there is beauty and there is strength. We all should know that diversity makes for a rich tapestry, and we must understand that all the threads of the tapestry are equal in value no matter their color.

-- Maya Angelou[1]

6.1 INTRODUCTION

As previously discussed one approach to improving conductivity of poly(ethyleneoxide), PEO, based polymer electrolytes has been to modify the polymer backbone by changing the heteroatom.[2,3] As second method that has also been extensively employed is the addition of side chains to PEO.[4,5] Flexible side chains serve to break the crystallinity of the system and provide coordination sites conducive to ion transport. In the case of poly(bis-methoxyethoxyethoxyphosphazene), MEEP, the two methods have been combined to produce a PEO analog with ethoxy side chains.[6,7] This material showed increased conductivity versus PEO, but the mechanical properties were not amenable to battery use.[7] A second instance of the mutual approach is that of poly(N-(2-(2-methoxyethoxy)ethyl)ethylenimine), LPEI-G2.[8] This material consists of ethoxy units tethered to nitrogens in the poly(ethylenimine), PEI, backbone. Conductivity of the non-optimzed systems is reported to be about an order of magnitude lower than that of the MEEP system, but the mechanical properties are superior to MEEP.[8]

The interactions between the cation, anion and polymer will largely govern the conductivity of the system. In an effort to more thoroughly understand these interactions, model compounds of the LPEI-G2 system have been studied. The model compounds presented here are N,N-dimethyl-(2-methoxyethyl)amine, G1MC, and N,N-dimethyl-(2-(2-methoxyethoxy)ethyl)amine, G2MC. These compounds model a single repeat unit of the polymers LPEI-G1 and LPEI-G2. Structures of these compounds are given in Figure 6-1.

The project has had several starts as different collaborative efforts between the physical chemistry group of Dr. Roger Frech and the organic chemistry group of Dr. Daniel Galtzhofer. Synthesis of the G2MC was performed by Dr. Lieyu Hu. Dr. Hu and Mr. Matt Meredith synthesized the G1MC. I prepared all analytical samples and collected and analyzed all IR and Raman spectroscopic data. It should be noted that the work presented

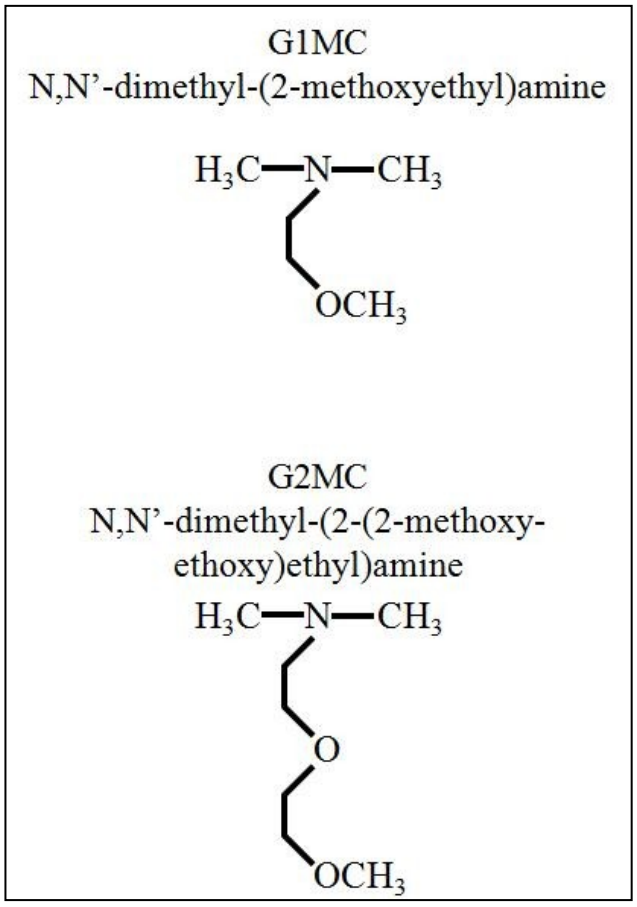

Figure 6-1: Structures and IUPAC names for G1MC and G2MC

here is an extremely sketchy characterization with much of the data not yet published. More details about the mixed nitrogen/oxygen heteroatom systems will soon be available from Mr. Meredith's and Mr. Rahul Kadam's dissertations.

6.2 SYNTHESIS AND APPEARANCE

N,N-dimethyl-(2-methoxyethyl)amine (G1MC) was synthesized via Ecshwieler-Clarke methylation of 2-methoxyethylamine by formaldehyde in formic acid.[9] The end product distilled over sodium carbonate and then over sodium metal in order to purify. G1MC is a readily flowing amber liquid whose viscosity appears similar to water. G1MC is capable of dissolving upwards of 1 mole of lithium trifluoromethanesulfonate, LiTf, per mole of compound.

N,N' dimethyl-(2-(2-methoxyethoxy)ethyl)amine (G2MC) was synzthesized similarly to the G1MC, using the Eschwieler-Clarke methylation of methoxy-ethoxyethylamine with formaldehyde in formic acid.[9] The G2MC was purified by distillation over sodium carbonate. G2MC is a thick dark amber liquid whose viscosity resembles that of thick molasses. It is able to solvate LiTf in concentrations greater than 2 moles of LiTf to each 1 mole of G2MC.

The highly hygroscopic nature of both materials required their storage over molecular sieves in an inert atmosphere glovebox. It also posed a number of handling challenges which significantly delayed the project. Despite extensive precautions, water was often taken up by the samples in the transfer between the

inert atmosphere glovebox and the IR sample chamber. This problem was magnified in the compound:LiTf complexes.

6.3 VIBRATIONAL SPECTROSCOPY OF G1MC AND G2MC

3.4.1 Backbone and Conformational Regions

Bands occurring in the IR spectral region from about 1000 to about 800 cm^{-1} result from motions of the polymer backbone and can be give information regarding the conformation of the chain. In PEO and PEO model compounds such as diglyme, these bands have been attributed to CH_2 rocking, C-C stretching, C-O stretching and some mixed modes of these motions.[10,11] In PEI and model compounds such as N,N-diemthylethylenediamine (N,N'-DMEDA) and tetramethylethylenediamine (TMEDA), bands in this region have been assigned to mixtures of CH bending, C-C stretching, C-N stretching modes.[12,13]

It is reasonable to assume that the same types of motions are responsible for the bands in G1MC and G2MC in this region. Figure 6-2 contains the IR absorbance spectra from TMEDA, G1MC, G2MC and diglyme in the 1000-800 cm^{-1} region. TMEDA is a model compound for PEI which consists of two completely methylated nitrogen atoms connected by an ethyl chain. In this case TMEDA could be thought of as the "backbone" of the G1MC and G2MC compounds. In the same way, diglyme, consisting of two methyl capped ether oxygen units, may be considered a model compound for PEO. In the case of the G1MC and G2MC, diglyme represents the "side chain" of the molecule. The G1MC has features in common with diglyme

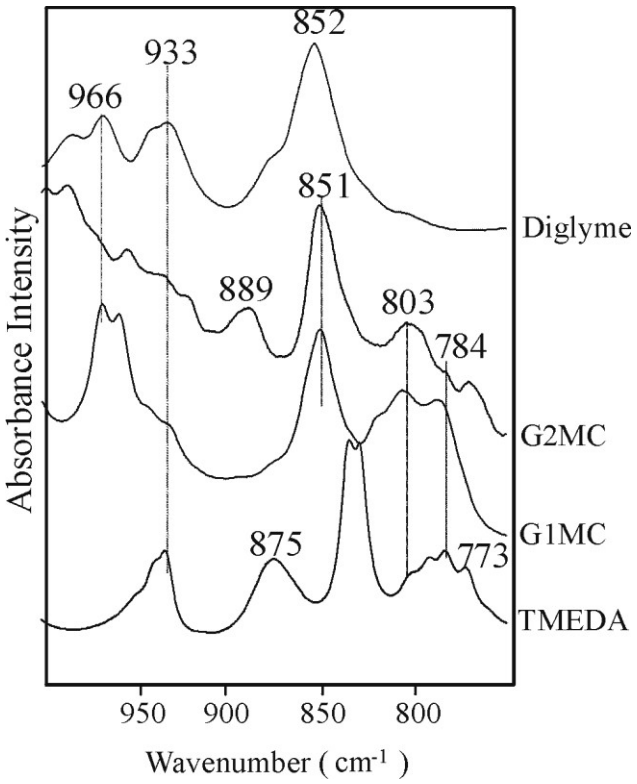

Figure 6-2: IR Absorbance spectra for the 1000-800 cm^{-1} region of diglyme, G1MC, G2MC and TMEDA.

and with TMEDA. The band at 851 or 852 cm^{-1} appears in the spectra of G1MC, G2MC and diglyme, but not in the TMEDA spectrum. This band likely relates to C-O stretching. The diglyme band at 985 cm^{-1} has an analog in the G1MC spectrum, but not in the G2MC spectrum. This is a little surprising since the methoxyethyoxy pattern of diglyme is present in G2MC, but not in G1MC. A broad feature of overlapping bands in the 770-850 cm^{-1} range appears in the spectra of G1MC, G2MC and TMEDA, but no analogous feature is present in the diglyme spectrum. The bands in this feature are likely due to the C-N stretching or motions involving the amino CH_3 groups. The broad 889 cm^{-1} band in G2MC may be related to the 875 cm^{-1} feature in TMEDA. The similar shape and relatively close frequencies suggest similar origins of the band.

The 1000-800 cm^{-1} region has been essential in differentiating conformations of PEO-based materials.[11] Knowledge of the G1MC and G2MC systems is

insufficient to make any assessments of probable conformations based only on IR spectra. However, adequate data is available to suggest that conformational changes occur upon salt addition.

As a side note, it should be noted that salt content is expressed as a ratio of moles of total heteroatoms to moles of lithium ion. For example, G1MC contains one nitrogen and one oxygen atom for a total of two heteroatoms. Therefore the heteroatom to lithium cation ratio is half the mole to mole ratio of the compound to the salt, so a heteroatom:Li^+ ratio of 20:1 corresponds to a G1MC:LiTf molar ratio of 10:1. It is important to clarify that ALL salt contents in this chapter are expressed as heteroatom:Li^+ ratios.

Figure 6-3 contains the 1000-800 cm^{-1} region of the IR absorbance spectra of neat G1MC and G2MC and for several LiTf complexes of the materials. The lower stack is for G1MC and its LiTf complexes, which range from 20:1 to 5:1 heteroatom:Li^+ moving up the stack. The upper stack contains the G2MC neat material and its 20:1 and 10:1 heteroatom:Li^+ complexes. Water absorption into the IR sample prevented the collection of high quality data beyond the 10:1 complex. Several changes occur in the G1MC system with low levels of salt. The split band at 966/957 cm^{-1} looses the higher frequency component, becoming a single symmetric band at 957 cm^{-1}. The 851 cm^{-1} band shifts slightly to 848 cm^{-1} and the broad feature of multiple overlapping bands from 770-840 cm^{-1} becomes a single band centered at 787 cm^{-1}. These data indicate that the conformation of the G1MC material changes with salt addition, which in turns suggests that cation coordination to one or more of

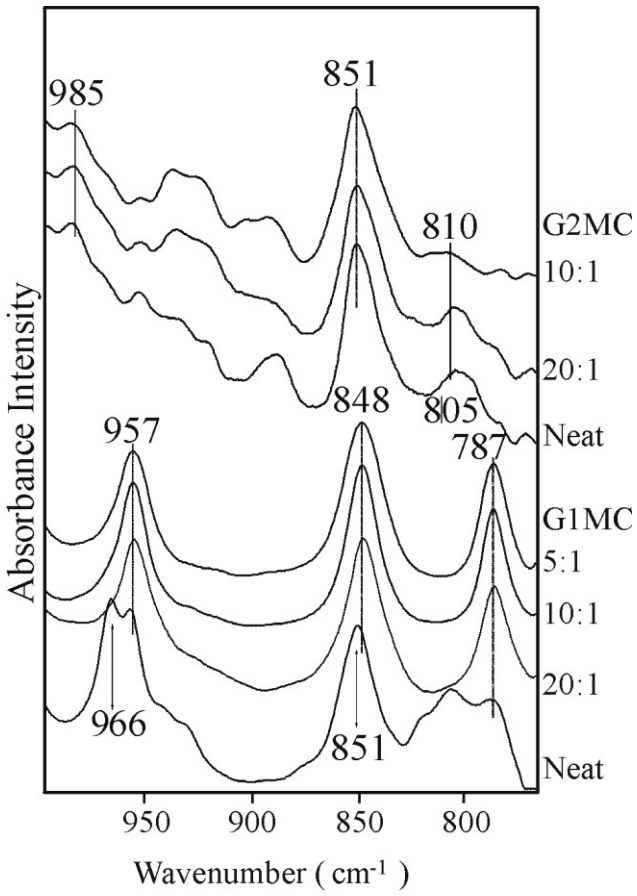

Figure 6-3: IR Absorbance spectra for the 1000-800 cm^{-1} region of neat G1MC and G2MC their complexes with lithium triflate of 20:1, 10:1 and 5:1 heteratom to Li^+ ratio.

the heteroatoms occurs. That spectral features associated with diglyme (966/957 cm^{-1}) are impacted by salt addition suggests that the oxygen atom may be involved with the coordination. However, results from both diglyme and monoglyme complexes with LiTf have identified the growth of a band at 877 cm^{-1} or 869 cm^{-1}, respectively, as positively indicating cation coordination.[14,15] This change may simply be indicative of a change in one more the dihedral angles involving the oxygen atom (i.e. C-O-C). The significant alteration of the broad overlapping feature also seen in TMEDA suggests involvement of the nitrogen atom in coordination. The change seen here is consistent with that seen by other workers where Li^+ coordination to TMEDA was confirmed via crystal structure.[13] This is strong evidence for cation coordination to the nitrogen atom. However, given the proclivity of lithium to be multi-coordinate, involvement of both

heteroatoms would not be unexpected. One interesting trend seen with the G1MC complexes is that no significant changes in the spectra occur with increased salt content. This suggests that a single preferred conformation is achieved with minimal salt addition.

Data for the G2MC system are shown in the upper part of Figure 6-3. Fewer changes are readily apparent in the G2MC system, though some are present. The band present at 805 cm^{-1} in the neat material shifts to 810 cm^{-1} and broadens with salt addition. The series of overlapping, broad bands of low intensity from about 880 cm^{-1} to around 900 cm^{-1} changes in shape and the band centers shift. Unfortunately, these bands are not well enough resolved to make intelligent comparisons to similar systems.

3.4.2 Ionic Association

A significant amount of information about the types of ionic associations occurring in the system is available in the vibrational bands associated with the anion motions. The bands most commonly used with lithium triflate are: the symmetric CF_3 bend, $\delta_s(CF_3)$ around 750-760 cm^{-1}, the symmetric SO_3 stretch, $\nu_s(SO_3)$ around 1030-1060 cm^{-1} and the asymmetric CF_3 stretch, $\nu_{as}(CF_3)$, around 1160-1190 cm^{-1}. These bands are well studied in PEO and PEO based electrolyte systems. [16-19] More recently, examination of these bands in amine-based systems indicated that while the bands did not maintain frequencies identical to those found in the ether oxygen systems, the frequencies were very similar and the trends remained the same. [20-22] To date, a systematic study of ionic association in nitrogen-oxygen mixed

heteroatom system has not been undertaken. However, it is reasonable to expect that increased degree of ionic association will continue to correspond to increased frequency of the bands.

Figure 6-4 contains the IR absorbance spectra for neat G1MC and several complexes with lithium triflate ranging from 20:1 (bottom) to 4:1 (top) heteroatom:Li^+. The far right panel contains the spectral range of 730-780 cm^{-1}, which corresponds to $\delta_s(CF_3)$. The frequencies of this mode have differed little between the PEO and the PEI based systems. At 20:1 heteroatom:Li^+ ratio, two overlapping bands are present. Deconvolution revealed the band centers to be at 757 cm^{-1} and 763 cm^{-1}; the bands have integrated intensities of 55% and 45% respectively. These frequencies are probably indicative of contact ion pair and the triple cation. Bandfitting did not indicate the presence of a "free" population, expected at a frequency around 754 cm^{-1}. In diglyme at this concentration, 23% of the population was found to be present as "free" ions.[23] In TMEDA, higher order aggregates and the absence of "free" ions have been reported at N:Li^+ of 20:1.[13] With increasing amounts of LiTf, the intensity of the 763 cm^{-1} band increases relative to the 757 cm^{-1} band suggesting the proportion of triple ion is also increasing. Around a ratio of 4:1 heteroatoms to Li^+, a shoulder on the 763 cm^{-1} is apparent. Using curvefitting, the center of this band is determined to be 769 cm^{-1}. This is may be indicative of the formation of a higher order aggregate such as $[Li_3Tf]^{+2}$ or the development of dimers type interactions. TMEDA has been shown to have such interactions that vibrate like higher order aggregates.[13]

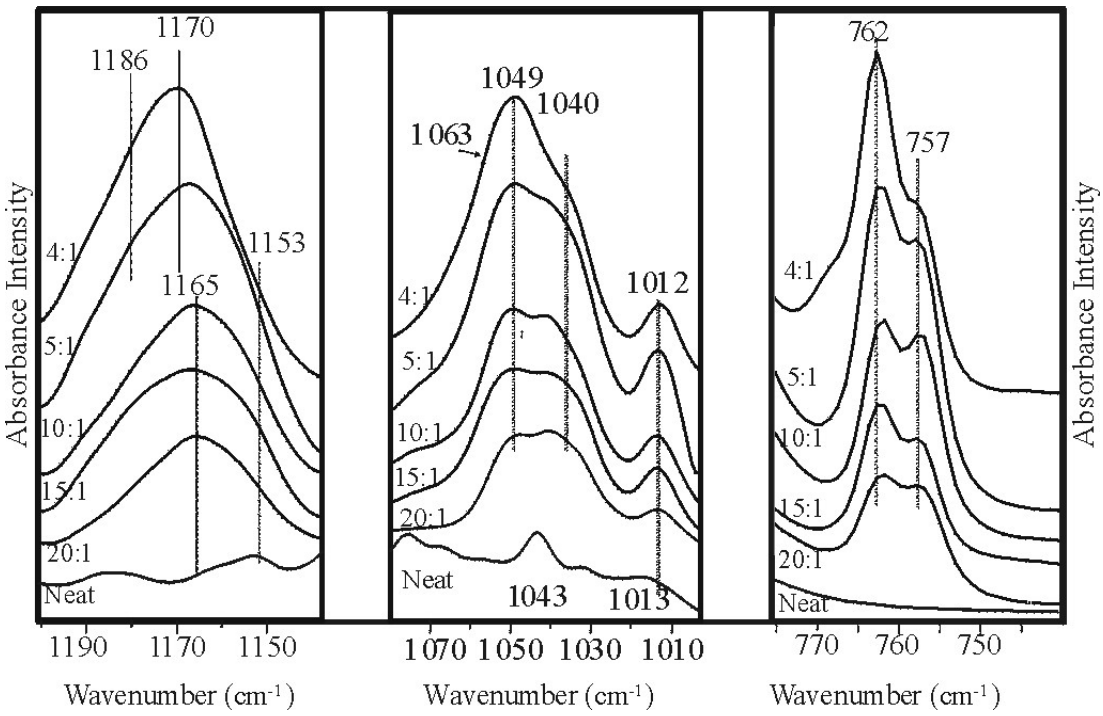

Figure 6-4: Ionic association regions of neat G1MC and G1MC:Litf complexes of 20:1, 15:1, 10:1 5:1 and 4:1 Heteratom:Li^+

The center panel of Figure 6-4 contains the $\nu_s(SO_3)$ region. An underlying G1MC band at 1043 cm^{-1} complicates the analysis of this region and precludes the use of integrated intensities to determine the relative percentages of ionic species. It is clear that increased salt concentration leads to higher order ionic associations. Bands centered at 1032, 1040 and 1049 cm^{-1} are present in the 20:1 heteroatom:Li^+ sample. The bands probably represent "free" ions, contact ion pairs and triple ions (or something vibrating like triple ions). At a salt content around 10:1 heteroatom:Li^+, a band centered at 1069 cm^{-1} begins to develop. This band indicates an even higher order aggregate or a species that vibrates like a higher order aggregate. Again this similar to the spectral behavior observed in TMEDA.[13]

Finally, the far left panel of Figure 3-4 illustrates the $\nu_{as}(CF_3)$ region of the G1MC:LiTf system. This region is the least well characterized of the three ionic association regions presented here. However, the trend of increased frequency relating increased aggregation is established (see Chapter 5 for a more thorough discussion). The behavior in this region is consistent with that seen in the other two regions. The system immediately achieves a high order of association and continues to shift in favor of higher aggregates with increased salt content. At 20:1 heteroatom:Li^+ a symmetric band centered at 1165 cm^{-1} appears. Deconvolution confirms the presence of side bands at 1178 and 1155 cm^{-1}. Integrated intensities indicate that about half the ions are contact ion pairs with the remaining population about equally divided between "free" ions and triple ions. This may be slightly misleading since a small G1MC band is present at 1153 cm^{-1} which may skew the curvefitting to favor the 1155 cm^{-1} band. Addition of lithium triflate continues to drive the system toward higher degrees of ionic association as seen by the broadening of the band and the gradual shift in the band center to a slightly higher frequency up to a composition of around 5:1 heteroatom:Li^+. Moving from 5:1 to 4:1 heteroatom:Li^+, the band narrows slightly and becomes slightly asymmetric with a high frequency tail. This band is composed of contributions from two bands: one centered at 1169 cm^{-1} (18%) and one centered at 1186 cm^{-1} (82%). Frequencies in this region have not been assigned conclusively to specific ionic associated species. The preliminary assignments given in Chapter 5 suggest these bands may be due to the triple ion and a higher order species. The G1MC system appears to experience

relatively high degree of ionic association even when containing a relatively small amount of salt.

3.5 CONCLUSIONS

A model compound for the LPEI-G2 polymer may be available in G2MC. However, the extremely hygroscopic nature of the compound greatly inhibits the collection of useable IR absorption data. The homolog compound, G1MC, is somewhat more forgiving. IR data indicate that G1MC andG2MC have some spectral features of amines and some spectral features of glymes. The addition of lithium triflate to the system alters the configuration of the chain connecting the nitrogen and oxygen atoms. It is not clear from the spectral data whether the cations associate more strongly with one heteroatom versus the other. Data from G1MC seems to more closely resemble that of TMEDA that it does diglyme. This hints at nitrogen coordination, but the evidence is not conclusive. A crystal structure and computational study is very much needed to more positively assign the vibrational modes. The G1MC system experiences mainly contact ion pair association and some triple ion at low salt levels, but evidence of a small amount "free" ion is present in two of the three anion regions presented here. This higher order of ionic association increases with increasing salt content.

Much work remains to fully character these mixed heteroatom systems. Many questions regarding the types of associations occurring the systems linger and the area is ripe for investigation. It is my delight that Rahul Kadam is using NMR

and other techniques to continue to investigate interactions in mixed heteroatom systems, so hopefully these systems can get the attention and interest they richly deserve.

3.7 REFERENCES

(1) Angelou, M. *Wouldn't Take Nothing for My Journey Now*; Bantam Paperback ed.; Bantam Books by arrangement with Random House: New York, 1994.

(2) Lee, Y.-C.; Ratner, M. A.; Shriver, D. F. *Solid State Ionics* **2001**, *138*, 273-276.

(3) Dupon, R.; Papke, B. L.; Ratner, M. A.; Shriver, D. F. *J. Electrochem. Soc.* **1984**, *131*, 586-9.

(4) Nishimoto, A.; Watanabe, M.; Ikeda, Y.; Kohjiya, S. *Electrochim. Acta* **1998**, *43*, 1177-1184.

(5) Ikeda, Y.; Wada, Y.; Matoba, Y.; Murakami, S.; Kohjiya, S. *Electrochim. Acta* **2000**, *45*, 1167-1174.

(6) Blonsky, P. M.; Shriver, D. F.; Austin, P.; Allcock, H. R. *Solid State Ionics* **1986**, *18-19*, 258-264.

(7) Allcock, H. R.; Napierala, M. E.; Olmeijer, D. L.; Cameron, C. G.; Kuharcik, S. E.; Reed, C. S.; O'Connor, S. J. M. *Electrochim. Acta* **1998**, *43*, 1145-1150.

(8) Snow, A. G.; Sanders, R. A.; Frech, R.; Glatzhofer, D. T. *Electrochim. Acta* **2003**, *48*, 2065-2069.

(9) Clarke, H. T.; Gillespie, H. B.; Weisshaus, S. Z. *J. Am. Chem. Soc.* **1933**, *55*, 4571-87.

(10) Yoshihara, T.; Tadokoro, H.; Murahashi, S. *J. Chem. Phys.* **1964**, *41*, 2902-11.

(11) Matsuura, H.; Fukuhara, K. *J. Polym. Sci., Part B: Polym. Phys.* **1986**, *24*, 1383-400.

(12) Boesch, S. E.; York, S. S.; Frech, R.; Wheeler, R. A. *PhysChemComm* **2000**, *1*, 1.

(13) Sanders, R. A.; Frech, R.; Khan, M. A. *J. Phys. Chem. B* **2003**, *107*, 8310-8315.

(14) Rhodes, C. P.; Frech, R. *Macromolecules* **2001**, *34*, 2660-2666.

(15) Rhodes, C. P., University of Oklahoma, 2001.

(16) Schantz, S.; Sandahl, J.; Borjesson, L.; Torell, L. M.; Stevens, J. R. *Solid State Ionics* **1988**, *28-30*, 1047-53.

(17) Frech, R.; Huang, W. *Solid State Ionics* **1994**, *72*, 103-7.

(18) Huang, W.; Frech, R.; Wheeler, R. A. *J. Phys. Chem.* **1994**, *98*, 100-10.

(19) Rhodes, C. P.; Frech, R. *Solid State Ionics* **1999**, *121*, 91-99.

(20) York, S.; Frech, R.; Snow, A.; Glatzhofer, D. *Electrochim. Acta* **2001**, *46*, 1533-1537.

(21) Sanders, R. A.; Frech, R.; Khan, M. A. *J. Phys. Chem. B* **2004**, *108*, 12729-12735.

(22) York, S. S.; Boesch, S. E.; Wheeler, R. A.; Frech, R. *PhysChemComm* **2002**, *5*, 99-111.

(23) Petrowsky, M.; Frech, R.; Suarez, S. N.; Jayakody, J. R. P.; Greenbaum, S. *J. Phys. Chem. B* **2006**, *110*, 23012-23021.

CHAPTER 7: CONCLUDING REMARKS

At the heart of science is an essential tension between two seemingly contradictory attitudes -- an openness to new ideas, no matter how bizarre or counterintuitive they may be, and the most ruthless skeptical scrutiny of all ideas, old and new. This is how deep truths are winnowed from deep nonsense. Of course, scientists make mistakes in trying to understand the world, but there is a built-in error-correcting mechanism: The collective enterprise of creative thinking and skeptical thinking together keeps the field on track.

-- Carl Sagan[1]

The chief results of this work include:

- Characterization of poly(propylenimine) and poly(N-methylpropylenimine) in terms of IR spectroscopy, thermal properties and conductivity behavior, including the discovery that PPI is not hygroscopic and the observation of a striking hysteresis effect in neat PMPI that suggests kinetic relaxation occurs on two time scale, with one being slower that the cooling rate of 5ºC min^{-1}.
- Determination that ionic association in PPI and PMPI is of a higher degree (even at low salt content) and is less dependent on temperature than the ethylene homologs, and the hypothesis that these differences may be due to the additional conformational freedom generated by the presence of the third backbone CH_2 group, which may allow stronger cation-heteroatom interactions in the propylene systems.

- Assignment of NH stretching bands to specific hydrogen bonding interactions in N,N'-DMEDA and N,N'-DMPDA.
- Hypothesis of the presence of a doubly intermolecular hydrogen-bonded species in N,N'-DMPDA.
- Determination that degree of ionic association is higher in N,N'-DMPDA:LiTf complexes than in N,N'-DMEDA:LiTf complexes and that N,N'-DMPDA:LiTf complexes are more robust against CCl_4 dilution.
- Determination that CCl_4 addition to N,N'-DMPDA and N,N'-DMEDA disrupts significant amounts of intermolecular hydrogen bonding and causes the collapse of the network formed through anion-cation-polymer interactions, which results in reduced cation-heteroatom interactions, increased hydrogen bonding and increased degree of ionic association.
- Proposal of assignments for vibrational bands to specific ionic association species based on the $\nu_{as}(CF_3)$ mode.

.

This work has furthered the understanding of the nature and impact of hydrogen bonding in these systems and has emphasized the importance of backbone spacing in ionic association in polymer electrolytes. As science should, the work has generated at least as many questions as it has answered. For example the finding that CCl_4 addition reduces cation-heteroatom interaction and increases both hydrogen bonding interactions and ionic association was surprising. A satisfactory specific mechanism for this phenomenon remains to be proposed. Likewise, crystal structures which

(hopefully) support the assignments of interactions provided here have not been obtained. These structures may also help answer the CCl_4 issue by providing a concrete structure for the ion-polymer network. In the absence of crystal structures, solid state NMR measurements may be useful to provide some information about interatomic distances in the materials. The use of other salts in N,N'-DMEDA and N,N'-DMPDA could further elucidate interaction of all types, including hydrogen bonding, occurring within the system. Another interesting issue raised, but not fully answered, in the process of this work is that of direct anionic interaction with the polymer. Traditionally, anion interaction with the heteroatoms has been modeled with the cation acting as a bridge between the anion and heteroatom. However, some results within this work offer the tantalizing possibility of direct interaction through N-H···O type interactions. This should be a route for further exploration. Finally, the rather preliminary results presented on the G-series offer a wider range of interesting possibilities, some of which are being explored now in the Glatzhofer lab by Rahul Kadam and Matt Meredith. I look forward to learning of their results.

Here's where we gotta be
Love and community
Laughter is eternity
If joy is real

-- Bono[2]

REFERENCES:

(1) Sagan, C., The fine art of baloney detection. *Parade Magazine* **1987**, (1 Feb), 12-13.

(2) U2, Get on Your Boots. On *No Line on the Horizon*, Eno, B.; Lanois, D.; Gaffney, D., Producers. Universal Island Records: New York, 2009.

THE END!